

Shear Behavior of Webs Post-Tensioned with Tendons Containing Flexible Fillers

Final Report

December 2021

Principal investigator:

H. R. Hamilton

Research assistant:

Devon Skelton

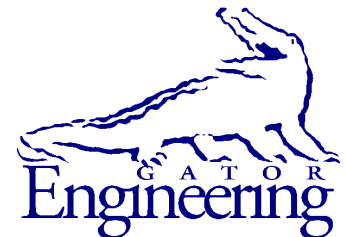
Department of Civil and Coastal Engineering
University of Florida
P.O. Box 116580
Gainesville, Florida 32611

Sponsor:

Florida Department of Transportation (FDOT)
Project Manager:
Bruno R. Vasconcelos

Contract:

UF Project No. 0035249 & 0035250
FDOT Contract No. BDV31-977-71



University of Florida

Engineering School of Sustainable Infrastructure and Environment
Department of Civil and Coastal Engineering
University of Florida
P.O. Box 116580
Gainesville, Florida 32611

Disclaimer

The opinions, findings, and conclusions expressed in this publication are those of the authors and not necessarily those of the State of Florida Department of Transportation.

Units of Measurement Conversion

SI* (MODERN METRIC) CONVERSION FACTORS APPROXIMATE CONVERSIONS TO SI UNITS

SYMBOL	WHEN YOU KNOW	MULTIPLY BY	TO FIND	SYMBOL
LENGTH				
in	inches	25.4	millimeters	mm
ft	feet	0.305	meters	m
yd	yards	0.914	meters	m
mi	miles	1.61	kilometers	km
AREA				
in ²	square inches	645.2	square millimeters	mm ²
ft ²	square feet	0.093	square meters	m ²
yd ²	square yard	0.836	square meters	m ²
ac	acres	0.405	hectares	ha
mi ²	square miles	2.59	square kilometers	km ²
VOLUME				
fl oz	fluid ounces	29.57	milliliters	mL
gal	gallons	3.785	liters	L
ft ³	cubic feet	0.028	cubic meters	m ³
yd ³	cubic yards	0.765	cubic meters	m ³
NOTE: volumes greater than 1000 L shall be shown in m ³				
MASS				
oz	ounces	28.35	grams	g
lb	pounds	0.454	kilograms	kg
T	short tons (2000 lb)	0.907	megagrams	Mg (or "t")
TEMPERATURE (exact degrees)				
°F	Fahrenheit	5(F-32)/9 or (F-32)/1.8	Celsius	°C
ILLUMINATION				
fc	foot-candles	10.76	lux	lx
fl	foot-Lamberts	3.426	candela/m ²	cd/m ²
FORCE and PRESSURE or STRESS				
kip	1000 pound force	4.45	kilonewtons	kN
lbf	pound force	4.45	newtons	N
lbf/in ²	pound force per square	6.89	kilopascals	kPa

*SI is the symbol for the International System of Units. Appropriate rounding should be made to comply with Section 4 of ASTM E380.

SI* (MODERN METRIC) CONVERSION FACTORS
APPROXIMATE CONVERSIONS FROM SI UNITS

SYMBOL	WHEN YOU KNOW	MULTIPLY BY	TO FIND	SYMBOL
LENGTH				
mm	millimeters	0.039	inches	in
m	meters	3.28	feet	ft
m	meters	1.09	yards	yd
km	kilometers	0.621	miles	mi
AREA				
mm ²	square millimeters	0.0016	square inches	in ²
m ²	square meters	10.764	square feet	ft ²
m ²	square meters	1.195	square yards	yd ²
ha	hectares	2.47	acres	ac
km ²	square kilometers	0.386	square miles	mi ²
VOLUME				
mL	milliliters	0.034	fluid ounces	fl oz
L	liters	0.264	gallons	gal
m ³	cubic meters	35.314	cubic feet	ft ³
m ³	cubic meters	1.307	cubic yards	yd ³
MASS				
g	grams	0.035	ounces	oz
kg	kilograms	2.202	pounds	lb
Mg (or "t")	megagrams (or "metric ton")	1.103	short tons (2000 lb)	T
TEMPERATURE (exact degrees)				
°C	Celsius	1.8C+32	Fahrenheit	°F
ILLUMINATION				
lx	lux	0.0929	foot-candles	fc
cd/m ²	candela/m ²	0.2919	foot-Lamberts	fl
FORCE and PRESSURE or STRESS				
kN	kilonewtons	0.225	1000 pound force	kip
N	newtons	0.225	pound force	lbf
kPa	kilopascals	0.145	pound force per square inch	lbf/in ²

*SI is the symbol for the International System of Units. Appropriate rounding should be made to comply with Section 4 of ASTM E380.

Technical Report Documentation Page

1. Report No.		2. Government Accession No.		3. Recipient's Catalog No.	
4. Title and Subtitle Shear Behavior of Webs Post-Tensioned with Tendons Containing Flexible Fillers				5. Report Date December 2021	
				6. Performing Organization Code	
7. Author(s) Skelton, D., and Hamilton, H. R.				8. Performing Organization Report No.	
9. Performing Organization Name and Address University of Florida Department of Civil & Coastal Engineering P.O. Box 116580 Gainesville, FL 32611-6580				10. Work Unit No. (TRAVIS)	
				11. Contract or Grant No. BDV31-977-71	
12. Sponsoring Agency Name and Address Florida Department of Transportation 605 Suwannee Street, MS 30 Tallahassee, FL 32399				13. Type of Report and Period Covered Final Report Feb. 2017-Dec. 2021	
				14. Sponsoring Agency Code	
15. Supplementary Notes					
<p>16. Abstract</p> <p>Post-tensioning provides several advantages, including smaller sections, longer spans, and reduction in cracking. The presence of post-tensioning (PT) tendon ducts in the girder web, however, may affect shear strength and serviceability. Ducts typically are injected with a high stiffness filler material like grout or a low stiffness flexible filler material such as wax. Previous shear strength testing has shown that web crushing is the dominant failure mode and main limiter of shear strength for girders with ducts. Limited research on shear strength of sections with ungrouted ducts led to the research covered in this report, in which full-scale girders were constructed with ungrouted (empty) ducts and then tested in shear.</p> <p>The research was divided into two phases of testing and investigated such variables as presence of duct, transverse reinforcement quantity, presence of top flange, web width, number of ducts, and duct-diameter-to-web-width ratio. The first phase included shear strength tests of six modified AASHTO Type III specimens. The specimens were precast and pretensioned; they also contained ducts of varying sizes but were not post-tensioned. Specimens were loaded in three-point bending at shear-span-to-depth ratios of 2.5 and 3. Four of the six specimens showed a web crushing failure at the duct location; specimens with larger duct sizes showed reduced shear strength. Specimens containing duct typically experienced localized diagonal cracking of the concrete cover over the duct followed by formation of diagonal web cracks through the full-depth of the web. The specimen with the largest duct-diameter-to-web-width ratio (0.64) experienced localized cracking at a relatively low applied shear of 19% of the shear strength. In the second phase of the experimental program, seven FIB-54 specimens were tested in shear, and similar behavior to the phase 1 specimens was noted.</p> <p>AASHTO LRFD, 9th Edition Bridge Design Specification shear design approach was evaluated using the test results from this and other research for ducts with duct-diameter-to-web-width ratio of 0.5 or less. Average shear strength ratios (V_{exp}/V_n) for specimens containing no ducts (solid web) in phase 1 and phase 2 were less than the comparable ratios for specimens containing ungrouted ducts.</p> <p>Based on the testing in this research, limiting the duct-diameter-to-web-width ratio to no more than 0.4 and limiting the calculated principal tensile stress in the concrete cover over the duct would have minimized the localized cracking that occurred in this testing.</p>					
17. Key Words Prestressed concrete, Shear, Post-tensioned, Florida I-Beam, Unbonded, Flexible Filler, Bridge Girder			18. Distribution Statement No restrictions		
19. Security Classif. (of this report) Unclassified		20. Security Classif. (of this page) Unclassified		21. No. of Pages 198	22. Price N/A

Acknowledgments

The authors would like to gratefully acknowledge and thank the Florida Department of Transportation (FDOT) for the financial support of this research project. The project was managed by Bruno Vasconcelos, and the authors thank him for his technical input and support throughout the project. The authors would like to thank the FDOT State Materials Office and Structures Research Center for their assistance with experimental and material testing. In particular, the authors would like to acknowledge Stephen Eudy, Christina Freeman, William Potter, Justin Robertson, and Paul Tighe.

The authors would like to thank Dura-Stress and its personnel for their support and contributions during the construction of our phase 1 and phase 2 test girders, especially Dr. Audi Sriboonlue and Mr. John Jarrett. Additionally, the authors would like to thank the many graduate students that contributed to the project, including Seaska Perez, Glenda Diaz, Satyajee Patil, and Eduardo Torres, for assistance with experimental testing and data collection.

Executive Summary

Post-tensioning is typically used in bridge construction because of its advantages over non-prestressed sections, such as allowing smaller sections, longer spans, and crack control. The presence of ducts in the web of post-tensioned girders leads to a discontinuity in the section, which can cause a reduction in the shear strength and affect serviceability. Ducts typically are injected with a high stiffness filler material like grout or a low stiffness flexible filler material such as wax.

The literature review for this research project noted previous shear strength tests performed on panels, prisms, and full-scale girders containing grout-filled ducts in the web. These tests indicated that web crushing was the dominant failure mode and main limiter of shear strength for girders. Limited research has been conducted on post-tensioned girders with ducts containing flexible filler. Such tests were conducted as part of the research reported herein to evaluate the serviceability and shear strength behavior of girders containing flexible filled post-tensioning tendons.

One outcome of the previous research was changes in shear design procedures. AASHTO LRFD Bridge Design Specifications, 9th Edition uses modified compression field theory to compute the nominal shear capacity of post-tensioned girders. This approach uses separate calculations for the concrete contribution and steel contribution to the overall shear capacity of a particular section. The design specifications require that an effective web width be used to determine the concrete contribution; the web width is reduced by the duct diameter for ungrouted ducts and is left at the full web width for grouted ducts. Although not specified directly, it is assumed that ducts containing flexible filler classified as ungrouted. Further adjustment is made in the shear capacity by adjusting the steel contribution using a duct factor for grouted ducts only; this factor reduces the steel contribution based on the ratio of duct diameter to web width.

The research was divided into two phases of testing. The first phase of the experimental program focused on shear strength tests of six modified AASHTO Type III specimens. The specimens were precast and pretensioned; they also contained ducts of varying sizes but were not post-tensioned. Specimens were loaded in three-point bending, at shear-span-to-depth ratios of 2.5 and 3; five of the specimens were designed to be tested in positive bending and the sixth in negative bending. Variables investigated included presence of post-tensioning duct, transverse reinforcement quantity, presence of top flange, web width, number of ducts and duct-diameter-to-web-width ratio. The primary purpose of these specimens was to test variable sensitivity in anticipation of larger scale shear strength tests. Four of the six specimens showed a web crushing failure at the duct location; specimens with larger duct sizes showed reduced shear strength. Specimens containing duct typically experienced localized diagonal cracking of the concrete cover over the duct followed by formation of diagonal web cracks through the full-depth of the web. The specimen with the largest duct-diameter-to-web-width ratio, experienced localized cracking at a relatively low applied shear of 19% of the shear strength.

In the second phase of the experimental program, seven FIB-54 specimens were tested in shear. These specimens contained one and two sets of ducts and were post-tensioned; duct-diameter-to-web-width ratio was varied among several of the specimens. Specimens were loaded in three-point bending at a shear-span-to-depth ratio of 2.5; two were loaded in negative bending, and five were loaded in positive bending. Each specimen was tested twice by performing a strength test on one end then moving the specimen to test the opposite end. Like phase 1, localized cracking typically occurred in the concrete cover over the duct at lower loads; as load was increased, full-depth web cracks formed. Positive bending specimens containing two ducts experienced localized cracking near the top duct location but no localized cracking at the bottom duct. This occurred due to the bottom duct proximity to the bottom flange where the section was thicker. Negative bending specimens experienced localized cracking occurred at similar loads in the concrete cover at both ducts for tests containing two ducts.

The AASHTO LRFD shear design approach was evaluated using the test results from this research as well as other researchers. It was found that average shear strength ratios (V_{exp}/V_n) for

specimens containing no ducts (solid web) in phase 1 and phase 2 were less than the comparable ratios for specimens containing ungrouted ducts. Furthermore, V_{exp}/V_n for grouted specimens in work by Moore et al. (2015) showed the same trend when compared to results from solid specimens. Note that this comparison includes only the specimens with a duct-diameter-to-web-width ratio of 0.5 or less. It can be concluded, based on the testing in this report, that the AASHTO LRFD approach is at least as conservative for girders containing ducts (either grouted or ungrouted) as it is for girders with solid webs.

Comparison of test results on specimens with and without ungrouted ducts indicated that there may be a potential for service-level localized cracking to occur at low principal stress levels. This cracking did not appear to affect the strength of the section under testing, but could result in long-term durability issues. Limiting principal stress in the concrete cover over the duct may reduce the probability of cracking.

Based on the testing in this research, limiting the duct-diameter-to-web-width ratio to no more than 0.4 and limiting the calculated principal tensile stress in the concrete cover over the duct to $2.6\sqrt{f'_c}$ would have minimized the localized cracking that occurred in this testing. This check would be in addition to the current principal stress check in AASHTO LRFD. Since this is a serviceability check rather than a safety check, another approach is to limit principal stresses in the concrete cover over the duct to $2.6\sqrt{f'_c}$ where the bridge is located in areas that are deemed to be harsh exposure conditions such as coastal bridges. The current limit of $3.5\sqrt{f'_c}$ could be used where the bridge is located in milder conditions.

Another alternative is to factor the duct diameter when calculating the effective web thickness (b_v) to ensure that the principal stresses are limited to $2.6\sqrt{f'_c}$. For the Phase 2 test specimens this factor is approximately 1.3.

Table of Contents

Disclaimer	ii
Units of Measurement Conversion	iii
Technical Report Documentation Page	v
Acknowledgments.....	vi
Executive Summary	vii
Table of Contents	ix
List of Figures	xii
List of Tables	xvii
1 Introduction.....	1
1.1 Research Objective	2
1.2 Research Approach	2
2 Prestressed I-Girders	3
2.1 Post-Tensioning Tendon Components.....	5
2.1.1 Grouted and Flexible Filler Materials.....	5
2.1.2 Bonded and Unbonded Tendons	5
3 Literature Review.....	7
3.1 Shear Behavioral Models.....	7
3.1.1 Shear Cracking in Prestressed Beams.....	7
3.1.2 Plastic Truss Models	10
3.1.3 Compression Field Approach	16
3.2 Current Shear Design Specifications	19
3.2.1 U.S. Design Specifications	20
3.2.2 International Design Specifications	22
3.2.3 Shear Design Using Effective Web Width	23
3.3 Panel Testing.....	24
3.3.1 Muttoni et al. (2006).....	24
3.3.2 Wald (2012)	26
3.4 Full-Scale Testing	33
3.4.1 Felan (2013).....	33
3.4.2 Shear Behavior of Spliced Post-Tensioned Girders (Moore et al. 2015)	34
3.5 Findings.....	37
4 Strength Tests on Modified AASHTO TYPE III Specimens	38
4.1 Introduction.....	38
4.2 Specimen Design	38
4.2.1 Included Variables	38
4.2.2 Excluded Variables	38
4.2.3 Cross-section.....	38
4.2.4 Strand Pattern.....	39
4.2.5 Duct Profile.....	40
4.2.6 Specified Material Properties.....	40
4.2.7 Test Matrix.....	40
4.3 Specimen Fabrication.....	41
4.3.1 Prestressing Strand Installation and Tensioning.....	41
4.3.2 Rebar Cage, Duct, and Internal Instrumentation Installation	45

4.3.3	Concrete Placement	48
4.3.4	Specimen Detensioning	52
4.4	Instrumentation	52
4.4.1	Strain	53
4.4.2	Displacement.....	54
4.5	Strength Test Results	55
4.5.1	Specimen SS1	56
4.5.2	Specimen SS2	57
4.5.3	Specimen SS3	59
4.5.4	Specimen SS4	61
4.5.5	Specimen SS5	63
4.5.6	Specimen NB1	64
4.6	Phase I Significant Results.....	66
5	Strength Tests on FIB-54 Specimens.....	67
5.1	Introduction.....	67
5.2	Specimen Design	67
5.2.1	Cross-section.....	68
5.2.2	Duct Profile.....	69
5.2.3	Specified Material Properties.....	70
5.2.4	Test Matrix.....	70
5.3	Specimen Fabrication.....	71
5.3.1	Prestressing Strand Installation and Tensioning	71
5.3.2	Rebar Cage, Duct, and Internal Instrumentation Installation	75
5.3.3	Concrete Placement	78
5.3.4	Specimen Detensioning	80
5.3.5	End Block and Deck Construction.....	81
5.4	Instrumentation	84
5.4.1	Strain.....	85
5.4.2	Displacement.....	87
5.5	Post-Tensioning Tendon Installation	87
5.5.1	Tendon Assembly	87
5.5.2	Instrumentation and Data Acquisition	89
5.5.3	Tendon Stressing Procedures	91
5.5.4	Load Cell Calibration.....	93
5.6	Specimen Test Procedure.....	96
5.7	Strength Test Results	97
5.7.1	Specimen P00.....	97
5.7.2	Specimen P34.....	99
5.7.3	Specimen P41.....	101
5.7.4	Specimen P50.....	103
5.7.5	Specimen P50R.....	105
5.7.6	Specimen N34.....	107
5.7.7	Specimen N50.....	109
5.8	Phase 2 Significant Results.....	111
6	Strength and Serviceability Analysis	112
6.1	Behavior at Service Load.....	112

6.2	Behavior at Ultimate Capacity	117
6.3	SDG Duct Reinforcement Analysis	119
6.4	Serviceability Analysis	123
6.5	Ultimate Shear Capacity Analysis	123
6.6	Effect of Duct Size	125
7	Summary and Conclusions	126
8	Implementation	128
8.1	Shear Strength	128
8.2	Serviceability	129
9	Future Research	130
	References	131
	Appendix A – Shear Strength Calculation Summary	133
	Appendix B – Cracking Loads Summary	139
	Appendix C – Principal Tensile Stress Summary	141
	Appendix D – Fabrication Drawings	144

List of Figures

Figure 1-1 Deviation of diagonal compressive stress in the vicinity of a voided duct.....	1
Figure 2-1 Examples of I-girder bridges: (a) simple span and (b) spliced	3
Figure 2-2 Simple span bridge with cast-in-place deck.....	3
Figure 2-3 Three-span bridge profile showing critical locations for shear investigation.	4
Figure 2-4 Example tendon profile for shear investigation.	4
Figure 2-5 Multi-strand post-tensioning tendon.	5
Figure 2-6 Girder with internal unbonded tendon containing flexible filler.	6
Figure 3-1 Shear stress diagram for simply supported girder under concentrated load (Dolan & Hamilton, 2019).	8
Figure 3-2 Mohr’s circle analysis of principal stresses at the neutral axis: (a) without prestressing and (b) with prestressing (Dolan & Hamilton, 2019)	9
Figure 3-3 Cracking in reinforced concrete beams: (a) web-shear crack (b) flexure-shear crack (Darwin et al., 2015)	9
Figure 3-4 Forces at a diagonal crack in a beam: (a) without shear reinforcement and (b) with shear reinforcement (Darwin et al., 2015)	10
Figure 3-5 Example of beam using a traditional truss model.	11
Figure 3-6 Calculated shear strength as a function of θ and shear reinforcement index ρ_v	11
Figure 3-7 Modified section-truss approach behavioral model for beams.	12
Figure 3-8 Free-body diagram at an end support for reinforced concrete member subjected to shear:	13
Figure 3-9 Failure modes predicted by rotating angle softened truss model for elements loaded in pure shear.	14
Figure 3-10 Average stress-strain curve for mild steel.	14
Figure 3-11 Cracked element model for fixed-angle truss model.	15
Figure 3-12 Constitutive properties used in fixed angle model:.....	16
Figure 3-13 Summarized compression field theory.....	17
Figure 3-14 Membrane element.....	18
Figure 3-15 Summarized MCFT for cracked elements.	19
Figure 3-16 Effective web width for shear calculations.	23
Figure 3-17 Compressive stress flow in panels under compressive force	25
Figure 3-18 Panel test results for empty and filled ducts compared to design code.....	25
Figure 3-19 Panel failure after shear testing	26
Figure 3-20 Panel testing parameters.....	27
Figure 3-21 Typical failure modes of panels	27
Figure 3-22 Compressive stress flow for various duct-diameter-to-thickness ratios	28
Figure 3-23 Plot of panel research showing η_D vs. δ	29
Figure 3-24 Steel duct and plastic duct strength comparison results.....	29
Figure 3-25 Grouted ducts vs. ungrouted ducts strength comparison results	30
Figure 3-26 Effect of through thickness reinforcement on shear strength.....	31
Figure 3-27 Results from varying grout-concrete strength ratio	31
Figure 3-28 Results from varying grout-concrete strength ratio	32
Figure 3-29 Typical test setup.....	33
Figure 3-30 Girder with plastic duct after failure	34
Figure 3-31 Localized and full-depth cracking of girders with PT ducts	35

Figure 3-32 Normalized shear stress at ultimate for plastic and steel ducts with duct-diameter-to-web-width ratio between 0.43 and 0.44	35
Figure 3-33 Shear strength ratio vs. transverse reinforcement ratio	36
Figure 3-34 λ_{duct} vs. duct-diameter-to-web-width ratio	37
Figure 4-1 Modified AASHTO Type III cross-section.....	39
Figure 4-2 Strand pattern for Modified AASHTO Type III sections	39
Figure 4-3 Specimen test setup for specimens:.....	41
Figure 4-4 Specimen orientation and strand cutting location.	41
Figure 4-5 Form release being sprayed on bottom liner	42
Figure 4-6 Typical plywood bulkhead for specimens.....	42
Figure 4-7 Prestressing strand insertion.....	43
Figure 4-8 PVC sheathing for strand debonding.	43
Figure 4-9 Prestressing strand stressing using monostrand jack	44
Figure 4-10 Prestressing strand jacking sequence	44
Figure 4-11 Strand debonding	44
Figure 4-12 Smooth duct with outside diameter: (a) 1.9-in. (b) 2.375 in. (c) 4.5-in.	45
Figure 4-13 Duct installation	46
Figure 4-14 Rebar cage assembly	46
Figure 4-15 Internal instrumentation	47
Figure 4-16 SS1 rebar cage assembly	47
Figure 4-17 SS2 rebar cage assembly	47
Figure 4-18 SS3 rebar cage assembly	47
Figure 4-19 SS4 rebar cage assembly	47
Figure 4-20 SS5 rebar cage assembly	48
Figure 4-21 NB1 rebar cage assembly	48
Figure 4-22 AASHTO Type III side form installation	48
Figure 4-23 Styrofoam attached to side form and glue.....	49
Figure 4-24 First concrete placement	49
Figure 4-25 Roughened top surface	50
Figure 4-26 Tarp covered specimens	50
Figure 4-27 Specimen second placement (a) plywood formwork (b) top flange rebar cage.....	51
Figure 4-28 Concrete placement and finished surface.....	51
Figure 4-29 Completed specimens.....	51
Figure 4-30 Detensioning sequence.....	52
Figure 4-31 Fully cut strands	52
Figure 4-32 Typical instrumentation layout for phase 1 specimens	53
Figure 4-33 60-mm foil-type concrete strain gauge	53
Figure 4-34 Rosette strain gauge	54
Figure 4-35 Linear potentiometer measuring strand slip.....	54
Figure 4-36 Laser displacement transducer	55
Figure 4-37 LVDT measuring web expansion.....	55
Figure 4-38 Shear-displacement results for specimen SS1.....	56
Figure 4-39 Specimen SS1 crack pattern after shear test	56
Figure 4-40 Concrete spalling under load point at peak load	57
Figure 4-41 Elevation view of specimen SS1 after strength test	57
Figure 4-42 Specimen SS2 load vs. displacement plot.....	58

Figure 4-43 Specimen SS2 crack pattern.....	58
Figure 4-44 Concrete spalling under load point at end of test.....	59
Figure 4-45 Specimen SS2 at end of destructive testing.....	59
Figure 4-46 Specimen SS3 load vs. displacement plot.....	60
Figure 4-47 Specimen SS3 crack pattern.....	60
Figure 4-48 Concrete spalling at, (a) web and (b) bottom flange at near support.....	60
Figure 4-49 Specimen SS3 at end of destructive testing.....	61
Figure 4-50 Specimen SS4 load vs. displacement plot.....	61
Figure 4-51 Specimen SS4 crack pattern.....	62
Figure 4-52 Shear failure of specimen SS4.....	62
Figure 4-53 Specimen SS4 (a) video screenshot at failure (b) half specimen after test.....	62
Figure 4-54 Specimen SS5 load vs. displacement plot.....	63
Figure 4-55 Specimen SS5 crack pattern.....	63
Figure 4-56 Concrete spalling at web.....	64
Figure 4-57 Specimen SS5 at end of destructive testing.....	64
Figure 4-58 Specimen NB1 load vs. displacement plot.....	65
Figure 4-59 Specimen NB1 crack pattern.....	65
Figure 4-60 Concrete spalling at web.....	65
Figure 4-61 Specimen NB1 at end of destructive testing.....	66
Figure 5-1 Specimen nomenclature.....	67
Figure 5-2 Duct reinforcement.....	68
Figure 5-3 Cross section of typical test specimen.....	69
Figure 5-4 Elevation view of typical specimen.....	69
Figure 5-5 Specimen test setup for (a) positive bending (b) negative bending.....	71
Figure 5-6 Specimen orientation and strand cutting location.....	71
Figure 5-7 FIB 54 steel bottom liner.....	72
Figure 5-8 Typical plywood bulkhead for specimens.....	72
Figure 5-9 Embedded steel bearing plate.....	72
Figure 5-10 Prestressing strand insertion.....	73
Figure 5-11 PVC Sheathing for strand debonding.....	73
Figure 5-12 Prestressing strand stressing using monostrand jack.....	74
Figure 5-13 Prestressing strand jacking sequence.....	74
Figure 5-14 Strand debonding.....	75
Figure 5-15 Duct installation.....	76
Figure 5-16 Rebar cage assembly.....	76
Figure 5-17 Internal instrumentation.....	77
Figure 5-18 P00 rebar cage assembly.....	77
Figure 5-19 P34 rebar cage assembly.....	77
Figure 5-20 P41 rebar cage assembly.....	77
Figure 5-21 P50 rebar cage assembly.....	77
Figure 5-22 P50R rebar cage assembly.....	78
Figure 5-23 N34 rebar cage assembly.....	78
Figure 5-24 N50 rebar cage assembly.....	78
Figure 5-25 FIB-54 side form installation.....	78
Figure 5-26 Concrete placement at girder bed for specimens.....	79
Figure 5-27 Roughened top surface.....	79

Figure 5-28	Tarp-covered specimens.....	80
Figure 5-29	Completed specimens.....	80
Figure 5-30	Detensioning sequence.....	81
Figure 5-31	Fully cut strands.....	81
Figure 5-32	End block construction: (a) end block platform (b) end block reinforcement cage (c) reinforcement cage inside end block (d) completed end block formwork.....	82
Figure 5-33	Deck construction: (a) deck reinforcement (b) deck formwork.....	83
Figure 5-34	End block concrete placement.....	83
Figure 5-35	Deck concrete placement.....	84
Figure 5-36	Completed concrete placement.....	84
Figure 5-37	Typical instrumentation layout for phase 2 specimens.....	85
Figure 5-38	60-mm foil-type concrete strain gauge.....	86
Figure 5-39	Rosette strain gauge.....	86
Figure 5-40	Fiber optic sensor.....	86
Figure 5-41	Laser displacement transducer.....	87
Figure 5-42	LVDT measuring web expansion.....	87
Figure 5-43	Geokon 850-kip hollow load cell and anchor head installation at dead-end.....	88
Figure 5-44	Anchor block and wedge plate at live end.....	88
Figure 5-45	Strand location for (a) specimen P34 and N34 (b) specimen P41 (c) specimen P50, P50R and N50.....	89
Figure 5-46	Multistrand jack pressure gauge and calibration sheet.....	90
Figure 5-47	Geokon 850-kip hollow load cell assembly.....	90
Figure 5-48	Multistrand jack installation for post-tensioning at live end.....	91
Figure 5-49	Plot of tendon force vs. time for specimen P50.....	93
Figure 5-50	Push test assembly with wedge plate.....	94
Figure 5-51	Push test assembly without wedge plate.....	94
Figure 5-52	Load cell assembly with square bottom plate.....	95
Figure 5-53	Nomenclature for positive and negative bending shear specimens containing ducts.....	96
Figure 5-54	Specimen P00 shear force vs. displacement plot (a) P00-1 (b) P00-2.....	98
Figure 5-55	Specimen P00 crack pattern for test (a) P00-1 (b) P00-2.....	99
Figure 5-56	Concrete spalling at web after peak shear force and unloading (a) P00-1 (b) P00-2.....	99
Figure 5-57	Specimen P34 shear force vs. displacement plot (a) P34-1 (b) P34-2.....	100
Figure 5-58	Specimen P34 crack pattern for test (a) P34-1 (b) P34-2.....	101
Figure 5-59	Concrete spalling at web after peak shear force and unloading (a) P34-1 (b) P34-2.....	101
Figure 5-60	Specimen P41 shear force vs. displacement plot (a) P41-1 (b) P41-2.....	102
Figure 5-61	Specimen P41 crack pattern for test (a) P41-1 (b) P41-2.....	103
Figure 5-62	Concrete spalling at web after peak shear force and unloading (a) P41-1 (b) P41-2.....	103
Figure 5-63	Specimen P50 shear force vs. displacement plot (a) P50-1 (b) P50-2.....	104
Figure 5-64	Specimen P50 crack pattern for test (a) P50-1 (b) P50-2.....	105
Figure 5-65	Concrete spalling at web after peak shear force and unloading (a) P50-1 (b) P50-2.....	105
Figure 5-66	Specimen P50R shear force vs. displacement plot (a) P50R-1 (b) P50R-2.....	106

Figure 5-67 Specimen P50R crack pattern for test (a) P50R-1 (b) P50R-2.....	107
Figure 5-68 Concrete spalling at web after peak shear force and unloading (a) P50R-1 (b) P50R-2.....	107
Figure 5-69 Specimen N34 shear force vs. displacement plot (a) N34-1 (b) N34-2.....	108
Figure 5-70 Specimen N34 crack pattern for test (a) N34-1 (b) N34-2.....	109
Figure 5-71 Concrete spalling at web after peak shear force and unloading (a) N34-1 (b) N34-2.....	109
Figure 5-72 Specimen N50 shear force vs. displacement plot (a) N50-1 (b) N50-2.....	110
Figure 5-73 Specimen N50 crack pattern for test (a) N50-1 (b) N50-2.....	111
Figure 5-74 Concrete spalling at web after peak shear force and unloading (a) N50-1 (b) N50-2.....	111
Figure 6-1 Localized cracks in concrete cover over duct for specimen with duct-diameter-to-web-width ratio (a) 0.34 (b) 0.50	113
Figure 6-2 Full-depth web cracks (a) no duct specimen (b) specimen with duct.....	113
Figure 6-3 Fiber optic sensor strain measurements at first cracks during loading	114
Figure 6-4 Crack identification within web of shear specimen	114
Figure 6-5 Locations for maximum principal tensile stress check	115
Figure 6-6 Simplified shear stress flow in I-girder containing voided duct	115
Figure 6-7 Normalized principal tensile strength vs. duct-diameter-to-web-width ratio for (a) cracking in concrete cover over duct (b) web cracking	116
Figure 6-8 Failure of ducted specimen (a) ungrouted (b) grouted specimen (Moore et al., 2015).	118
Figure 6-9 Peak shear force vs. duct-diameter-to-web-width ratio of positive bending tests for (a) phase 1 (b) phase 2 (c) Moore et al. (2015) shear tests.....	119
Figure 6-10 Duct reinforcement for I-girders containing post-tensioning ducts as required by FDOT SDG (Structures Design Guidelines, 2021).....	120
Figure 6-11 Specimen P50R SDG duct reinforcement.....	121
Figure 6-12 Localized cracking comparison for specimen (a) P50-1 (b) P50R-1 (c) P50-2 (d) P50R-2.	122
Figure 6-13 Web cracking comparison for specimen (a) P50-1 (b) P50R-1 (c) P50-2 (d) P50R-2.	122
Figure 6-14 Effect of duct-diameter-to-web-width ratio on normalized AASHTO LRFD shear strength ratio	124

List of Tables

Table 3-1	Table showing k factor for various codes.....	24
Table 3-2	Table showing panel test results.....	26
Table 3-3	Panel testing results of varying δ	28
Table 3-4	Comparison of panel and girder with plastic duct strength test results.....	34
Table 4-1	Table showing material properties and specifications.....	40
Table 4-2	Modified AASHTO TYPE III specimens test matrix.	40
Table 4-3	Specimen fabrication event summary.	41
Table 4-4	Duct size and material summary	45
Table 4-5	Summary of general instrumentation	53
Table 5-1	Table showing material properties and specifications.....	70
Table 5-2	Phase 2 specimen matrix	70
Table 5-3	Specimen fabrication event summary	71
Table 5-4	Duct size and material summary	75
Table 5-5	Summary of general instrumentation	85
Table 5-6	Summary of data acquisition during post-tensioning.....	91
Table 5-7	Tendon elongations (in.).....	92
Table 5-8	Tendon force measured at jack after each incremental increase in jacking force	93
Table 5-9	Summary of push test configurations and results.....	95
Table 5-10	Dead-end load cell reading before and after calibration	95
Table 5-11	Summary of specimen test dates and duct information.....	96
Table 6-1	Normalized principal tensile stress* at which localized cracks formed.....	116
Table 6-2	Normalized principal tensile stress* at which web cracks formed.....	117
Table 6-3	Summary of cracking loads and peak shear force for specimen P50 and P50R.	121
Table 6-4	Normalized strength ratio using AASHTO 9 th Edition MCFT provisions.....	124
Table 6-5	Normalized strength ratio using AASHTO 9 th Edition LRFD Segmental provisions.	125
Table 6-6	Normalized strength ratio using ACI 318-19 provisions.	125
Table 6-7	Normalized strength ratio comparison of solid and duct specimens using AASHTO 9 th Edition MCFT provisions.	125
Table A-1	Phase 1 nominal strength calculation summary using AASHTO LRFD, 9th Edition MCFT.....	133
Table A-2	Phase 1 nominal strength calculation summary using AASHTO LRFD, 9th Edition Segmental procedure.....	134
Table A-3	Phase 1 nominal strength calculation summary using ACI 318-19.....	135
Table A-4	Phase 2 nominal strength calculation summary using AASHTO LRFD, 9th Edition MCFT.....	136
Table A-5	Phase 2 nominal strength calculation summary using AASHTO LRFD, 9th Edition Segmental procedure.....	137
Table A-6	Phase 2 nominal strength calculation summary using ACI 318-19.....	138
Table B-7	Summary of duct- and web-cracking shear forces for phase 1 and phase 2 tests.	139
Table B-8	Summary of duct- and web-cracking loads for Texas research girders.....	140
Table C-9	Summary of principal tensile stresses for phase1 and phase 2 tests.....	141
Table C-10	Summary of principal tensile stresses for Texas research girders.	142

Table C-11 Principal tensile stress and rosette principal tensile stress comparison for phase1 and phase 2. 143

1 Introduction

Prestressed concrete is widely used as a cost-effective and efficient method of bridge construction and offers several unique advantages over other systems. Bonded multi-strand post-tensioning tendons have typically been the primary method of prestressing long-span spliced-girder and box-girder bridges in Florida. To attain bonded tendons, however, a cementitious grout must be injected into the tendon and allowed to harden. Recent years have seen durability issues arise in grouted tendons from poor grouting practice or poor material performance. To address this issue, Florida Department of Transportation (FDOT) has implemented the use of flexible fillers (petroleum wax) in lieu of cementitious grout as the primary choice for corrosion protection of post-tensioning tendons.

Flexible filler use in post-tensioned concrete bridge construction is relatively new in the United States with little to no shear behavior investigation being done on girders with multi-strand post-tensioning (PT) tendons containing flexible filler. These types of tendons, however, have been used in the nuclear industry, cable stay bridges, and in bridges located in Europe for corrosion protection of PT tendons. Flexible filler has a very low stiffness and for the purposes of analyzing the structural behavior of girders the tendons should be considered unbonded. Bond is not developed along the length of unbonded tendons, so their post-tensioning force is transferred at anchorages and along the length of deviated ducts.

Ducts of unbonded tendons effectively reduce the thickness of the girder web, which induces stresses to deviate around the duct causing high compressive and tensile stresses in the concrete adjacent to the duct; if the duct occupies a significant portion of the web thickness, then the web may crush at a lower shear stress than a solid web of the same thickness (Figure 1-1).

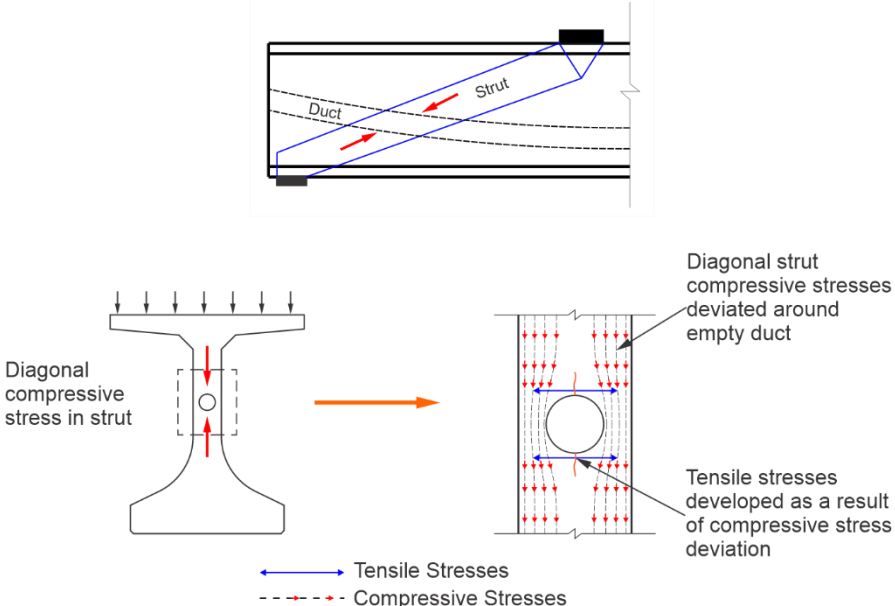


Figure 1-1 Deviation of diagonal compressive stress in the vicinity of a voided duct

This report focuses on the shear behavior of girders with PT tendons containing flexible filler and how the introduction of this new filler material impacts the local and global behavior. Chapter 2 provides background on prestressed I-girder and post-tensioning components. The

literature review in Chapter 3 includes shear behavioral models, current shear design approaches, and previous shear testing as they relate to girders with hollow ducts in the web. Chapter 4 presents the experimental strength test performed on modified AASHTO type III specimens, test setup and shear strength test results. Chapter 5 covers the full-scale experimental strength tests performed on FIB-54 specimens.

1.1 Research Objective

Experimental work was conducted to achieve the following objectives:

- Evaluate the sensitivity of girders containing post-tensioning tendons to various variables at ultimate and service level.
- Evaluate the effectiveness of current design codes for determining the shear strength of girders containing ungrouted post-tensioning tendons.
- Develop strategies for implementing the results into the shear design requirements of AASHTO LRFD for girders containing ungrouted post-tensioning tendons.

1.2 Research Approach

The efforts conducted to accomplish the research objective can be divided into two (2) major components:

- Phase 1 strength test of AASHTO Type III girders to determine which variables would be most critical to the shear test investigation. Results were used to refine the Phase 2 test program.
- Phase 2 strength test of FIB-54s closer representation of a typical post-tensioned bridge girder configuration to investigate the shear behavior.

2 Prestressed I-Girders

Florida bridges are commonly constructed using precast, prestressed I-girders (Figure 2-1). A typical precast simple-span bridge is shown in Figure 2-2 and an example of a post-tensioned spliced I-girder bridge, based on the Wonderwood bridge, is shown below in Figure 2-3 and Figure 2-4.

Both simple span and spliced girder construction allows for the economical construction of long span bridges. Simple-span construction is easier to construct because it uses a simpler design and construction process than spliced girder systems. However, simple-span construction span lengths are limited by the shipping and handling of the precast girder. Spliced girder construction uses post-tensioning tendons with efficient profiles to create continuity. Multiple precast segments are joined at spliced locations, creating longer spans with fewer interior supports than simple-span bridges thus reducing substructure costs. The elimination of interior supports also improves driver safety by reducing the chances of vehicle collisions.



Figure 2-1 Examples of I-girder bridges: (a) simple span and (b) spliced

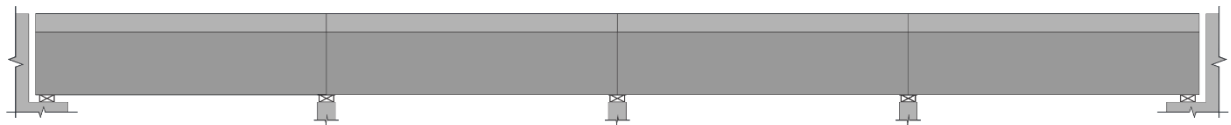


Figure 2-2 Simple span bridge with cast-in-place deck.

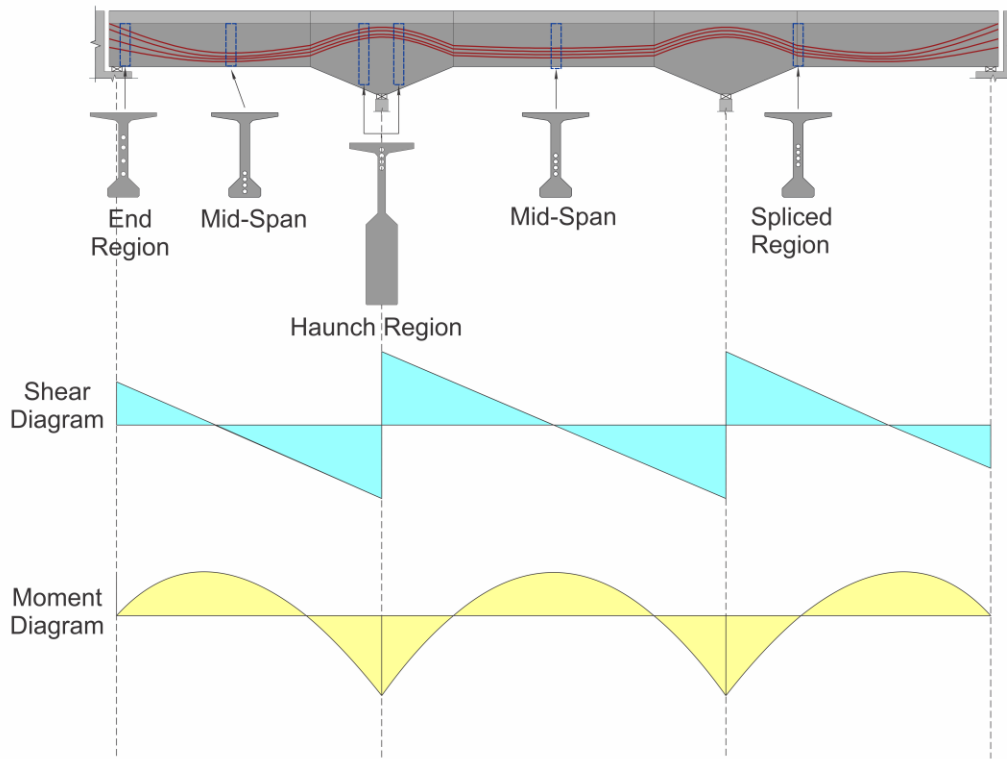


Figure 2-3 Three-span bridge profile showing critical locations for shear investigation.

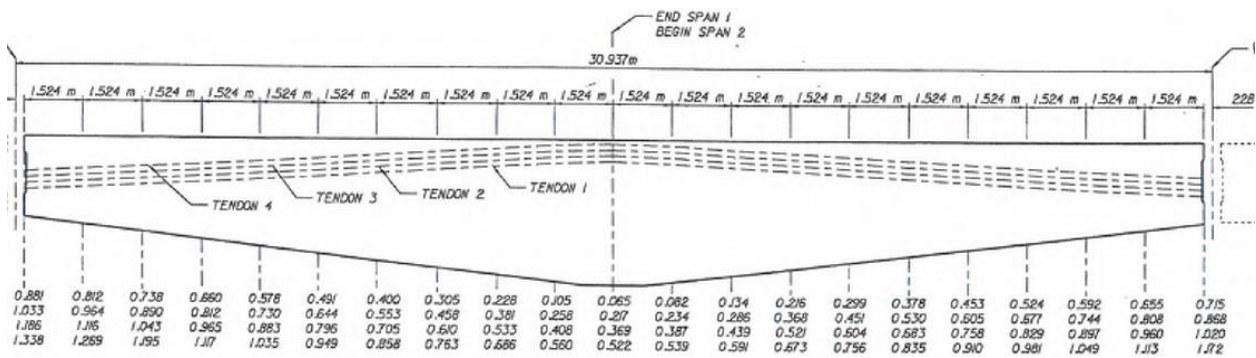


Figure 2-4 Example tendon profile for shear investigation.

2.1 Post-Tensioning Tendon Components

Post-tensioning tendons are defined as “a single or group of prestressing strands and their anchorage assemblies, which impart the prestress force to a structural member.” (Post-Tensioning Institute, 2007) Generally, post-tensioning tendons, shown in Figure 2-5, are comprised of the following components:

- Grout port/Inlet port – Filler material is injected through here after the strands have been tensioned.
- Wedge plate/Anchor Head – Hold the wedges in place and transfer the forces from the prestressing strands to the bearing plate.
- Bearing plate – Transfers the prestress force into the structure.
- Duct – Contains the prestressing strands along with filler material and defines the tendon profile when cast into the section.

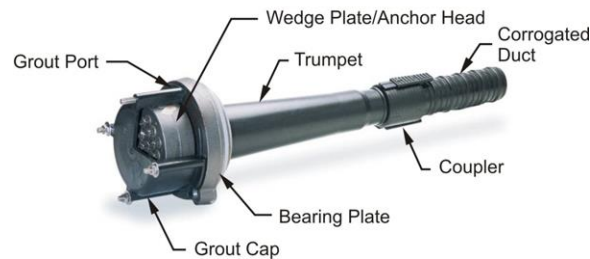


Figure 2-5 Multi-strand post-tensioning tendon. (Theryo, Hartt, & Paczkowski, 2013)

2.1.1 Grouted and Flexible Filler Materials

Traditionally PT ducts were filled with cementitious grout that hardened to compressive strengths that are comparable to that of the member concrete. Grout is a filler injected into PT tendons comprised of cementitious materials, potable water, and admixtures. The grout provides structural bond between the prestressing strand and surrounding concrete. In addition, the grout provides corrosion protection for the prestressing strands.

Alternatively, ducts can be filled with flexible fillers such as petroleum wax or grease, which provide corrosion protection, but do not provide structural bond. Flexible fillers are injected into the tendon similar to that of grout. One key difference is that the filler is heated to achieve the flowability for injection.

2.1.2 Bonded and Unbonded Tendons

Bonded tendons are typically filled with cementitious grout. These types of tendons are integral to the concrete structure, the cementitious grout bonds the strands to the surrounding concrete and does not allow relative movement between the concrete and the grout. Corroged ducts are used to enforce the bond. The ribs of the duct in conjunction with the stiffness of the grout create the bond to the surrounding concrete.

Post-tensioning tendons that are not connected to the surrounding concrete are considered unbonded. The prestressing strand is not bonded so relative movement is allowed between the strands and surrounding concrete. An unbonded tendon's prestressing strand force is transferred typically at the anchorage by end blocks. Internal or external tendons containing flexible filler are considered unbonded while external tendons containing cementitious grout are unbonded.



Figure 2-6 Girder with internal unbonded tendon containing flexible filler.

3 Literature Review

3.1 Shear Behavioral Models

Shear failure is an undesirable failure mode due to its sudden nature. Predicting shear behavior is difficult because shear behavior is heavily dependent on the tensile strength of concrete, which is highly variable. The effect of shear loading on a concrete beam results in diagonal tension, which typically leads to diagonal cracking. This cracking is controlled using stirrups, vertical reinforcement, which crosses these diagonal cracks, thus stabilizing the post-cracking behavior.

The uncertainty associated with shear strength prediction is partially reflected in the relatively low strength reduction factors compared to flexure used in various design codes. Typically diagonal tensile stresses, which are a result of the combination of shear stress and longitudinal flexural stress, are a major concern in shear analysis and design for beams. (Darwin, Dolan, & Nilson, 2015)

The application of prestressing, to some degree, offsets the diagonal tension stresses caused by shear. To better understand this effect in prestressed beams, shear cracking is discussed in Section 3.1.1. The use of stirrups leads to plastic truss behavior that is discussed in Section 4.2 and includes several variations of models used to analyze reinforced concrete beams. Section 3.1.3 covers the compression field approaches, which are a classification of plastic truss analytical model that is used in the current AASHTO LRFD Bridge Design Specification, 9th Edition (hereafter referred to as AASHTO).

3.1.1 Shear Cracking in Prestressed Beams

Understanding shear behavior requires an understanding of the formation of diagonal cracks. Before the section has cracked, first principles can be used to analyze the beam. Once the section has cracked, a shear behavioral model, such as the plastic truss approach, can be used to analyze the member. The behavior before cracking is similar in beams with or without reinforcement.

A simply supported prestressed beam under a concentrated load, shown in Figure 3-1, experiences a bending moment, axial force, and internal shear force. Before cracking, the concrete can be assumed to behave in a linear-elastic manner. A Mohr's circle analysis of the principal stresses and principal stress orientation at the neutral axis is shown in Figure 3-2. The diagonal principal stress causes the diagonal crack, and the principal angle corresponds to the crack angle. For beams without prestressing, we can expect the diagonal cracks to form at an angle of 45 degrees to the longitudinal axis of the beam (Figure 3-2a). Prestressed beams require a larger shear force to form the diagonal crack; in addition, the angle of these diagonal cracks is typically shallower, as illustrated in the Mohr's circle analysis (Figure 3-2b)

Web-shear cracks typically form near the neutral axis where diagonal tension is maximum (Figure 3-3a); these cracks may also propagate to the level of the reinforcement and cause bond failure. Web shear cracks generally occur in sections with a large shear force and small bending moment. The formation of the crack happens when the shear stress exceeds the tensile strength of the concrete, beam tests have shown this occurs on average around $3.5\sqrt{f_c}$. (Darwin et al., 2015)

Flexure-shear cracks occur in beams where the shear force and bending moment were large; these cracks were typically more common than web-shear cracks. The crack is initiated as a flexural crack, which then propagates upwards into the web as load is increased. As the crack

propagates, the angle generally decreases because of the diagonal tensile stresses near the neutral axis of the beam (Figure 3-3 (b)). The shear stress required to form this diagonal tension crack is conservatively estimated as $1.9\sqrt{f_c}$ (Darwin et al., 2015).

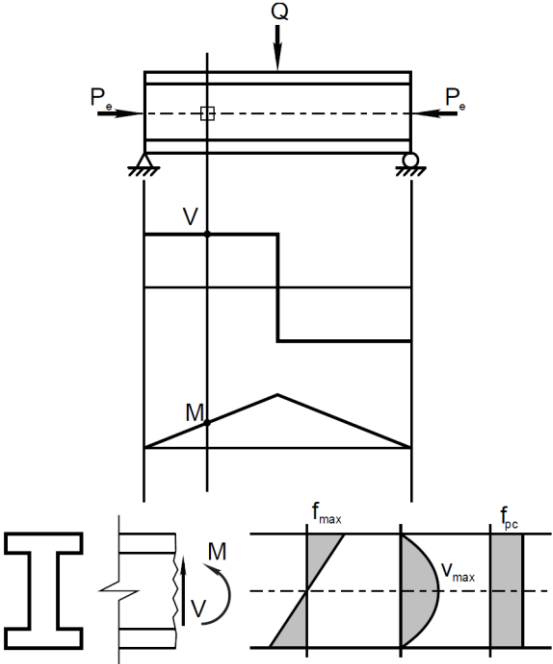


Figure 3-1 Shear stress diagram for simply supported girder under concentrated load (Dolan & Hamilton, 2019).

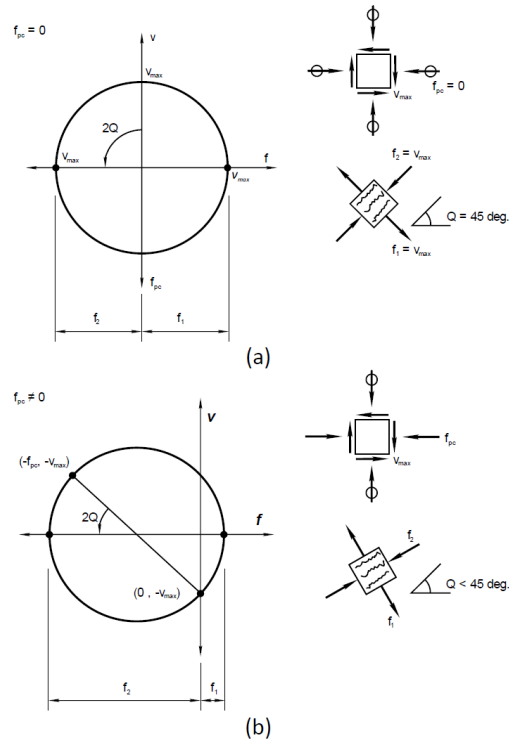


Figure 3-2 Mohr's circle analysis of principal stresses at the neutral axis: (a) without prestressing and (b) with prestressing (Dolan & Hamilton, 2019)

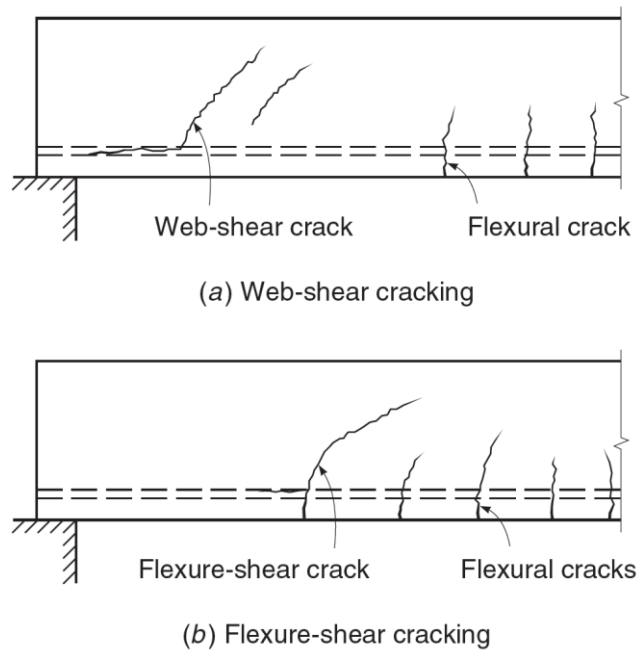


Figure 3-3 Cracking in reinforced concrete beams: (a) web-shear crack (b) flexure-shear crack (Darwin et al., 2015)

After diagonal cracks have formed in beams with no shear reinforcement, diagonal cracks may grow suddenly from the tension face into the compression face of the member, which can lead to a catastrophic failure with little to no warning.

The use of vertical shear reinforcement introduces additional mechanisms to resist the shear stresses and to control diagonal cracking, shown in Figure 3-3b. The additional mechanism of resistance leads to increased ductility and further warning before an impending failure. The vertical reinforcement does this in the following ways:

- Shear reinforcement resists the diagonal crack growth, which slows the propagation of the crack into the compression zone. This allows more of the compression zone to remain intact and resist the applied forces in the compression zone.
- The diagonal crack width is reduced, which increases the interface forces at the crack location and makes them more reliable.
- Shear reinforcement ties the longitudinal steel to the rest of the concrete section. This helps to prevent splitting of the concrete along the longitudinal steel and also increases the resistance of the shear force resisted by dowel action (Darwin et al., 2015)

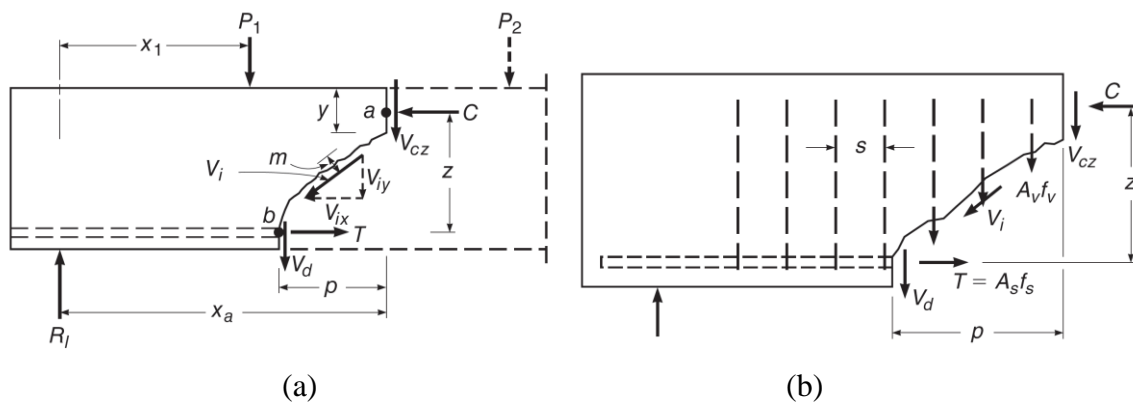


Figure 3-4 Forces at a diagonal crack in a beam: (a) without shear reinforcement and (b) with shear reinforcement (Darwin et al., 2015)

3.1.2 Plastic Truss Models

A prestressed concrete beam with shear reinforcement can be modelled as a truss by considering the stirrups as vertical web members and the concrete in diagonal compression as diagonal web members; top and bottom chords are formed by the flexural compression zone and reinforcement (Figure 3-5).

The traditional truss approach assumes that compression struts are parallel to the diagonal tension cracks and no stress transfer occurs across the cracks, which yields lower predicted strengths than experimental tests. These early models assumed no tensile stresses were carried by the cracked concrete and the diagonal compressive stresses were 45 degrees to the longitudinal axis, which led to the conservative results (Ramirez & Dilger, 2000).

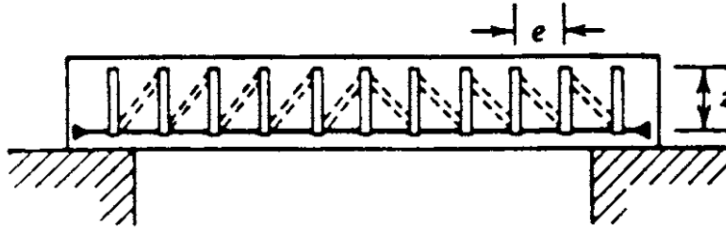


Figure 3-5 Example of beam using a traditional truss model (Ramirez & Breen, 1991).

Improvements were made to the traditional truss model where Mörsh suggested the possibilities of diagonal truss angles different than 45 degrees. This variable angle model (Figure 3-6) became a viable model for shear and torsion in prestressed and reinforced concrete. The fully plastic model assumes that the capacity of the web is achieved when the shear reinforcement yields while the concrete crushes simultaneously. The plot shows the inclination angle of the struts, θ , as a function of shear reinforcement index, ρ_v . Mörsh's traditional 45 degree truss model which assumes a constant strut angle, is shown to predict a lower capacity than that of a fully plastic variable-angle truss.

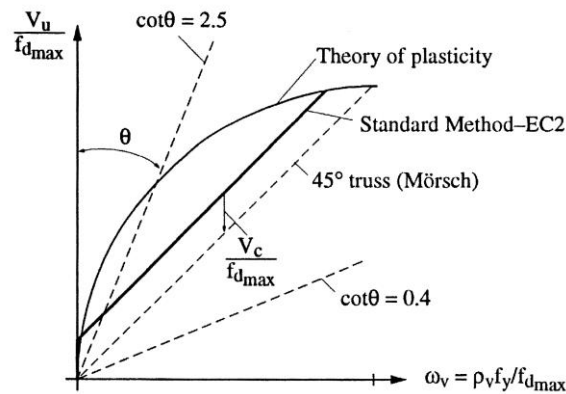


Figure 3-6 Calculated shear strength as a function of θ and shear reinforcement index ρ_v (Ramirez & Dilger, 2000).

3.1.2.1 Modified Sectional Truss Approach

The modified sectional-truss approach proposes the inclusion of a V_c term which allows for the efficient design of beams with low shear stresses. This model is also applicable for lightly loaded beams and B-type regions not requiring vertical shear reinforcement. The behavioral model assumes a beam with vertical shear reinforcement consists of parallel chord trusses with diagonals forming a uniform compression field, shown in Figure 3-7. A variable truss angle is used for this model with limits from 25 degrees to 65 degrees for prestressed beams. The K factor represents the beneficial effect of prestressing to increasing the shear capacity after cracking. The K-factor is derived from a Mohr's circle of an element at the neutral axis of a prestressed beam before diagonal cracking. The K value is limited to a lower bound of 1, which represents where the stress in the extreme tension fiber due to the factored load and prestress exceeds $6\sqrt{f'_c}$, up to a value of 2 (Ramirez & Breen, 1991).

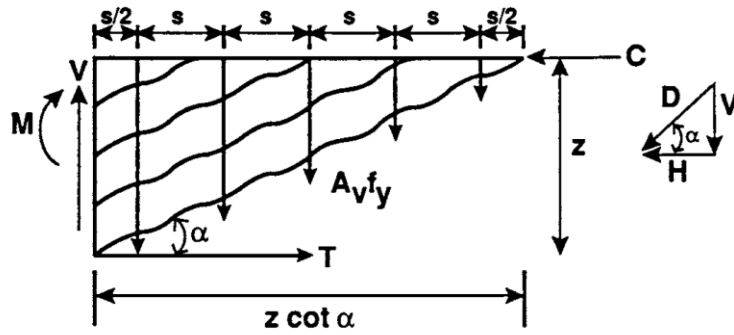


Figure 3-7 Modified section-truss approach behavioral model for beams(Julio A. Ramirez & Breen, 1991).

The nominal strength takes the familiar form:

$$V_n = V_s + V_c \quad (1)$$

$$V_c = K \frac{\sqrt{f_c}}{6} b_w 0.9d \quad (2)$$

$$K = \left[1 + \frac{f_{pc}}{f_t} \right]^{0.5} \quad (3)$$

$$V_s = A_v f_{yv} 0.9d \frac{\cot \theta}{s} \quad (4)$$

where:

- f_c = specified compressive strength of concrete
- b_w = web width or circular diameter
- f_{pc} = normal stress at neutral axis
- f_t = principal diagonal tension stress
- A_v = area of shear reinforcement within distance s
- f_{yv} = stirrup yield strength
- $0.9d$ = flexural lever arm or effective truss depth
- α = angle of incline struts
- s = stirrup spacing

3.1.2.2 Truss Model with Crack Friction

This model assumes forces are transferred across cracks by friction (Reineck, 1991). A free body diagram generated by separation along a crack in the B region of a concrete member with transverse reinforcement, shown in Figure 3-8. Equilibrium of the free body diagram is then used to create equations 5 and 6 The vertical component V_f , shown in Figure 3-8(b), is the combined friction forces, T_f and N_f . These friction forces are additive with the shear force carried by the stirrups. This is the case for all design methods that contain a concrete contribution term.

The crack inclination, β_{cr} , is assumed to be 45 degrees for non-prestressed concrete members but for prestressed members a flatter angle is typical. The angle of the principal compressive stress at the neutral axis of the uncracked section is typically assumed as the crack angle. (Loov & Patnaik, 1994)

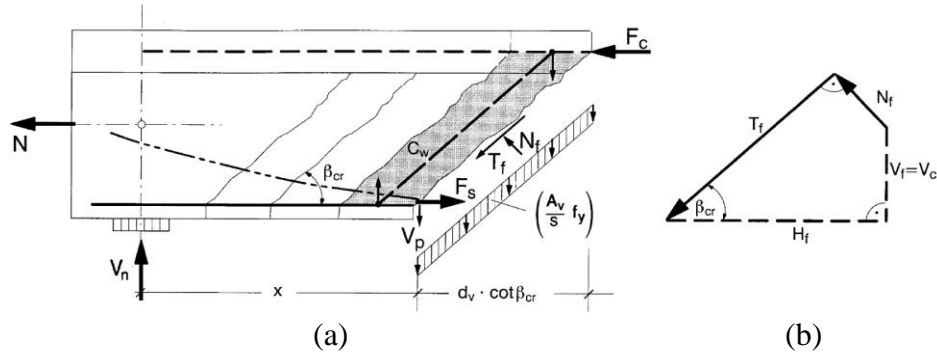


Figure 3-8 Free-body diagram at an end support for reinforced concrete member subjected to shear: (a) free-body diagram showing forces across a crack (b) forces due to friction (Reineck, 1991)

$$V_n = V_s + V_c + V_p \quad (5)$$

where:

V_n = nominal shear strength

V_s = shear force carried by the stirrups

V_c = sum of the vertical components of the tangential friction forces at the crack T_f , and the normal force at the crack N_f

V_p = vertical component of force in prestressing tendon

$$V_s = A_v f_y d_v \frac{\cot \beta_{cr}}{s} \quad (6)$$

where:

A_v = area of shear reinforcement within distance s

f_y = stirrup yield stress

d_v = lever arm

β_{cr} = crack inclination

s = stirrup spacing

3.1.2.3 Rotating Angle Softened Truss Model

A truss model developed by Pang & Hsu (1995) accounts for the tensile stresses in diagonally cracked concrete called the rotating angle softened truss model. The model assumes that the principal stress angle coincides with the principal strain angle for cracked concrete, shown in Figure 3-11.

As the shear stresses increase, this angle decreases but the creators of the model limit the model's applicability to angles between 33 degrees and 57 degrees, for angles outside this range,

a fixed angle should be used. (Pang & Hsu, 1995) The model can predict failure modes based on reinforcement ratios in the longitudinal and transverse directions, shown in Figure 3-9.

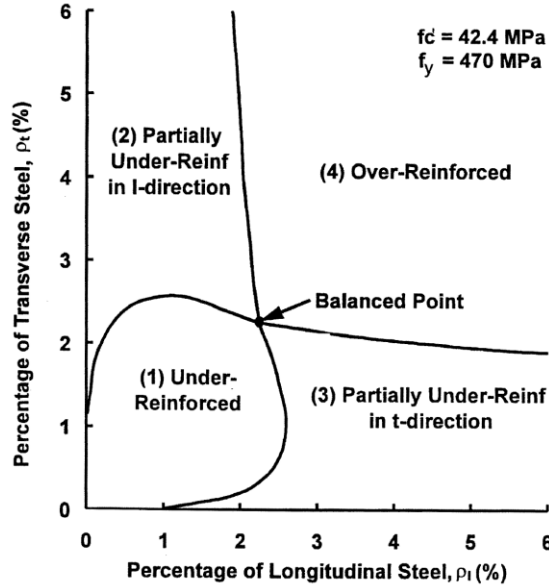


Figure 3-9 Failure modes predicted by rotating angle softened truss model for elements loaded in pure shear (Pang & Hsu, 1995).

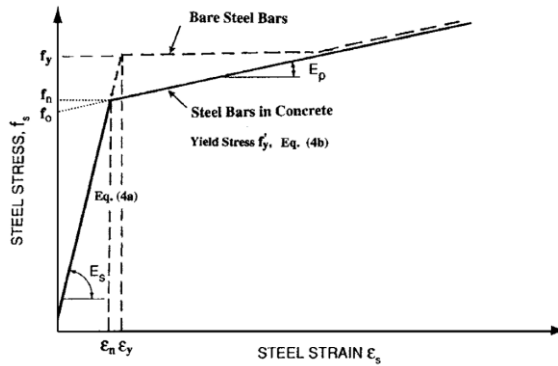


Figure 3-10 Average stress-strain curve for mild steel (Pang & Hsu, 1995).

Equilibrium equations in terms of average stresses, mild steel average stresses are shown in Figure 3-10 and equations 7 to 9 below, and compatibility equations in terms of average strains are used to develop the relationships shown below:

$$f_s = E_s \varepsilon_s \quad \text{if} \quad \varepsilon_s \leq \varepsilon_n \quad (7)$$

$$f_s = f_y \left[(0.91 - 2B) + (0.02 + 0.25B) \frac{E_s}{f_y} \varepsilon_s \right] \left[1 - \frac{2 - \alpha_2 / 45}{1000\rho} \right] \quad \text{if} \quad \varepsilon_s > \varepsilon_n \quad (8)$$

$$\varepsilon_n = \frac{f_y}{E_s} (0.93 - 2B) \left[1 - \frac{2 - \alpha_2/45}{1000\rho} \right] \quad (9)$$

$$B = \frac{\left(\frac{f_{cr}}{f_y}\right)^{1.5}}{\rho} \quad (10)$$

3.1.2.4 Fixed Angle Softened Truss Model

The rotating angle softened truss model assumed that the angle of the compressive struts rotates with the post cracking principal compressive stresses. This meant there were no shear stresses along the crack which meant the model did not account for the concrete contribution to shear strength. As a result, the fixed angle softened truss model was developed to predict the concrete contribution to shear strength. This model assumes the concrete strut remains parallel to the initial crack orientation. The initial orientation is dependent on the direction of the principal stress just before cracking, shown in Figure 3-11. (Pang & Hsu, 1996) Equilibrium and compatibility is then used to develop an expression, based on constitutive properties shown in Figure 3-12, for the shear yield strength of concrete, shown in equation 11, where the first term is the concrete contribution, V_c , and the second term is the shear reinforcement contribution, V_s .

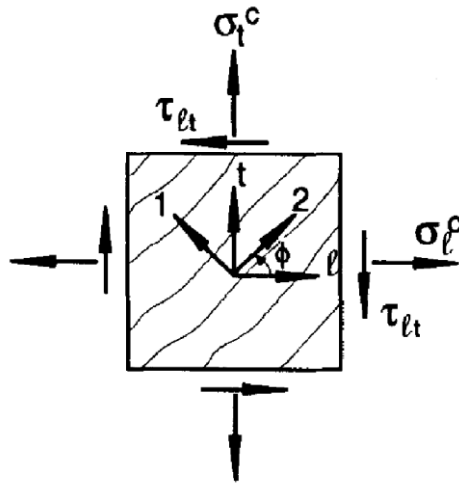


Figure 3-11 Cracked element model for fixed-angle truss model. (Pang & Hsu, 1996)

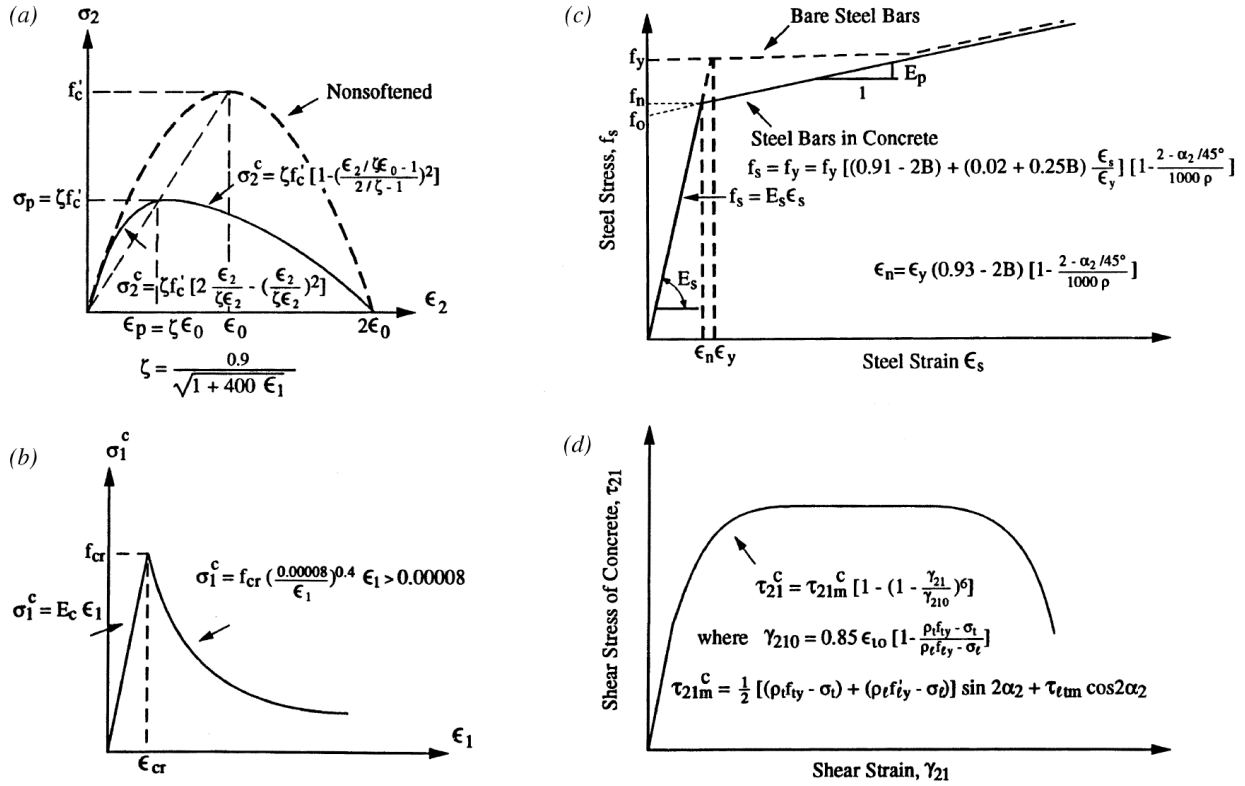


Figure 3-12 Constitutive properties used in fixed angle model: (a) compressive stress-strain curve concrete (b) average tensile stress-strain curve for concrete (c) average stress-strain curve mild steel (d) average stress-strain curve for concrete in shear (Ramirez & Dilger, 2000).

$$\tau_{lt} = \frac{(\tau_{21}^c)^2}{2\sqrt{\rho_l f_{ly} \rho_t f_{ty}}} + \sqrt{\rho_l f_{ly} \rho_t f_{ty}} \quad (11)$$

where:

τ_{lt} = shear yield strength

τ_{21}^c = average shear stress in the 2-1 direction

ρ_l = steel reinforcement ratio in the longitudinal direction

ρ_t = steel reinforcement ratio in the transverse direction

f_{ly} = mild steel yield stress in the longitudinal direction

f_{ty} = mild steel yield stress in the transverse direction

3.1.3 Compression Field Approach

The compression field approach was developed based on the tension field theory derived by Wagner (1929) for steel plate girders. The tension field theory uses deformations within the system to determine the angle of inclination of the tensile stresses which is assumed to be the same as the angle of inclination for the principal tensile strains.

Procedures using the relationship that determines the angle of inclination, θ , by considering deformations in the transverse and longitudinal reinforcements along with the diagonally stressed concrete became known as compression field approaches. Using the

relationships shown in Figure 3-13 load-deformation can be predicted for a section subjected to shear.

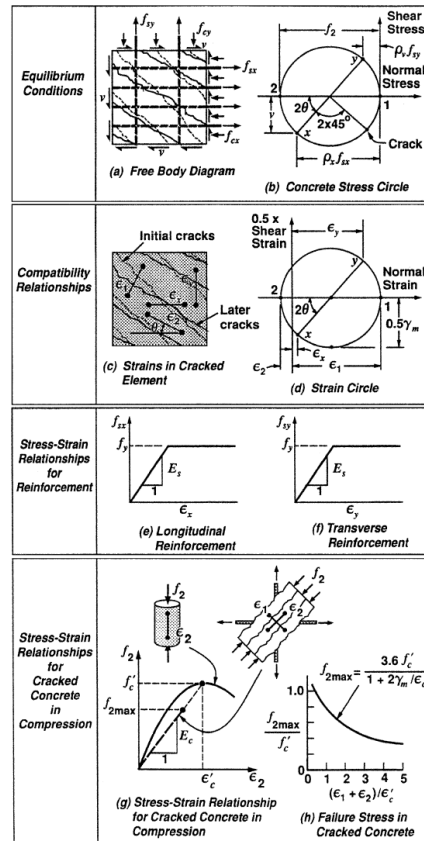


Figure 3-13 Summarized compression field theory (Ramirez & Dilger, 2000).

3.1.3.1 Compression Field Theory

Procedures were developed for determining the angle of inclination (Mitchell & Collins, 1974), θ , for members loaded in torsion which further developed to apply for members loaded in shear, which became known as compression field theory (CFT) (Ramirez & Dilger, 2000). Applied shear stresses to cracked reinforced concrete causes tensile stresses to develop in the transverse and longitudinal reinforcement and causes compressive stresses in the concrete. This theory assumes once concrete cracks no tension can develop. Using equilibrium conditions shown in Figure 3-13 gives the following relationships for the applied shear stress and the concrete and reinforcement stresses:

$$\rho_v f_{sy} = f_{cy} = v \tan \theta \quad (12)$$

$$\rho_x f_{sx} = f_{cx} = v \cot \theta \quad (13)$$

$$f_2 = v(\tan \theta + \cot \theta) \quad (14)$$

where:

ρ_v = steel reinforcement ratio in the transverse direction

- ρ_x = steel reinforcement ratio in the longitudinal direction
- f_2 = compressive stress in cracked concrete
- θ = compressive stress, f_2 , angle with respect to longitudinal axis
- f_{sx} = tensile stress in longitudinal reinforcement
- f_{sy} = tensile stress in transverse reinforcement
- v = applied shear stress

3.1.3.2 Modified Compression Field Theory

The modified compression field theory, also known as MCFT, was developed from the previously discussed compression field theory. This theory has been used to develop the current general design procedure for shear design in AASHTO LRFD. The major difference between the two theories are that MCFT considers tensile stresses in the concrete and uses experimentally verified stress-average strain relationships. (Vecchio & Collins, 1986) A small membrane element is considered for the definition of the problem, shown in Figure 3-14, with the following fundamental assumptions:

- For each strain state there exists only one corresponding stress state, loading history will not be considered
- Stresses and strains will be averaged over areas or distances large enough to include several cracks
- Reinforcing bars will be perfectly bonded at the boundaries of the elements, i.e., no slip.
- Longitudinal and transverse reinforcing bars are uniformly distributed over the element

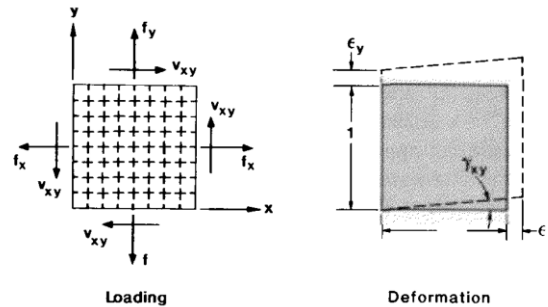


Figure 3-14 Membrane element. (Vecchio & Collins, 1986)

MCFT has proven suitable for predicting the response of beams loaded in shear, flexure, and axial loads. The model considers compatibility, equilibrium and the material stress-strain relationships to solve for principal stresses and angles with consideration given to local stress conditions at crack locations, the theory is summarized in Figure 3-15. (Vecchio & Collins, 1986)

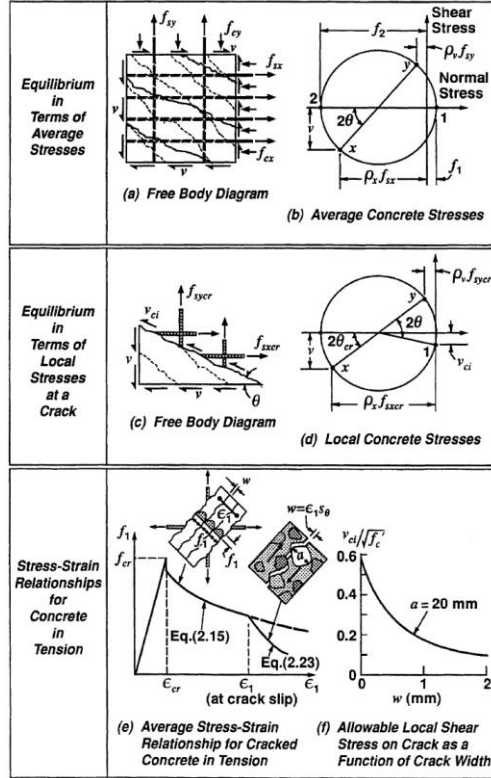


Figure 3-15 Summarized MCFT for cracked elements (Ramirez & Dilger, 2000).

$$\rho_v f_{sy} = f_{cy} = v \tan \theta - f_1 \quad (15)$$

$$\rho_x f_{sx} = f_{cx} = v \cot \theta - f_1 \quad (16)$$

$$f_2 = v(\tan \theta + \cot \theta) - f_1 \quad (17)$$

where:

ρ_v = steel reinforcement ratio in the transverse direction

ρ_x = steel reinforcement ratio in the longitudinal direction

f_2 = compressive stress in cracked concrete

θ = compressive stress, f_2 , angle with respect to longitudinal axis

f_{sx} = tensile stress in longitudinal reinforcement

f_{sy} = tensile stress in transverse reinforcement

v = applied shear stress

f_1 = principal tensile stress in concrete

3.2 Current Shear Design Specifications

U.S. and European shear design codes have incorporated behavioral models to determine service level behavior and nominal strengths. The following section explores how design codes have incorporated behavioral models.

3.2.1 U.S. Design Specifications

3.2.1.1 ACI 318-19

ACI 318 calculates the nominal shear strength for prestressed sections as $V_n = V_s + V_c$, similarly to other design codes. The concrete contribution, V_c , uses the modified truss approach described in section 3.1.2 while the steel contribution, V_s , is calculated using a similar approach as the truss model with crack friction with a crack angle of 45 degrees. The presence of post-tensioned ducts is not directly addressed. (ACI Committee 318, 2019)

$$V_c = \min \left(\frac{V_{ci}}{V_{cw}} \right) \quad (18)$$

$$V_{ci} = \max \left(\begin{array}{c} 0.6\lambda \sqrt{f_c} b_w d_p + V_d + \frac{V_i M_{cre}}{M_{max}} \\ 1.7\lambda \sqrt{f_c} b_w d \end{array} \right) \quad (19)$$

$$M_{cre} = \left(\frac{1}{y_t} \right) (6\lambda \sqrt{f_c} + f_{pe} - f_d) \quad (20)$$

$$V_{cw} = (3.5\lambda \sqrt{f_c} + 0.3f_{pc}) b_w d_p + V_p \quad (21)$$

$$V_s = \frac{A_v f_{yt} d}{s} \quad (22)$$

3.2.1.2 AASHTO LRFD (9th) Edition General Shear Procedure

The nominal shear strength V_n according to AASHTO LRFD, 9th Edition (2020) is calculated as the lesser of $V_n = V_s + V_c + V_p$ or $V_n = 0.25f_c b_v d_v + V_p$ using the following equations:

$$V_n = \min \left(\begin{array}{c} 0.0316\beta\lambda \sqrt{f_c} b_v d_v + \frac{A_v f_y d_v (\cot\theta + \cot\alpha) \sin\alpha}{s} \lambda_{duct} + V_p \\ 0.25f_c b_v d_v + V_p \end{array} \right) \quad (23)$$

$$\lambda_{duct} = 1 - \delta \left(\frac{\phi_{duct}}{b_w} \right)^2 \quad (24)$$

This approach uses separate calculations for the concrete contribution, steel contribution, and the vertical component of prestressing, if any, to the overall shear capacity of a particular section. For ungrouted ducts, the presence of PT ducts is addressed by subtracting the duct diameter from the gross web width, b_w , to obtain an effective web width, b_v . For grouted ducts the transverse reinforcement contribution, V_s , is modified by a shear strength reduction factor, λ_{duct} , to account for the presence of PT ducts; this factor is a function of the duct diameter ϕ_{duct} , gross web width b_w , and duct diameter correction factor, which is taken as 2.0 for grouted

ducts. The duct diameter correction factor is taken as 1.0 for ungrouted ducts. Although not specified directly, it is assumed that ducts containing flexible filler are classified as ungrouted.

3.2.1.3 AASHTO LRFD (9th) Edition Alternative Shear Design Procedure for Segmental Girders

The alternative shear design procedure is based on research done by Breen and Ramirez (1991). The alternative design procedure removes the unnecessary conservatism found when using the general design procedure for calculating the nominal shear capacity. The steel contribution is based on the 45 degree truss model and does not follow the variable angle described in the research done by Breen and Ramirez (1991). The nominal shear strength V_n is to be determined as the lesser of the following:

$$V_n = V_c + V_s \quad (25)$$

$$V_n = 0.379 \lambda \sqrt{f'_c} b_v d \quad (26)$$

where:

$$V_c = 0.0632K \lambda \sqrt{f'_c} b_v d \quad (27)$$

$$V_s = \frac{A_v f_{yt} d}{s} \quad (28)$$

$$K = \sqrt{1 + \frac{f_{pc}}{0.0632 \lambda \sqrt{f'_c}}} \leq 2.0 \quad (29)$$

where:

b_v = steel reinforcement ratio in the transverse direction

d = steel reinforcement ratio in the longitudinal direction

f'_c = compressive stress in cracked concrete

f_{pc} = compressive stress, f_2 , angle with respect to longitudinal axis

s = tensile stress in longitudinal reinforcement

A_v = tensile stress in transverse reinforcement

λ = applied shear stress

3.2.2 International Design Specifications

3.2.2.1 Australian Standard 2017

The Australian concrete code calculates the nominal shear strength of a prestressed beam subjected to shear force, bending moment, and axial force based on a truss analogy. The code uses the sum of the concrete contribution, V_{uc} , and the shear reinforcement contribution, V_{us} , to determine the shear strength. The angle, θ_v , between the concrete strut and longitudinal axis is conservatively 45 degrees or varies from 30 degrees to 45 degrees. Grouted tendons are accounted for by using an effective web width which is determined by subtracting the summation of half the duct diameter at the horizontal level across the web from the web width. UngROUTED tendons are not considered in this code (Australia, 2017).

$$V_u = \min \left(\begin{array}{l} 0.2f_c' b_v d_o + P_v \\ \beta_1 \beta_2 \beta_3 b_v d_o \left[\frac{(A_{st} + A_{pt}) f_c'}{b_v d_o} \right]^{\frac{1}{3}} + V_o + P_v + \frac{A_v f_y d_v \cot \theta_v}{s} \end{array} \right) \quad (30)$$

3.2.2.2 JSCE No. 15 2007

JSCE No. 15 developed its procedure to calculate nominal shear strength using the truss analogy. The shear strength is calculated by adding the concrete contribution, V_{cd} , the shear reinforcement contribution, V_{sd} , and the vertical component of the prestressing force, V_{ped} . The presence of PT ducts is addressed by reducing the gross web width, b , to an effective web width, b_r . The web width is reduced by subtracting half the diameter of the duct for grouted tendons and 1.2 times the diameter of the duct for ungrouted tendons from the gross web width. (Uomoto et al., 2008)

$$V_{yd} = V_{cd} + V_{sd} + V_{ped} \quad (31)$$

$$V_{cd} = \beta_d \beta_p \beta_n f_{vcd} b_w \frac{d}{\gamma_b} \quad (32)$$

$$V_{sd} = \left[\frac{A_w f_{wyd} (\sin \alpha_s + \cos \alpha_s)}{S_s} + \frac{A_{pw} \sigma_{pw} (\sin \alpha_p + \cos \alpha_p)}{S_p} \right] \frac{z}{\gamma_b} \quad (33)$$

$$V_{ped} = P_{ed} \sin \frac{\alpha_p}{\gamma_b} \quad (34)$$

3.2.2.3 Eurocode 2 (2014)

A truss analogy is used to develop the nominal shear strength, (V_{rd}), equations for Eurocode 2. The presence of PT ducts is addressed by reducing the gross web width, b_w , to an effective web width, $b_{w,nom}$. For grouted ducts with duct diameter larger than one-sixth the web width, half of the duct diameter is subtracted from the web. No reduction is applied for grouted ducts with duct diameter smaller than one-sixth of the web width. For ungrouted ducts, the web width is reduced by subtracting 1.2 times the diameter of the duct from the gross web width. (Narayanan, 2014) For members with vertical shear reinforcement the shear strength is calculated as:

$$V_{rd} = \min \left(\frac{A_{sw} f_{ywd} z \cot \theta}{s} \right) \frac{s}{\alpha_{cw} b_w z v_1 f_{cd}} \quad (35)$$

$$\frac{1}{(\cot \theta + \tan \theta)}$$

3.2.2.4 FIB 2010

A truss analogy is used to develop the nominal shear strength, V_{Rd} , equations for FIB 2010. The code uses the sum of the concrete contribution, $V_{Rd,c}$, and the shear reinforcement contribution, $V_{Rd,s}$, to determine the shear strength. The presence of PT ducts is addressed by reducing the gross web width, b_w , to an effective web width, $b_{w,nom}$. For metal grouted ducts half of the duct diameter is subtracted from the web and for grouted plastic ducts 0.8 times the duct diameter is subtracted. For ungrouted ducts the web width is reduced by subtracting 1.2 times the diameter of the duct from the gross web width. (Fib, 2013)

3.2.3 Shear Design Using Effective Web Width

Shear design specifications generally address the presence of PT ducts by reducing the actual web thickness to an effective web width (Figure 3-16) that is used when calculating the concrete contribution. This is done by subtracting the actual web width by the product of the duct diameter and the diameter correction factor, shown in equation 36. The effective web width is used in the shear design calculations as a substitute for the actual web width.

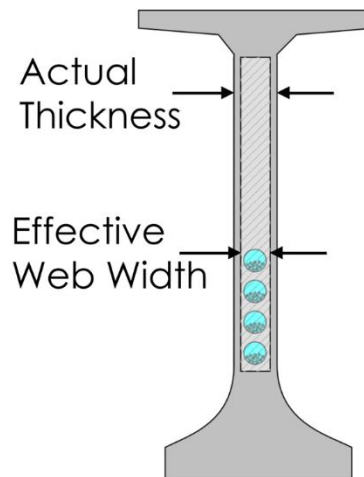


Figure 3-16 Effective web width for shear calculations.

$$b_{eff} = b_w - k \cdot \sum \phi \quad (36)$$

where:

b_{eff} = effective web width

b_w = web width

k = "diameter correction factor"

ϕ = duct diameter

The diameter correction factor, k , varies among the design codes for the same variables (Table 3-1). This k factor varies in codes based on the filler material, grouted or ungrouted, and the duct material, steel, or plastic. The k factor is not addressed in ACI 318.

Table 3-1 Table showing k factor for various codes.

Design Code	Section	Grouted Steel Duct	Ungouted Steel Duct	Grouted Plastic Duct	Ungouted Plastic Duct
AASHTO General Shear	5.7.3.3	0	1	0.5	1
AASHTO Segmental Shear	5.12.5.3.8	0	1	0.5	1
Australian Standard 2017	8.2.6	0.5	Not addressed	0.5	Not addressed
JSCE No. 15 2007	3.4-(1)	0.5	1.2	0.5	1.2
Eurocode 2 (2014)	6.2.3-6	0.5	1.2	1.2	1.2
FIB 2010	7.3-15	0.5	1.2	0.8	1.2

3.3 Panel Testing

Extensive panel tests have been conducted beginning in the 1960s that investigate the effect of introducing ducts into concrete sections. Panel tests have been found to be economical and allowed researchers to conduct numerous tests on multiple variables. Results of these tests were used to determine the factors that have a significant effect on shear strength for actual bridge girders.

3.3.1 Muttoni et al. (2006)

Muttoni investigated the effect that introducing a duct into the web of a concrete girder has on its shear strength (Muttoni, Burdet, & Hars, 2006). Previous panel tests that showed ducts introduced into the web of a concrete girder reduces its shear strength, which makes locations of high shear a primary concern. Ducts were not expected to have a significant effect on flexural or axial strength.

The presence of a duct causes the compressive stress field to deviate around or through the duct depending on the stiffness of the filler material (Figure 3-17). Ungouted duct stress fields deviate around the void causing transverse tensile stresses to develop just above and below the void location. Conversely stiff filler material causes the compressive stress field to deviate towards the duct causing larger tensile stresses to develop at a location farther away from the duct.

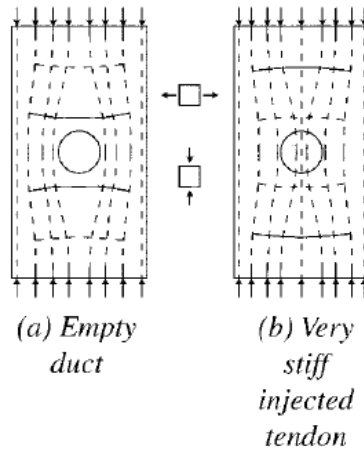


Figure 3-17 Compressive stress flow in panels under compressive force (Muttoni et al., 2006).

Twelve specimens were cast in the laboratory and four precracked panels were extracted from a bridge built in 1967. Figure 3-18 shows a comparison of test results with expected values from design codes AASHTO, EUROCODE 2, CEB and BS 5400 (Muttoni et al., 2006). A correction factor, k , based on duct type, ungrouted vs. steel or plastic, is used to adjust the width of the web to account for the reduction in shear.

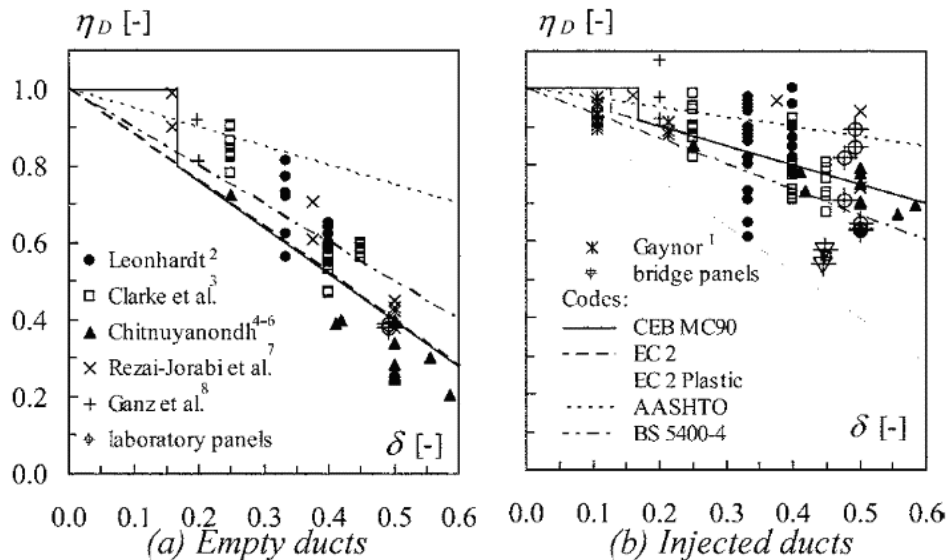


Figure 3-18 Panel test results for empty and filled ducts compared to design code. (Muttoni et al., 2006)

The results showed that panels with HDPE plastic ducts experienced a 40% strength loss while the panels with steel ducts experienced a 15% strength loss. Precracked panels from an actual bridge experienced a 44% loss in strength, which was attributed to cracked concrete. A summary of the panel tests conducted by Muttoni et. al. is shown below is shown in Figure 3-19.

Table 3-2 Table showing panel test results(Muttoni et al., 2006).

Specimen	First series, laboratory panels												Second series, bridge panels			
	W1	W2	W3	W4	W5	W6	W7	W8	W9	W10	W11	W12	W21	W22	W23	W24
	HDPE		None		Steel		Steel		HDPE		Steel 1967		Steel 1967		None	
Duct	Injected		—		Injected		Empty		Injected		Injected		Injected		—	
\varnothing_D , in. (mm)	2.48 (63)	2.48 (63)	0 (0)	0 (0)	2.44 (62)	2.44 (62)	2.44 (62)	2.44 (62)	2.48 (63)	2.48 (63)	2.36 (60)	2.36 (60)	2.36 (60)	2.36 (60)	0 (0)	0 (0)
δ	0.50	0.50	0	0	0.50	0.50	0.50	0.50	0.50	0.50	0.48	0.48	0.45	0.45	0	0
Injected	Yes	Yes	—	—	Yes	Yes	No	No	Yes	Yes	Yes	Yes	Yes	Yes	—	—
f'_c , psi (MPa)	5278 (36.4)	5452 (37.6)	5250 (36.2)	5415 (37.3)	5076 (35)	5154 (35.5)	5352 (36.9)	5116 (35.3)	5434 (37.5)	5304 (36.6)	4984 (34.4)	5329 (36.7)	7818 (53.9)	6846 (47.2)	6962 (48)	6846 (47.2)
t , days	22	30	21	28	16	18	25	17	29	23	14	24 years	36 years	36 years	36 years	36 years
β , degrees	0	0	—	—	0	0	0	0	34	34	0	0	52	50	—	—
N_R , kips (kN)	386 (1718)	396 (1763)	607 (2700)	627 (2790)	501 (2228)	538 (2393)	248 (1103)	228 (1013)	389 (1733)	388 (1725)	413 (1838)	508 (2258)	464 (2066)	433 (1924)	719 (3200)	736 (3276)
N_{R_s} , kips (kN)	29 (129)	31 (139)	46 (203)	45 (202)	42 (187)	46 (205)	27 (91)	21 (120)	22 (100)	23 (100)	36 (161)	41 (181)	0 (0)	0 (0)	23 (102)	21 (94)
N_{R_c} , kips (kN)	357 (1589)	365 (1624)	561 (2497)	582 (2588)	459 (2040)	492 (2188)	221 (982)	207 (921)	367 (1633)	365 (1625)	377 (1677)	467 (2076)	464 (2066)	433 (1924)	696 (3098)	715 (3182)
$\frac{N_{R_c}}{b_w \cdot c}$, psi (MPa)	3072 (21.2)	3140 (21.6)	4829 (33.3)	5005 (34.5)	3946 (27.2)	4231 (29.2)	1900 (13.1)	1781 (12.3)	3158 (21.8)	3142 (21.7)	3242 (22.4)	4015 (27.7)	3720 (25.6)	3479 (24)	6117 (42.2)	6153 (42.4)
$\frac{N_{R_c}}{b_w \cdot c \cdot f'_c}$	0.58	0.58	0.92	0.92	0.78	0.82	0.35	0.35	0.58	0.59	0.65	0.75	0.48	0.51	0.88	0.90
η_D	0.63	0.62	1.00	1.00	0.84	0.89	0.38	0.38	0.63	0.64	0.71	0.82	0.54	0.57	0.99	1.01

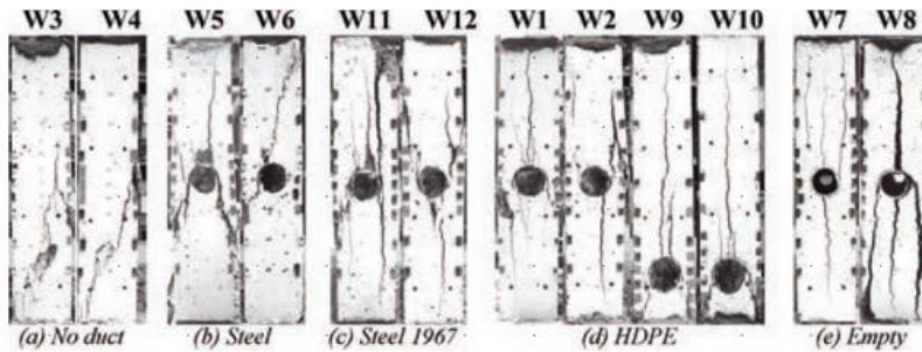


Figure 3-19 Panel failure after shear testing(Muttoni et al., 2006).

3.3.2 Wald (2012)

Wald (2012) investigated the effect of different variables on the shear strength of concrete panels. The purpose of the research was to investigate the portion of I-girder sections containing a duct subjected to a compressive force and determine the reduction in strength due to the presence of this duct. The results were used to modify existing code and determine an appropriate reduction factor to find the shear strength of members with post-tensioning ducts.

One hundred panels were fabricated for testing; 76 panels contained at least one post-tensioning duct while 24 panels had no ducts. All the panels were 24 in. x 24 in. with varying thicknesses. Nine 5-in., eighty-one 7-in. and ten 9-in. panels were constructed for testing. The primary parameters for the panel tests are shown below in Figure 3-20. The strength reduction (η_b) caused by varying these parameters were investigated.

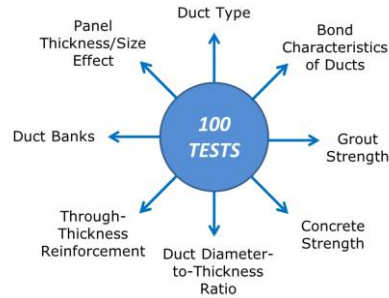


Figure 3-20 Panel testing parameters (Wald, 2012)

Generally, panels failed when a splitting crack formed parallel to the face of the specimen (Figure 3-21). In addition to the splitting failure, the specimens with plastic duct were noted to have debonded. Specimens with plastic ducts also had a lower crushing strength when compared to those with steel ducts (Figure 3-24). The researcher attributed the reduced strength to the poor bond between the concrete and smooth plastic duct surface. A short investigation was conducted to improve bond strength, but none of the trial methods provided a significant increase in bond strength.

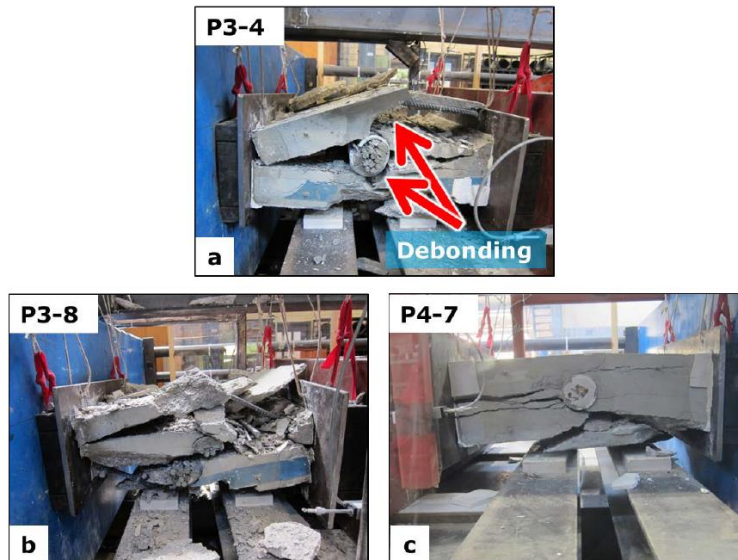


Figure 3-21 Typical failure modes of panels (Wald, 2012).

Duct diameter-to-thickness ratio was found to have a significant effect on the crushing strength of the panels. This is attributed to the increased deviation angle (Figure 3-22) of the compressive stress field leading to increased tensile stresses in the concrete.

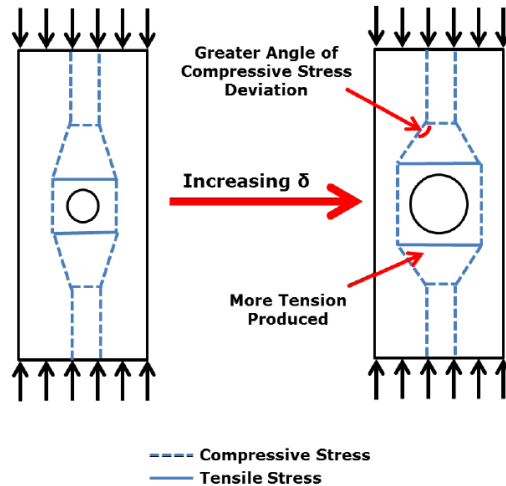


Figure 3-22 Compressive stress flow for various duct-diameter-to-thickness ratios (Wald, 2012).

Shear strength tests were done varying duct-diameter-to-thickness ratios for seven panels, which showed an increase duct-diameter-to-thickness ratio caused a drop in shear strength (Table 3-3).

Table 3-3 Panel testing results of varying δ (Wald, 2012).

Specimen	f_{concrete} (ksi)	f_{grout} (ksi)	Φ (in.)	Nominal δ	Measured δ	η_D
P7-8	10.6	4.9	2.375	0.34	0.37	0.43
P3-3	9.4	5.3	3	0.43	0.43	0.37
P3-4	9.4	5.3	3	0.43	0.43	0.36
P3-6	9.4	5.3	3	0.43	0.43	0.35
P4-5	8.2	4.7	3	0.43	0.42	0.39
P9-3	10.2	6.3	3	0.43	0.43	0.35
P8-3	11.2	6.0	3.375	0.48	0.48	0.28

The results were plotted and compared to previous panel testing results which also showed a trend of decreasing shear strength with increased duct-diameter-to-thickness ratio (Figure 3-27).

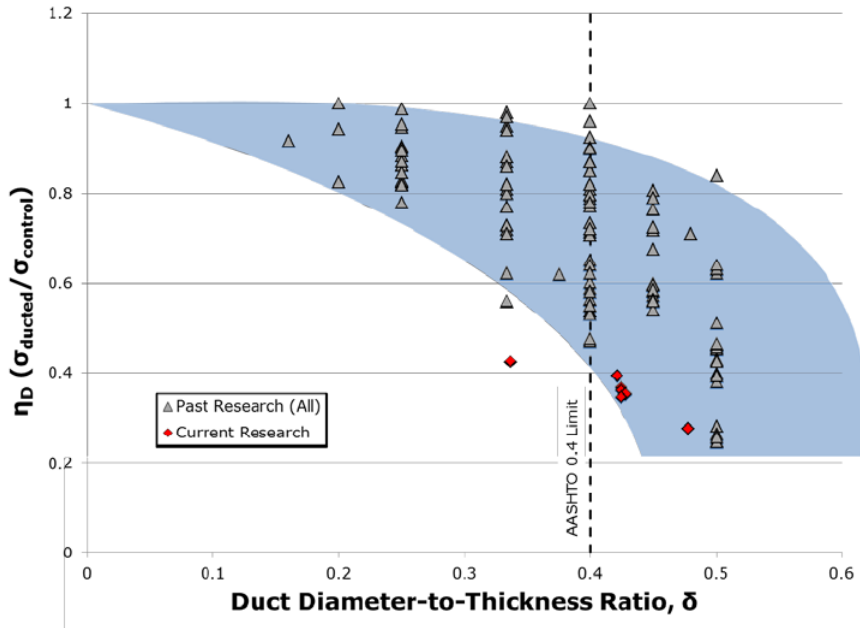


Figure 3-23 Plot of panel research showing η_D vs. δ (Wald, 2012).

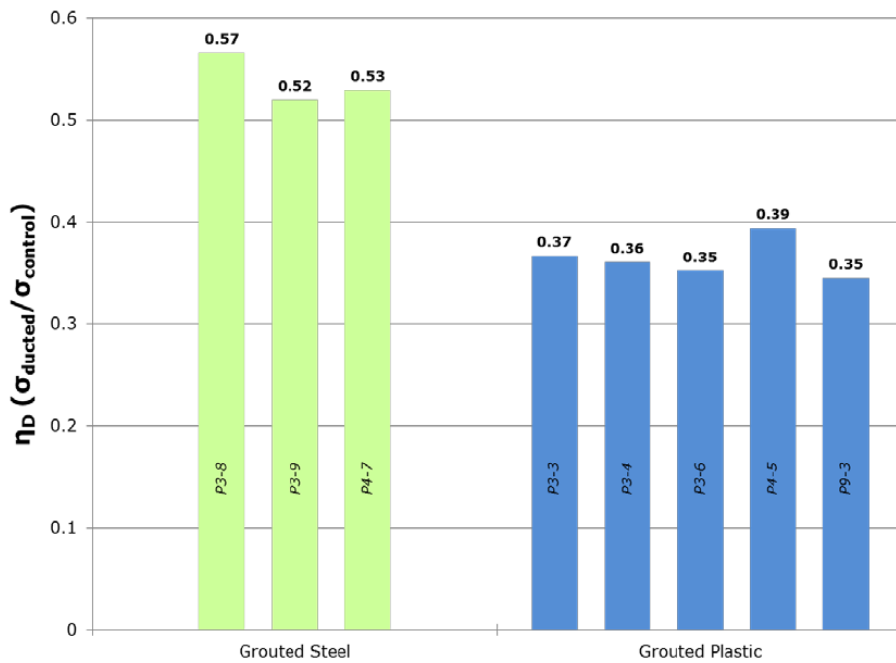


Figure 3-24 Steel duct and plastic duct strength comparison results (Wald, 2012).

The effect of having grouted ducts vs. non-grouted ducts was also investigated and grouted ducts were found to have higher strength compared to non-grouted ducts (Figure 3-25).

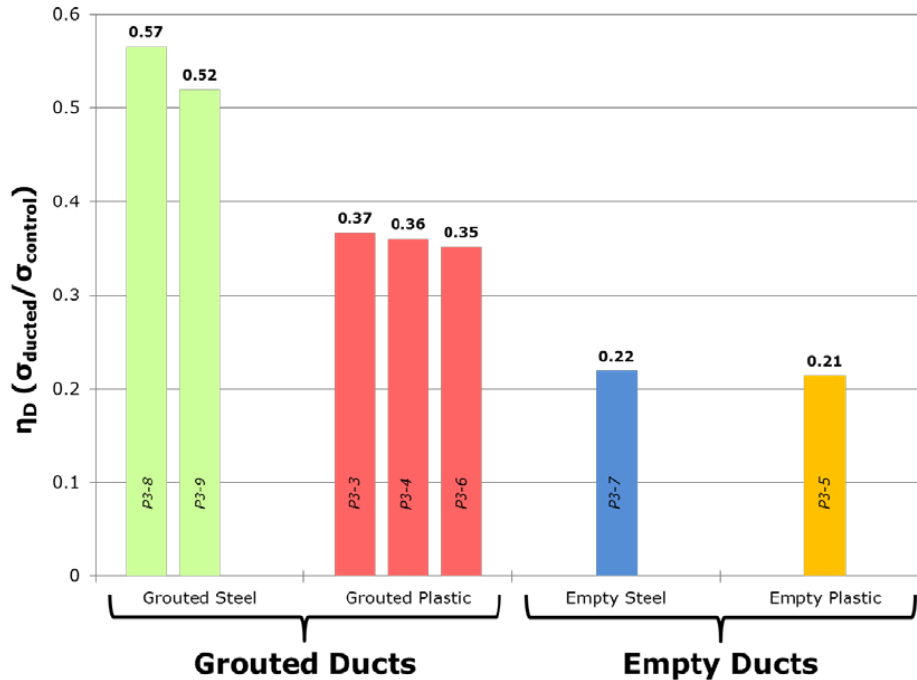


Figure 3-25 Grouted ducts vs. ungrouted ducts strength comparison results (Wald, 2012).

Through-thickness reinforcement has been found to be beneficial in improving the shear strength of panels with ducts (Figure 3-26). The researcher recommends the use of through-thickness reinforcement around the duct and tied at every other vertical mild reinforcement. The amount and location of the through-thickness reinforcement had a more significant effect on shear strength than the shape of the through thickness reinforcement. The researcher suggests using simpler through thickness reinforcement shapes at discrete locations instead of complicated shapes that may slow specimen fabrication.

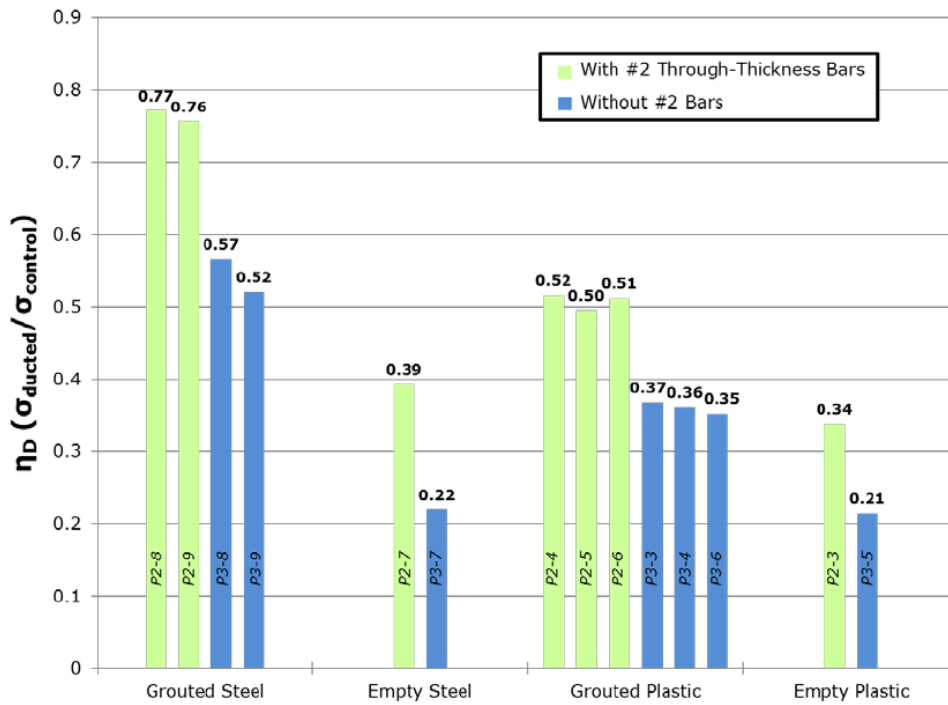


Figure 3-26 Effect of through thickness reinforcement on shear strength (Wald, 2012).

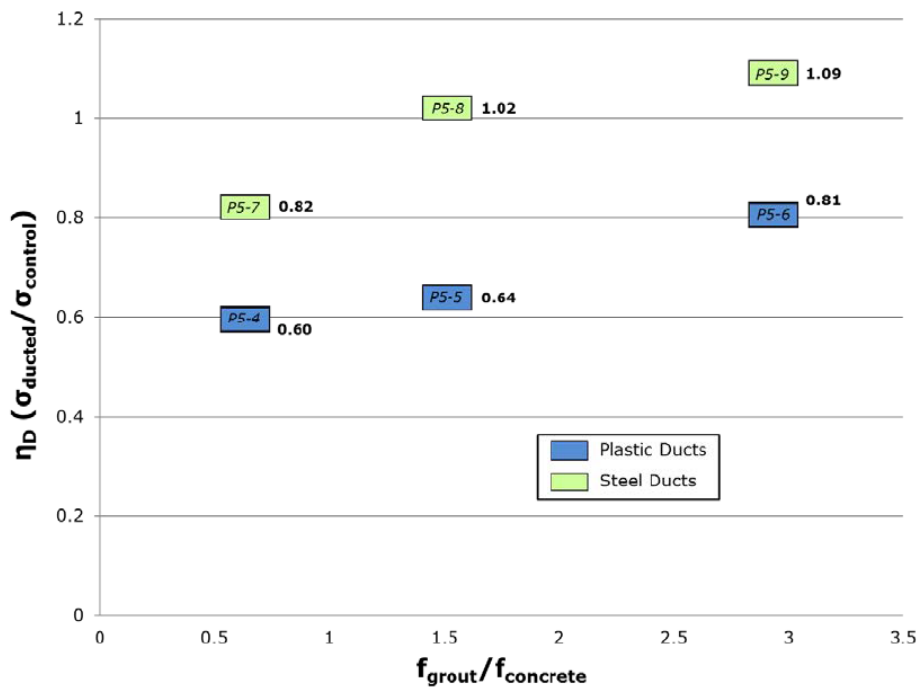


Figure 3-27 Results from varying grout-concrete strength ratio (Wald, 2012).

The effect of grout compressive strength on shear panel strength was investigated by varying grout strength relative to concrete strength. Higher grout-to-concrete strength ratios resulted in a significant rise in shear strength for panels with steel ducts while panels with plastic ducts had a less significant increase in strength for increasing grout-to-concrete ratios. Plastic ducts experienced debonding during testing at the failure load, which was thought to be cause of the reduced strength. Steel ducts remained well-bonded during all testing, which led to a larger increase in strength at higher grout-to-concrete strength ratios.

An increase in concrete compressive strength resulted in an apparent greater reduction in shear capacity (Figure 3-28). The primary failure mode of panels with PT duct was a “splitting” failure, which depended primarily on tensile strength of the panel, while panels without ducts failed primary by crushing, which depends primarily on the compressive strength of the panel. The tensile strength of concrete increases by the square root of the compressive strength, which leads to little benefit to preventing the “splitting” failure for large increases in concrete strength. Thus, the shear strength of panels without ducts increases significantly compared to panels with PT ducts for increasing concrete compressive strength.

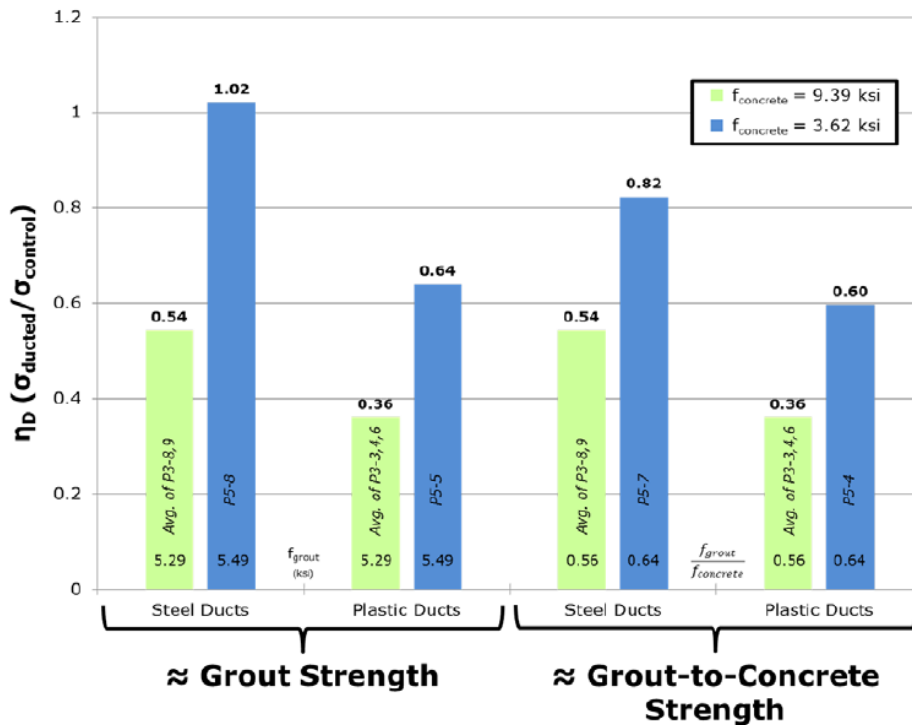


Figure 3-28 Results from varying grout-concrete strength ratio (Wald, 2012).

Panel tests had as much as 60% reduction in strength for panels with PT ducts when compared to solid panels. Wald (2012) indicated that they did not expect the panel tests to simulate the behavior of actual girders with PT ducts. Furthermore, they indicated that although some of the test variables had considerable effect on panel strength, these same variables were not expected to have as much influence on the behavior of full-scale girders. For example, Wald (2012) indicated that through-thickness reinforcement is not expected to have much of an effect on full-scale girders due to the presence of stirrups and the restraint created by the flanges.

For future full-scale testing the researcher has suggested a few major variables be investigated such as:

- Filler type
- Duct type
- Duct diameter-to-thickness ratio
- Web thickness
- Through-thickness reinforcement, suggested by the researcher to be substituted for girders in full-scale tests.

3.4 Full-Scale Testing

Little data is currently available on the shear strength of I-girder webs containing PT tendons, particularly those with ungrouted ducts. Although numerous panel tests with PT ducts have been done to economically investigate the sensitivity of shear strength to different variables, these tests do not capture the entirety of full-scale girder behavior due to missing conditions such as transverse tension and horizontal shearing. (Williams et al., 2015)

3.4.1 Felan (2013)

Felan (2013) built upon the research done by Wald (2012) by investigating the shear strength of two 30-ft long by 46-in. deep bulb-tee girders, one with a plastic duct in the web and the other without a duct in the web. Two prestressing strands stressed to 1 kip were used to support the plastic duct during construction, but the specimen was not post-tensioned. These girders were simply supported with two elastomeric bearing pads and load was applied at the center of the span until failure.

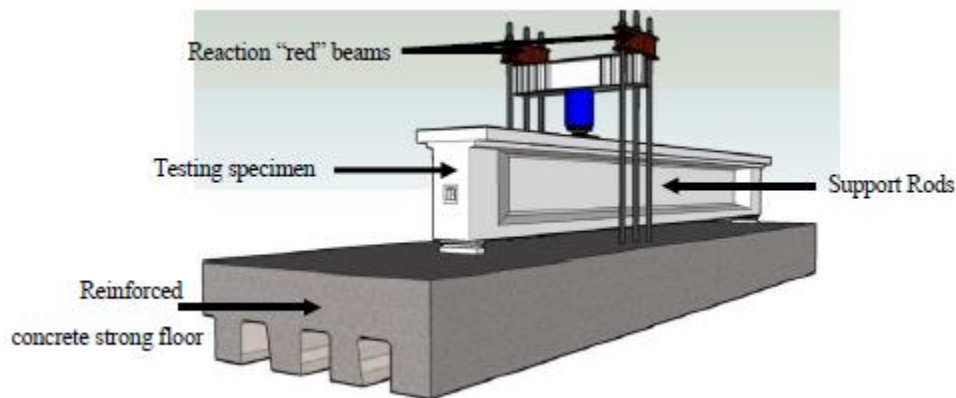


Figure 3-29 Typical test setup (Felan, 2013).

The control girder experienced a shear induced anchorage failure at 533 kip, where the AASHTO LRFD method predicted a shear failure at 525 kip. The girder with the plastic duct experienced a web crushing failure at a load of 465 kip, using the AASHTO 2012 General Shear method a k-factor of 0.25 predicted a failure of 515 kip. To more accurately predict the web crushing failure load observed using AASHTO 2012 General Shear method, a k-factor of one would be required, which gives a failure load of 460 kip.

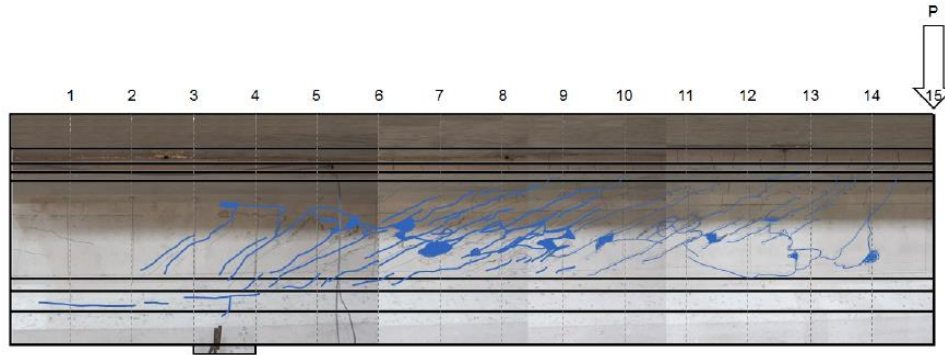


Figure 3-30 Girder with plastic duct after failure (Felan, 2013).

The testing of a full-scale girder showed that the panel test was not an accurate predictor of full-scale shear strength reduction. A panel with similar variables (Wald, 2012) experienced approximately 60% strength losses while the full-scale test experienced a 13% loss, a significant difference from panel testing.

Test specimens for future research were recommended to be full-scale girders rather than panels to ensure that the results are valid. Another recommended variable by the researcher was introducing the post-tensioned force of the duct, which may influence the shear strength.

Table 3-4 Comparison of panel and girder with plastic duct strength test results (Wald, 2012).

Specimen	f_{concrete} [ksi]	f_{grout} [ksi]	[in.]	Nominal δ	η_D
P7-8	10.62	4.86	2.375	0.339	0.43
P3-3	9.39	5.29	3	0.429	0.37
P3-4	9.39	5.29	3	0.429	0.36
P3-6	9.39	5.29	3	0.429	0.35
P4-5	8.17	4.66	3	0.429	0.39
P9-3	10.19	6.25	3	0.429	0.35
P8-3	11.16	5.98	3.375	0.482	0.28
Tx46 w/ plastic duct	9.70	8.60	3	0.429	0.86

3.4.2 Shear Behavior of Spliced Post-Tensioned Girders (Moore et al. 2015)

Moore et al. (2015) conducted eleven shear tests on seven 50-ft long by 62-in. deep bulb-tee girders in an effort to evaluate their strength and serviceability. Specimens containing ducts were post-tensioned to a nominal force of 527 kips. Also, a PT Evaluation Database, containing 34 shear tests, was developed to isolate shear tests that would be directly applicable to spliced post-tensioned bridges. Shear behavior was evaluated based on adjusting the following variables:

- i) Presence of post-tensioning duct
- ii) Duct material
- iii) Duct diameter
- iv) Web width
- v) Transverse reinforcement ratio

Girders that contained post-tensioning duct experienced service load level cracking localized around the duct at around 35% of the failure load and full-depth cracking occurred at approximately 50% of the failure load (Figure 3-31). The control specimen experienced full-depth hairline cracks at the same percentage of ultimate load that localized cracking occurred for the PT duct specimens. At failure, all girders containing ducts experienced localized web crushing in the concrete surrounding the duct, while the control girder experienced full-depth web crushing at ultimate load.

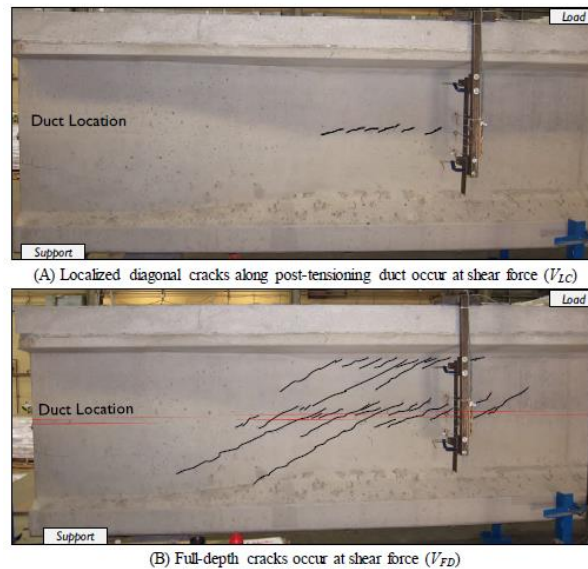


Figure 3-31 Localized and full-depth cracking of girders with PT ducts (Moore et al., 2015).

The duct material did not affect the failure mode or shear strength reduction as shown in a plot of normalized shear stress (Figure 3-32). All specimens experienced localized cracking at the duct location followed by full-depth cracks at the failure load. The report suggests that there is no need to differentiate between duct materials for strength reduction calculations.

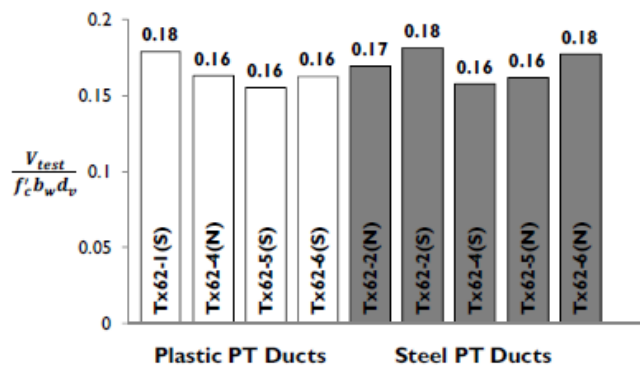


Figure 3-32 Normalized shear stress at ultimate for plastic and steel ducts with duct-diameter-to-web-width ratio between 0.43 and 0.44 (Moore et al., 2015).

The failure mechanism was the same for all specimens containing a PT duct as stated before. A duct-diameter-to-web-width ratio of 0.33 to 0.44 was used for testing and there was no

observable difference in the failure mechanism, which was localized web crushing. Specimens with a duct width-to-web width ratio of 0.33 failed at a shear stress of $0.20f'_c$ while specimen with a ratio of 0.44 failed between a stress of $0.16f'_c$ and $0.18f'_c$.

The researchers found that an increase in transverse reinforcement ratio tended to reduce the shear strength ratios (Figure 3-33). These values become unconservative beyond the AASHTO general upper nominal shear strength limit, $V_n=0.25 f'_c b_w d_v$.

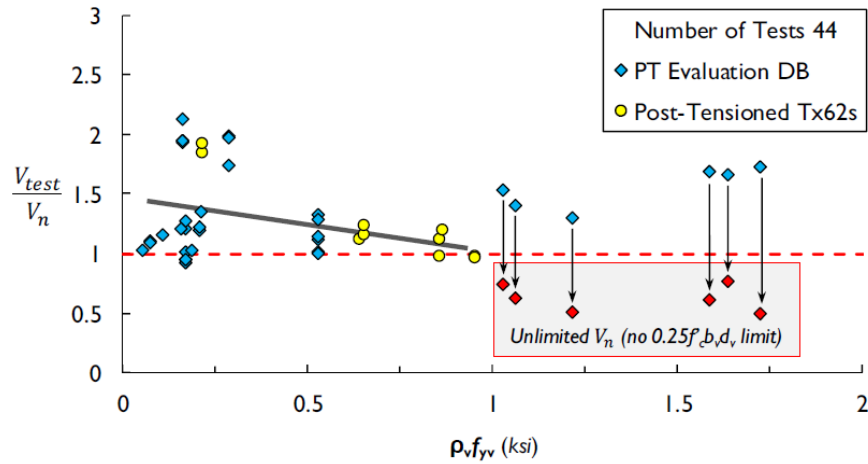


Figure 3-33 Shear strength ratio vs. transverse reinforcement ratio (Moore et al., 2015).

The researcher proposed a modification to AASHTO LRFD shown in the following two equations:

$$V_n = \min \left\{ \begin{array}{l} \beta \sqrt{f'_c} b_w d_v + \frac{A_s f_y}{s} d_v \lambda_{duct} \cot \theta \\ 0.25 f'_c b_w d_v \end{array} \right\} + V_p \quad (37)$$

$$\lambda_{duct} = 1 - \delta \left(\frac{\phi_{duct}}{b_w} \right)^2 \geq 0 \quad (38)$$

where:

- λ_{duct} = quadratic reduction factor applied to V_s that accounts for the presence of PT duct
- f'_c = concrete compressive strength
- b_w = minimum gross width within a depth of d_v
- d_v = effective shear depth calculated using AASHTO general
- ϕ_{duct} = the outside PT duct diameter
- V_p = vertical component of prestressing force after losses
- δ = duct diameter correction factor, 2.0 for grouted ducts

These equations modify the transverse reinforcement contribution to shear strength, V_s and is intended to replace the current nominal shear strength calculations for webs containing a PT duct. This method was implemented in AASHTO LRFD 9th edition.

A quadratically reducing term, λ_{duct} (Figure 3-34), is introduced to modify the V_s term when calculating nominal shear strength. The effective web width term is removed from calculations and the gross web width, b_w , is used instead for nominal shear strength calculations.

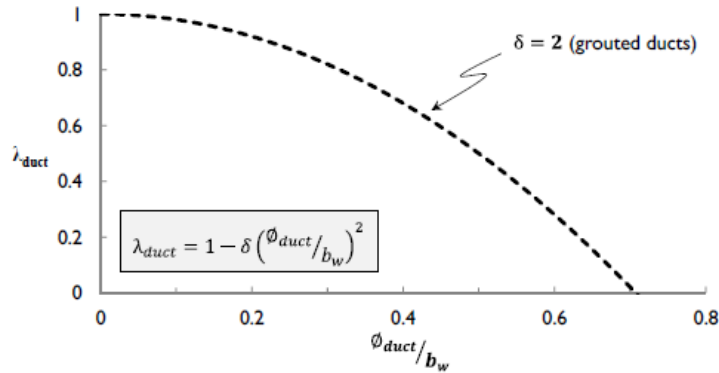


Figure 3-34 λ_{duct} vs. duct-diameter-to-web-width ratio (Moore et al., 2015).

3.5 Findings

The key findings from the literature review can be summarized as follows:

- Diagonal tensile stresses cause shear cracking and is a major concern for shear analysis.
- Nominal shear strength is made up of the concrete contribution, V_c , the vertical reinforcement, V_s , and the vertical component of the prestressing tendon, V_p .
- Design codes typically account for the presence of PT ducts by using an effective web width to determine the nominal shear strength.
- AASHTO 9th Edition introduced a shear reduction factor for transverse reinforcement contribution to determine nominal shear strength for grouted ducts.
- Panel tests were inexpensive and effective for determining variable sensitivity but did not accurately mimic the behavior of large-scale girders.
- Full-scale specimens experienced localized cracking near the duct location prior to full-depth diagonal web cracks.
- Failure mode of full-scale specimens containing PT ducts was web crushing at the duct location.

4 Strength Tests on Modified AASHTO TYPE III Specimens

4.1 Introduction

Firstly, an investigation was done using six modified AASHTO Type III precast specimens to determine variables critical in influencing the shear behavior of I-girders containing PT ducts. The modified AASHTO Type III sections were fabricated at a precast plant experienced with fabrication of bridge girders for FDOT. These sections were smaller than sections used in spliced bridge girder construction but would still have wide top and bottom flanges with a thin web which would be representative of the typical I-girder. For the purposes of reducing initial complexity anchorage systems and prestressing strands were not installed. Also, these specimens have been designed to fail in shear.

4.2 Specimen Design

In preparation for the specimen fabrication variables were chosen to be included or excluded in this preliminary investigation on the influence on the shear behavior, based on literature review and an existing bridge investigation. A modified AASHTO TYPE III cross-section based on the existing bridge investigation was selected. A test matrix based on the chosen variables and cross section is also presented.

4.2.1 Included Variables

Based on the literature review the following key variables were considered:

- Inclusion and exclusion of flanges
- Duct diameter
- Web width
- Duct-diameter-to-web-width ratio
- Transverse reinforcement ratio
- Number of ducts

4.2.2 Excluded Variables

Based on previous research, the following variables were excluded that were not considered significant for this experiment:

- Concrete strength
- Grout strength
- Duct bond
- Duct material
- Through thickness reinforcement

4.2.3 Cross-section

Based on existing bridge investigations a modified AASHTO Type III cross section was chosen for the phase 1 experimental test, shown in Figure 4-1. The specimens were fabricated at a precaster using an AASHTO Type III bottom liner and side forms while the deck was made from custom plywood forms. The cross sections were modified to include a wide top flange like a typical I-girder cross-sections used in spliced bridge construction. The top flange dimensions were 2 ft. wide by 6 in. thick.

Concrete was placed in two separate pours and the top of each specimen was roughened after the first placement, except for specimen SS1 (Figure 4-1 (a)) which had a trowel finish.

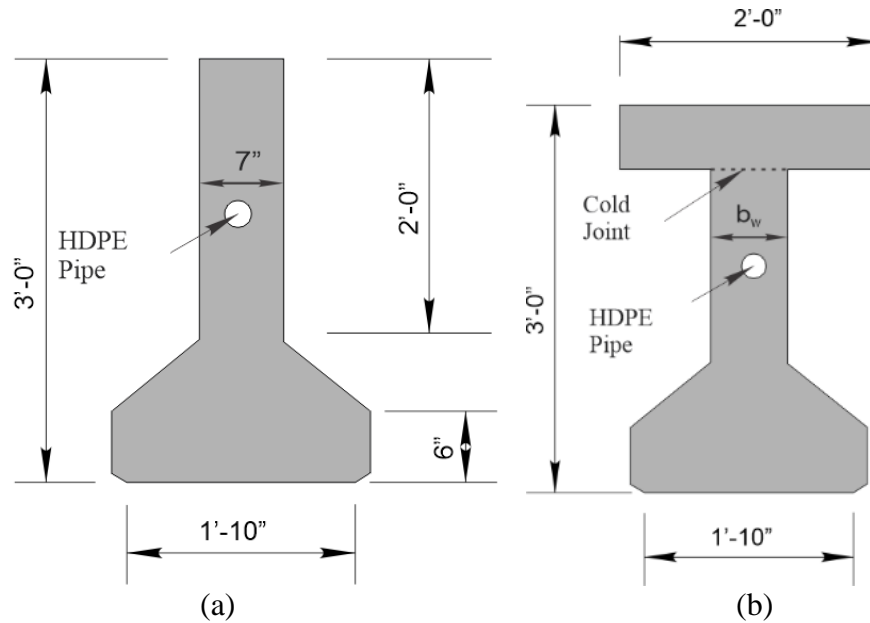


Figure 4-1 Modified AASHTO Type III cross-section. (a) SS1 (b) other specimens

4.2.4 Strand Pattern

Prestressing strands were the primary flexural reinforcement for the simply supported sections. These strands were limited to a quantity that would not cause excessive cracking due to the prestress force but provide sufficient flexural resistance to ensure a shear failure during testing. The prestressing strand pattern, shown in Figure 4-2, was identical for all specimens but debonding was used to vary the applied prestress force for certain specimens.

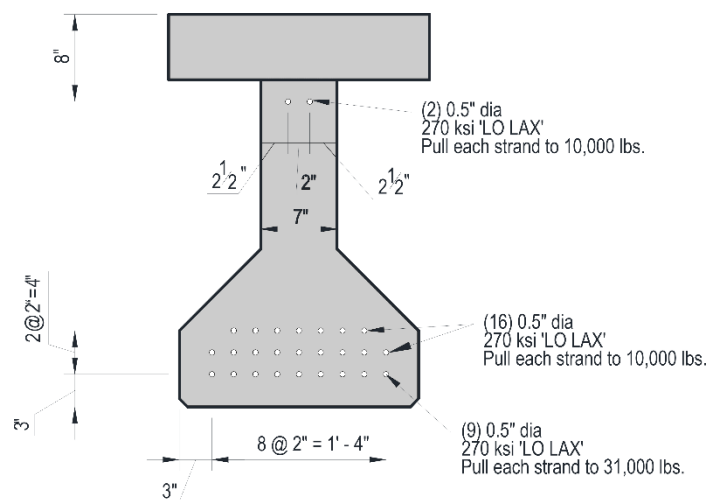


Figure 4-2 Strand pattern for Modified AASHTO Type III sections

4.2.5 Duct Profile

A parabolically draped tendon profile was chosen for the simply supported section, and the cantilever supported section. The tendon was ungrouted which is representative of the low stiffness flexible filler material. The positive bending section is intended to represent the end span of a three-span continuous splice girder while the negative bending section represents the haunch region of the bridge. The shape and location of the parabola is shown in Figure 4-3.

4.2.6 Specified Material Properties

The following specified material properties and specifications used for these specimens:

Table 4-1 Table showing material properties and specifications.

Material	Specification
Precast Concrete	8500 psi 28-day compressive strength 5000 psi compressive strength at prestress release
Prestressing Strand	ASTM 416 0.5-in diameter 7-wire strand 270 ksi ultimate strength Low relaxation
Mild Reinforcement	ASTM 615 Grade 60 60 ksi yield strength

4.2.7 Test Matrix

Based on the variables discussed in the previous sections a test matrix was developed, shown below in Table 4-2. Two type of support conditions were considered simply supported (SS), shown in Figure 4-3 (a), and negative bending (NB), shown in Figure 4-3 (b). Span to depth ratios were kept greater than 2 to prevent deep beam behavior during testing.

Table 4-2 Modified AASHTO TYPE III specimens test matrix.

Specimen	Flange	Filler	Duct Diameter O/D (in.)	Web Width (in.)	Duct Diameter-to-web thickness ratio	Number of ducts	Transverse Reinforcement
SS-1	Bottom	Empty	1.9	7	0.27	1	(2) #3 @ 12"
SS-2	Both	Empty	1.9	7	0.27	1	(2) #3 @ 12"
SS-3	Both	Empty	2.375	7	0.34	1	(2) #4 @ 12"
SS-4	Both	N/A	N/A	7	N/A	N/A	(2) #4 @ 12"
SS-5	Both	Empty	4.5	7	0.64	1	(2) #4 @ 12"
NB-1	Both	Empty	2.375	9	0.26	2	(2) #4 @ 12"

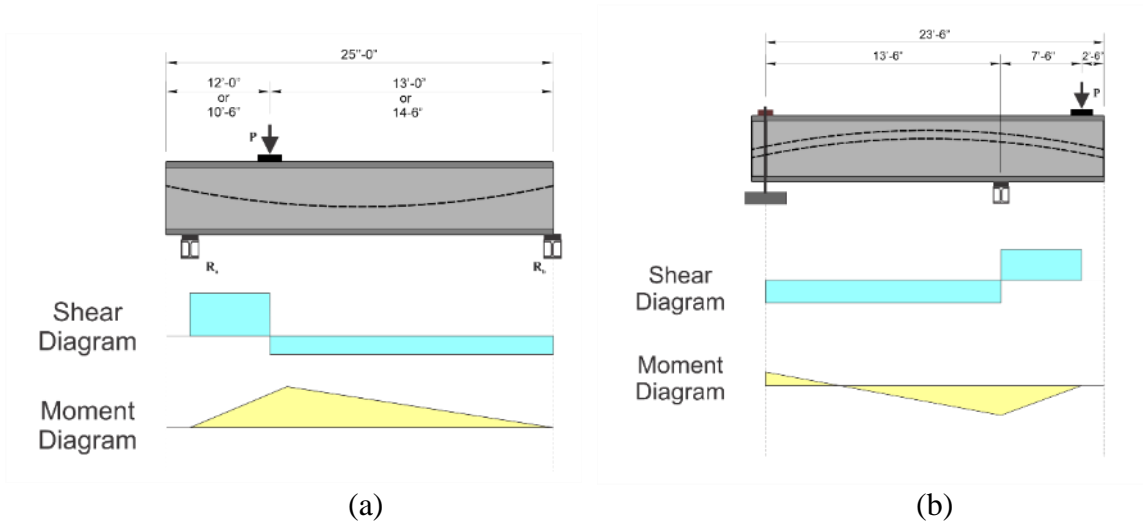


Figure 4-3 Specimen test setup for specimens: (a) positive bending (b) negative bending

4.3 Specimen Fabrication

Specimens, except SS1, were constructed in two stages, the first phase used the AASHTO Type III side forms to construct the bottom portion of the specimens and the final phase used plywood forms to construct the top flange. Specimen orientation on the prestressing bed and the strand cut locations are shown in Figure 4-4. Table 4-3 presents a summary of key event dates during fabrication.

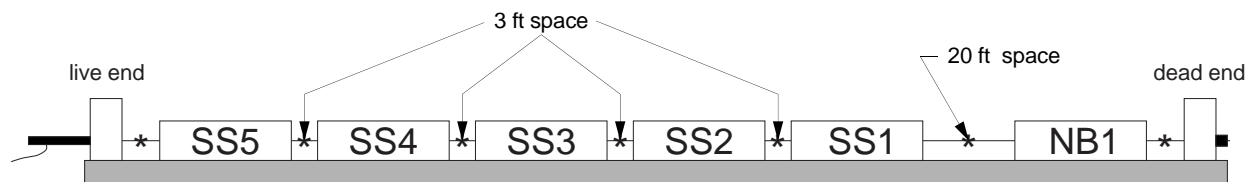


Figure 4-4 Specimen orientation and strand cutting location.

Table 4-3 Specimen fabrication event summary.

Specimen	Prestressing strands tensioned	First Pour	Second Pour	Detensioning
*SS1	Feb. 18, 2019	Feb. 20, 2019	N/A	March 1, 2019
SS2	Feb. 18, 2019	Feb. 20, 2019	Feb. 25, 2019	March 1, 2019
SS3	Feb. 18, 2019	Feb. 20, 2019	Feb. 26, 2019	March 1, 2019
SS4	Feb. 18, 2019	Feb. 20, 2019	Feb. 27, 2019	March 1, 2019
SS5	Feb. 18, 2019	Feb. 20, 2019	Feb. 27, 2019	March 1, 2019
NB1	Feb. 18, 2019	Feb. 20, 2019	Feb. 22, 2019	March 1, 2019

*Specimen SS1 required a single pour because it did not have a top flange.

4.3.1 Prestressing Strand Installation and Tensioning

AASHTO Type III bottom liners of 22 in. width were first installed on the fabrication bed with a modified 24 in. bottom liner being used for specimen NB1 to create the 9 in. web required for that specimen. Form release was sprayed along the entire length of the bed shown in Figure

4-5. Plywood bulkheads (Figure 4-6) were used and holes were drilled to allow prestressing strands and duct to be inserted.



Figure 4-5 Form release being sprayed on bottom liner



Figure 4-6 Typical plywood bulkhead for specimens

Strands were inserted individually, Figure 4-7, from the dead-end through the plywood bulkheads and out the live end. Strands were debonded as indicated on engineering drawings for specimens NB1 and SS1 using PVC tube sheathing shown in Figure 4-8.



Figure 4-7 Prestressing strand insertion.

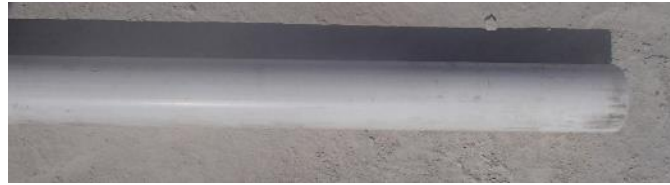


Figure 4-8 PVC sheathing for strand debonding.

Tensioning of the strands was done using a monostrand hydraulic jack shown in Figure 4-9. The bottom layer of strands were stressed to a target force of 31.55 kip while all other strands were stressed to 10.55 kip, within a tolerance of ± 2.5 percent. Jacking force was verified against elongation measurements. Tensioning pattern is shown in Figure 4-10.

4.3.2 Rebar Cage, Duct, and Internal Instrumentation Installation

Ducts, shown in Figure 4-12, were installed prior to assembling the rebar cage due to the access required to fit each duct. The ducts were installed by first cutting a circular hole in the plywood bulkhead and then manually inserting the duct in the cutouts as shown in Figure 4-13. The duct sizes used for each specimen is summarized in Table 4-4.



(a)



(b)



(c)

Figure 4-12 Smooth duct with outside diameter: (a) 1.9-in. (b) 2.375 in. (c) 4.5-in.

Table 4-4 Duct size and material summary

Specimen	Material	Outside Diameter (in.)
SS1	PVC	1.9
SS2	PVC	1.9
SS3	HDPE	2.375
SS4	None	None
SS5	HDPE	4.5
NB1	HDPE	2.375 (Two)



Figure 4-13 Duct installation

Mild steel reinforcement, Figure 4-14, was assembled as per fabricator engineering drawings and internal instrumentation was placed as per instrumentation drawings, Figure 4-15, in Task 4. Ducts were supported using U shaped #3 mild steel rebars at 4 feet minimum spacings. Completed rebar cages are shown from Figure 4-16 to Figure 4-21.



Figure 4-14 Rebar cage assembly



Figure 4-15 Internal instrumentation



Figure 4-16 SS1 rebar cage assembly



Figure 4-17 SS2 rebar cage assembly



Figure 4-18 SS3 rebar cage assembly



Figure 4-19 SS4 rebar cage assembly



Figure 4-20 SS5 rebar cage assembly



Figure 4-21 NB1 rebar cage assembly

4.3.3 Concrete Placement

AASHTO Type III side forms were assembled around the rebar cages in preparation for concrete placement. A rubber-tired gantry crane was used to move the side form into position and laborers locked the side form into place, shown in Figure 4-22. The side form for specimen SS1 was adjusted to create the desired cross section by gluing custom cut pieces of Styrofoam on the form shown in Figure 4-23.



Figure 4-22 AASHTO Type III side form installation



Figure 4-23 Styrofoam attached to side form and glue

Concrete placement was done in two separate placements and the top of each specimen was roughened after the first placement, shown in Figure 4-24 and Figure 4-25, except for specimen SS1 which had a trowel finish. Class VI 8500 psi self-consolidating concrete mix was prepared at a batch plant on-site for both placements and delivered to the prestress bed. A concrete vibrator was used only for specimen SS5 due to the large duct and small concrete cover to ensure proper concrete consolidation around the duct. Concrete cylinders were taken from each concrete batch by the research team and the precast plant quality control team. Girders were covered with tarp, shown in Figure 4-26, after the first concrete placement.



Figure 4-24 First concrete placement



Figure 4-25 Roughened top surface



Figure 4-26 Tarp covered specimens

Tarps were removed the following day and reusable plywood formwork, shown in Figure 4-27, was installed in preparation for the second concrete placement. The rebar cage for the top flange was installed followed by the final concrete placement. The top flange concrete surface was given a trowel finish. Plywood forms were removed the day after concrete placement for the top flange. Two 4x8 field cured cylinders were tested before detensioning. The average concrete strength after two days was 6611 psi and the specified release strength was 5000 psi.



(a)



(b)

Figure 4-27 Specimen second placement (a) plywood formwork (b) top flange rebar cage



Figure 4-28 Concrete placement and finished surface



Figure 4-29 Completed specimens

4.3.4 Specimen Detensioning

Strands were cut in the sequence shown in Figure 4-30 using an acetylene torch and at the locations shown in Figure 4-4. Each location was inspected before proceeding on to the next strand in the sequence. Strands were inspected at the end of detensioning to ensure all strands were fully cut shown in Figure 4-31.

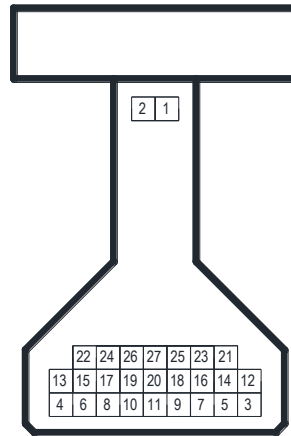


Figure 4-30 Detensioning sequence



Figure 4-31 Fully cut strands

4.4 Instrumentation

Preliminary FEA modeling was used to determine instrumentation locations for measurements such as compressive strains near the load button, flexural cracks, mild steel strains, strand slip, prestressing strand strains and shear stress measurements. Internal gauges were installed during the fabrication of each specimen while external gauges were installed at the Structures Research Center. Gages were placed in strategic locations to capture key stages of testing along with initial test conditions. The general instrumentation and what was measured is shown in Table 4-5. An example of an overall instrumentation layout is shown in Figure 4-32.

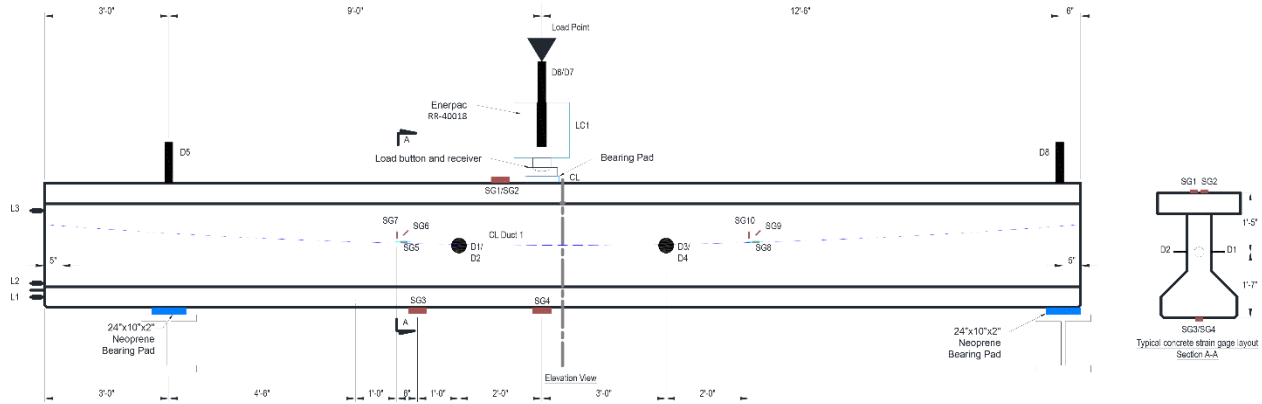


Figure 4-32 Typical instrumentation layout for phase 1 specimens

Table 4-5 Summary of general instrumentation

Stage	Prestressing strand strain	Mild steel strain	Concrete strain	Displacement	Actuator force
Stressing	X				
Shear Test	X	X	X	X	X

4.4.1 Strain

Concrete strain gauges were 60-mm foil-type gauge, shown in Figure 4-33, while internal mild steel strain gauges were 5-mm foil-type gauge. Strain gauges near the load button were used to determine an imminent compressive failure which signaled the approaching completion of the test. Strain gauges at the bottom of the beam were used to measure the strain before the first flexural cracks. Steel strain gauges were attached on the stirrups and used to measure the strains during testing, particularly leading up to concrete cracking and until failure. Rosette strain gauges, shown in Figure 4-34, were located in the shear test region and were used to determine principal shear stresses and angles. Vibrating wire gauges were used to determine the final prestress force on test day.

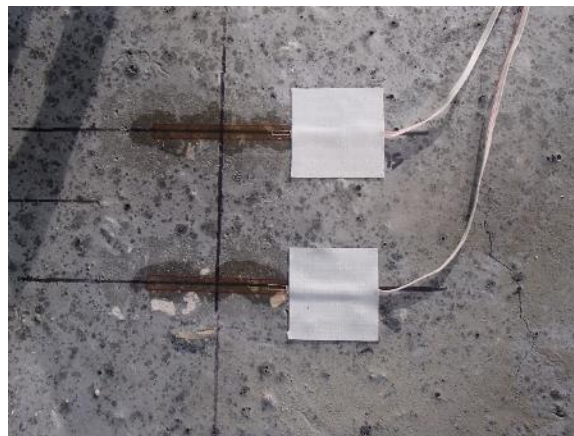


Figure 4-33 60-mm foil-type concrete strain gauge

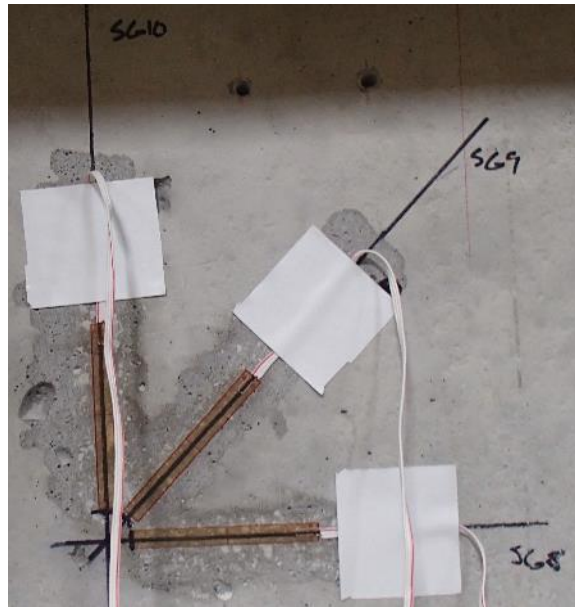


Figure 4-34 Rosette strain gauge

4.4.2 Displacement

Strand slip was measured using linear potentiometer, shown in Figure 4-35. Vertical displacements were measured using laser transducers placed at strategic locations, shown in Figure 4-36. Web expansion was measured using LVDTs, shown in Figure 4-37.



Figure 4-35 Linear potentiometer measuring strand slip



Figure 4-36 Laser displacement transducer

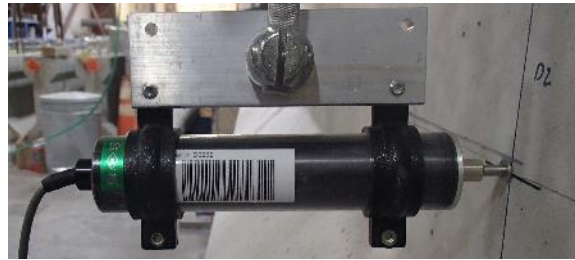


Figure 4-37 LVDT measuring web expansion

4.5 Strength Test Results

The following section contains results from the strength tests performed on the AASHTO TYPE III specimens. Strength test results are presented in terms of superimposed shear, which is the shear due to the applied load and does not include the self-weight of the specimen.

Displacement results are presented as the vertical displacement occurring at the load point. The displacement at the load point was taken as the average of the two displacements measured by the laser transducers at the load point. The effect of the bearing pad was removed from the displacement readings.

Specimens were tested at the FDOT Structures Research Center in Tallahassee, FL. Specimens were placed in a reaction frame supported on a 24 in. x 10 in. x 2 in. composite elastomeric bearing pad. Load was applied using an Enerpac RR-40018 actuator at a rate 0.2 kip/sec. Load was held at anticipated load that would cause web shear cracks, and cracks were visually inspected and marked. Loading was then continued at a rate of 0.2 kip/sec until failure, pausing every 20 kips to inspect cracks and crack growth. The test was terminated once a shear failure or compressive failure of the concrete occurred.

Continuous readings of displacements, strains, and load were taken during each shear test. Vibrating wire gauge readings were taken before the test to determine the stress in the strands at the time of loadings. Concrete cylinders corresponding to each specimen were tested to determine the compressive strength at the time of testing.

4.5.1 Specimen SS1

The primary purpose of specimen SS1 was to investigate the effect the flange has on the shear behavior of a girder containing a post-tensioning duct. The specimen was simply supported and intended to replicate the positive bending region of a continuous spliced girder bridge. The shear-span-to-depth ratio for this test was 2.5.

Specimen SS1 was loaded until the first flexural cracks were observed at 88 kip. Load was held and all cracks were marked and identified. Once markings were completed, specimen was loaded until the concrete under the load point was crushed. The first web shear crack occurred at 114 kip, and the peak shear at 134 kip. The displacement at peak load was 0.92 in. Loading was stopped once there was significant concrete spalling under the load point. Shear-displacement and crack pattern are shown in Figure 4-38 and Figure 4-39 respectively. Specimen SS1 experienced a nodal failure, shown in Figure 4-40, at the load point.

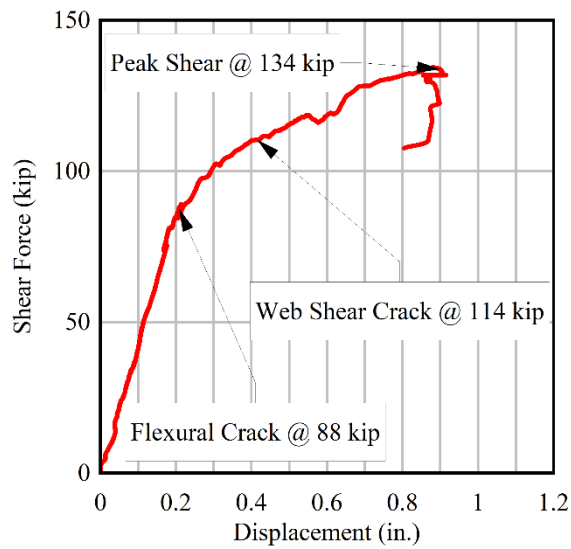


Figure 4-38 Shear-displacement results for specimen SS1

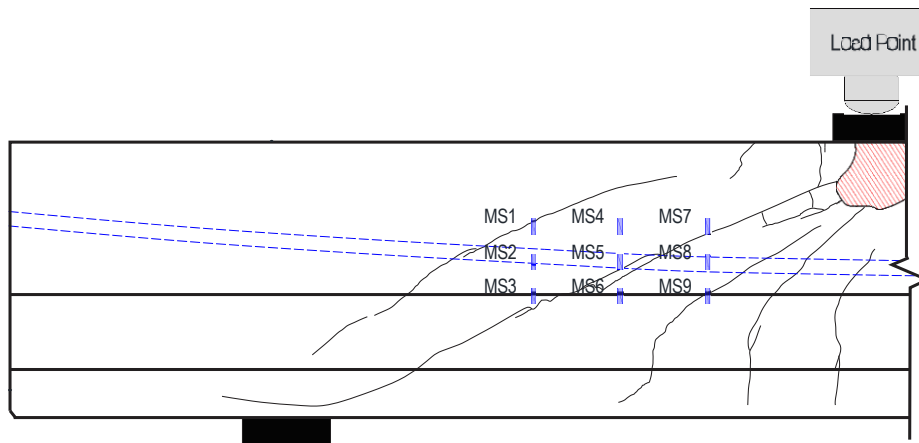


Figure 4-39 Specimen SS1 crack pattern after shear test



Figure 4-40 Concrete spalling under load point at peak load

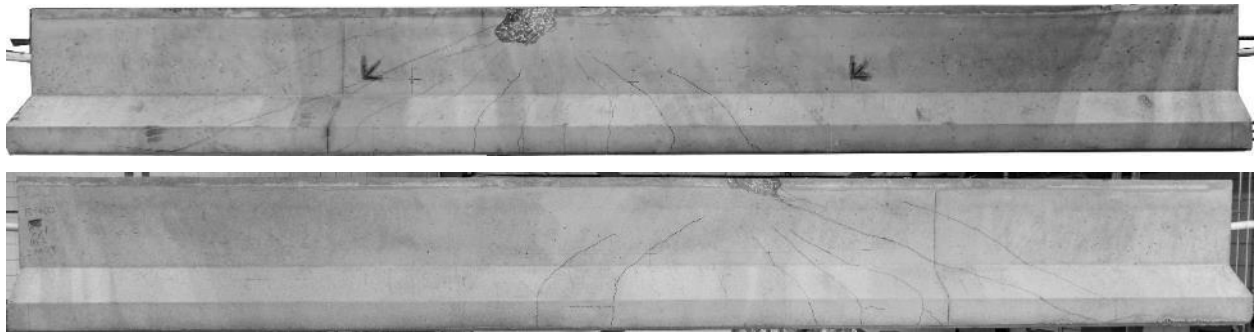


Figure 4-41 Elevation view of specimen SS1 after strength test

4.5.2 Specimen SS2

The primary purpose of specimen SS2 was to investigate the effect including the flange has on the shear behavior of a girder containing a post-tensioning duct. The specimen was simply supported and intended to replicate the positive bending region of a continuous spliced girder bridge. The shear-span-to-depth ratio for this test was 2.5.

Duct and web diagonal cracks occurred simultaneously at a shear force of 103 kip. Load was held and all cracks were marked and identified. Loading continued and the first flexural crack was noted at 142 kip, and the peak shear was 179 kip. The displacement at peak load was 0.46 in. Loading was stopped once web shear cracks extended through the thickness of the top flange indicating the onset of a compression failure.

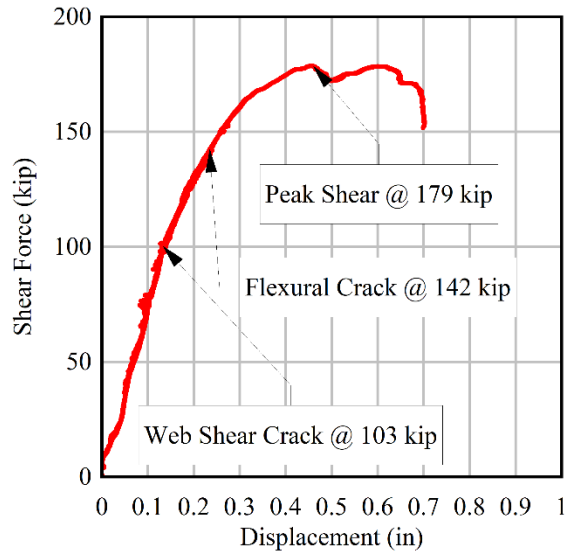


Figure 4-42 Specimen SS2 load vs. displacement plot

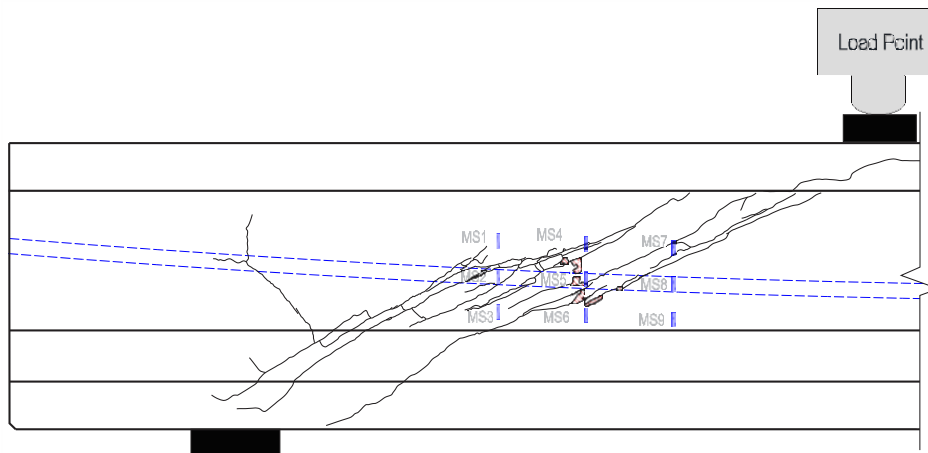


Figure 4-43 Specimen SS2 crack pattern

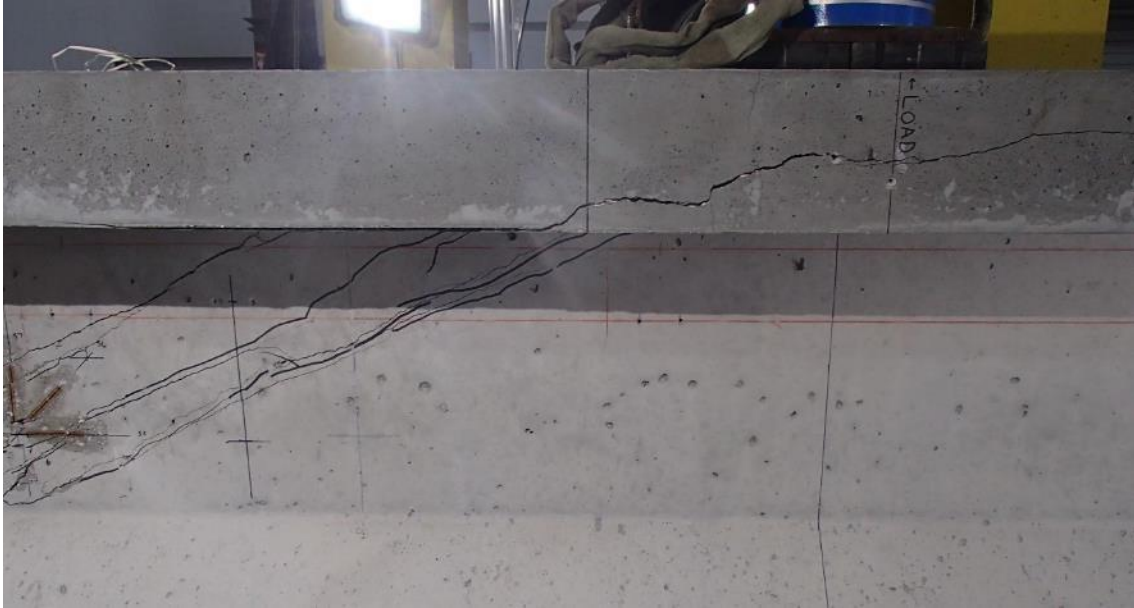


Figure 4-44 Concrete spalling under load point at end of test



Figure 4-45 Specimen SS2 at end of destructive testing

4.5.3 Specimen SS3

The primary purpose of specimen SS3 was to investigate the effect of varying duct size on the shear behavior of a girder containing a post-tensioning duct. The specimen was simply supported and intended to replicate the positive bending region of a continuous spliced girder bridge. The shear-span-to-depth ratio for this test was 3.

The specimen was loaded until localized cracking at the duct location was observed at 94 kip. Load was held and all cracks were marked and identified. Loading continued until the first flexural crack was noted at 102 kip, the peak load was 212 kip. The displacement at peak load was 1.28 in. Loading was stopped once web shear spalling occurred along with spalling of the bottom flange near the support.

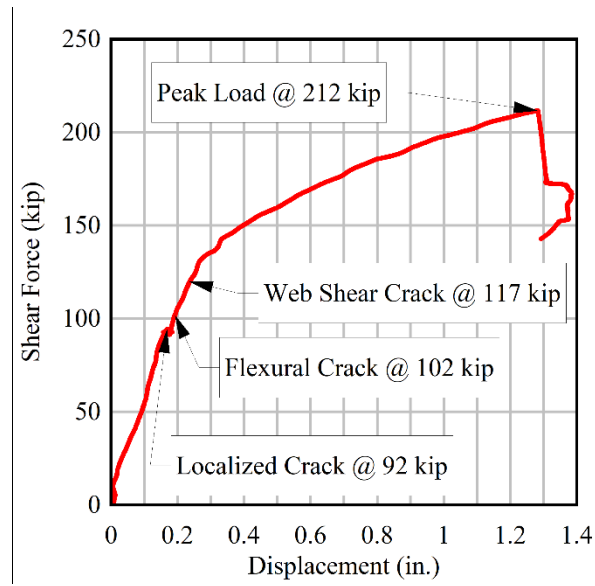


Figure 4-46 Specimen SS3 load vs. displacement plot

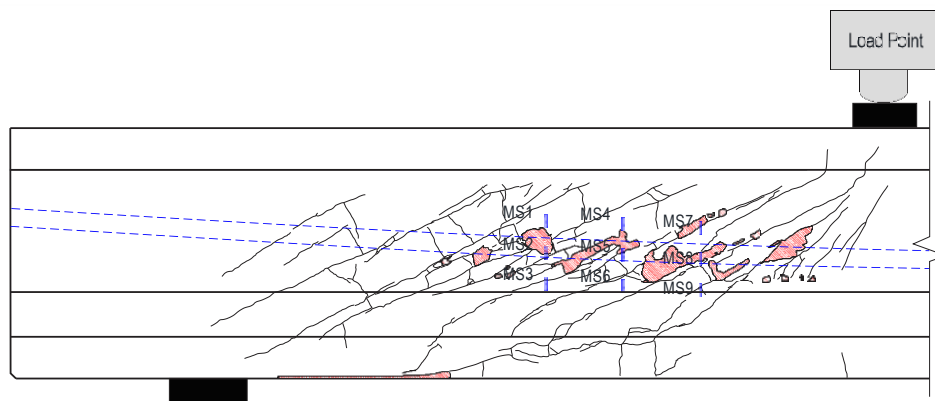


Figure 4-47 Specimen SS3 crack pattern



Figure 4-48 Concrete spalling at, (a) web and (b) bottom flange at near support.

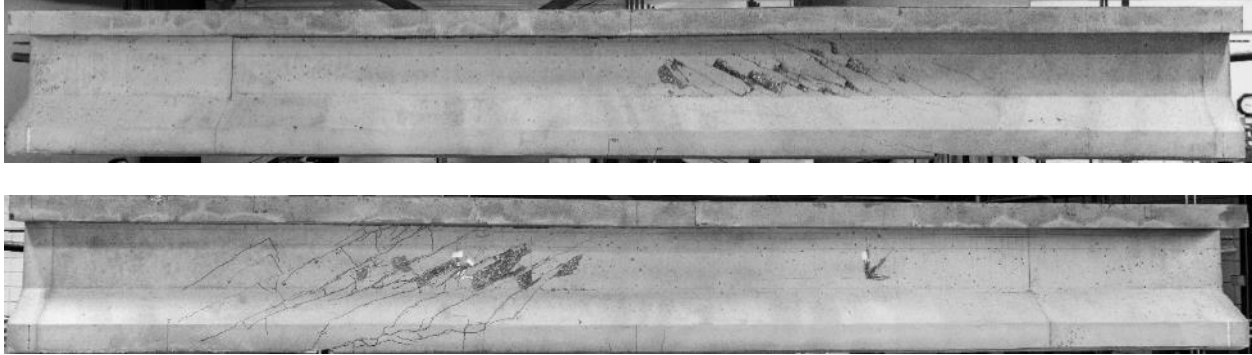


Figure 4-49 Specimen SS3 at end of destructive testing

4.5.4 Specimen SS4

The primary purpose of specimen SS4 was to be a control specimen that consisted of a solid web. The specimen was simply supported and intended to replicate the positive bending region of a continuous spliced girder bridge. The shear-span-to-depth ratio for this test was 3.

Specimen was loaded and the first flexural cracks at 118 kip were observed. Load was held and all cracks were marked and identified. Loading continued and the first web shear cracks were observed at 168 kip, and the peak load was 228 kip. The displacement at peak load was 1.54 in. The specimen experienced a web shear failure at the peak load along and produced concrete projectiles.

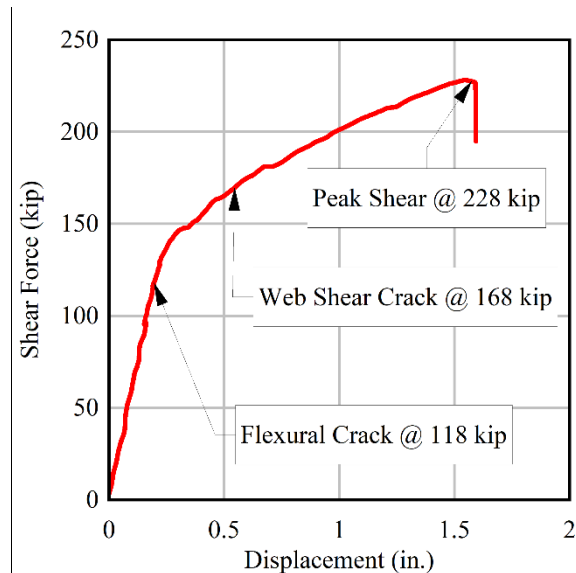


Figure 4-50 Specimen SS4 load vs. displacement plot

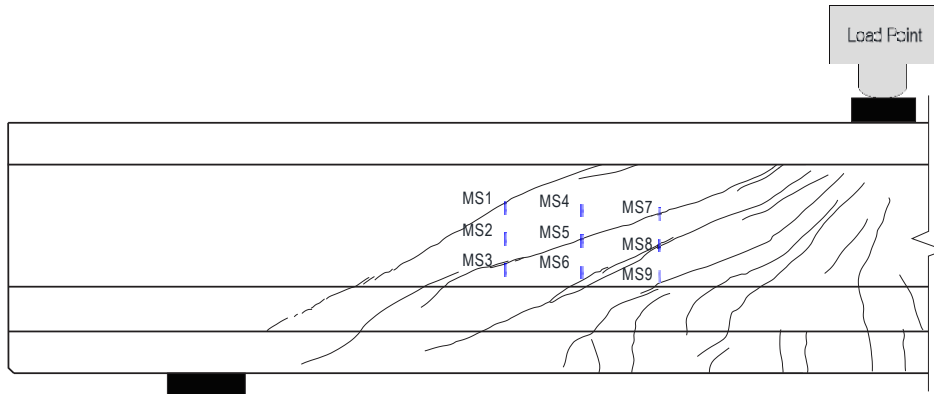


Figure 4-51 Specimen SS4 crack pattern



Figure 4-52 Shear failure of specimen SS4

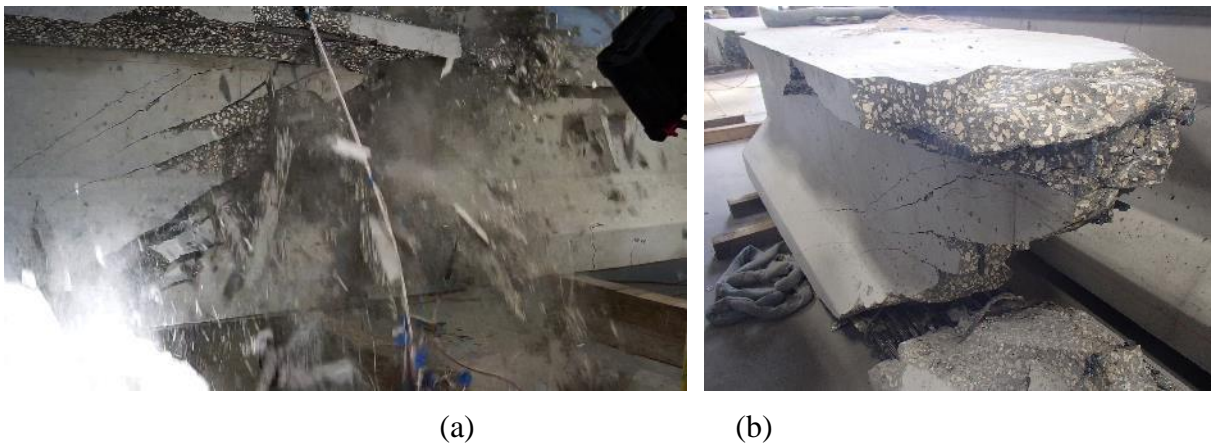


Figure 4-53 Specimen SS4 (a) video screenshot at failure (b) half specimen after test

4.5.5 Specimen SS5

The primary purpose specimen SS5 was to investigate the effect of an extreme duct size with very little clear cover on the shear behavior of a girder containing a post-tensioning duct. The specimen was simply supported and intended to replicate the positive bending region of a continuous spliced girder bridge. The shear-span-to-depth ratio for this test was 3.

Specimen was loaded until diagonal localized cracks formed in the concrete over the duct appeared at 29 kip. Loading was continued until full-depth web shear cracks appeared at 81 kip. Loading was paused when cracks appeared; cracks were marked and identified. Once markings were completed, loading was continued until failure. Specimen failure was at a peak shear force of 153 kip. The displacement at peak load was 0.42 in. Loading was stopped once spalling occurred along the location of the duct and there was a significant drop in peak shear force.

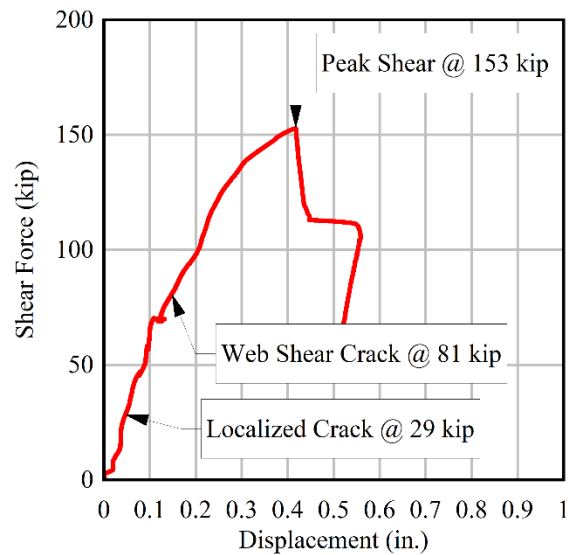


Figure 4-54 Specimen SS5 load vs. displacement plot

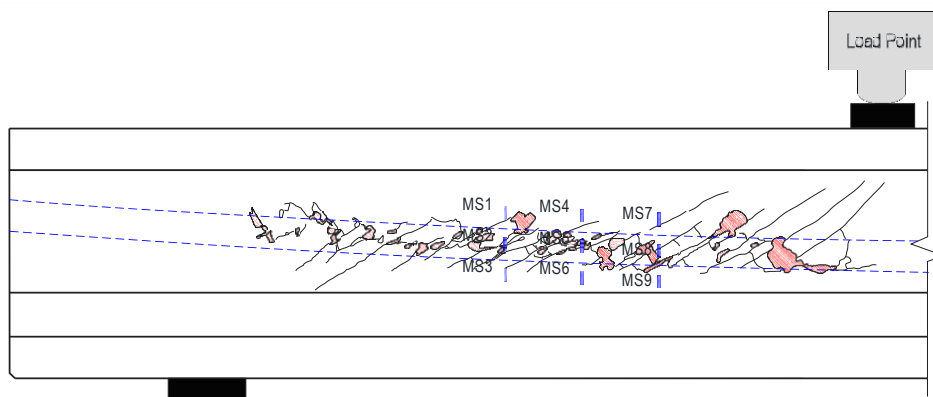


Figure 4-55 Specimen SS5 crack pattern



Figure 4-56 Concrete spalling at web



Figure 4-57 Specimen SS5 at end of destructive testing

4.5.6 Specimen NB1

The primary purpose of this specimen was to investigate the effect of having multiple ducts and a thicker web has on the shear strength of a section. The specimen support conditions were intended to replicate the negative bending region of a continuous spliced girder bridge.

Specimen was loaded and held at an applied load of 45 kip, and then at 90 kip. All cracks were marked and identified at each increment. Once markings were completed, loading was continued to the next increment. Specimen failure occurred at a peak shear force of 233 kip at a displacement of 3.08 in. Testing was halted once concrete spalled at the near support.

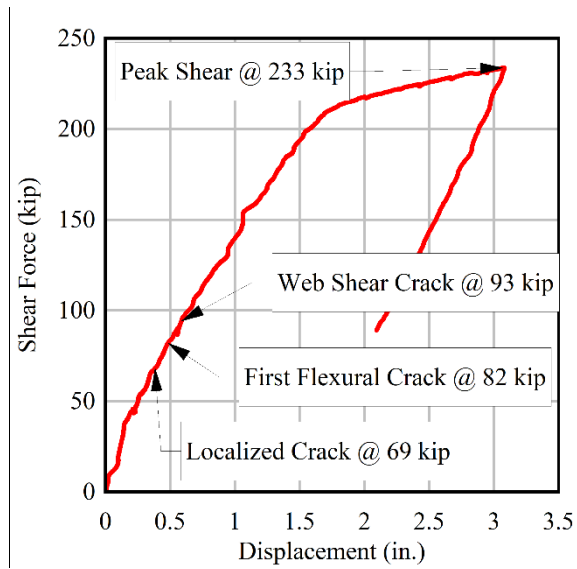


Figure 4-58 Specimen NB1 load vs. displacement plot

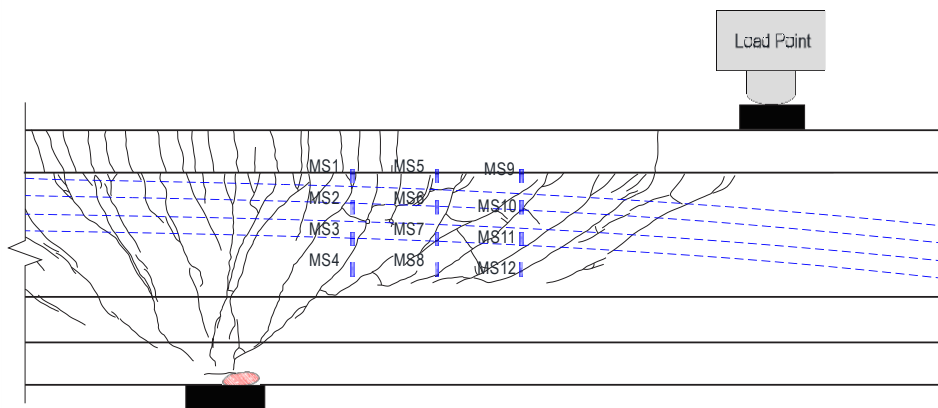


Figure 4-59 Specimen NB1 crack pattern

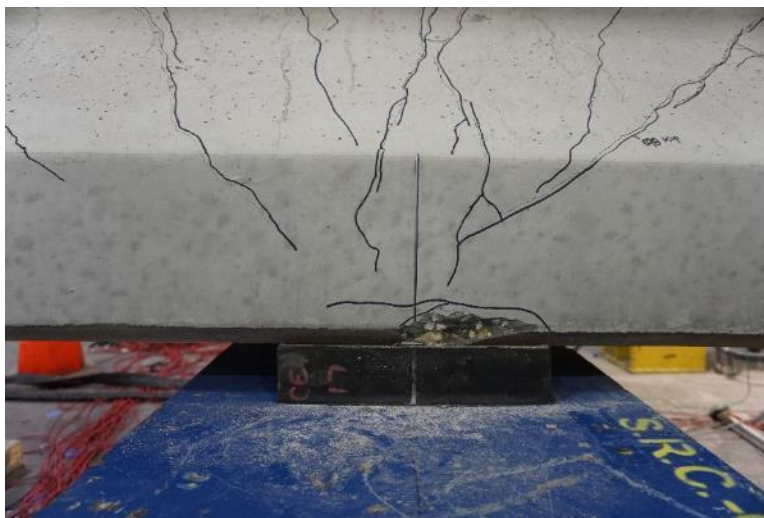


Figure 4-60 Concrete spalling at web

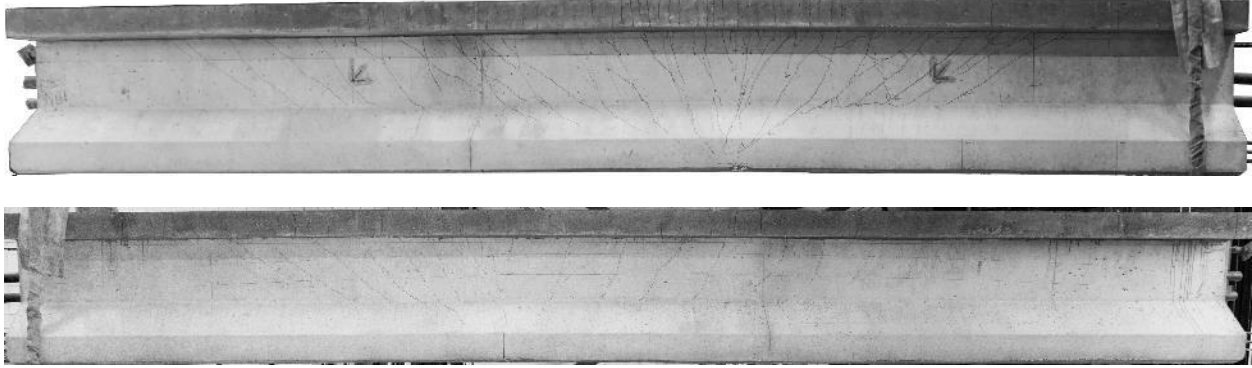


Figure 4-61 Specimen NB1 at end of destructive testing

4.6 Phase I Significant Results

The key findings from the strength tests performed on the modified AASHTO Type III specimens can be summarized as follows:

- Presence of a top flange resulted in an increase in peak shear of 25%.
- All specimens except SS1 and NB1 experienced a web crushing failure at the duct location. Specimen SS1 experienced a nodal failure at the load point and NB1 experienced a nodal failure at the near support.
- Specimens containing duct typically experienced localized diagonal cracking at the duct location followed by diagonal web cracks through the full-depth of the web.
- The specimen with the largest duct-diameter-to-web-width ratio, specimen SS5, experienced localized cracking at 19% of peak shear strength.
- As duct size increased peak shear force decreased. The specimen with the smallest duct, SS3, had a peak shear of 212 kip compared to specimen SS5 which had a peak shear of 153 kip.
- The amount of transverse reinforcement was increased (by approximately a factor of 2) from #3 spaced at 12 in. (SS2) to #4 spaced at 12 in. (SS3). The shear strength of SS3 was approximately an 18% higher than that of SS2 even though the duct-diameter-to-web-width ratio for SS3 was larger. The increase in shear reinforcement appears to have offset the loss in shear strength due to the larger duct ratio.
- Test NB1 was the only phase 1 specimen containing multiple ducts; no discernable behavior changes were noted in this specimen that might have been caused by the presence of two ducts. No localized cracking occurred in this test, which was likely due to the low web width-to-duct diameter ratio of 0.26.

5 Strength Tests on FIB-54 Specimens

5.1 Introduction

The test procedure developed for testing the FIB-54 specimens was based on the results of the modified AASHTO Type III specimens. The subsequent test matrix in this section contains specimens tested in positive and negative bending. A major addition was the inclusion of a post-tensioned tendon in specimens containing ducts and end blocks that house the anchorage. Specimens having varying duct sizes along with no duct, single duct, or multiple ducts will be investigated. The specimens were designed to be tested twice. Due to the limitations of the actuator available at the testing lab, specimens had a constant web thickness of 7 in. to ensure the specimens could be tested beyond the expected ultimate shear force.

5.2 Specimen Design

The duct-diameter-to-thickness ratios ranged from 0.34 to 0.50 to capture test data over a wide range of duct sizes. The specimen naming convention is shown in Figure 5-1. Specimens contained a single duct continuous from end-to-end with a post-tensioning tendon. A second duct was placed in one end of the specimen and terminated at mid-span. Each specimen was tested at each end, which provided data on single and multiple duct arrangements. All specimens used steel tie-wire to secure ducts in place for concrete placement. Specimen P50R contained duct reinforcement as specified in SDG (Structures Design Guidelines, 2021) (Figure 5-2).

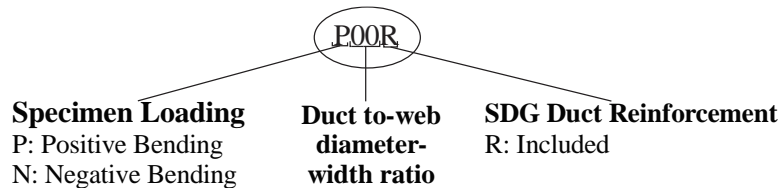


Figure 5-1 Specimen nomenclature

Figure 4.5.1-1: Webs of I-Girder and U-Girder Bridges Reinforcing Requirements

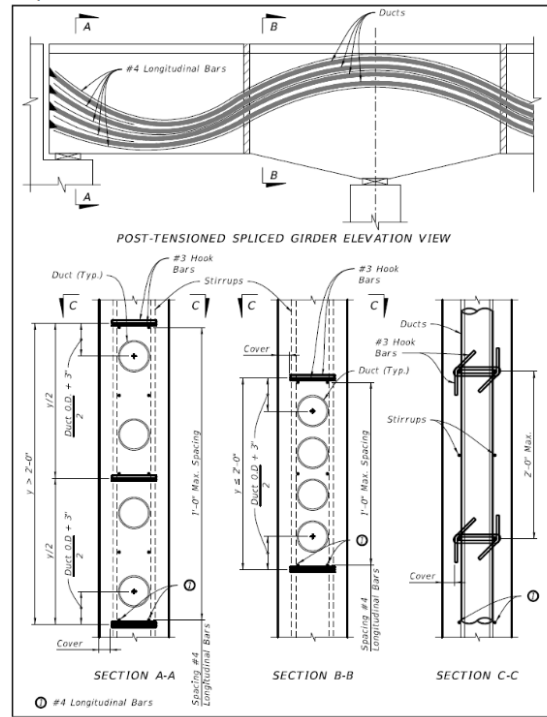


Figure 5-2 Duct reinforcement (Structures Design Guidelines, 2021)

5.2.1 Cross-section

An FIB-54 cross-section, shown in Figure 5-3, was used for each specimen. The total length of each specimen was 50 ft. which included a 3 ft. rectangular end block and 44 ft. precast section shown in Figure 5-4. The end block was designed to house the anchorage assembly which was post-tensioned at the Structures Research Center. The specimens were fabricated at a precaster using FIB-54 side forms and FIB bottom liner and the deck and end blocks were made from custom plywood forms at the Structures Research Center. The cross section was intended to replicate full-scale typical I-girder cross-sections used in spliced bridge construction.

Concrete placement was done in three separate placements. The first concrete placement was the precast girder at the concrete precaster, the second concrete placement was the cast-in-place end block and the final placement was the cast-in-place deck. The top of each specimen was roughened after the first placement and second placement in preparation for the cast-in-place deck placement.

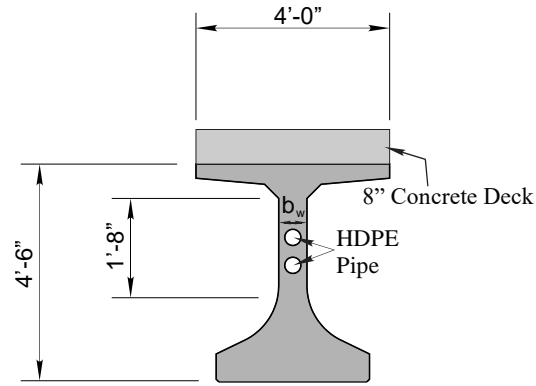


Figure 5-3 Cross section of typical test specimen

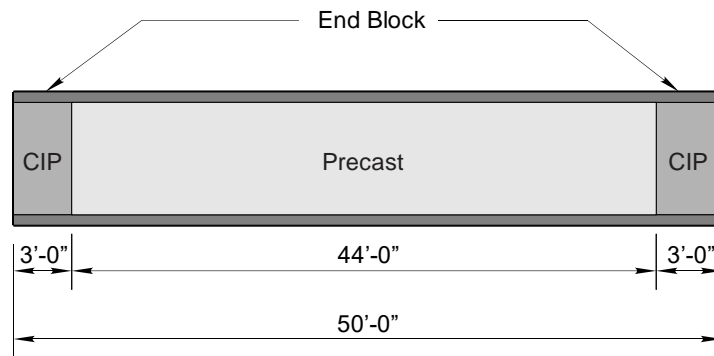


Figure 5-4 Elevation view of typical specimen

5.2.2 Duct Profile

A parabolically draped tendon profile was chosen for the simply supported section, and the cantilever supported section. The tendon was ungrouted which is representative of the low stiffness flexible filler material. Post-tensioning tendons were inserted in the duct that continued from one end of the section to the other while the duct that terminated at mid-span remained empty. The positive bending section is intended to represent the end span of a three-span continuous splice girder while the negative bending section represents the haunch region of the bridge. The shape and location of the parabola is shown in Figure 5-5.

5.2.3 Specified Material Properties

The following specified material properties and specifications used for these specimens:

Table 5-1 Table showing material properties and specifications.

Material	Specification
Precast Concrete	8500 psi 28-day compressive strength 5000 psi compressive strength at prestress release
Prestressing Strand	ASTM 416 0.6-in diameter 7-wire strand 270 ksi ultimate strength Low relaxation
Mild Reinforcement	ASTM 615 Grade 60 60 ksi yield strength

5.2.4 Test Matrix

Based on the variables discussed in the previous sections a test matrix was developed, shown below in Table 4-2. Two type of support conditions were considered simply supported (SS), shown in Figure 4-3 (a), and negative bending (NB), shown in Figure 4-3 (b). Span to depth ratios were kept greater than 2 to prevent deep beam behavior during testing.

Table 5-2 Phase 2 specimen matrix

Specimen	Duct Diameter O/D (in.)	Web Width (in)	Diameter-to-thickness ratio	Transverse Reinforcement
P00	N/A	7	0	(2) #4 @ 12"
P34	2.375	7	0.34	(2) #4 @ 12"
P41	2.875	7	0.41	(2) #4 @ 12"
P50	3.5	7	0.50	(2) #4 @ 12"
P50R	3.5	7	0.50	(2) #4 @ 12"
N34	2.375	7	0.34	(2) #4 @ 12"
N50	3.5	7	0.50	(2) #4 @ 12"

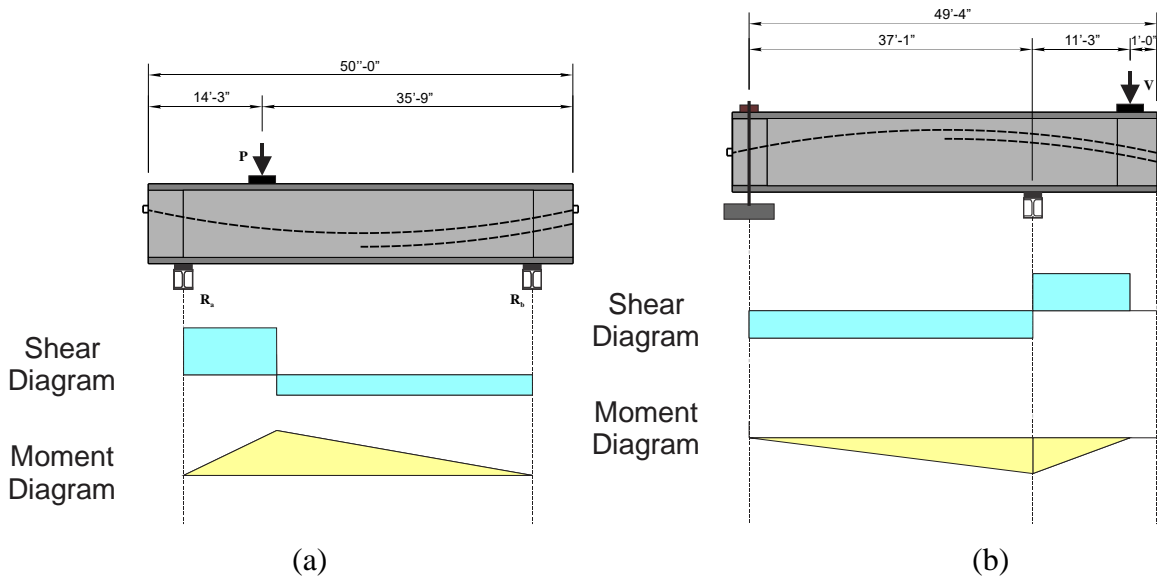


Figure 5-5 Specimen test setup for (a) positive bending (b) negative bending

5.3 Specimen Fabrication

Specimens were constructed using FIB54 side forms and FIB bottom liner. Specimen orientation on the prestressing bed and the strand cut locations are shown in Figure 5-6. Table 5-3 presents a summary of key event dates during fabrication.

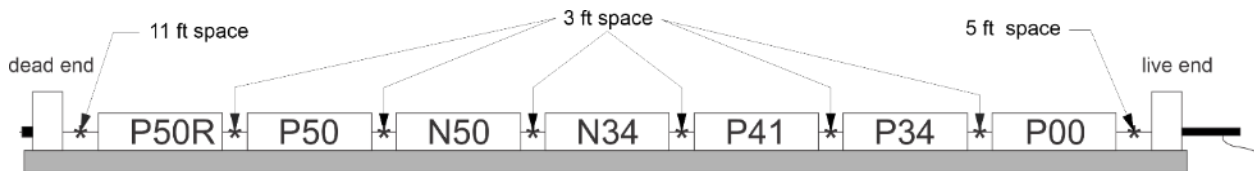


Figure 5-6 Specimen orientation and strand cutting location

Table 5-3 Specimen fabrication event summary

Specimen	Prestressing strands tensioned	Concrete placement	Detensioning
P00	January 28 th 2020	January 31 st 2020	February 4 th 2020
P34	January 28 th 2020	January 31 st 2020	February 4 th 2020
P41	January 28 th 2020	January 31 st 2020	February 4 th 2020
P50	January 28 th 2020	January 31 st 2020	February 4 th 2020
P50R	January 28 th 2020	January 31 st 2020	February 4 th 2020
N34	January 28 th 2020	January 31 st 2020	February 4 th 2020
N50	January 28 th 2020	January 31 st 2020	February 4 th 2020

5.3.1 Prestressing Strand Installation and Tensioning

FIB bottom liners, shown in Figure 5-1, of width 38-in. were first installed on the fabrication bed. Form release was sprayed along the entire length of the bed shown in Figure 5-1. Plywood bulkheads, Figure 5-8, were used and holes were drilled to allow prestressing strands and duct to be inserted. Steel bearing plates were attached to the bottom liner using epoxy (Figure 5-9) to allow embedment in the precast specimens during concrete placement.



Figure 5-7 FIB 54 steel bottom liner



Figure 5-8 Typical plywood bulkhead for specimens



Figure 5-9 Embedded steel bearing plate

Strands were inserted individually by pulling the strand from the spool placed at the dead-end anchor through the plywood bulkheads and terminating at the live end anchor (Figure 5-10). Strands were debonded as indicated on engineering drawings for specimens N34 and N50 using HDPE tube sheathing shown in Figure 5-11.



Figure 5-10 Prestressing strand insertion



Figure 5-11 PVC Sheathing for strand debonding

Tensioning of the strands was done using a monostrand hydraulic jack shown in Figure 5-12. The bottom layer of strands were stressed to a target force of 44.6 kip while all other strands were stressed to 10 kip, within a tolerance of ± 2.5 percent. Jacking force was verified against elongation measurements. Tensioning pattern is shown in Figure 5-13.



Figure 5-12 Prestressing strand stressing using monostrand jack

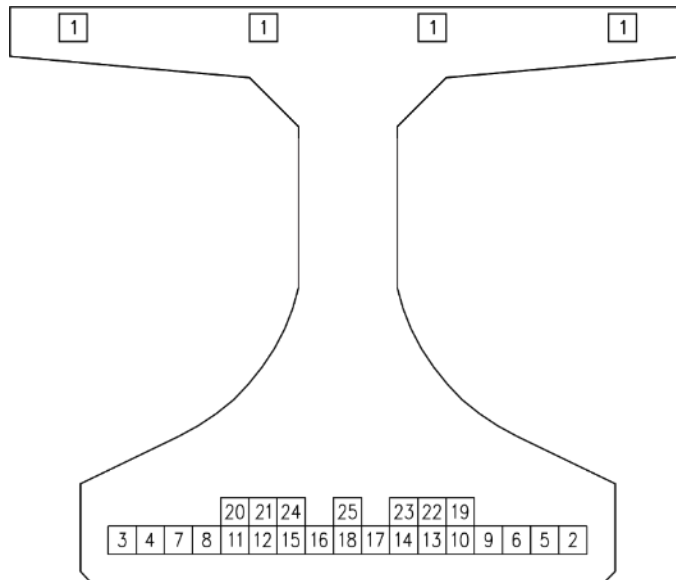


Figure 5-13 Prestressing strand jacking sequence

Following strand tensioning, the PVC tube sheathing used for debonding was securely fastened using tie wire and duct tape as shown in Figure 5-14. Debonding was 21.5 feet from each end leaving a 1-ft bonded length at the mid-length of the beam.



Figure 5-14 Strand debonding.

5.3.2 Rebar Cage, Duct, and Internal Instrumentation Installation

Ducts were installed prior to assembling the rebar cage due to the access required to fit each duct. The ducts were installed by first cutting a circular hole in the plywood bulkhead and then manually inserting the duct in the cutouts as shown in Figure 5-15. The duct sizes used for each specimen are summarized in Table 5-4.

Table 5-4 Duct size and material summary

Specimen	Material	Outside Diameter (in.)
P00	None	N/A
P34	HDPE	2.375
P41	PVC	2.875
P50	HDPE	3.5
P50R	HDPE	3.5
N34	HDPE	2.375
N50	HDPE	3.5



Figure 5-15 Duct installation.

Mild steel reinforcement, Figure 5-16, was assembled as per fabricator engineering drawings and internal instrumentation was placed as per instrumentation drawings, Figure 5-17, in Task 4. Ducts were supported using steel tie wire at 4 feet minimum spacings. Completed rebar cages are shown in Figure 5-18 to Figure 5-23. Reinforcement between the beam and future end blocks was inserted through the bulkhead to facilitate connection to the end blocks which were to be cast at the FDOT Structures Research Center.



Figure 5-16 Rebar cage assembly.



Figure 5-17 Internal instrumentation.



Figure 5-18 P00 rebar cage assembly.



Figure 5-19 P34 rebar cage assembly.



Figure 5-20 P41 rebar cage assembly.



Figure 5-21 P50 rebar cage assembly.



Figure 5-22 P50R rebar cage assembly.



Figure 5-23 N34 rebar cage assembly.



Figure 5-24 N50 rebar cage assembly.

5.3.3 Concrete Placement

FIB-54 side forms were assembled around the rebar cages in preparation for concrete placement. A rubber-tired gantry crane was used to move the side form into position and laborers locked the side form into place, shown in Figure 5-25.



Figure 5-25 FIB-54 side form installation.

An 8500 psi self-consolidating concrete mix was prepared at the fabricator's on-site batch plant and delivered to the girder bed once side forms had been securely installed. Vibration was

not necessary due to the use of a self-consolidating mix; Figure 5-26 shows the concrete being placed using a Tuckerbilt concrete buggy. Once concrete placement was complete, the top of the girders were roughened in preparation for deck installation which would be done at the FDOT Research Center (Figure 5-27). Concrete cylinders were taken from each concrete batch by the research team and the precast plant quality control team. Girders were covered with a tarp during curing after the concrete placement (Figure 5-28).



Figure 5-26 Concrete placement at girder bed for specimens



Figure 5-27 Roughened top surface



Figure 5-28 Tarp-covered specimens

5.3.4 Specimen Detensioning

Two 4x8 field cured cylinders were tested before detensioning. The average compressive strength at release was 7975 psi and the specified release strength was 6000 psi.

Strands were cut in the sequence shown in Figure 5-30 using an acetylene torch and at the locations shown in Figure 5-6. Strands were cut simultaneously to prevent uneven stresses during detensioning (Figure 5-30) . Strands were inspected during and at the end of detensioning to ensure all strands were fully cut (Figure 5-31).



Figure 5-29 Completed specimens

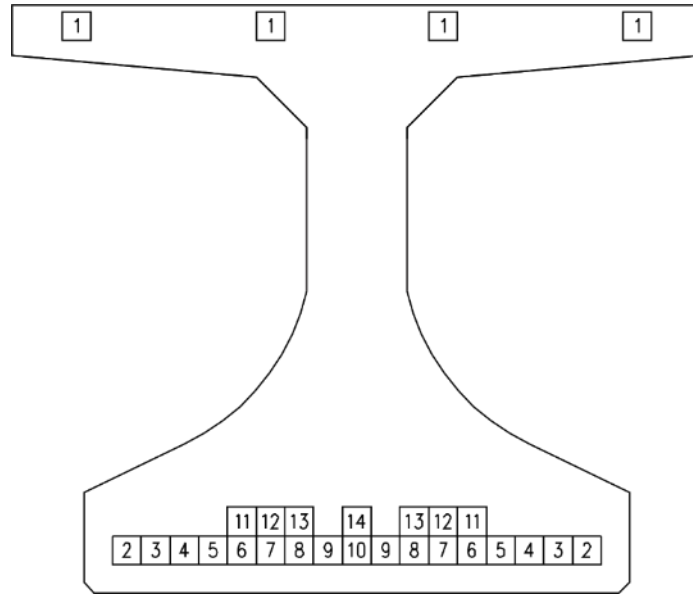


Figure 5-30 Detensioning sequence



Figure 5-31 Fully cut strands

5.3.5 End Block and Deck Construction

Precast girders were shipped to the Marcus H. Ansley Structures Research Center in Tallahassee, FL for deck and end block construction followed by post-tensioning.

The end block reinforcing cages were assembled prior to placement into the formwork and lifted in to place on the end block platform once complete. #4 mild steel starter bars which projected 3 ft from the face of the precast section were used to resist tension and shear forces between the end block and precast girder joint. End block forms were constructed using plyboards and plyforms and secured to the precast girder and sealed in preparation for concrete placement (Figure 5-32).



(a)



(b)



(c)



(d)

Figure 5-32 End block construction: (a) end block platform (b) end block reinforcement cage (c) reinforcement cage inside end block (d) completed end block formwork

Once the end block formwork was constructed longitudinal and transverse deck reinforcement was installed, shown in Figure 5-33. Plywood forms and plyboards were then affixed to the top flange and secured with threaded rods, shown in Figure 5-33.



(a)

(b)

Figure 5-33 Deck construction: (a) deck reinforcement (b) deck formwork

Concrete was prepared by a local ready mix plant. 6500 psi concrete was used for the end blocks and 4500 psi for the deck. Concrete placement was done inside of the laboratory in two separate placements one for the end block, shown in Figure 5-34 and the other for the deck, shown in Figure 5-35. Concrete was transported from the mix truck to the girder via a bucket and crane. Consolidation was done using hand-held vibrators. A completed specimen is shown in Figure 5-36.



Figure 5-34 End block concrete placement



Figure 5-35 Deck concrete placement



Figure 5-36 Completed concrete placement

5.4 Instrumentation

Similar to phase 1 specimens, preliminary FEA modeling was used to determine instrumentation locations for measurements such as compressive strains near the load button, flexural cracks, mild steel strains, strand slip, prestressing strand strains and shear stress measurements. Internal gauges were installed during the fabrication of each specimen while external gauges were installed at the Structures Research Center. Gages were placed in strategic locations to capture key stages of testing along with initial test conditions. The general instrumentation and what was measured is shown in Table 4-5. An example of an overall instrumentation layout is shown in Figure 4-32.

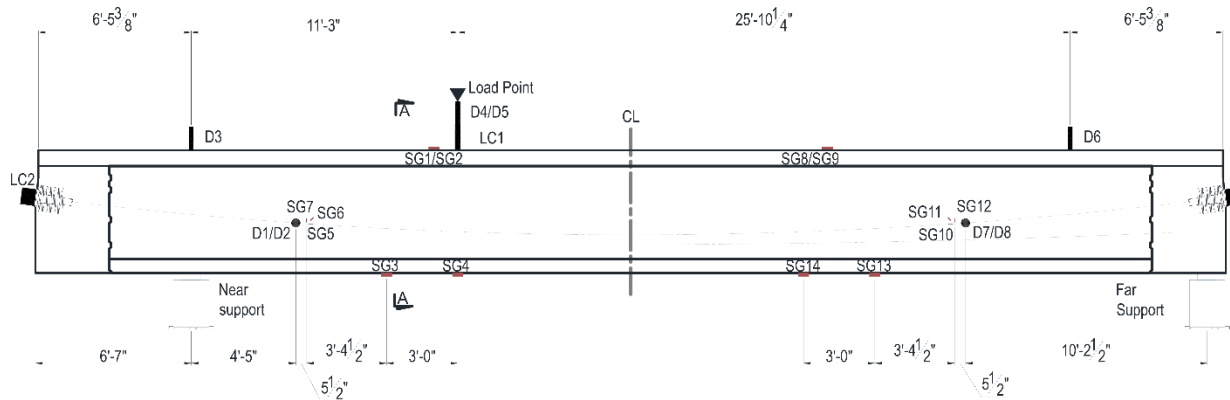


Figure 5-37 Typical instrumentation layout for phase 2 specimens

Table 5-5 Summary of general instrumentation

Stage	Prestressing strand strain	Mild steel strain	Concrete strain	Displacement	Load Cell Readings
Stressing	X				
Post-tensioning					X
Shear Test	X	X	X	X	X

5.4.1 Strain

Concrete strain gauges were 60-mm foil-type gauge, shown in Figure 5-38, while internal mild steel strain gauges were 5-mm foil-type gauge. Strain gauges near the load button was used to determine an imminent compressive failure which signaled the approaching completion of the test. Strain gauges at the bottom of the beam were used to measure the strain before the first flexural cracks. Steel strain gauges were attached on the stirrups and used to measure the strains during testing, particularly leading up to concrete cracking and until failure. Rosette strain, shown in Figure 5-39, gauges located in the shear test region and were used to determine principal shear stresses and angles. Vibrating wire gauges were used to determine the final prestress force on test day. Ormocer coated fiber optic sensors, shown in Figure 5-40, were used to take continuous strain readings within the web during strength tests.

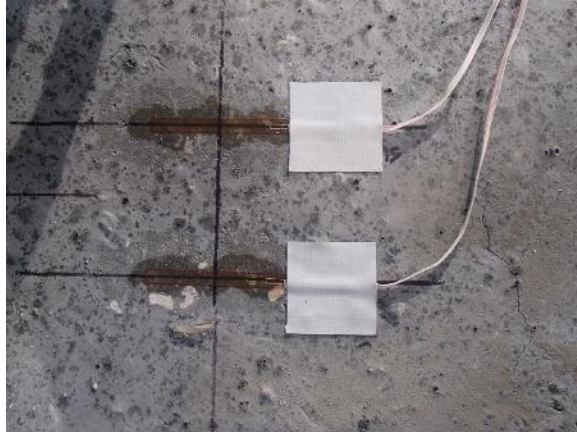


Figure 5-38 60-mm foil-type concrete strain gauge

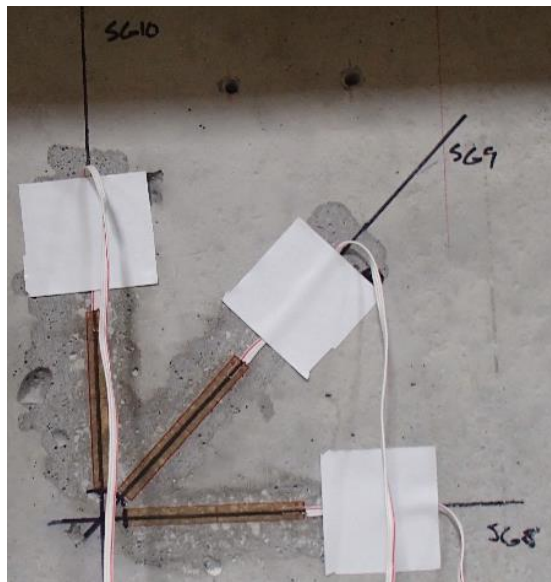


Figure 5-39 Rosette strain gauge



Figure 5-40 Fiber optic sensor

5.4.2 Displacement

Vertical displacements were measured using laser transducers placed at strategic locations, shown in Figure 5-41. Web expansion was measured using LVDTs, shown in Figure 5-42.



Figure 5-41 Laser displacement transducer

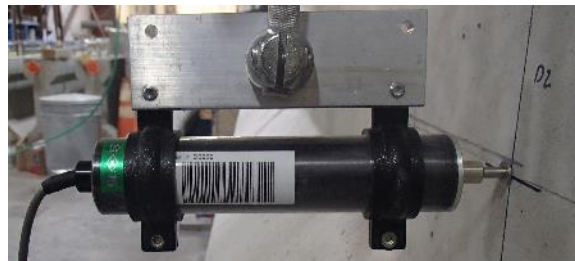


Figure 5-42 LVDT measuring web expansion

5.5 *Post-Tensioning Tendon Installation*

5.5.1 Tendon Assembly

Installation of the post-tensioning tendon consisted of hand-pushing single prestressing strands into the duct from the dead-end. To ensure that the strands in the tendon were parallel and untwisted, each strand was numbered so that it could be inserted in its respective location in the dead and live end wedge plates (Figure 5-45). To prevent installed strands from obstructing the subsequent strand installation, the installation was ordered from bottom to top. This allowed the previously installed strands to rest on the bottom of the duct and the subsequent strands to be installed over the top of the bundle of strand already in the duct.

The tendon was threaded through a Geokon 850-kip hollow load cell that was installed under the tendon wedge plate at the dead-end. At the live end, the wedge plate was installed against the anchor with sufficient strand length to allow the jack to grip and stress the tendon (Figure 5-43 and Figure 5-44).



Figure 5-43 Geokon 850-kip hollow load cell and anchor head installation at dead-end



Figure 5-44 Anchor block and wedge plate at live end

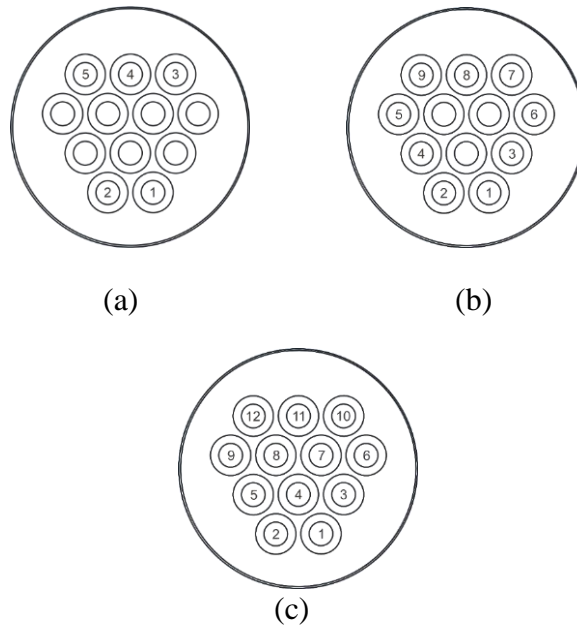
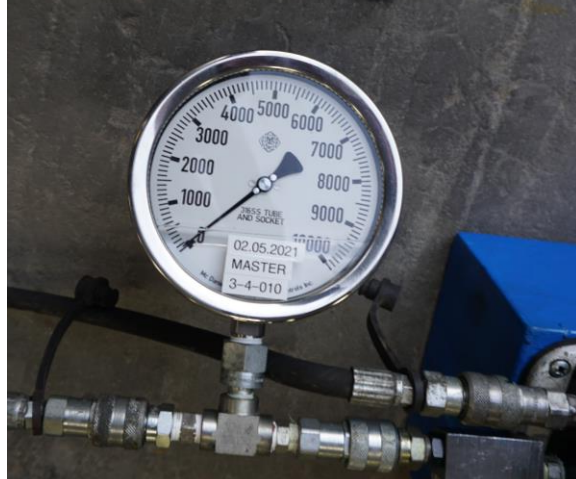


Figure 5-45 Strand location for (a) specimen P34 and N34 (b) specimen P41 (c) specimen P50, P50R and N50

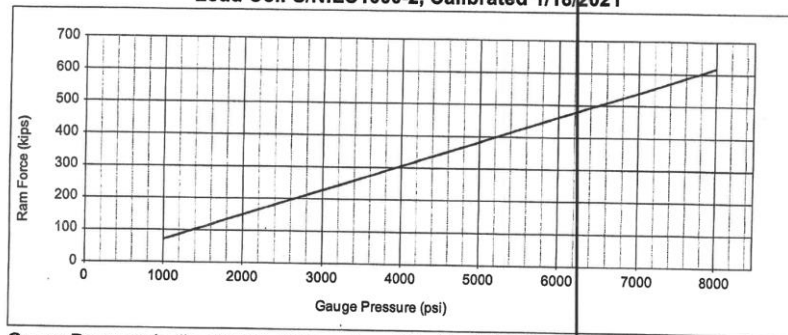
5.5.2 Instrumentation and Data Acquisition

Data were collected before, during and after post-tensioning. At the live end, tendon force was determined using a pressure gauge connected to the jack pump; the pressure was converted to load using the calibration sheet shown in Figure 5-46. Strain readings were taken at midspan using internal vibrating wire gauges. The pressure and strain readings were recorded at 5%, 20%, 40%, 60%, 80%, and 100% of the target jacking force.

At the dead-end, tendon force was measured continuously using a Geokon 850-kip hollow load cell. A load cell assembly was specifically manufactured to ensure the load cell only bears on the face of the anchorage and not the concrete while allowing a tendon of (12) 0.6-in. dia. 7-wire prestressing strands to pass through unobstructed. The assembly also positioned the load cell to ensure concentric application of the tendon force to load cell. Table 5-6 shows instrumentation used to gather data during the post-tensioning operation and at what stage it was collected.



Load Cell S/N:LC1000-2, Calibrated 1/18/2021



$$\text{Gauge Pressure (psi)} = (12.81 * \text{Ram Force (kips)}) + 89.37$$

Figure 5-46 Multistrand jack pressure gauge and calibration sheet

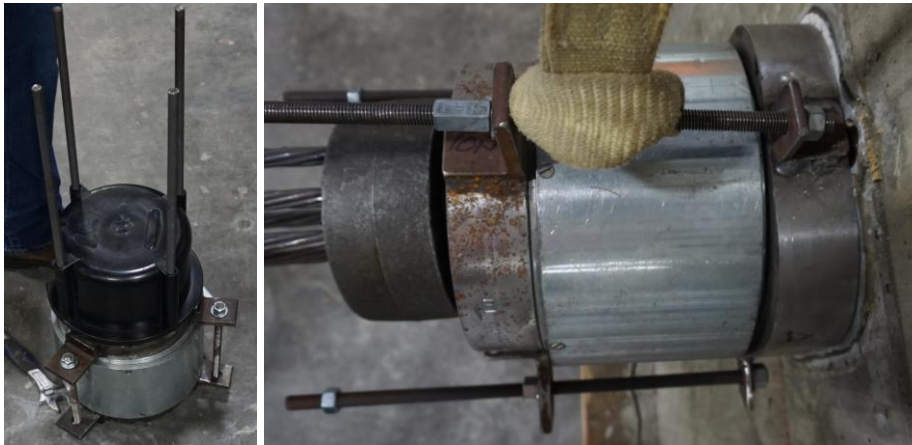


Figure 5-47 Geokon 850-kip hollow load cell assembly

Table 5-6 Summary of data acquisition during post-tensioning

Stage	Live End Jack Pressure	Mid Span Concrete Strain	Elongation Measurement	Dead End Tendon Force*
Before Jacking		X		X
5% P_{jack}	X	X		X
20% P_{jack}	X	X	X	X
40% P_{jack}	X	X	X	X
60% P_{jack}	X	X	X	X
80% P_{jack}	X	X	X	X
100% P_{jack}	X	X	X	X
After Jack Release		X		X

*Dead-end tendon force was collected continuously

5.5.3 Tendon Stressing Procedures

After the deck and end block concrete attained the minimum specified compressive strength (4.5 ksi and 6.5 ksi respectively), each tendon was stressed incrementally to a target prestress of $0.8f_{pu}$ or 46.9 kip/strand (Figure 5-48). Tendons were stressed to 5%, 20%, 40%, 60%, 80%, and 100% of the target tendon force with a pause at each increment. At 5% of the target tendon force the anchorage system was inspected to ensure proper alignment of the wedge plates and load cell. At 20% of the target force, strands were marked and elongation readings were taken at each subsequent 20% hold. The final elongation was taken at the 100% P_{jack} before the jack was released.

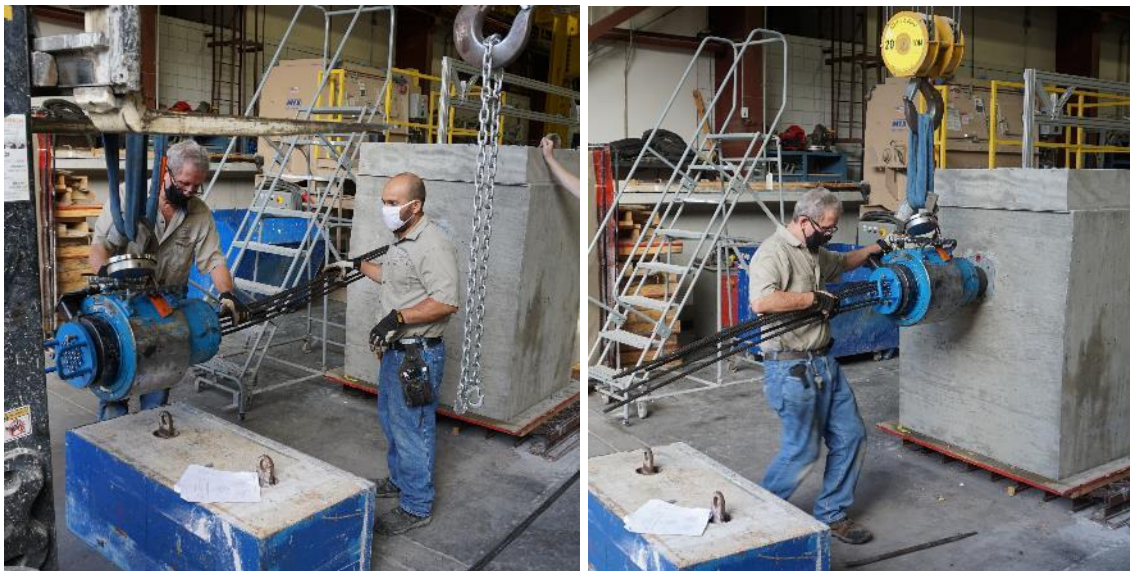


Figure 5-48 Multistrand jack installation for post-tensioning at live end

Theoretical elongations were calculated using equation 39 and actual elongations were calculated using equation 40. Actual elongations were calculated using an adjusted elongation

for 0% to 20% of P_{jack} and the measured elongations at 20%, 40%, 60%, 80% and 100% of P_{jack} before the jack was released. Table 5-7 shows the total tendon elongations measured during the stressing operation from 20% to 100% of the target prestress force.

$$\Delta_{theoretical} = \frac{P_{jack} * L_{tendon}}{A_{pt} * E_{ps}} \quad 39)$$

where:

- P_{jack} = Target prestress force
- L_{tendon} = Length of tendon
- A_{pt} = Total area of prestressing steel inside tendon
- E_{ps} = Modulus of elasticity of prestressing steel

$$\Delta_{actual} = \Delta_{adjusted} + (\Delta_{20\%-40\%} + \Delta_{40\%-60\%} + \Delta_{60\%-80\%} + \Delta_{80\%-100\%}) \quad 40)$$

where:

- $\Delta_{adjusted} = \frac{(\Delta_{20\%-40\%} + \Delta_{40\%-60\%} + \Delta_{60\%-80\%} + \Delta_{80\%-100\%})}{4}$
- $\Delta_{20\%-40\%}$ = Measured elongation from 20% to 40% P_{jack}
- $\Delta_{40\%-60\%}$ = Measured elongation from 40% to 60% P_{jack}
- $\Delta_{60\%-80\%}$ = Measured elongation from 60% to 80% P_{jack}
- $\Delta_{80\%-100\%}$ = Measured elongation from 80% to 100% P_{jack}

Table 5-7 Tendon elongations (in.)

Specimen	Theoretical Elongation	Actual Elongation	Difference
P34	5.1	4.9	3.5%
P41	5.1	4.8	6.5%
P50	5.1	5.5	7.3%
P50R	5.1	5.2	2.6%
N34	5.1	5.2	2.6%
N50	5.1	5.3	4.1%

An example of the tendon force vs. time is shown in Figure 5-49. The entire stressing operation required 30 minutes. Stressing was paused at each increment for approximately 2 minutes to take readings and to inspect the specimen. Detailed data of the jacking forces based on the calibrated pressure gauge provided with the hydraulic jack are shown in Table 5-8. The forces shown in the table were measured at the indicated fraction of the target jacking force (P_{jack}).

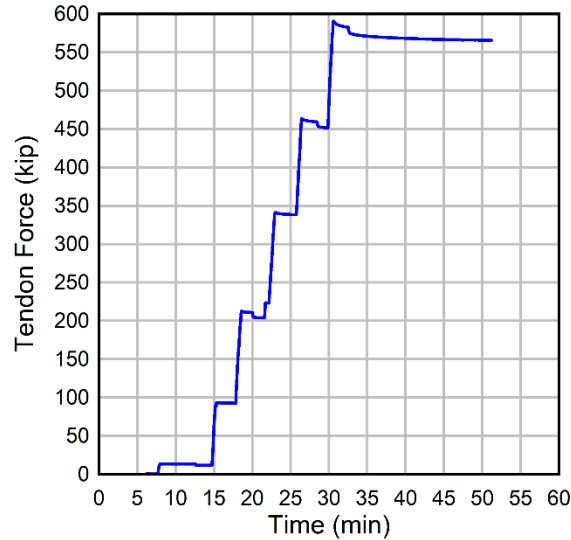


Figure 5-49 Plot of tendon force vs. time for specimen P50

Table 5-8 Tendon force measured at jack after each incremental increase in jacking force

Specimen	5% P_{jack} (kip)	20% P_{jack} (kip)	40% P_{jack} (kip)	60% P_{jack} (kip)	80% P_{jack} (kip)	100% P_{jack} (kip)
P34	9	50	92	138	187	232
P41	21	85	170	248	369	422
P50	28	112	225	338	450	560
P50R	28	111	224	338	448	564
N34	12	47	95	141	180	233
N50	28	114	223	338	450	563

5.5.4 Load Cell Calibration

Readings from the load cell during and following tendon stressing were outside the range of expected values. Geokon literature indicates that “...load cell readings can be affected profoundly by eccentric loading, uneven and/or warped bearing plates, or frictional effects on the bearing surfaces.” To accommodate field conditions, Geokon literature strongly suggests that the user calibrate their load cell under the conditions that it will be used. To address the unique conditions of the test setup used in this research, a calibration of the Geokon 850-kip hollow load cell was conducted against a Tovey 1000-kip load cell.

The push test was performed for various assembly configurations. The typical assembly consisted of (2) round steel ring plates stacked on top of each other, loaded against the wedge plate which was on top of the Geokon 850-kip hollow load cell (Figure 5-50). Some configurations did not include a wedge plate (Figure 5-51). A load offset of 0 in. represents the centered condition. The push test setup was intended to mimic the dead-end load cell assembly.

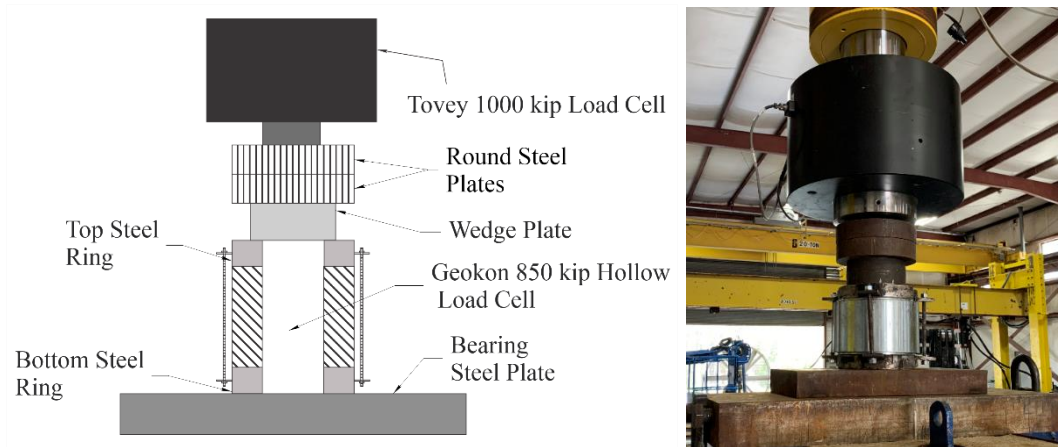


Figure 5-50 Push test assembly with wedge plate

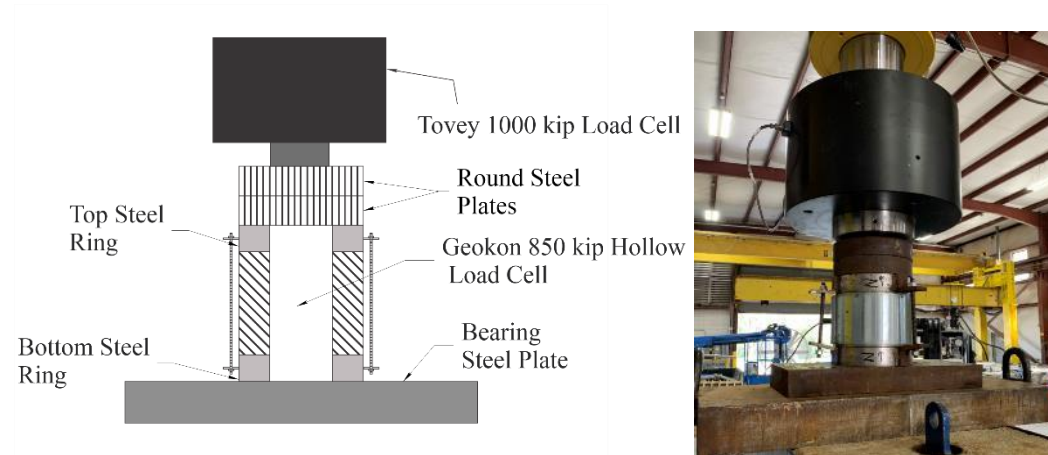


Figure 5-51 Push test assembly without wedge plate

The push test was done three times for each configuration to a load of 600 kip and the average of the three runs was used to determine the difference between the Geokon load cell and Tovey load cell. The verification showed that the Geokon load cell overestimated the load measured by the Tovey load cell between 3% and 19%. A summary of the push test configurations and difference in reading between the Geokon and Tovey load cell are shown below in Table 5-9. Configurations 10 to 13 used a square bottom ring plate with rounded corners to increase the bearing surface area between the load cell assembly and end block shown in Figure 5-52. The difference decreased by 5% to 6% on average for this configuration.

The results of the push test were used to adjust the readings from the Geokon 850-kip load cell for each specimen. The corresponding percent difference for the configuration that matched the specimen assembly was used to reduce the Geokon 850-kip load cell summarized in Table 5-10.

Table 5-9 Summary of push test configurations and results

Configuration number	Load cell designation	Load offset (in.)	Wedge plate	Ring plate thickness	Difference (%)
1	10	0	Yes	2 in. x 9¼ in.	19
2	10	5/16	Yes	2 in. x 9¼ in.	18
3	10	0	No	2 in. x 9¼ in.	15
4	11	0	yes	2 in. x 9¼ in.	16
5	11	0	no	2 in. x 9¼ in.	13
6	10	0	yes	1½ in. x 9¼ in.	12
7	10	0	no	1½ in. x 9¼ in.	6
8	11	0	Yes	1½ in. x 9¼ in.	9
9	11	0	No	1½ in. x 9¼ in.	3
10	10	0	Yes	2 in. x 9¼ in.	15
11	10	0	No	2 in. x 9¼ in.	9
12	11	0	Yes	2 in. x 9¼ in.	10
13	11	0	No	2 in. x 9¼ in.	5



Figure 5-52 Load cell assembly with square bottom plate.

Table 5-10 Dead-end load cell reading before and after calibration

Specimen	Calibration Number	Dead-end force before calibration		Dead-end force after calibration	
		Before Release (kip)	After Release (kip)	Before Release (kip)	After Release (kip)
P34	8	221	218	201	199
P41	6	456	439	402	386
P50	8	589	567	537	517
P50R	1	642	619	520	502
N34	10	261	257	223	220
N50	12	577	564	520	508

5.6 Specimen Test Procedure

Following completion of construction and installation of instrumentation, specimens were moved into the loading frame for load testing. Specimens were tested incrementally by applying load close to one support and then moving the load to the opposite end of the specimen for an additional test. This provided two tests per specimen. For specimens containing ducts the end containing two ducts were tested first followed by the end with a single duct.

Nomenclature for each load test is shown in Figure 5-53. Table 5-11 shows the test dates. Specimens were designated by the specimen name followed by 1 or 2 indicating the number of ducts at that end. P00 was a solid web specimen with no ducts, which resulted in identical characteristics at each end of the specimen. Consequently, labels P00-1 and P00-2 were arbitrarily assigned to each end of the specimen.

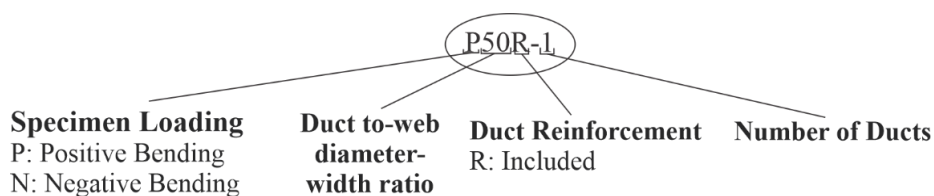


Figure 5-53 Nomenclature for positive and negative bending shear specimens containing ducts

Table 5-11 Summary of specimen test dates and duct information

Designation	Duct size (in.)	Duct reinforcement	Number of ducts	Test date
P00-1	No duct	no	0	04-01-2021
P00-2	No duct	no	0	04-09-2021
P34-1	2.375	no	1	11-09-2020
P34-2	2.375	no	2	11-04-2020
P41-1	2.875	no	1	11-23-2020
P41-2	2.875	no	2	11-16-2020
P50-1	3.5	no	1	12-03-2020
P50-2	3.5	no	2	12-02-2020
P50R-1	3.5	yes	1	03-04-2021
P50R-2	3.5	yes	2	03-01-2021
N34-1	2.375	no	1	06-15-2021
N34-2	2.375	no	2	05-28-2021
N50-1	3.5	no	1	06-18-2021
N50-2	3.5	no	2	05-25-2021

Once the specimens were in place, load was increased at a load rate of 0.25 kip/sec. Load was increased to specified load levels and held. At each load hold, specimens were inspected for cracks. If found, cracks were marked to enhance visibility. Once load exceeded levels that were deemed safe for marking cracks, loading was continued until the test was terminated. The first test on each specimen was terminated prior to destruction of the specimen to prevent undue damage from occurring at the opposite end of the girder. This procedure was followed to ensure

that the second test on the specimen would not be significantly affected by the damage caused by the first test.

Specimens were tested in three-point bending using a shear-span-to-depth ratio of 2.5. Specimens will be tested in positive and negative bending as shown in Figure 5-5. Each specimen will be tested at each end to allow comparison of one-duct vs. two-duct configuration.

5.7 Strength Test Results

The following section contains results from the strength tests performed on FIB-54 specimens. Strength test results are presented in terms of superimposed shear, which is the shear due to the applied load and does not include the self-weight of the specimen.

Displacement results are presented as the vertical displacement occurring at the load point. The displacement at the load point was taken as the average of the two displacements measured by the laser transducers at the load point. The effect of the bearing pad was removed from the displacement readings.

Specimens were tested at the FDOT Structures Research Center in Tallahassee, FL. Specimens were placed in between a reaction frame supported on a 24 in. x 10 in. x 2 in. composite elastomeric bearing pad. Load was applied using a 1000-kip Enerpac actuator at a rate 0.25 kip/sec. Load was held at anticipated load that would cause web shear cracks and cracks were visually inspected and marked. Loading was then continued at a rate of 0.25 kip/sec until failure but pausing every 20 kips to inspect cracks and crack growth. The test was terminated once a shear failure or compressive failure of the concrete occurred.

Continuous readings of displacements, strains and load were taken during each shear test. Vibrating wire gauge readings were taken before the test to determine the stress in the strands at the time of loadings. Concrete cylinders corresponding to each specimen were tested to determine the compressive strength at the time of testing.

5.7.1 Specimen P00

The primary purpose of this specimen was to investigate the shear behavior of a control specimen that does not contain a post-tensioning tendon. The specimen was simply supported and intended to replicate the positive bending region of a continuous spliced girder bridge. The specimen was tested at both ends.

The specimen was loaded, and applied load was held at 200, 240, 280, and 320 kip. Visible cracks were marked and identified. The first full-depth web cracks were observed at shear forces of 200 kip and 210 kip for tests P00-1 and P00-2, respectively. Loading continued until the peak shear of 483 kip and 522 kip for tests P00-1 and P00-2, respectively. The displacement at peak shear force was 0.65 in. and 0.94 in. for tests P00-1 and P00-2, respectively. Loading was stopped at end 1 once any web spalling occurred to preserve end 2 for testing. Phase 1 solid specimen, SS4, experienced a sudden web crushing failure immediately after the peak load. It was important to end the test early due to the nature of the failure observed in phase 1. The loading was stopped at end 2 once a significant amount of web spalling occurred.

Shear force versus displacement plots are shown in Figure 5-54 for specimen P00. Crack figures and specimen images after shear strength test are shown in Figure 5-55, and Figure 5-56 respectively.

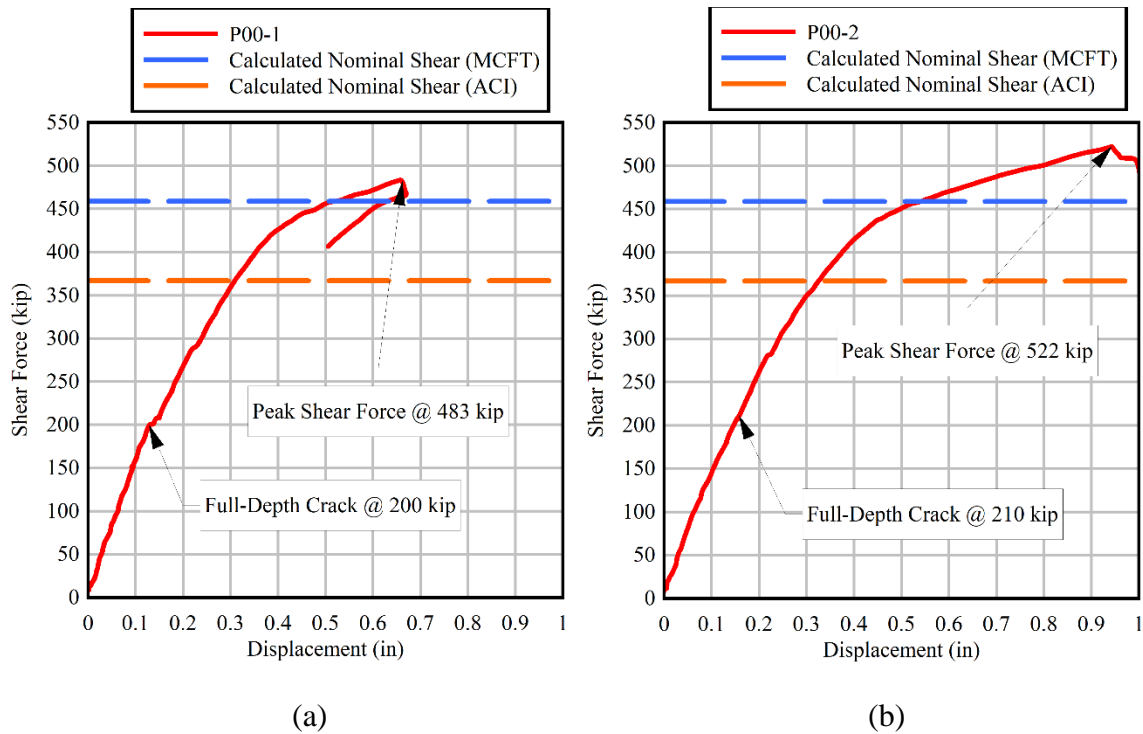
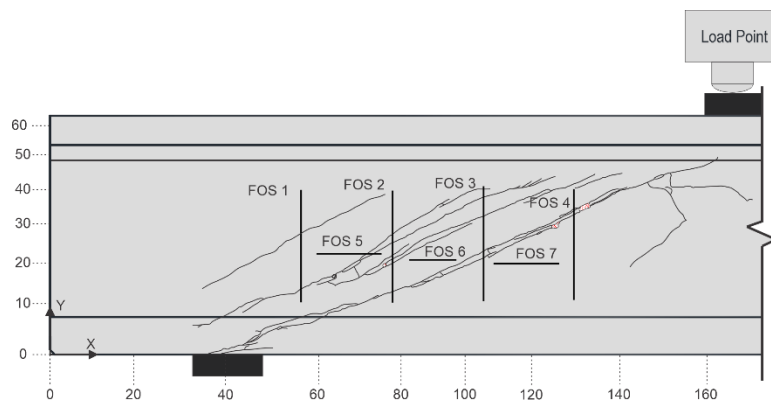
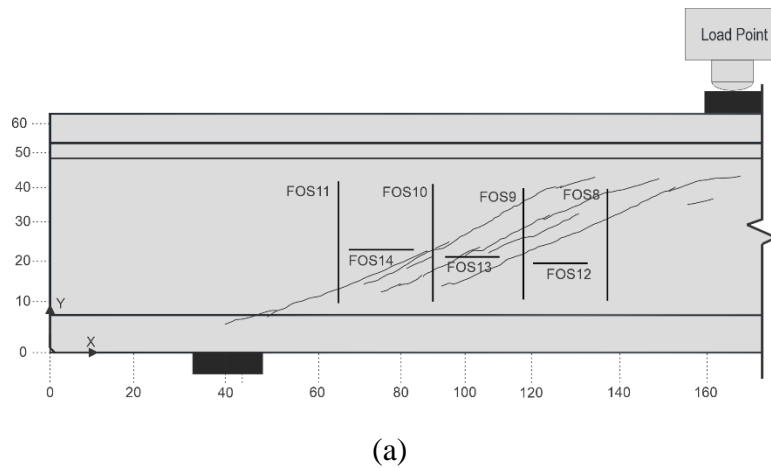


Figure 5-54 Specimen P00 shear force vs. displacement plot (a) P00-1 (b) P00-2



(b)

Figure 5-55 Specimen P00 crack pattern for test (a) P00-1 (b) P00-2



Figure 5-56 Concrete spalling at web after peak shear force and unloading (a) P00-1 (b) P00-2.

5.7.2 Specimen P34

The primary purpose of this specimen was to investigate the effect of varying duct size on the shear behavior of a girder containing a post-tensioning duct, with five strands stressed to 80% f_{pu} . The specimen was simply supported and intended to replicate the positive bending region of a continuous spliced girder bridge. The specimen was tested at both ends: one containing a single duct and the other test region containing two ducts.

During testing applied load was held at 120, 140, 160, and 180 kip any observed cracks were marked and identified. Cracks near the duct location were observed at a shear force of 188 kip at end 1 and 150 kip at end 2. The first large web shear crack was observed at 250 kip for P34-1 and 236 kip for P34-2. Loading continued until the peak load 512 kip and 506 kip for tests P34-1 and P34-2, respectively. The displacement at peak shear force was 0.60 in. and 0.55 in. for tests P34-1 and P34-2 respectively. Loading was stopped for test P34-2 once any web spalling occurred to preserve the specimen for test P34-1. The loading was stopped at end 1 once a significant amount of web spalling occurred.

Shear force versus displacement plots are shown in Figure 5-57 for specimen P34. Crack figures and specimen images after shear strength test are shown in Figure 5-58, and Figure 5-59 respectively.

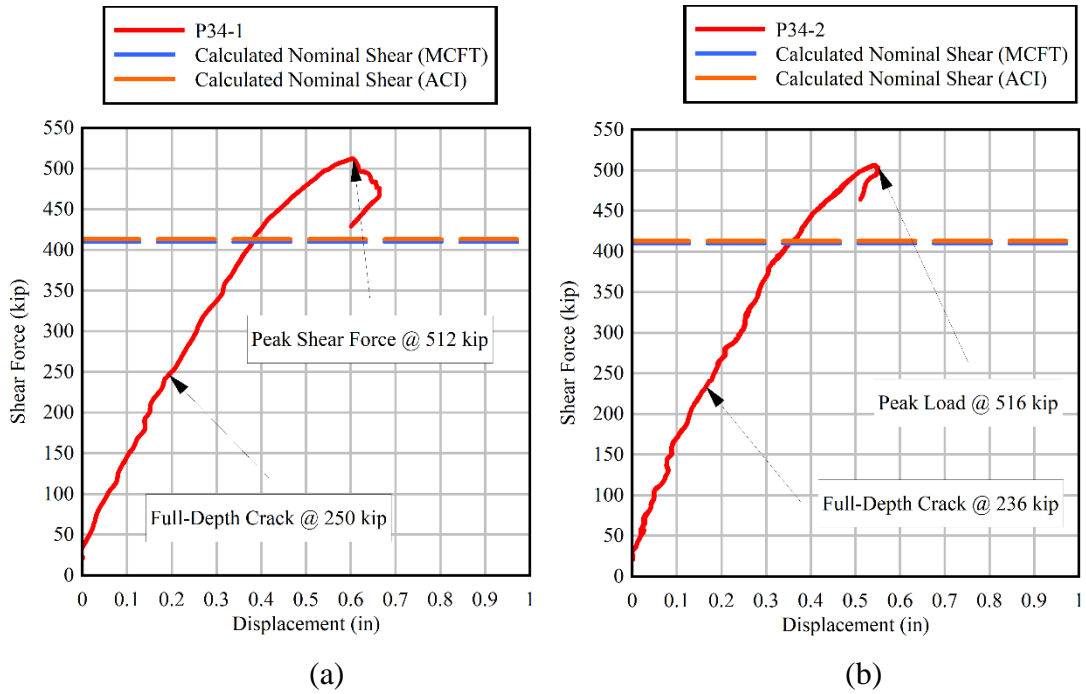
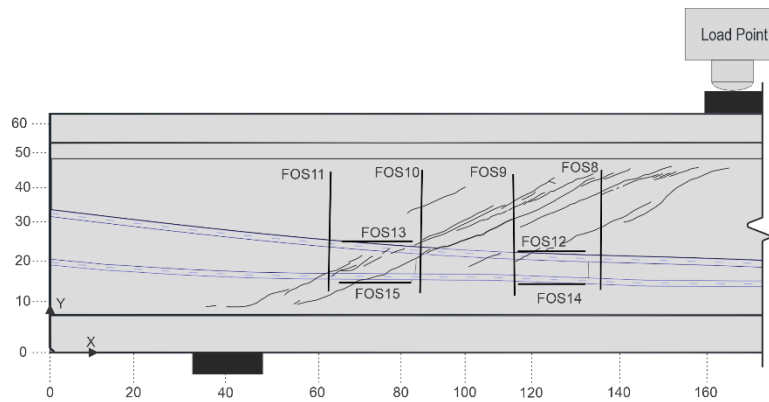
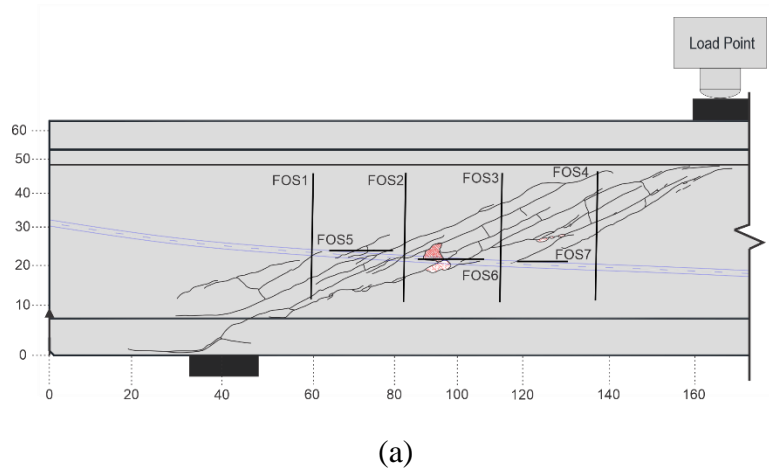


Figure 5-57 Specimen P34 shear force vs. displacement plot (a) P34-1 (b) P34-2



(b)

Figure 5-58 Specimen P34 crack pattern for test (a) P34-1 (b) P34-2



(a)

(b)

Figure 5-59 Concrete spalling at web after peak shear force and unloading (a) P34-1 (b) P34-2.

5.7.3 Specimen P41

The primary purpose of this specimen was to investigate the effect of varying duct size on the shear behavior of a girder containing a post-tensioning duct, with nine strands stressed to 80% f_{pu} . The specimen was simply supported and intended to replicate the positive bending region of a continuous spliced girder bridge. The specimen was tested at both ends: one containing a single duct and the other test region containing two ducts.

The specimen was loaded, and applied load was held at 160, 200, 240, and 280 kip. Any observed cracks were marked and identified. Cracks near the duct location were observed at a shear force of 188 kip and 198 kip for tests P41-1 and P41-2, respectively. The first full-depth web cracks were observed at shear forces of 236 kip and 290 kip for tests P41-1 and P41-2, respectively. Loading continued until the peak shear of 516 kip and 545 kip for tests P41-1 and P41-2, respectively. The displacement at peak shear force was 0.52 in. and 0.54 in. for tests P41-1 and P41-2 respectively. Loading was stopped at end 2 once any web spalling occurred. The loading was stopped at end 1 once a significant amount of web spalling occurred near the duct location.

Shear force versus displacement plots are shown in Figure 5-60 for specimen P41. Crack figures and specimen images after shear strength test are shown in Figure 5-61, and Figure 5-62 respectively.

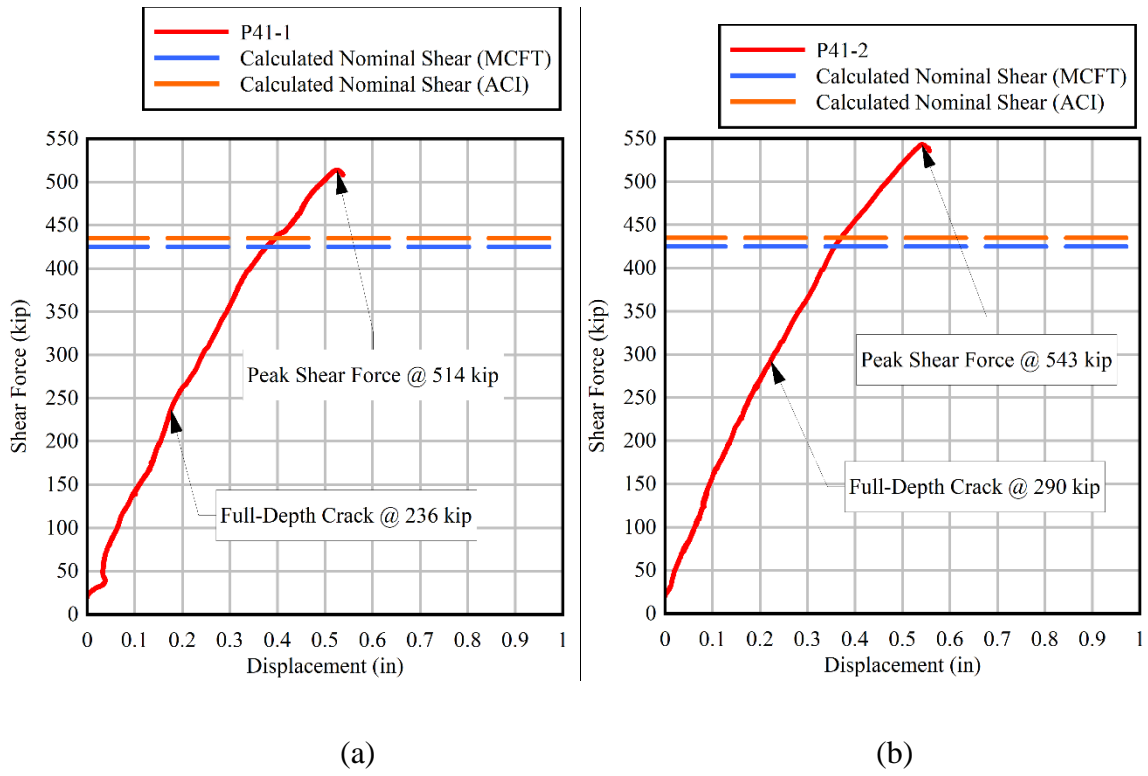
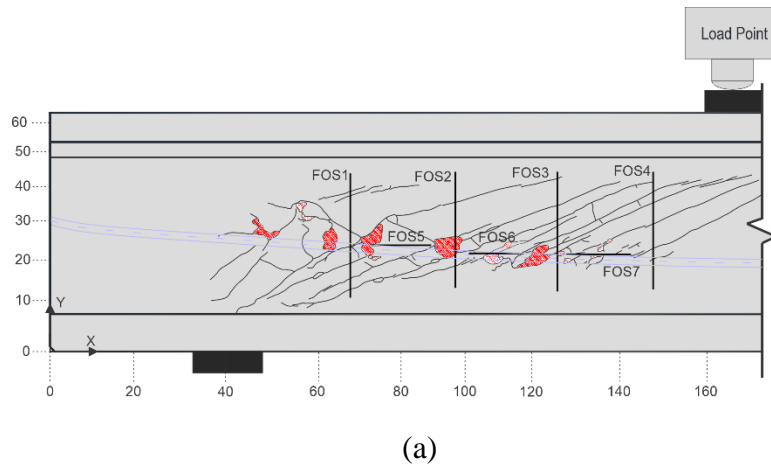
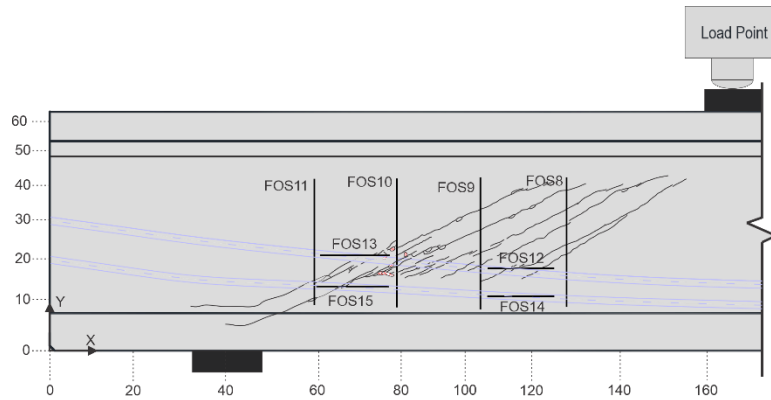


Figure 5-60 Specimen P41 shear force vs. displacement plot (a) P41-1 (b) P41-2





(b)

Figure 5-61 Specimen P41 crack pattern for test (a) P41-1 (b) P41-2



(a)

(b)

Figure 5-62 Concrete spalling at web after peak shear force and unloading (a) P41-1 (b) P41-2.

5.7.4 Specimen P50

The primary purpose of this specimen was to investigate the effect of varying duct size on the shear behavior of a girder containing a post-tensioning duct, with twelve strands stressed to 80% f_{pu} . The specimen was simply supported and intended to replicate the positive bending region of a continuous spliced girder bridge. The specimen was tested at both ends: one containing a single duct and the other test region containing two ducts.

The specimen was loaded, and applied load was held at 80, 120, 160, 200, 240, and 280 kip any observed cracks were marked and identified. Cracks near the duct location were observed at a shear force 150 kip for tests P50-1 and P50-2. The first full-depth web cracks were observed at shear forces of 307 kip and 286 kip for tests P50-1 and P50-2, respectively. Loading continued until the peak shear of 470 kip and 473 kip for tests P50-1 and P50-2, respectively. The displacement at peak shear force was 0.42 in. for both tests P50-1 and P50-2. Loading was stopped at end 2 once any web spalling occurred. The loading was stopped at end 1 once a significant amount of web spalling occurred.

Shear force versus displacement plots are shown in Figure 5-63 for specimen P50. Crack figures and specimen images after shear strength test are shown in Figure 5-64, and Figure 5-65 respectively.

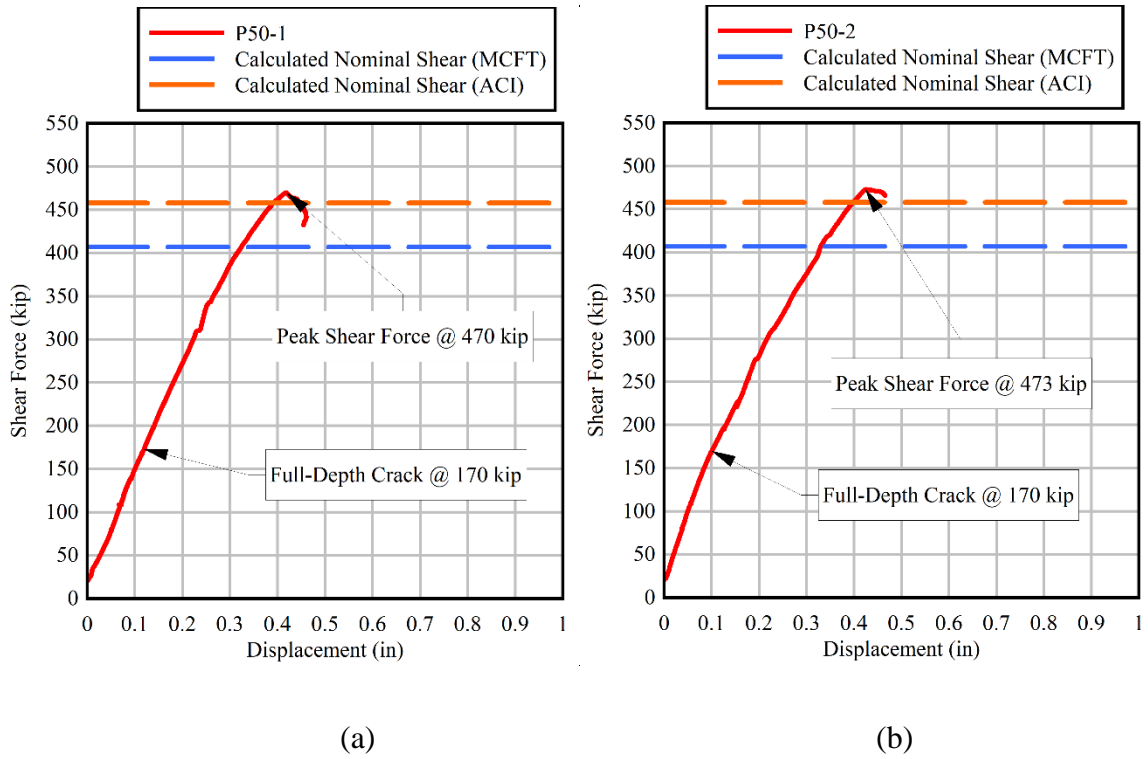
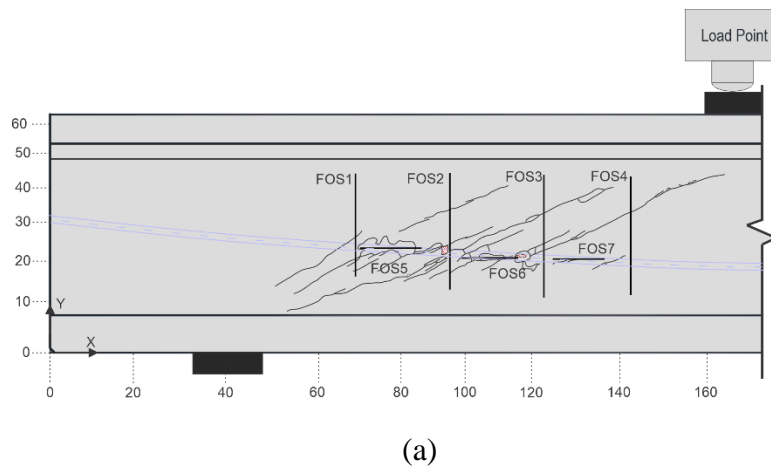
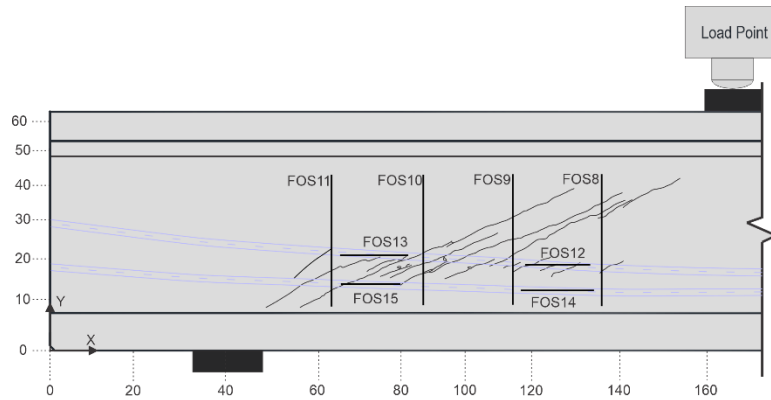


Figure 5-63 Specimen P50 shear force vs. displacement plot (a) P50-1 (b) P50-2





(b)

Figure 5-64 Specimen P50 crack pattern for test (a) P50-1 (b) P50-2



(a)

(b)

Figure 5-65 Concrete spalling at web after peak shear force and unloading (a) P50-1 (b) P50-2.

5.7.5 Specimen P50R

The primary purpose of this specimen was to investigate the effect of varying duct size on the shear behavior of a girder containing a post-tensioning duct, with twelve strands stressed to 80% f_{pu} , and the effect that including SDG reinforcement has on shear behavior. The specimen was simply supported and intended to replicate the positive bending region of a continuous spliced girder bridge. The specimen was tested at both ends: one containing a single duct and the other test region containing two ducts.

The specimen was loaded, and applied load was held at 80, 120, 160, 200, 240, and 280 kip any observed cracks were marked and identified. Cracks near the duct location were observed at a shear force 150 kip for tests P50R-1 and P50R-2. The first full-depth web cracks were observed at shear forces of 325 kip and 300 kip for tests P50R-1 and P50R-2, respectively. Loading continued until the peak shear of 533 kip and 536 kip for tests P50R-1 and P50R-2, respectively. The displacement at peak shear force was 0.49 in. and 0.47 in. for tests P50R-1 and P50R-2 respectively. Loading was stopped at end 2 once any web spalling occurred. The loading was stopped at end 1 once a significant amount of web spalling occurred.

Shear force versus displacement plots are shown in Figure 5-66 for specimen P50R. Crack figures and specimen images after shear strength test are shown in Figure 5-67, and Figure 5-68 respectively.

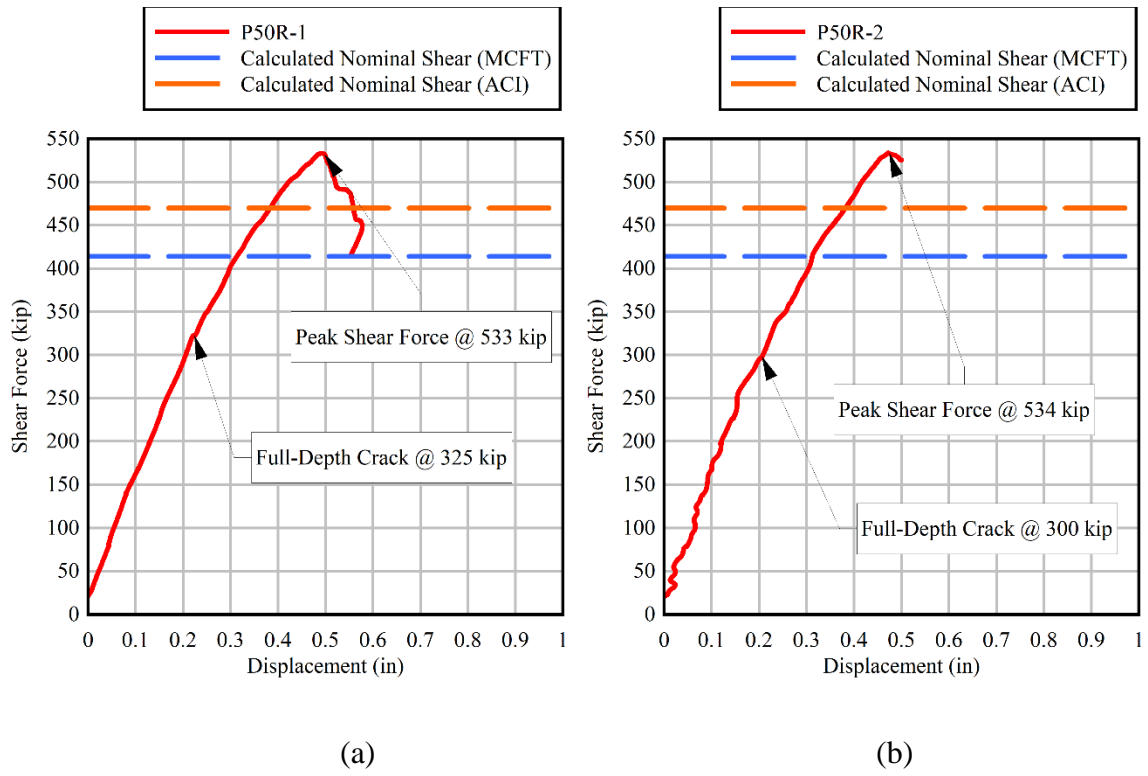
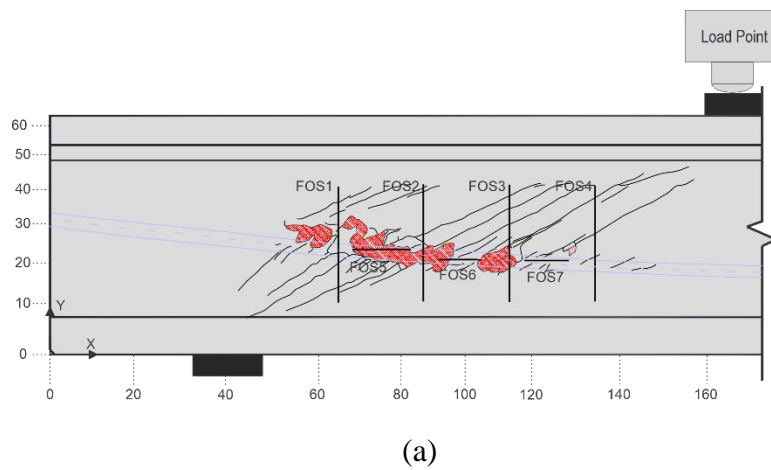
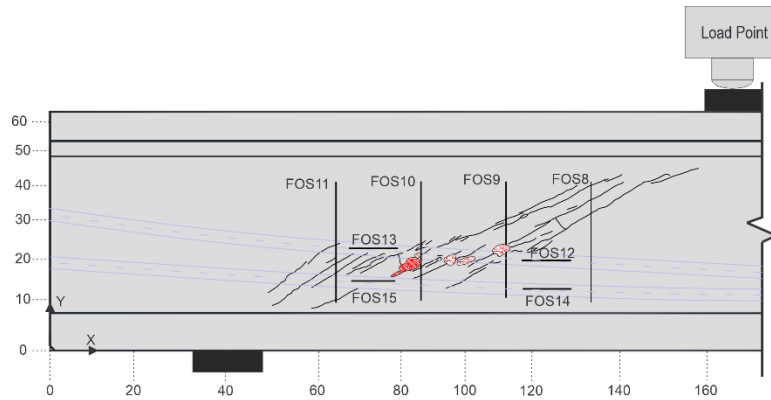


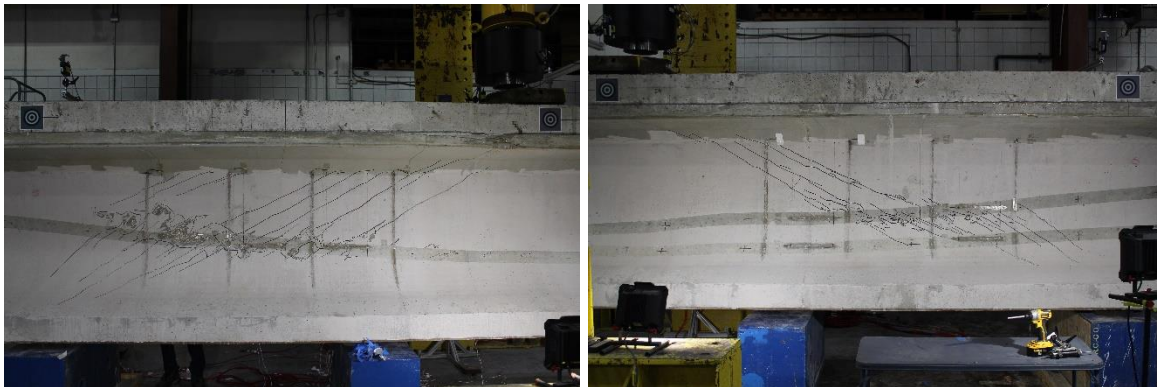
Figure 5-66 Specimen P50R shear force vs. displacement plot (a) P50R-1 (b) P50R-2





(b)

Figure 5-67 Specimen P50R crack pattern for test (a) P50R-1 (b) P50R-2



(a)

(b)

Figure 5-68 Concrete spalling at web after peak shear force and unloading (a) P50R-1 (b) P50R-2.

5.7.6 Specimen N34

The primary purpose of this specimen was to investigate the effect of varying duct size on the shear behavior of a girder containing a post-tensioning duct, with five strands stressed to 80% f_{pu} . The specimen replicates the negative bending region at the interior pier of a continuous spliced girder bridge with high shear. The specimen was tested at both ends: one containing a single duct and the other test region containing two ducts.

The specimen was loaded, and applied load was held at 120, 160, and 200 kip and any observed cracks were marked and identified. Cracks near the duct location were observed at a shear force 150 kip for tests N34-1 and N34-2. The first full-depth web cracks were observed at shear forces of 205 kip and 210 kip for tests N34-1 and N34-2, respectively. Loading continued until the peak shear of 382 kip and 290 kip for tests N34-1 and N34-2, respectively. The displacement at peak shear force was 4.34 in. and 1.28 in. for tests N34-1 and N34-2 respectively. Loading was stopped at end 2 once a drop in force occurred during loading. The loading was stopped at end 1 once spalling occurred at the near support.

Shear force versus displacement plots are shown in Figure 5-69 for specimen N34. Crack figures and specimen images after shear strength test are shown in Figure 5-70, and Figure 5-71 respectively.

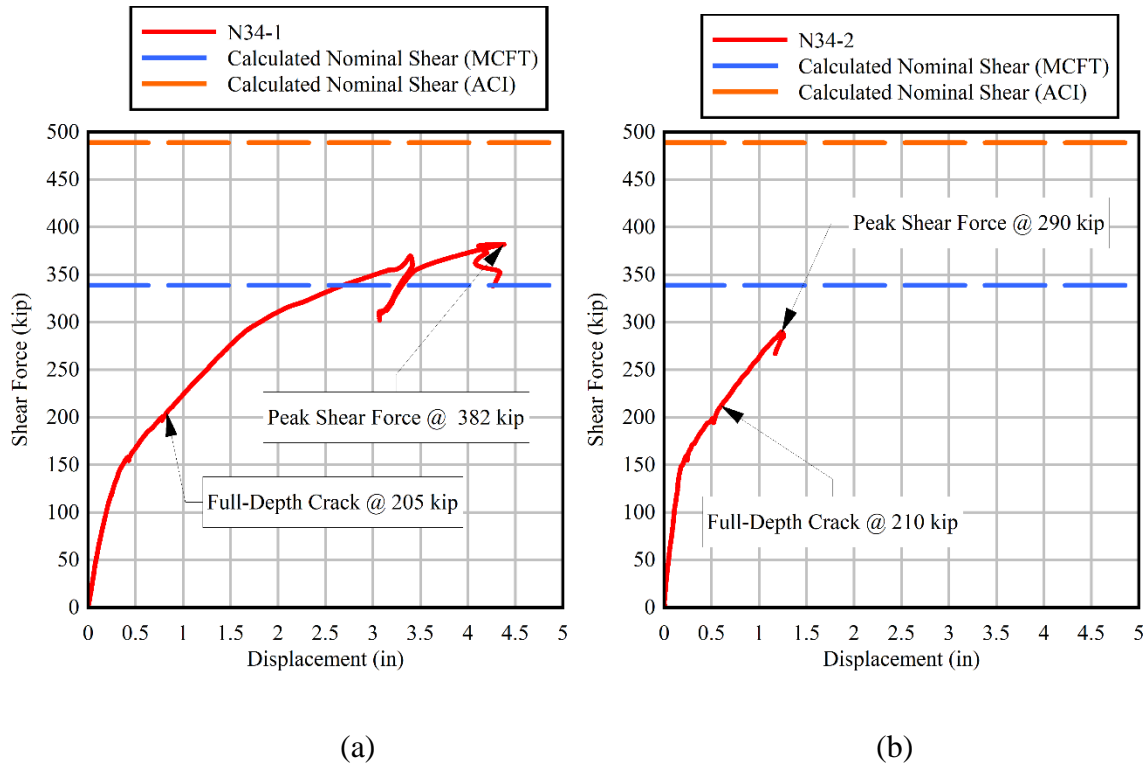
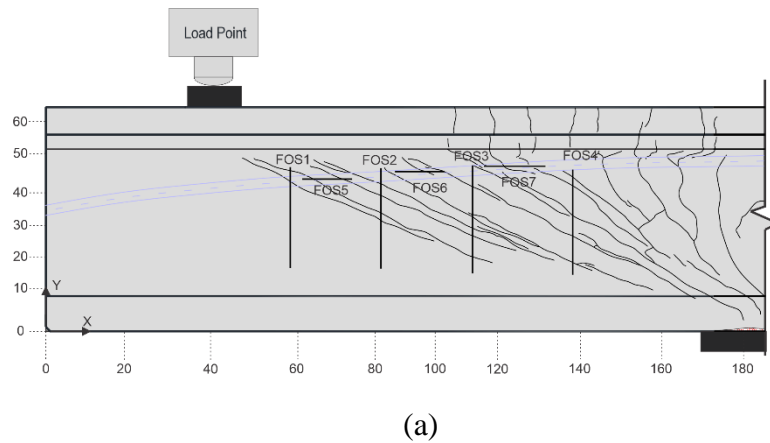
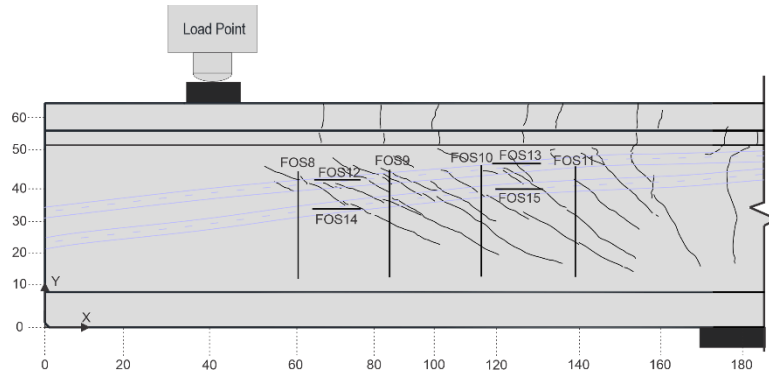


Figure 5-69 Specimen N34 shear force vs. displacement plot (a) N34-1 (b) N34-2





(b)

Figure 5-70 Specimen N34 crack pattern for test (a) N34-1 (b) N34-2



(a)

(b)

Figure 5-71 Concrete spalling at web after peak shear force and unloading (a) N34-1 (b) N34-2.

5.7.7 Specimen N50

The primary purpose of this specimen was to investigate the effect of varying duct size on the shear behavior of a girder containing a post-tensioning duct, with twelve strands stressed to 80% f_{pu} . The specimen replicates the negative bending region at the interior pier of a continuous spliced girder bridge with high shear. The specimen was tested at both ends: one containing a single duct and the other test region containing two ducts.

The specimen was loaded, and applied load was held at 120, 160, and 200 kip any observed cracks were marked and identified. Cracks near the duct location were observed at an applied load of 150 kip for tests N50-1 and 140 kip for tests N50-2. The first full-depth web cracks were observed at shear forces of 220 kip and 250 kip for tests N50-1 and N50-2, respectively. Loading continued until the peak shear of 434 kip and 399 kip for tests N50-1 and N50-2, respectively. The displacement at peak shear force was 2.75 in. and 1.44 in. for tests N34-1 and N34-2 respectively. Loading was stopped at end 2 once any web spalling occurred. The loading was stopped at end 1 once a compression failure occurred at the support.

Shear force versus displacement plots are shown in Figure 5-72 for specimen N50. Crack figures and specimen images after shear strength test are shown in Figure 5-73, and Figure 5-74 respectively.

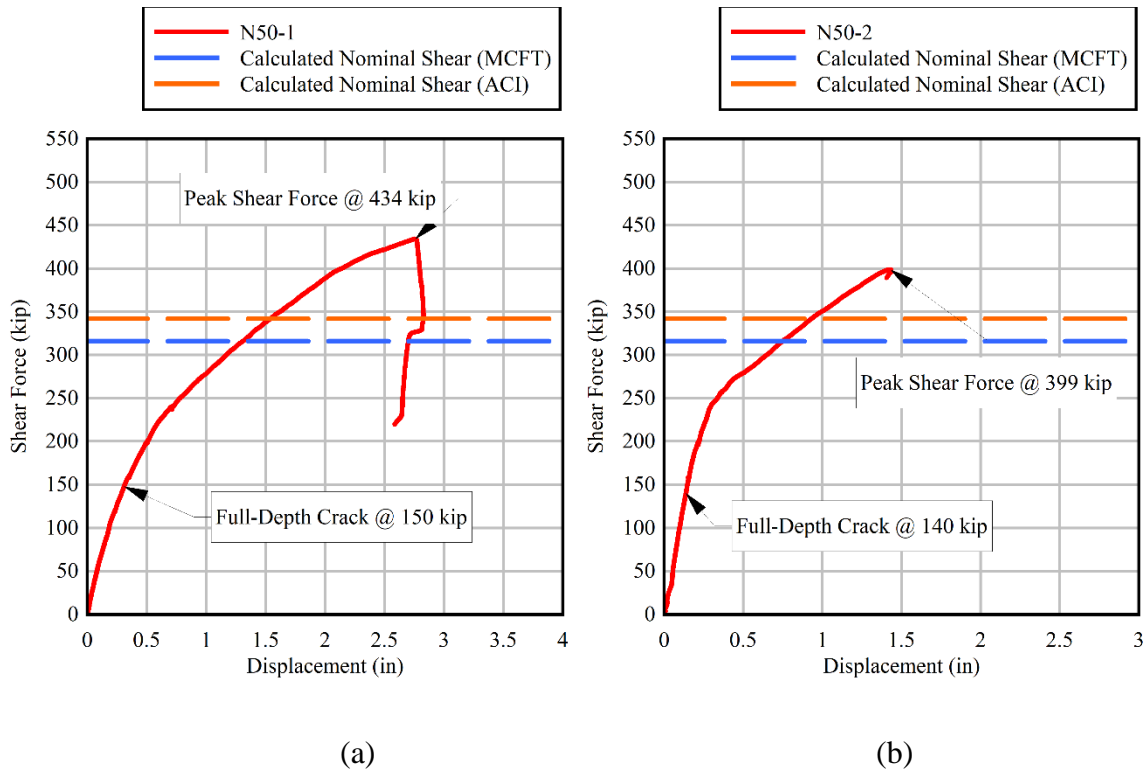
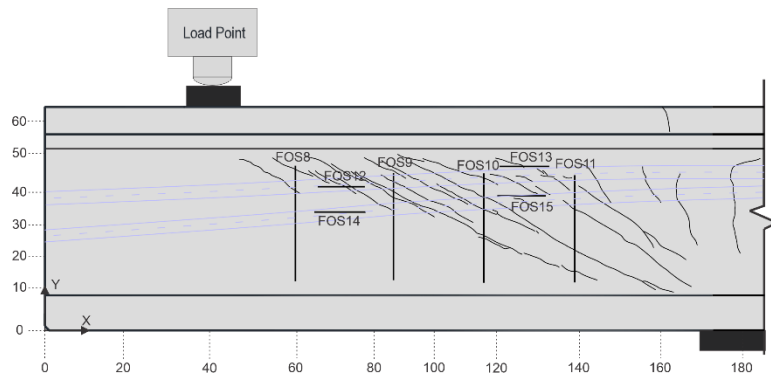
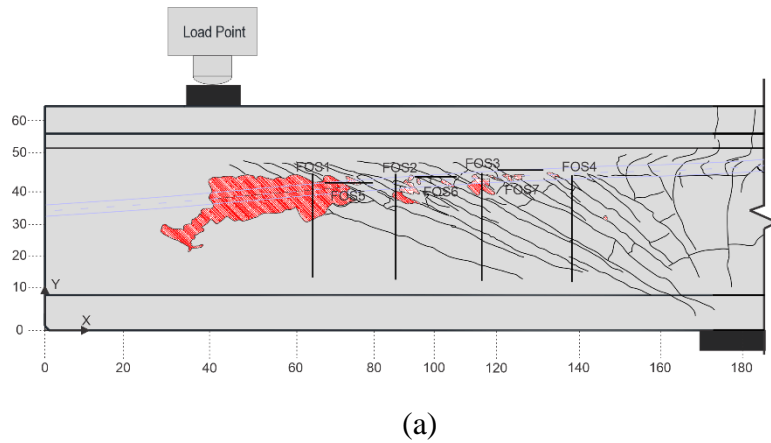


Figure 5-72 Specimen N50 shear force vs. displacement plot (a) N50-1 (b) N50-2



(b)

Figure 5-73 Specimen N50 crack pattern for test (a) N50-1 (b) N50-2



Figure 5-74 Concrete spalling at web after peak shear force and unloading (a) N50-1 (b) N50-2.

5.8 Phase 2 Significant Results

The key findings from the strength tests performed on FIB-54 specimens can be summarized as follows:

- Localized diagonal cracking near the duct location occurred for specimens containing post-tensioning ducts followed by diagonal full-depth web cracks.
- Specimens containing post-tensioning ducts experienced a web crushing failure at the duct location.
- Generally, cracking occurred at similar shear forces for both test regions of each specimen regardless of the quantity of ducts. Localized cracking occurred at a slightly lower shear force for the final test region of a specimen. Damage from the previous test typically caused the localized cracking to occur earlier.
- Positive bending specimens containing two ducts experienced localized cracking near the top duct location but no localized cracking at the bottom duct. This occurred due to the bottom duct proximity to the bottom flange where the section was thicker. Negative bending specimens experienced localized cracking simultaneously for both ducts for tests containing two ducts.

6 Strength and Serviceability Analysis

In general, the shear strength of specimens with ungrouted ducts was reduced when compared to that of specimens with solid webs. Furthermore, fiber optic strain data indicated that short, localized cracks formed in the concrete cover over the ungrouted ducts at lower applied shear than full-depth web cracks that typically form in solid webs. Consequently, it may be advisable to limit both strength and serviceability limit states to ensure adequate safety and service life.

Further analysis is provided on the service and ultimate capacity behavior of the phase 1 and 2 specimens in this chapter. In addition, test results from Moore et al. (2015) were included in the analysis to provide some perspective related to grouted ducts. The results of all three sets of data were then compared with calculations using design specification requirements from AASHTO LRFD Bridge Design Specifications, 9th Edition (AASHTO, 2020), and ACI 318-19 (ACI Committee 318, 2019). Based on the analysis of the results, recommendations were made for calculating shear capacity and checking serviceability of girder webs containing ungrouted ducts.

6.1 Behavior at Service Load

Specimens that contained ducts exhibited localized cracking at the duct as load was increased; this was followed by the formation of full-depth web cracks as the load was increased further. Localized cracks were characterized by small diagonal cracks in the concrete cover over ducts that were oriented at angles ranging between 22 deg. and 26 deg. from horizontal (Figure 6-1). It was observed that as the duct diameter increased, the quantity of localized cracks would increase along the length of the duct. Localized cracking typically occurred between 20 and 40 percent of the peak shear force and would occur at a relatively lower load as the duct-diameter-to-web-width ratio increased. In addition, based on visual observations, initial localized cracks occurred at lower loads on the specimens with larger duct diameters; the initial length was also shorter than those on the specimens with smaller duct diameters. This was thought to occur due to the locally high principal tensile stresses in the relatively narrower concrete cover over the larger ducts. But because the cracks formed at lower applied loads, the principal tensile stresses were not yet elevated enough to cause the cracks to extend into the web away from the duct. This was visually observed in the initial cracking in both phase 1 and phase 2 testing.

Full-depth web cracks typically extended over the height of the web between the top and bottom flange and generally formed as extensions of the localized cracks that had already formed at lower load levels (Figure 6-2). Web cracks were oriented at angles ranging between 22 deg. and 28 deg. from horizontal. Web cracks occurred between 50 and 70 percent of the peak shear force. Specimens without ducts had fewer initial full-depth web cracks compared to specimens with ducts.

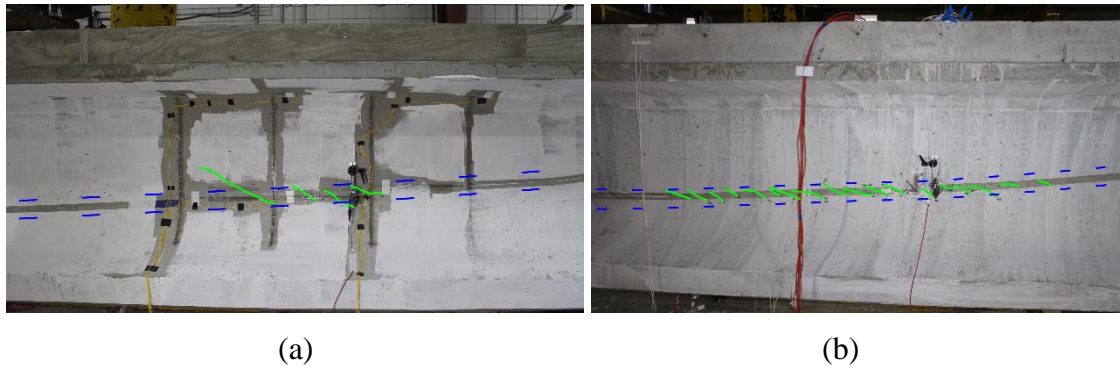


Figure 6-1 Localized cracks in concrete cover over duct for specimen with duct-diameter-to-web-width ratio (a) 0.34 (b) 0.50

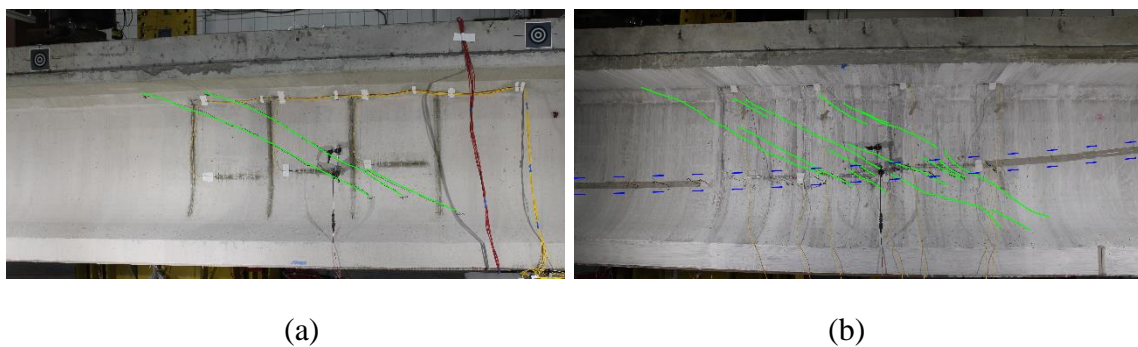


Figure 6-2 Full-depth web cracks (a) no duct specimen (b) specimen with duct

As indicated in AASHTO LRFD, 9th Edition (§5.9.2.3.3) for post-tensioned girders with internal and/or external tendons, principal tensile stresses are limited under the Service III limit state. The principal tensile stresses were to be determined using the combination of axial and shear stress that maximize the principal tensile stress. For precast sections made composite with a cast-in-place deck, the principal tensile stress at both the noncomposite and composite neutral axes should be checked using the shear stress and axial stress at each location.

Principal tensile stresses were calculated using Mohr's circle analysis for phase 1 and phase 2 and Moore et al. (Moore et al., 2015) shear tests were calculated at both the composite and noncomposite neutral axis. The principal stresses were calculated at the applied shear required to form the first and web crack. Crack formation was detected using data from rosette strain gauges and visual observations for phase 1 specimens. Phase 2 specimens used fiber optic sensor data, rosette strain data and visual observations to identify duct and web cracks. Fiber optic sensors measured strain at discrete locations along the length of the fiber sensor while rosette strain gauges measured strain at a single location. Figure 6-3 shows strain readings along fiber optic sensors at a shear force when the first crack was detected. The sharp rise in strain along the height indicates where initial cracks occurred and match with visual observations shown in Figure 6-4. Fiber optic sensors were able to detect cracks before they were observed visually and gave a specific load at which the crack formed.

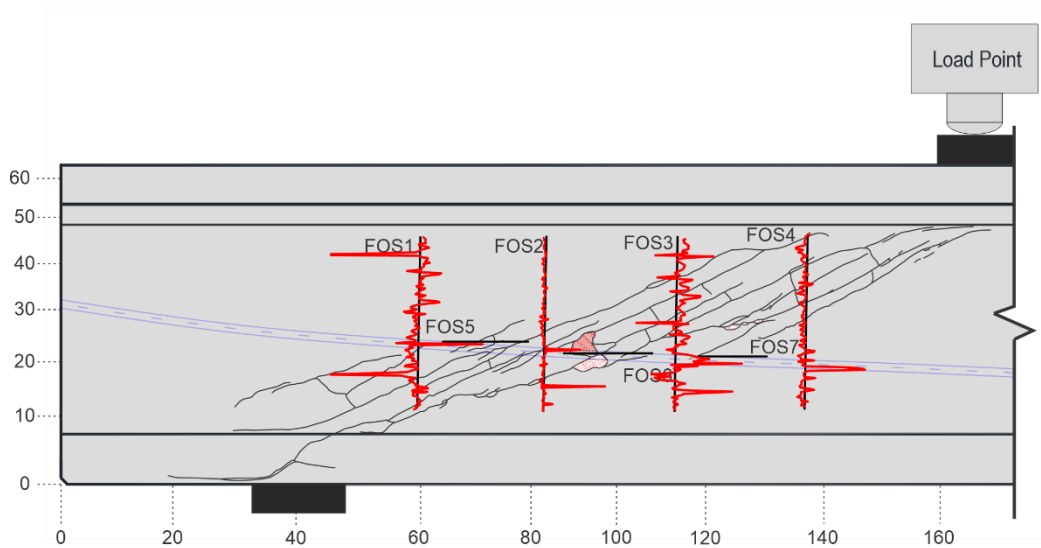


Figure 6-3 Fiber optic sensor strain measurements at first cracks during loading

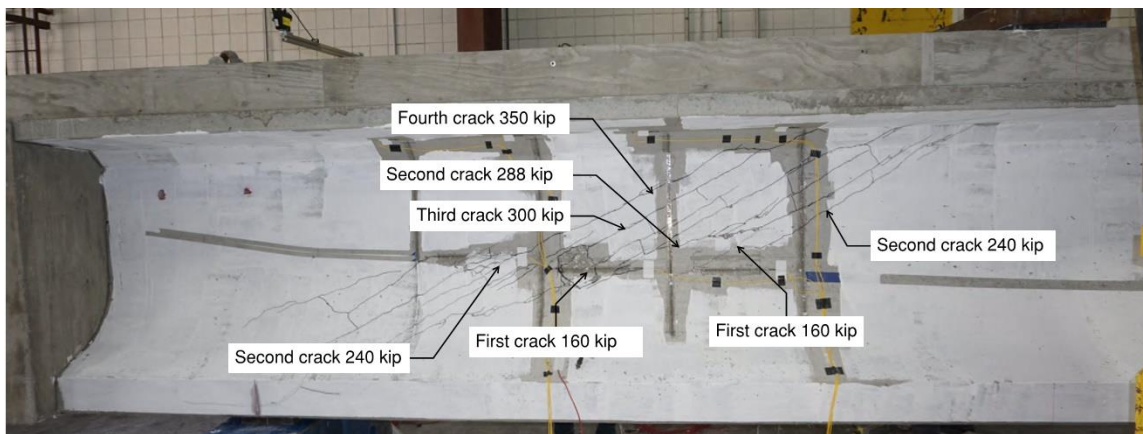


Figure 6-4 Crack identification within web of shear specimen

Principal tensile stresses were also calculated at the duct location where localized cracking was first detected by the fiber optic sensors to determine the shear force when cracking occurred as described previously. Locations as shown in Figure 6-5 were checked to find the maximum principal tensile stresses during loading. When calculating principal tensile stresses at the neutral axis for the composite and noncomposite section the gross web width was used. For principal tensile stress calculations at the centerline of duct, an effective web width equal to the gross web width minus the duct diameter was used for ungrouted ducts while the gross web width was used for grouted ducts. An effective web width was used to account for the “weakened” area at the duct location caused by the increased tensile stresses due to the deviation of compressive stresses from applied loads around the duct shown in Figure 6-6. The results were normalized against the square root of the concrete compressive strength.

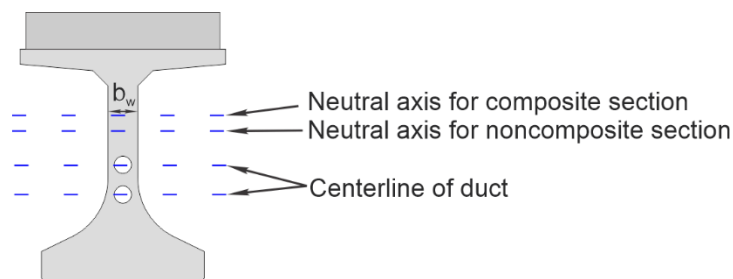


Figure 6-5 Locations for maximum principal tensile stress check

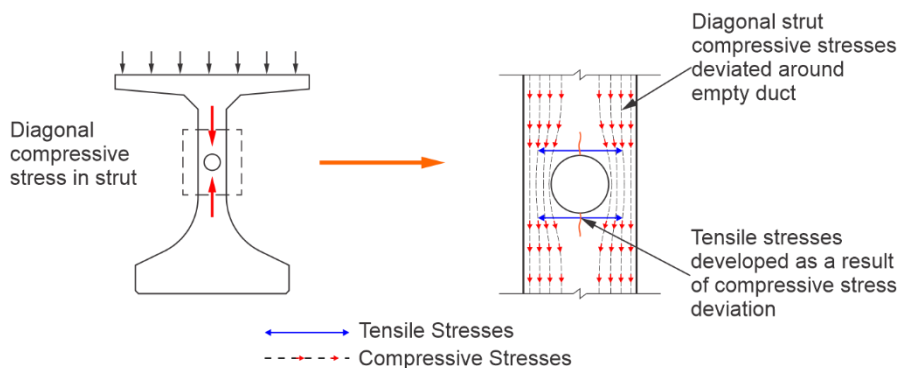


Figure 6-6 Simplified shear stress flow in I-girder containing voided duct

Figure 6-7 shows principal tensile stresses normalized against the square root of compressive strength versus duct-diameter-to-web-width ratio. Solid specimen results were plotted on localized crack plot using principal tensile stresses at either the composite or noncomposite neutral axis, whichever is larger. Figure 6-7 shows localized cracks occurred at lower normalized principal tensile stresses as duct-diameter-to-web-width ratio increased for both grouted and ungrouted tests. The reduction in normalized principal stresses that caused localized cracking was more significant for duct-diameter-to-web-width ratios greater than 0.4. Also, Figure 6-7 shows web cracking occurred at lower tensile stresses for ungrouted ducts compared to grouted ducts due to the damage at the duct location. Although cracking occurred at the duct location for grouted specimens, the high stiffness grout filler allowed the section to maintain stiffness and resist higher tensile stresses before web cracking. Specimens with ungrouted ducts were unable to resist principal tensile stresses as well as grouted specimens causing web cracking to occur earlier.

Each end of phase 2 specimens was shear tested. The first test on each specimen was terminated prior to destruction to prevent undue damage from occurring at the opposite end of the girder. This procedure was followed to ensure that the second test on the specimen would not be significantly affected by the damage caused by the first test. In some cases, however, it is suspected that the first test caused some cracking to occur to the second end of the specimen, which may have affected the loads at which cracking was detected during the second test. For example, after test P50-2 cracking was observed near the duct within the test region for P50-1. During test P50-1 localized cracking occurred at a lower applied shear force than P50-2. This trend occurred in most of the second tests for phase 2 specimens and had a more significant effect on localized cracking between tests on a specimen.

Table 6-1 shows that the phase 2 specimens had a mean normalized principal tensile stress at localized cracking at 2.82 and 3.02 for the second test and first test, respectively. This

highlighted that the first test damaged the second test region causing localized cracking to happen earlier. Normalized principal tensile stresses for localized cracking had more variation than web cracking shown in Table 6-2. The higher coefficient of variation for localized cracking compared to full-depth cracking shows that localized crack formation can be more inconsistent. Phase one tests had a high coefficient of variation for both duct and full-depth cracking. One explanation is that localized cracking may have occurred at the same time as web cracking for most specimens due to specimens having relatively shallow web depths. Another is that fiber optics were able to detect cracks earlier and more consistently on the phase 2 specimens than the rosette and visual inspection did on the phase 1 specimens.

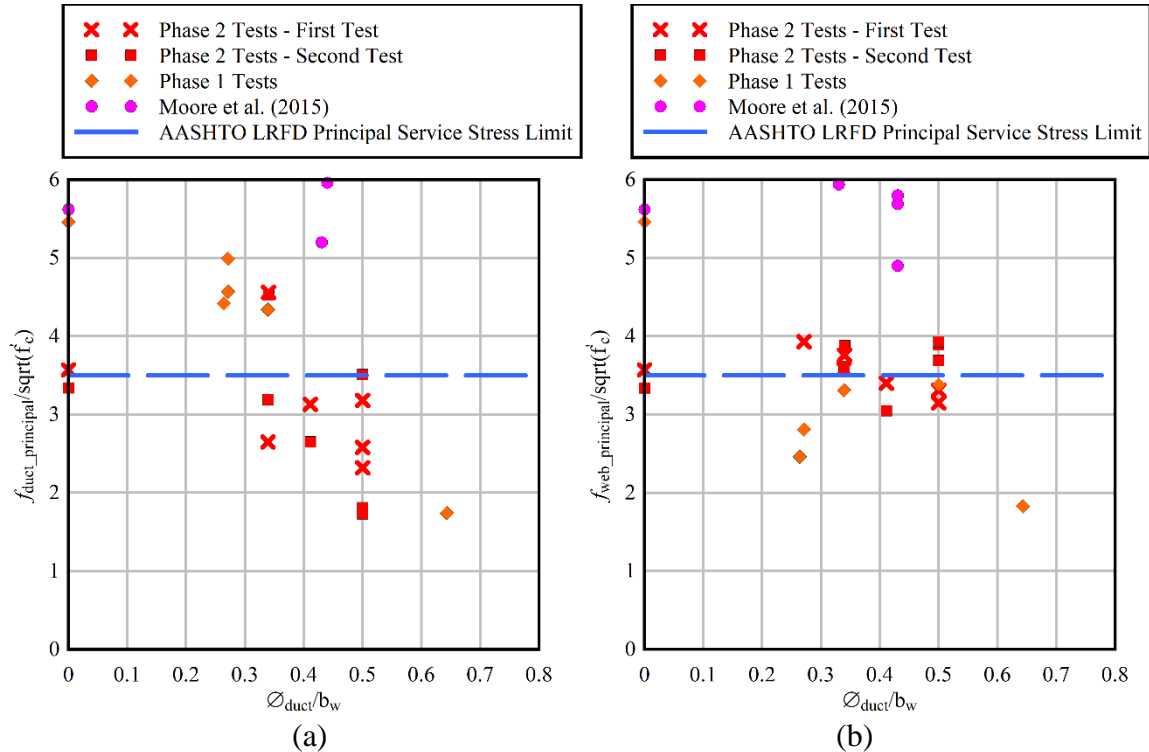


Figure 6-7 Normalized principal tensile strength vs. duct-diameter-to-web-width ratio for (a) cracking in concrete cover over duct (b) web cracking

Table 6-1 Normalized principal tensile stress* at which localized cracks formed

	Mean	COV
Phase 1	3.8	0.31
Phase 2 – First Test	3.07	0.23
Phase 2 – Second Test	2.82	0.33
Moore et al. (2015)	7.0	0.22

* Shear stress was calculated using an effective web width equal to the gross web width minus duct diameter.

Table 6-2 Normalized principal tensile stress* at which web cracks formed

	Mean	COV
Phase 1	3.11	0.38
Phase 2 – First Test	3.44	0.05
Phase 2 – Second Test	3.61	0.08
Moore et al. (2015)	6.23	0.12

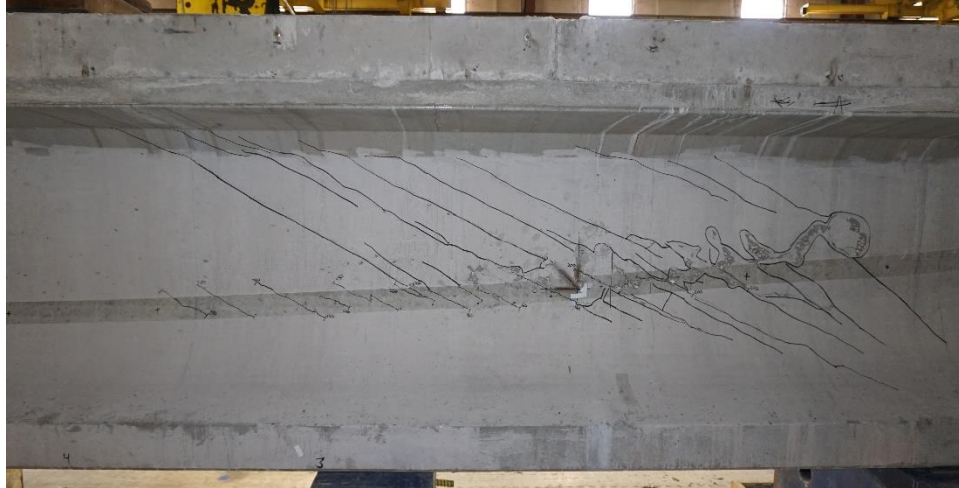
* Shear stress was calculated using the gross web width

6.2 Behavior at Ultimate Capacity

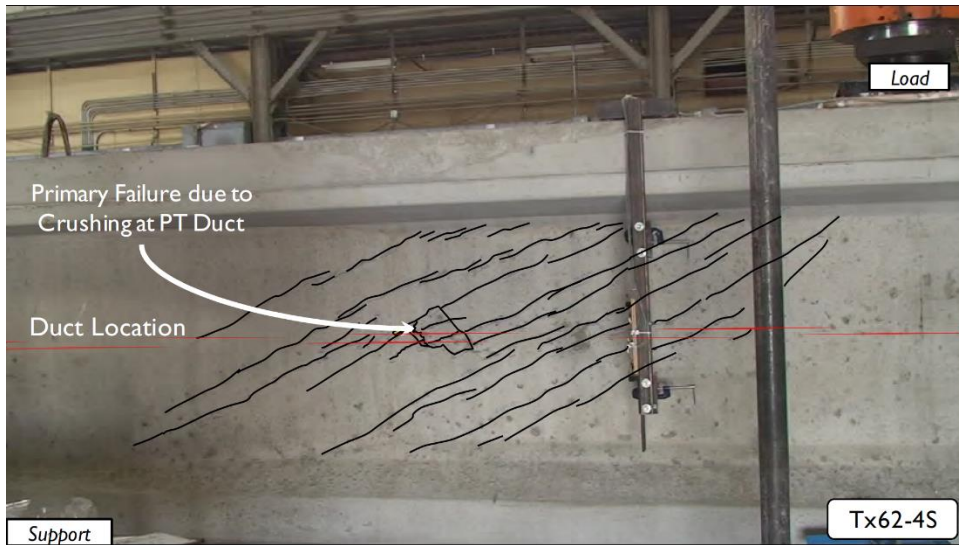
Figure 6-8 shows that the failure mode for both grouted and ungrouted specimens at ultimate capacity was web crushing at the duct. The duct and full-depth cracks that formed during service level loads would lengthen and widen until concrete near the duct location crushed at the peak shear force. Although the presence and size of ducts influenced the peak shear force for the shear tests, web crushing failure mode was consistent for specimens containing a duct.

The duct-diameter-to-web-width ratio had a significant effect on the shear capacity for ungrouted girders in phase 1 and phase 2 of this research due to the ducts being ungrouted, which reduced the diagonal axial stiffness of the web; conversely, grouted ducts maintain the axial stiffness of the solid web and thus had less effect on the shear capacity as reported in Moore et al. (2015).

AASHTO LRFD, 9th Edition incorporates an effective web width, which reduces the concrete contribution, V_c , to account for the effect of the ungrouted duct on ultimate shear capacity for girders containing ungrouted post-tensioning duct. Girders containing grouted duct modify the transverse reinforcement contribution, V_s , to account for the effect of the grouted duct on ultimate shear capacity. Figure 6-9 shows the peak shear forces for tests performed for the three research projects. The negative bending tests have been removed from phase 1 and phase 2 results for clarity due to positive bending specimens having different configurations. As duct diameter increases the general trend is that the peak shear force decreases for both grouted and ungrouted specimens as shown in Figure 6-9. Generally, specimens that were tested twice had similar peak shear forces for both tests unlike what was seen with localized cracking.



(a)



(b)

Figure 6-8 Failure of ducted specimen (a) ungrouted (b) grouted specimen (Moore et al., 2015).

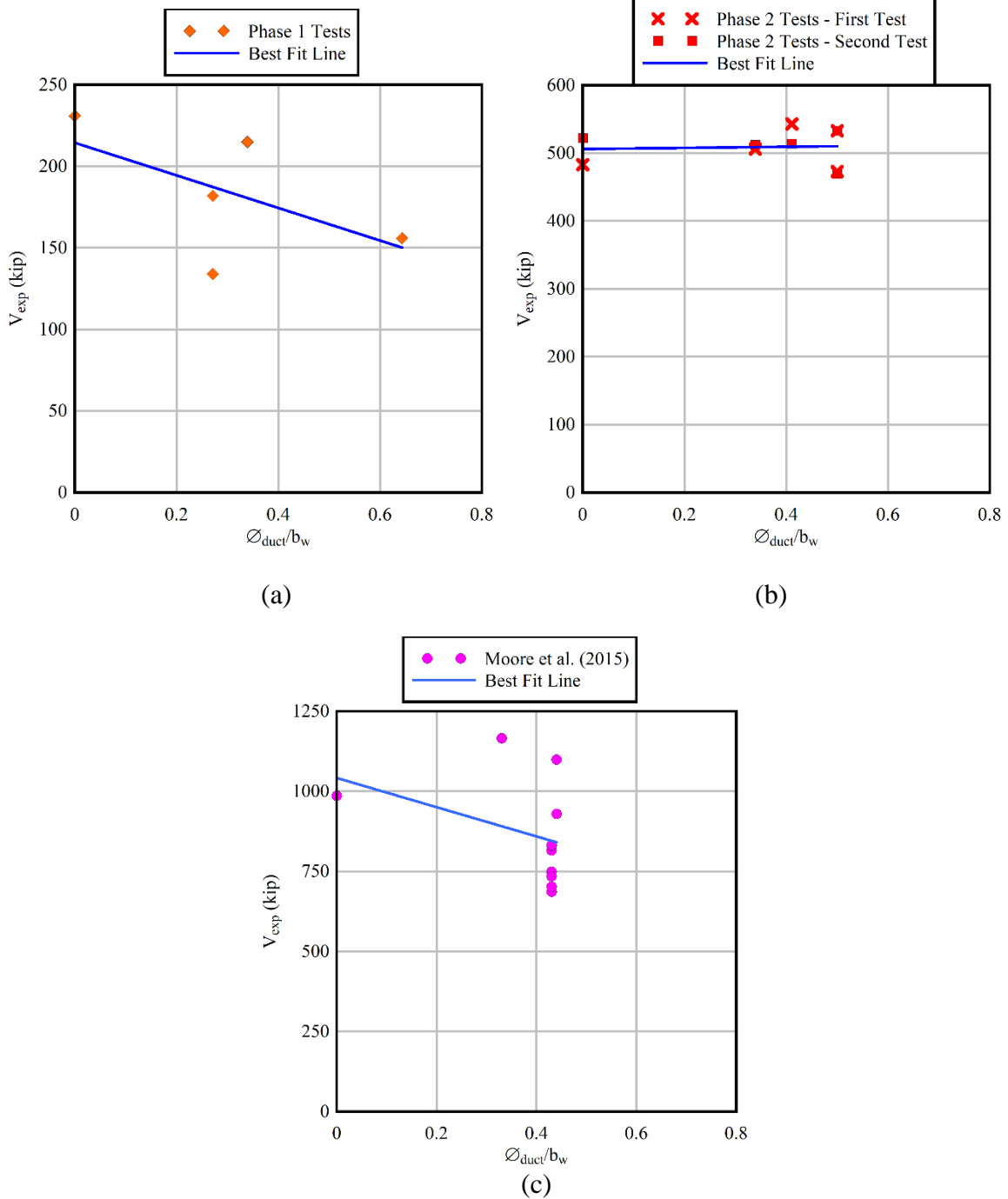


Figure 6-9 Peak shear force vs. duct-diameter-to-web-width ratio of positive bending tests for (a) phase 1 (b) phase 2 (c) Moore et al. (2015) shear tests.

6.3 SDG Duct Reinforcement Analysis

Lateral tension ties were used near the ducts in P50R in accordance with the Structures Design Guidelines January 2021 (SDG). The effectiveness of this reinforcement was investigated by comparing tests performed on specimen P50 and P50R, which were of identical design with the exception of the lateral tension ties used in P50R. Specimen P50R contained duct

reinforcement per FDOT SDG 2021 consisting of #3 hook bars spaced at 2 ft. longitudinally and #4 longitudinal bars near the duct location and detailed as shown in Figure 6-10 and Figure 6-11.

Diagonal localized cracks were observed during testing in both specimen P50R and P50 (Figure 6-12). Localized cracking patterns exhibited similar location, quantity, and orientation in both specimens. Web cracking patterns, shown in Figure 6-13, also had similar quantity, location, and orientation in both specimens.

A summary of the shear forces required to cause localized cracking and web cracking along with the peak shear forces for specimens P50 and P50R are shown in Table 6-3. Shear forces required to cause localized cracking in the two specimens agreed well with a difference of approximately 7%. This small difference is likely due to the variability in tensile strength of concrete of specimen P50 and P50R, which were 11.7 ksi and 13.5 ksi, respectively.

Web cracking occurred at shear forces of 286 kip and 307 kip for specimen P50 and 297 kip and 320 kip for P50R. P50R web cracking occurred at approximately 4% higher than specimen P50. The peak shear force for specimen P50R was approximately 13% higher than specimen P50. The normalized shear strength ratio for specimen P50R was approximately 12% higher than specimen P50.

In summary, there was no clear advantage provided by the tension ties with respect to improved cracking behavior. Localized cracking and web cracking occurred at similar shear forces when comparing P50 and P50R. There was an increase in peak shear strength when comparing both specimens. Testing more specimens containing the SDG duct reinforcement would be required to refine our understanding of the behavior and clarify the improvement resulting from the use of duct reinforcement.

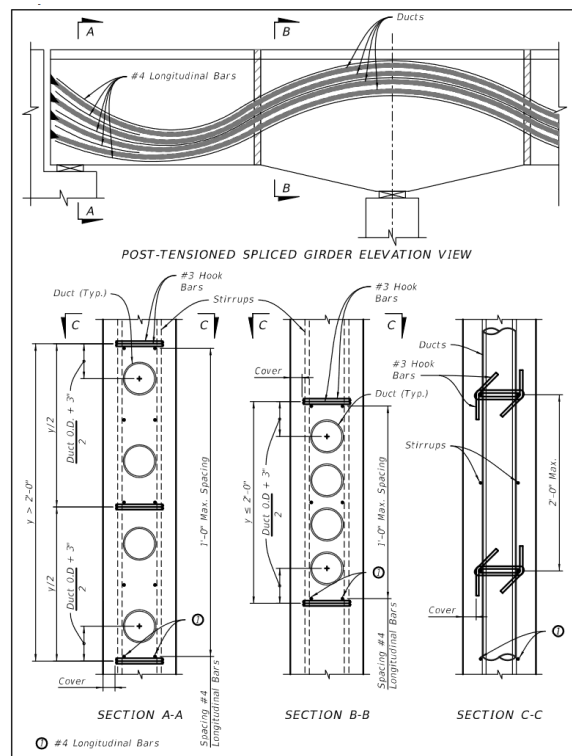


Figure 6-10 Duct reinforcement for I-girders containing post-tensioning ducts as required by FDOT SDG (Structures Design Guidelines, 2021).



Figure 6-11 Specimen P50R SDG duct reinforcement.

Table 6-3 Summary of cracking loads and peak shear force for specimen P50 and P50R.

Test	Localized crack Shear Force (kip)	Web Crack Shear Force (kip)	Peak Shear Force (kip)	$\frac{V_{exp}}{V_n}$
P50-1	150	307	470	1.15
P50-2	170	286	473	1.16
P50R-1	140	320	533	1.29
P50R-2	160	297	533	1.29

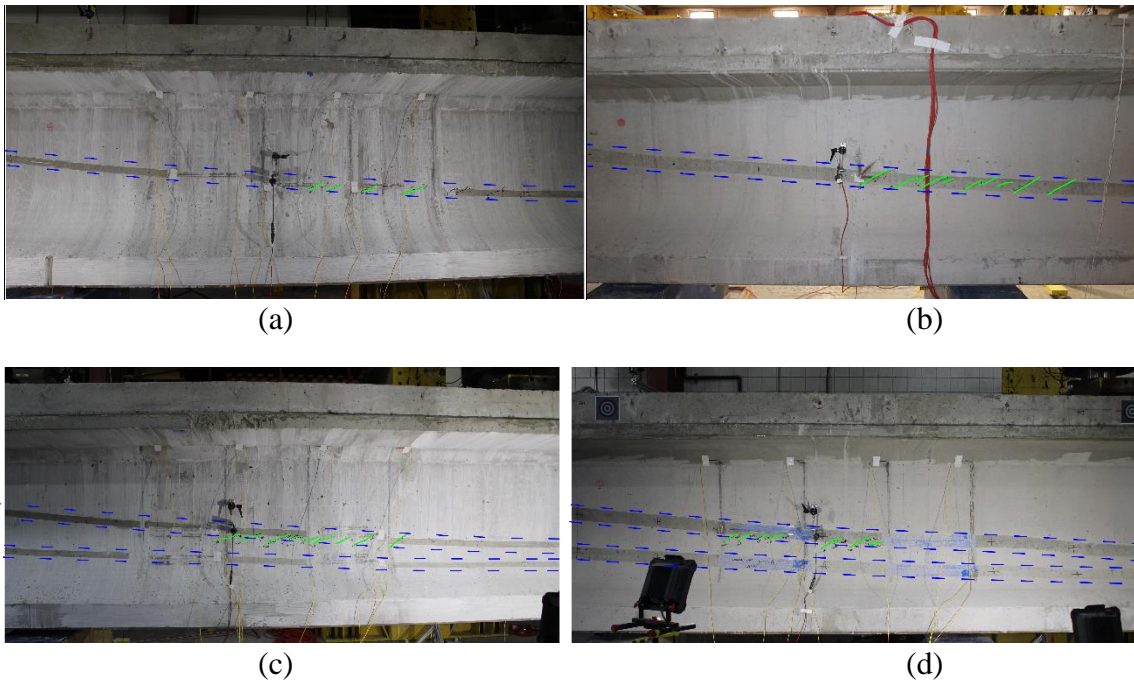


Figure 6-12 Localized cracking comparison for specimen (a) P50-1 (b) P50R-1 (c) P50-2 (d) P50R-2.

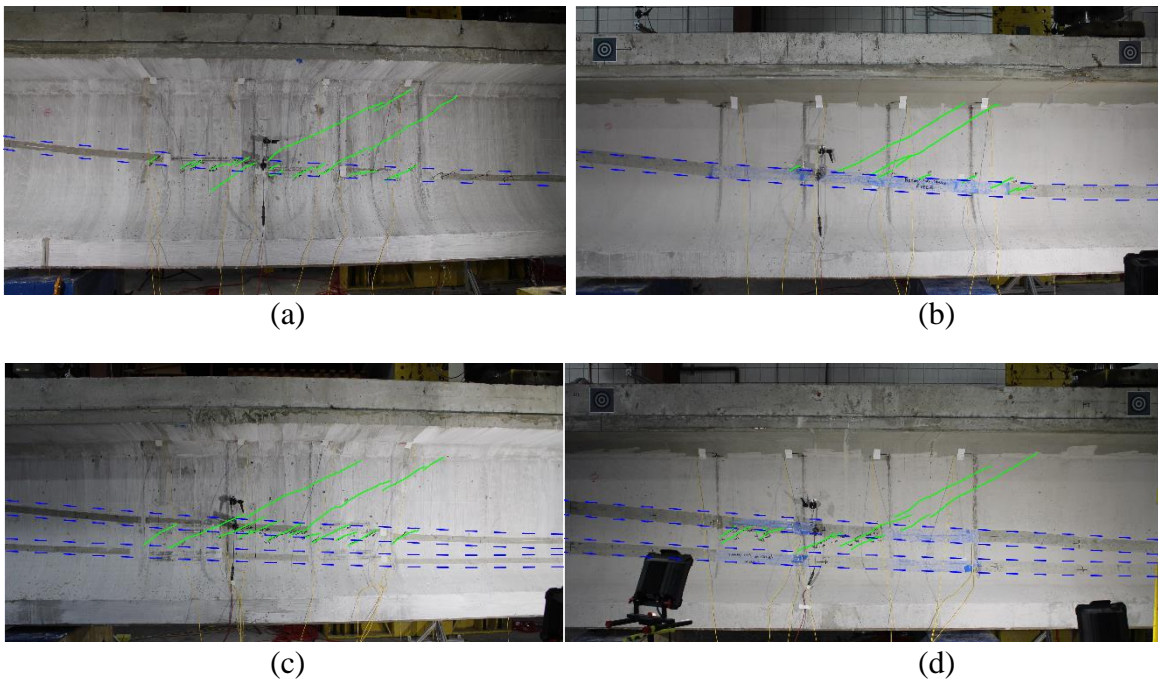


Figure 6-13 Web cracking comparison for specimen (a) P50-1 (b) P50R-1 (c) P50-2 (d) P50R-2.

6.4 Serviceability Analysis

Figure 6-7a shows 11 ungrouted tests and one solid specimen test from phase 2 were below the tensile stress limit of $3.5\sqrt{f'_c}$ according to AASHTO 9th Edition Service III limit. Localized cracking occurred at a normalized principal tensile stress ratio as low as 1.7 and 2.6 for tests with a duct-diameter-to-web-width ratio of 0.5 and 0.4 respectively. For specimens with duct-diameter-to-web-width ratio of no more than 0.4, the principal stresses under the Service III combination were no less than $2.6\sqrt{f'_c}$ when duct cracks formed.

Comparison of test results on specimens with and without grouted ducts indicate that there may be a potential problem with service level cracking locally in the concrete adjacent to an ungrouted duct. This principal tensile stress check could be added to design specifications to limit the probability of cracking from shear stresses under service load conditions. Based on the testing in this research, limiting the duct-diameter-to-web-width ratio to no more than 0.4 and limiting the calculated principal tensile stress in the concrete at the duct to $2.6\sqrt{f'_c}$ would have prevented the cracking that occurred in this testing. This check would be in addition to the current principal stress check in AASHTO LRFD, 9th Edition.

6.5 Ultimate Shear Capacity Analysis

AASHTO LRFD, 9th Edition §5.7.3.3 shear design provisions modify the nominal strength of girders with ungrouted ducts by subtracting the entire duct diameter from the width of the web to provide an effective width that is used to determine the concrete contribution to shear capacity (V_c). Using this approach, nominal shear capacity was calculated for the phase 1 and phase 2 tests as well as the Moore et al. (2015) tests. In addition, alternative shear design procedures for segmental bridges were used from AASHTO LRFD §5.12.5.3.8c. Finally, ACI 318-19 was used to calculate the nominal shear capacity. Experimental results were compared to the calculated nominal strength by dividing the maximum measured shear force at a distance equal to the depth of the section from the support closest to the load point (V_{exp}) by the calculated nominal shear strength (V_n). AASHTO LRFD and Segmental Provisions use a reduced effective web width for their shear design procedure while ACI 318-19 uses the gross web width when calculating nominal shear.

Figure 6-14 shows the shear strength ratios using AASHTO LRFD for all specimens. In general, shear strength ratios (V_{exp}/V_n) vary between 1.2 and 1.5 for most of the grouted and ungrouted specimens. The shear strength ratio was less than one for two tests. One test was a phase 1 specimen with a duct-diameter-to-web-width ratio of 0.64. This demonstrates that the AASHTO LRFD shear capacity calculations gave an unconservatively high value of shear capacity for webs with large ducts used in this testing. The other ratio is from the phase 2 test N34-2, which was terminated at the first sign of spalling during the testing; this test was terminated to avoid undue damage to the opposite end of the beam. It is likely that the full shear capacity had not been reached for this test.

It is interesting to note that the strength ratios V_{exp}/V_n of the specimens with ducts exceed those of the solid specimens, indicating that the calculated shear strengths were more conservative for specimens with ducts (both grouted and ungrouted) than those with solid webs. This holds for the tests in this report and those from Moore et al. and appears to be true up to and including a duct ratio of 0.5. At a duct ratio of 0.64, however, the tested strength is less than the calculated capacity.

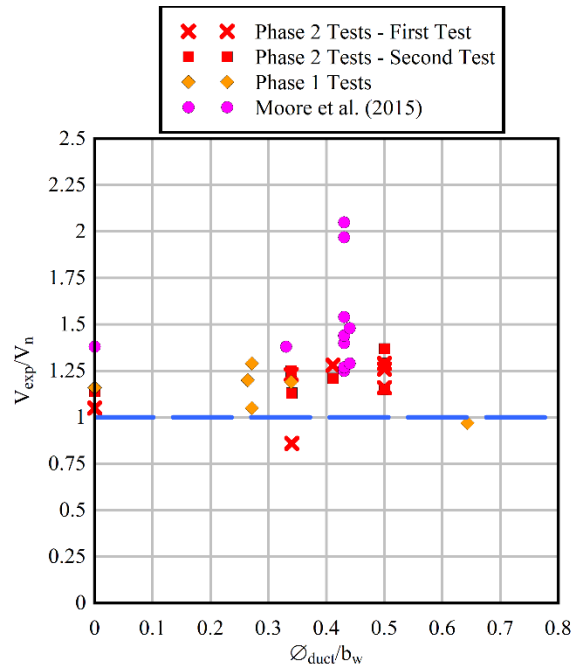


Figure 6-14 Effect of duct-diameter-to-web-width ratio on normalized AASHTO LRFD shear strength ratio

Table 6-4 summarizes the data shown in Figure 6-14.

Table 6-5 and Table 6-6 provide comparison of strength ratios calculated using the AASHTO Segmental procedures and ACI 318-19, respectively. Detailed results are provided in Appendix A.

The AASHTO Segmental Procedure exceeded V_{exp} by more than 70 percent for the three sets of data. ACI 318-19 resulted in a mean ratio that was closer to 1.0 for phase 1 and 2, than for the Moore et al. (2015) tests and the data was more scattered when compared to AASHTO LRFD. AASHTO LRFD produced the most results with a mean just above 1.0 and lowest variability.

Table 6-7 shows that the average normalized strength ratio for specimens containing ducts for each testing program was higher than the average ratio for solid specimens, which indicates that the AASHTO LRFD approach is at least as conservative for girders containing ducts (either grouted or ungrouted) as it is for girders with solid webs.

Table 6-4 Normalized strength ratio using AASHTO 9th Edition MCFT provisions.

AASHTO MCFT	Phase 1	Phase 2	Moore et al. (2015)
Mean	1.14	1.19	1.50
COV	0.10	0.11	0.18
$\frac{V_{exp}}{V_n} < 1.0$	1 of 7	1 of 14	0 of 11

Table 6-5 Normalized strength ratio using AASHTO 9th Edition LRFD Segmental provisions.

AASHTO Segmental Alternative Shear Design Procedure	Phase 1	Phase 2	Moore et al. (2015)
Mean	1.62	1.90	2.14
COV	0.14	0.16	0.24
$\frac{V_{exp}}{V_n} < 1.0$	0 of 7	0 of 14	0 of 11

Table 6-6 Normalized strength ratio using ACI 318-19 provisions.

ACI 318-19	Phase 1	Phase 2	Moore et al. (2015)
Mean	1.09	1.13	1.73
COV	0.24	0.14	0.23
$\frac{V_{exp}}{V_n} < 1.0$	2 of 7	2 of 14	0 of 11

Table 6-7 Normalized strength ratio comparison of solid and duct specimens using AASHTO 9th Edition MCFT provisions.

	Phase 1	Phase 2	Moore et al. (2015)
Solid Specimen Mean	1.16	1.09	1.38
Duct Specimen Mean	1.23	1.21	1.52

6.6 Effect of Duct Size

Figure 6-7 shows duct and web cracking occurring at principal tensile stresses below the AASHTO LRFD Service III limit in specimens that had duct ratios above 0.34 and 0.27 respectively. The general trend was that as the duct size increased cracking occurred at lower normalized principal tensile stress. A more significant drop in normalized tensile stress required to cause cracking occurred for duct sizes greater than 0.4. Duct sizes greater than 0.5 cracked as low as half of the AASHTO 9th Edition Service III principal tensile stress limit.

Normalized shear strength values, shown in Figure 6-14, were greater than one for the three research programs up to a duct-diameter-to-web-width ratio of 0.50, except test N34-2. Test N34-2 and SS5 had a normalized shear strength ratio less than one. Specimen SS5 had a duct-diameter-to-web-width ratio of 0.64 which severely reduced the shear strength of the specimen. Test N34-2 was stopped prematurely to preserve the other shear test region for a subsequent test.

7 Summary and Conclusions

The objective of this research was to evaluate the sensitivity of girders containing post-tensioning tendons to important variables on shear strength and service load performance and to compare the results to the shear design provisions of AASHTO LRFD for girders containing ungrouted post-tensioning tendons.

The research was divided into two phases of testing. The first phase of the experimental program focused on shear strength tests of six modified AASHTO Type III specimens. The specimens were precast and pretensioned; they also contained ducts of varying sizes but were not post-tensioned. Specimens were loaded in three-point bending at shear-span-to-depth ratios of 2.5 and 3; five of the specimens were designed to be tested in positive bending and the sixth in negative bending. Variables investigated included presence of post-tensioning duct, transverse reinforcement quantity, presence of top flange, web width, number of ducts and duct-diameter-to-web-width ratio. The primary purpose of these specimens was to test variable sensitivity in anticipation of larger scale shear strength tests. Significant findings of phase 1 testing were:

- Presence of a top flange resulted in an increase in peak shear of 25%.
- All specimens except SS1 and NB1 experienced a web crushing failure at the duct location. Specimen SS1 experienced a nodal failure at the load point and NB1 experienced a nodal failure at the near support.
- Specimens containing duct typically experienced localized diagonal cracking at the duct location followed by diagonal web cracks through the full-depth of the web.
- The specimen with the largest duct-diameter-to-web-width ratio, specimen SS5, experienced localized cracking at 19% of peak shear strength.
- As duct size increased peak shear force decreased. The specimen with the smallest duct, SS3, had a peak shear of 212 kip compared to specimen SS5 which had a peak shear of 153 kip.
- The amount of transverse reinforcement was increased (by approximately a factor of 2) from #3 spaced at 12 in. (SS2) to #4 spaced at 12 in. (SS3). The shear strength of SS3 was approximately an 18% higher than that of SS2 even though the duct-diameter-to-web-width ratio for SS3 was larger. The increase in shear reinforcement appears to have offset the loss in shear strength due to the larger duct ratio.
- Test NB1 was the only phase 1 specimen containing multiple ducts; no discernable behavior changes were noted in this specimen that might have been caused by the presence of two ducts. No localized cracking occurred in this test, which was likely due to the low web width-to-duct diameter ratio of 0.26.

In the second phase of the experimental program seven FIB-54 specimens were tested in shear. These specimens contained one and two sets of ducts and were post-tensioned; duct-diameter-to-web-width ratio was varied among several of the specimens. Specimens were loaded in three-point bending at a shear-span-to-depth ratio of 2.5; two were loaded in negative bending and five were loaded in positive bending. Each specimen was tested twice by performing a strength test on one end then moving the specimen to test the opposite end region for a second test. Significant findings of phase 2 testing were:

- Localized diagonal cracking near the duct location occurred for specimens containing post-tensioning ducts followed by diagonal full-depth web cracks.
- Specimens containing post-tensioning ducts experienced a web crushing failure at the duct location.
- Generally, cracking occurred at similar shear forces for both test regions of each specimen regardless of the quantity of ducts. Localized cracking occurred at a slightly lower shear force for the final test region of a specimen. Damage from the previous test typically caused the localized cracking to occur earlier.
- Positive bending specimens containing two ducts experienced localized cracking near the top duct location but no localized cracking at the bottom duct. This occurred due to the bottom duct proximity to the bottom flange where the section was thicker. Negative bending specimens experienced localized cracking simultaneously for both ducts for tests containing two ducts.

Analysis of phase 1 and 2 test results generated further insight into service and ultimate behavior. In addition, comparison with AASHTO LRFD design procedures were made for both service and strength limit states with the result of this research and that of Moore et al. (2015). Following were findings of this analysis:

Service

- Specimens containing grouted and ungrouted post-tensioning ducts experienced localized cracking along the location of the duct during strength tests.
- Localized cracks occurred in 11 ungrouted specimens below the principal tensile stress limit specified in AASHTO LRFD Service III stress limits ($3.5\sqrt{f'_c}$).
- For the testing described in this report, localized cracking in concrete cover over ungrouted ducts occurred at principal stresses as low as $1.7\sqrt{f'_c}$. Furthermore, duct-diameter-to-web-width ratios greater than 0.4 tended to have localized cracking occur at lower principal stresses than specimens with duct-diameter-to-web-width ratios less than 0.4.

Ultimate Capacity

- Specimens containing ducts experienced a failure mode of web crushing at the duct location the three research programs.
- Using AASHTO LRFD, 9th Edition MCFT provisions, nominal strength for girders with ungrouted ducts agrees well with the calculated nominal strength for solid webs.
- For specimens with duct-diameter-to-web-width ratio up to 0.5, AASHTO LRFD, 9th Edition MCFT shear provisions provided a strength ratio V_{exp}/V_n greater than 1.0. For the single specimen at 0.64 the ratio was 0.93. The LRFD shear provisions produced a nominal strength in all cases that was greater than the tested strength by an average ratio of 1.36 for duct diameter ratio 0.5 or less.

8 Implementation

8.1 Shear Strength

The nominal shear strength V_n according to AASHTO LRFD, 9th Edition (2020) is calculated as the lesser of $V_n = V_s + V_c + V_p$ or $V_n = 0.25f'_c b_v d_v + V_p$ using the following equations:

$$V_n = \min \left(0.0316\beta\lambda\sqrt{f'_c}b_v d_v + \frac{A_v f_y d_v (\cot\theta + \cot\alpha) \sin\alpha}{s} \lambda_{duct} + V_p \right) \quad (41)$$

$$\lambda_{duct} = 1 - \delta \left(\frac{\Phi_{duct}}{b_w} \right)^2 \quad (42)$$

This approach uses separate calculations for the concrete contribution, steel contribution, and the vertical component of prestressing, if any, to the overall shear capacity of a particular section. For ungrouted ducts, the presence of PT ducts is addressed by subtracting the duct diameter from the gross web width, b_w , to obtain an effective web width, b_v . For grouted ducts the transverse reinforcement contribution, V_s , is modified by a shear strength reduction factor, λ_{duct} , to account for the presence of PT ducts; this factor is a function of the duct diameter Φ_{duct} , gross web width b_w , and duct diameter correction factor, which is taken as 2.0 for grouted ducts. The duct diameter correction factor is taken as 1.0 for ungrouted ducts. Although not specified directly, it is assumed that ducts containing flexible filler are classified as ungrouted.

Note that FDOT Structures Design Guide modifies the equation for V_c and upper limit on V_n as follows:

$$V_c = 0.379\sqrt{f'_c}b_v d_v \quad (43)$$

$$V_n = 0.15\sqrt{f'_c}b_v d_v + V_p \quad (44)$$

Under the testing conducted in this research, the failure mode was consistently web crushing at the duct as was indicated in the literature for other such testing. Although the presence and size of ducts influenced the peak shear force for the shear tests, web crushing failure mode was consistent for specimens containing an ungrouted duct.

In evaluating the AASHTO LRFD approach, average shear strength ratios (V_{exp}/V_n) for specimens containing no ducts (solid web) in phase 1 and phase 2 were less than the comparative ratios for specimens containing ungrouted ducts. Furthermore, V_{exp}/V_n for grouted specimens in work by Moore et al. (2015) showed the same trend when compared to results from solid specimens. Note that this comparison includes only the specimens with a duct-diameter-to-web-width ratio of 0.5 or less. It can be concluded, based on the testing compared in this report, that the AASHTO LRFD approach is at least as conservative for girders containing ducts (either grouted or ungrouted) as it is for girders with solid webs.

8.2 Serviceability

AASHTO LRFD §5.9.2.3.3 limits principal tensile concrete stresses in post-tensioned girders with internal and/or external tendons under the Service III limit state. The principal tensile stresses are to be determined using the combination of axial and shear stress that maximize the principal tensile stress. For precast sections made composite with a cast-in-place deck, the principal tensile stress at both the noncomposite and composite neutral axes should be checked using the shear stress and axial stress at each location.

In this research, test specimens that contained ungrouted ducts exhibited localized cracking at the duct as load was increased; this was followed by the formation of full-depth web cracks as the load was increased further. Localized cracks were characterized by small diagonal cracks in the concrete cover over the duct location that were oriented at angles ranging between 22 deg. and 26 deg. from horizontal. Localized cracking typically occurred between 20 to 40 percent of the peak shear force and would occur at a relatively lower load as the duct-diameter-to-web-width ratio increased.

Comparison of test results on specimens with and without ungrouted ducts indicate that there may be a potential for service level cracking occurring locally in the concrete adjacent to an ungrouted duct. While the cracking does not appear to result in a reduced strength, it is possible that the presence of duct cracking could have long-term durability issues. To reduce the probability of localized cracking from shear stresses under service load conditions, one option is to limit principal tensile stresses in the concrete cover over the duct.

Based on the testing in this research, limiting the duct-diameter-to-web-width ratio to no more than 0.4 and limiting the calculated principal tensile stress in the concrete cover over the duct to $2.6\sqrt{f'_c}$ would have prevented the cracking that occurred in this testing. This check would be in addition to the current principal stress check in AASHTO LRFD. Since this is a serviceability check rather than a safety check, another approach is to limit principal stresses in the concrete cover over the duct to $2.6\sqrt{f'_c}$ where the bridge is located in areas that are deemed to be harsh exposure conditions such as coastal bridges. The current limit of $3.5\sqrt{f'_c}$ could be used where the bridge is located in milder conditions.

Another alternative is to factor the duct diameter when calculating the effective web thickness (b_v) to ensure that the principal stresses are limited to $2.6\sqrt{f'_c}$. For the Phase 2 test specimens this factor is approximately 1.3.

9 Future Research

- Variations in shear reinforcement quantities on the shear strength should be investigated.
- Creep and shrinkage in the concrete cover over the duct can create high concrete strains. The combined effect of these strains and the shear stresses should be investigated.
- The behavior for thin webbed sections is expected to behave like I-girders containing post-tensioning ducts. Further exploration is recommended for different cross sections such as box girders and pier caps

References

- AASHTO. (2020). AASHTO-LRFD Bridge Design Specifications, 9th Edition. In *American Association of State Highway and Transportation Officials*. Washington D.C.
- ACI Committee 318. (2019). 318-19 Building Code Requirements for Structural Concrete and Commentary. In *Building Code Requirement for Structural Concrete*. Farmington Hills, MI: American Concrete Institute. <https://doi.org/10.14359/51716937>
- Australia, C. of S. (2017). Australian Standard ® Bridge design Part 5 : Concrete. In *Concrete* (2nd ed., Vol. 04). Sydney, Australia: Council of Standards Australia.
- Darwin, D., Dolan, C. W., & Nilson, A. (2015). *Design Of Concrete Structures* (15th ed.). New York, NY: Mc Graw Hil.
- Dolan, C. W., & Hamilton, H. R. (2019). *Prestressed Concrete*. Cham, Switzerland: Springer International Publishing. <https://doi.org/10.1007/978-3-319-97882-6>
- Felan, J. (2013). *Shear Strength and Effects of HDPE Plastic Post-Tensioning Duct on a Prestressed Girder (Master thesis)*, University of Texas, Austin, Texas. Austin, Texas.
- Fib. (2013). Interface Characteristics. In *fib Model Code for Concrete Structures 2010* (pp. 152–189). Weinheim, Germany: Ernst and Sohn. <https://doi.org/10.1002/9783433604090.ch6>
- Loov, R. E., & Patnaik, A. K. (1994). Horizontal Shear Strength of Composite Concrete Beams With a Rough Interface. *PCI Journal*, 39(1), 48–69. <https://doi.org/10.15554/pcij.01011994.48.69>
- Mitchell, D., & Collins, M. P. (1974). Diagonal Compression Field theory-A Rational Model For Structural Concrete in Pure Torsion. *ACI Journal Proceedings*, 71(8), 396–408. <https://doi.org/10.14359/7103>
- Moore, A., Williams, C., Al-Tarafany, D., Felan, J., Massey, J., Nguyen, T., ... Ghannoum, W. (2015). *Shear Behavior of Spliced Post-Tensioned Girders* (Vol. 7). Austin, Texas.
- Muttoni, A., Burdet, O. L., & Hars, E. (2006). Effect of duct type on shear strength of thin webs. *ACI Structural Journal*, 103(5), 729–735.
- Narayanan, R. S. (2014). BS EN1992-1-1:2004+A1:2014- Eurocode 2: Design of concrete structures-Part 1-1: General rules and rules for buildings. *Civil Engineering*, 144(6), 1–230.
- Pang, X. B., & Hsu, T. T. C. (1995). Behavior of reinforced concrete membrane elements in shear. *ACI Structural Journal*, 92(6), 665–679. <https://doi.org/10.14359/9661>
- Pang, X. D., & Hsu, T. T. C. (1996). *Fixed Angle Softened Truss Model for Reinforced Concrete*.

(93), 197–207.

Post-Tensioning Institute. (2007). *Training and Certification of Field Personnel for Bonded Post-Tensioning* (3rd ed.). Farmington Hills, MI: Post-Tensioning Institute.

Ramirez, J A, & Dilger, W. H. (2000). ACI 445R-99 Recent Approaches to Shear Design of Structural Concrete Reported by Joint ACI-ASCE Committee 445. *Structural Concrete*, 99(Reapproved), 1–55.

Ramirez, Julio A., & Breen, J. E. (1991). Evaluation of a Modified Truss-Model Approach for Beams in Shear. In *ACI Structural Journal*.

Reineck, K.-H. (1991). Modelling of Members with Transverse Reinforcement. In *IABSE Colloquium Structural Concrete, IABSE Report, Zurich, 62*.

Structures Design Guidelines. (2021). Structures Design Guidelines. In *Florida Department of Transportation*. Tallahassee, Florida.

Theryo, T. S., Hartt, W. H., & Paczkowski, P. (2013). *Guidelines for Sampling, Assessing, and Restoring Defective Grout in Prestressed Concrete Bridge Post-Tensioning Ducts*. Tampa, FL. Retrieved from

<https://www.fhwa.dot.gov/publications/research/infrastructure/structures/bridge/13028/index.cfm>

Uomoto, T., Ishibashi, T., Nobuta, Y., Satoh, T., Kawano, H., Takewaka, K., & Uji, K. (2008). Standard Specifications for Concrete Structures-2007 by Japan Society of Civil Engineers. In *Concrete Journal* (Vol. 46). https://doi.org/10.3151/coj1975.46.7_3

Vecchio, F. J., & Collins, M. P. (1986). Modified Compression-Field Theory for Reinforced Concrete Elements Subjected To Shear. *Journal of the American Concrete Institute*, 83(2), 219–231. <https://doi.org/10.14359/10416>

Wald, D. (2012). *Experimental Investigation of Crushing Capacity of I-Girder Webs Containing Post-Tensioning Ducts*. University of Texas at Austin.

Williams, C., Moore, A., Al-Tarafany, D., Bayrak, O., Jirsa, J., Ghannoum, W., & Street, G. (2015). *Behavior of the Splice Regions of Spliced I-Girder Bridges (FHWA 0-6652-2)* (Vol. 7). Austin, Texas.

Appendix A – Shear Strength Calculation Summary

Table A-1 Phase 1 nominal strength calculation summary using AASHTO LRFD, 9th Edition MCFT.

Test	f_{girder} (ksi)	f_{flange} (ksi)	b_{web} (in)	b_v (in)	Φ_{duct} (in)	A_{ps} (in ²)	f_{po} (ksi)	d_v (in)	V_u (kip)	M_u (kip-ft)	ϵ_s (in/in) $\times 10^3$	β	Θ (deg)	V_c (kip)	V_s (kip)	V_n (kip)	$V_{n,limit}$ (kip)	V_{exp}^* (kip)	$\frac{V_{exp}}{V_n}$
SS1	10.2	N/A	7	5.1	1.9	2.14	128	28.8	126	378	0.153	4.31	29.5	63.8	62.4	130	375	136	1.05
SS2	9.28	9.33	7	5.1	1.9	3.83	109	30.3	141	423	0.035	5.33	28.5	73.3	67.4	141	358	182	1.29
SS3	10	9.59	7	4.625	2.375	3.83	98	30.8	181	543	0.165	4.27	29.6	60.7	121	181	356	215	1.19
SS4	11	10.3	7	7	None	3.83	98.3	31.3	199	597	0.475	3.54	30.7	81.3	118	199	603	231	1.16
SS5	10.2	11	7	3.5	4.5	3.83	187	30.8	160	480	0.101	4.84	29.0	37.2	124	161	192	156	0.97
NB1	10.6	10.3	9	6.625	2.375	0.31	63.7	28.2	198	594	0.102	4.46	29.4	85.8	112	198	496	237	1.20
Mean																			1.22
COV																			0.14

Table A-2 Phase 1 nominal strength calculation summary using AASHTO LRFD, 9th Edition Segmental procedure.

Test	f_{girder} (ksi)	f_{deck} (ksi)	b_{web} (in)	b_v (in)	Φ_{duct} (in)	A_{ps} (in ²)	f_{pc} (ksi)	d (in)	K	V_c (kip)	V_s (kip)	V_n (kip)	$V_{n.limit}$ (kip)	V_{exp} (kip)	$\frac{V_{exp}}{V_n}$
SS1	10.2	N/A	7	5.1	1.9	2.14	0.67	32.0	2.00	66	39	105	375	136	1.30
SS2	9.28	9.33	7	5.1	1.9	3.83	0.782	31.2	2.00	61	38	100	358	182	1.82
SS3	10	9.59	7	4.625	2.375	3.83	0.764	31.2	2.00	58	70	127	356	215	1.69
SS4	11	10.3	7	7	None	3.83	0.768	30.9	2.00	91	69	160	603	231	1.44
SS5	10.2	11	7	3.5	4.5	3.83	0.776	31.2	2.00	31	70	101	192	156	1.54
NB1	10.6	10.3	9	6.625	2.375	0.31	0.265	33.0	1.51	59	64	124	496	237	1.91
Mean															1.71
COV															0.11

Table A-3 Phase 1 nominal strength calculation summary using ACI 318-19.

Test	f_{girder} (ksi)	f_{flange} (ksi)	b_w (in)	d_p (in)	Φ_{duct} (in)	A_{ps} (in ²)	f_{pc} (ksi)	V_{cw} (kip)	V_{ci} (kip)	V_c (kip)	V_s (kip)	V_n (kip)	V_{exp} (kip)	$\frac{V_{exp}}{V_n}$
SS1	10.2	N/A	7	32	1.9	2.14	0.67	124	177	124	39.3	163	136	0.83
SS2	9.28	9.33	7	31	1.9	3.83	0.782	125	280	125	38.3	163	182	1.1
SS3	10	9.59	7	31	2.375	3.83	0.764	126	278	126	69.6	196	215	1.1
SS4	11	10.3	7	30.9	None	3.83	0.768	129	283	129	69.1	198	231	1.2
SS5	10.2	11	7	31.2	4.5	3.83	0.776	128	282	128	69.6	197	156	0.8
NB1	10.6	10.3	9	28	2.375	0.31	0.265	114	93	93	64.3	157	237	1.5
Mean														1.15
COV														0.20

Table A-4 Phase 2 nominal strength calculation summary using AASHTO LRFD, 9th Edition MCFT.

Test	f_{girder} (ksi)	f_{deck} (ksi)	b_w (in)	b_v (in)	A_{ps} (in ²)	f_{po} (ksi)	d_v (in)	V_u (kip)	M_u (kip-ft)	ϵ_s (in/in) $\times 10^3$	β	Θ (deg)	V_c (kip)	V_s (kip)	V_p (kip)	V_n (kip)	$V_{n.limit}^*$ (kip)	V_{exp} (kip)	$\frac{V_{exp}}{V_n}$
P00-1**	12.8	5.29	7.00	7.00	5.21	176	56.3	460	2070	-0.0026	4.81	29.0	215	244	0	459	1270	483	1.05
P00-2***	12.8	5.29	7.00	7.00	5.21	176	56.3	460	2070	-0.0026	4.81	29.0	215	244	0	459	1270	522	1.14
P34-1***	11.7	5.45	7.00	4.63	5.21	177	56.0	410	1845	-0.0740	5.08	28.7	142	245	23	410	758	512	1.25
P34-2**	11.7	5.45	7.00	4.63	5.21	177	56.0	410	1845	-0.0740	5.08	28.7	142	245	23	410	758	506	1.23
P41-1***	12.0	7.97	7.00	4.13	5.21	176	56.5	425	1912	-0.119	5.27	28.6	135	249	41	425	700	514	1.21
P41-2**	12.0	7.97	7.00	4.13	5.21	176	56.5	425	1912	-0.119	5.27	28.6	135	249	41	425	700	543	1.28
P50-1***	11.7	6.70	7.00	3.50	5.21	171	55.9	407	1831	-0.0762	5.09	28.7	108	245	55	407	571	470	1.15
P50-2**	11.7	6.70	7.00	3.50	5.21	171	55.9	407	1831	-0.0762	5.09	28.7	108	245	55	407	571	473	1.16
P50R-1***	13.5	7.40	7.00	3.50	5.21	177	56.0	415	1868	-0.0764	5.08	28.7	116	245	55	414	664	533	1.29
P50R-2**	13.5	7.40	7.00	3.50	5.21	177	56.0	415	1868	-0.0764	5.08	28.7	116	245	55	414	664	533	1.29
N34-1***	12.7	7.90	7.00	4.63	0.87	36	51.0	339	1525	0.0818	4.52	29.3	120	218	22	339	749	382	1.13
N34-2**	12.7	7.90	7.00	4.63	0.87	36	51.0	339	1525	0.0818	4.52	29.3	120	218	22	339	749	290	0.86
N50-1***	13.7	8.80	7.00	3.50	0.87	37	50.7	316	1422	0.0264	4.71	29.1	97.6	218	52	316	607	434	1.37
N50-2**	13.7	8.80	7.00	3.50	0.87	37	50.7	316	1422	0.0264	4.71	29.1	97.6	218	52	316	607	399	1.26
Mean																			1.19
COV																			0.11
* $V_{n.limit} = f_{girder} * b_v * d_v + V_p$																			
** End region of specimen tested first																			
*** End region of specimen tested second																			

Table A-5 Phase 2 nominal strength calculation summary using AASHTO LRFD, 9th Edition Segmental procedure.

Test	\hat{f}_{girder} (ksi)	\hat{f}_{block} (ksi)	\hat{f}_{deck} (ksi)	b_w (in)	b_v (in)	Φ_{duct} (in)	A_{ps} (in ²)	f_{pc} (ksi)	d_v (in)	K	V_c (kip)	V_s (kip)	V_n (kip)	$V_{n,limit}$ (kip)	V_{exp} (kip)	$\frac{V_{exp}}{V_n}$
P00-1	12.8	N/A	5.29	7.00	7.00	0.00	5.21	0.530	58.4	1.83	169	140	309	1270	483	1.56
P00-2	12.8	N/A	5.29	7.00	7.00	0.00	5.21	0.530	58.4	1.83	169	140	309	1270	522	1.69
P34-1	11.7	8.57	5.45	7.00	4.63	2.38	5.21	0.848	58.4	2.00	117	140	257	758	512	1.99
P34-2	11.7	8.57	5.45	7.00	4.63	2.38	5.21	0.848	58.4	2.00	117	140	257	758	506	1.97
P41-1	12.0	9.53	7.97	7.00	4.13	2.88	5.21	0.919	58.4	2.00	106	140	246	700	514	2.09
P41-2	12.0	9.53	7.97	7.00	4.13	2.88	5.21	0.919	58.4	2.00	106	140	246	700	543	2.21
P50-1	11.7	9.80	6.70	7.00	3.50	3.50	5.21	1.03	58.4	2.00	88.4	140	229	571	470	2.05
P50-2	11.7	9.80	6.70	7.00	3.50	3.50	5.21	1.03	58.4	2.00	88.4	140	229	571	473	2.07
P50R-1	13.5	7.40	7.40	7.00	3.50	3.50	5.21	1.05	58.4	2.00	95	140	235	664	533	2.27
P50R-2	13.5	7.40	7.40	7.00	3.50	3.50	5.21	1.05	58.4	2.00	95	140	235	664	533	2.27
N34-1	12.7	8.60	7.90	7.00	4.63	2.38	0.868	1.89	59.0	1.60	98	142	240	749	382	1.59
N34-2	12.7	8.60	7.90	7.00	4.63	2.38	0.868	1.89	59.0	1.60	98	142	240	749	290	1.21
N50-1	13.7	8.40	8.80	7.00	3.50	3.50	0.868	2.09	59.0	1.88	91	142	233	607	434	1.87
N50-2	13.7	8.40	8.80	7.00	3.50	3.50	0.868	2.09	59.0	1.88	91	142	233	607	399	1.72
Mean																1.90
COV																0.16

Table A-6 Phase 2 nominal strength calculation summary using ACI 318-19.

Test	\hat{f}_{girder} (ksi)	\hat{f}_{block} (ksi)	\hat{f}_{deck} (ksi)	b_w (in)	d_p (in)	Φ_{duct} (in)	A_{ps} (in ²)	\hat{f}_{pc} (ksi)	V_{cw} (kip)	V_{ci} (kip)	V_c (kip)	V_s (kip)	V_n (kip)	V_{test} (kip)	$\frac{V_{exp}}{V_n}$
P00-1	12.8	N/A	5.29	7.00	58.4	0.00	5.21	0.530	227	264	227	140	367	483	1.32
P00-2	12.8	N/A	5.29	7.00	58.4	0.00	5.21	0.530	227	264	227	140	367	522	1.42
P34-1	11.7	8.57	5.45	7.00	58.4	2.38	5.21	0.848	273	270	251	140	413	512	1.24
P34-2	11.7	8.57	5.45	7.00	58.4	2.38	5.21	0.848	273	270	251	140	413	506	1.23
P41-1	12.0	9.53	7.97	7.00	58.4	2.88	5.21	0.919	295	275	275	140	435	514	1.18
P41-2	12.0	9.53	7.97	7.00	58.4	2.88	5.21	0.919	295	275	275	140	435	543	1.25
P50-1	11.7	9.80	6.70	7.00	58.4	3.50	5.21	1.03	317	274	274	140	458	470	1.03
P50-2	11.7	9.80	6.70	7.00	58.4	3.50	5.21	1.03	317	274	274	140	458	473	1.03
P50R-1	13.5	7.40	7.40	7.00	58.4	3.50	5.21	1.05	330	281	281	140	470	533	1.13
P50R-2	13.5	7.40	7.40	7.00	58.4	3.50	5.21	1.05	330	281	281	140	470	533	1.13
N34-1	12.7	8.60	7.90	7.00	52.0	2.38	0.868	1.89	364	346	346	125	362	382	1.06
N34-2	12.7	8.60	7.90	7.00	52.0	2.38	0.868	1.89	364	346	346	125	362	290	0.80
N50-1	13.7	8.40	8.80	7.00	52.0	3.50	0.868	2.09	412	398	398	125	420	434	1.03
N50-2	13.7	8.40	8.80	7.00	52.0	3.50	0.868	2.09	412	398	398	125	420	399	0.95
Mean															1.13
COV															0.14

Appendix B – Cracking Loads Summary

Table B-7 Summary of duct- and web-cracking shear forces for phase 1 and phase 2 tests.

Test	Duct Cracking Shear Force		Web Cracking Shear Force	
	V_{duct}	V_{duct}/V_{exp}	V_{web}	V_{web}/V_{exp}
SS1	114	0.58	114	0.58
SS2	103	0.57	103	0.57
SS3	92	0.43	117	0.54
SS4	N/A	N/A	168	0.73
SS5	29	0.19	81	0.52
NB1	69	0.29	93	0.39
P00-1	N/A	N/A	272	0.56
P00-2	N/A	N/A	283	0.54
P34-1	175	0.34	247	0.48
P34-2	150	0.30	250	0.49
P41-1	176	0.34	267	0.52
P41-2	190	0.35	290	0.53
P50-1	150	0.32	307	0.65
P50-2	170	0.36	286	0.60
P50R-1	140	0.26	320	0.60
P50R-2	160	0.30	297	0.56
N34-1	160	0.42	205	0.54
N34-2	150	0.52	210	0.72
N50-1	150	0.35	274	0.63
N50-2	140	0.35	250	0.63

Table B-8 Summary of duct- and web-cracking loads for Texas research girders.

Test	Duct Cracking Load		Web Cracking Load	
	V_{duct}	V_{duct}/V_{exp}	V_{web}	V_{duct}
Tx62-1(S)	196	0.29	371	0.54
Tx62-2(S)	272	0.33	478	0.59
Tx62-2(N)	286	0.38	476	0.64
Tx62-3(S)	N/A	N/A	404	0.41
Tx62-4(S)	364	0.44	546	0.66
Tx62-4(N)	281	0.34	539	0.65
Tx62-5(S)	272	0.39	469	0.67
Tx62-5(N)	331	0.45	452	0.61
Tx62-6(S)	319	0.34	699	0.75
Tx62-6(N)	315	0.29	669	0.61
Tx62-7(S)	411	0.35	600	0.51

Appendix C – Principal Tensile Stress Summary

Table C-9 Summary of principal tensile stresses for phase1 and phase 2 tests.

Test	Duct crack ratio	Duct crack principal tensile stress (psi)	Web crack ratio	Web crack principal tensile stress (psi)
SS1	4.99	504	3.93	397
SS2	4.57	440	2.81	270
SS3	4.34	436	3.31	332
SS4	N/A	N/A	5.46	572
SS5	1.74	176	1.83	185
NB1	4.42	454	2.46	253
P00-1	N/A	N/A	3.57	405
P00-2	N/A	N/A	3.34	378
P34-1	3.19	345	3.61	391
P34-2	2.65	286	3.58	387
P41-1	2.65	290	3.05	334
P41-2	3.13	343	3.4	372
P50-1	1.81	196	3.69	399
P50-2	2.58	279	3.15	341
P50R-1	1.73	187	3.89	421
P50R-2	2.32	251	3.31	358
N34-1	4.53	511	3.88	437
N34-2	4.56	513	3.76	424
N50-1	3.51	411	3.93	461
N50-2	3.18	373	3.38	395

Table C-10 Summary of principal tensile stresses for Texas research girders.

Test	Duct crack ratio	Duct crack principal tensile stress (psi)	Web crack ratio	Web crack principal tensile stress (psi)
Tx62-1(S)	5.20	535	4.90	504
Tx62-2(S)	7.79	853	6.59	725
Tx62-2(N)	8.29	907	6.48	704
Tx62-3(S)	N/A	N/A	5.62	609
Tx62-4(S)	10.55	1245	7.09	837
Tx62-4(N)	7.21	841	6.92	807
Tx62-5(S)	7.09	792	5.69	634
Tx62-5(N)	9.64	1075	5.80	647
Tx62-6(S)	6.25	695	7.28	809
Tx62-6(N)	5.96	684	6.65	763
Tx62-7(S)	7.02	775	5.94	656

Table C-11 Principal tensile stress and rosette principal tensile stress comparison for phase1 and phase 2.

Test	Calculated Principal Tensile Stress		Rosette Principal Tensile Stress (psi)	
	Duct Crack (psi)	Web Crack (psi)	Duct Crack (psi)	Error
SS1	504	397	468	7.7%
SS2	440	270	528	16.6%
SS3	436	332	432	0.9%
SS4	N/A	572	569	0.6%
SS5	176	185	181	2.8%
NB1	454	253	400	13.5%
P00-1	N/A	405	690	41.4%
P00-2	N/A	378	458	17.5%
P34-1	345	391	Error	Error
P34-2	286	387	369	22.4%
P41-1	290	334	704	58.8%
P41-2	343	372	573	40.1%
P50-1	196	399	405	51.6%
P50-2	279	341	569	50.9%
P50R-1	187	421	630	70.3%
P50R-2	251	358	931	73.0%
N34-1	511	437	472	8.2%
N34-2	513	424	496	3.5%
N50-1	411	461	786	47.7%
N50-2	373	395	670	44.4%

Appendix D – Fabrication Drawings

GENERAL NOTES

- INDIVIDUAL PRECAST MEMBER PIECE DETAILS ARE NOT REQUIRED TO BE SUBMITTED FOR APPROVAL AS SUFFICIENT INFORMATION FOR THEIR FABRICATION IS CONTAINED IN THE CONTRACT DRAWINGS, F.D.O.T. STANDARD INDEX DRAWINGS AND SPECIFICATIONS FOR ROAD AND BRIDGE CONSTRUCTION. THESE DRAWINGS ARE INTENDED TO MEET THE REQUIREMENTS FOR PRECAST MEMBER SUBMITTALS AND ARE TO BE USED IN CONJUNCTION WITH THE PREVIOUSLY MENTIONED DOCUMENTS.
- THE COMPOSITE NEOPRENE BEARING PADS ARE TO BE FURNISHED AND INSTALLED BY THE G.C.
- PRIOR TO PRODUCTION OF PRECAST MEMBERS THE FOLLOWING INFORMATION NEEDS TO BE SUPPLIED REGARDING MATERIALS FURNISHED TO PRECASTER FOR EMBEDMENT INTO BEAMS.

S.I.P. FORM CLIPS

ARE THEY REQUIRED? NO
 WHERE ARE THEY TO BE LOCATED? _____
 WHAT IS THEIR SPACING? _____
 WHAT IS THEIR EXACT TYPE? _____
 WHAT ARE THEIR DIMENSIONS? _____

STEEL HANGERS

ARE THEY REQUIRED? NO
 WHERE ARE THEY TO BE LOCATED? _____
 WHAT IS THEIR SPACING? _____
 WHAT IS THEIR EXACT TYPE? _____
 WHAT ARE THEIR DIMENSIONS? _____

BRACING

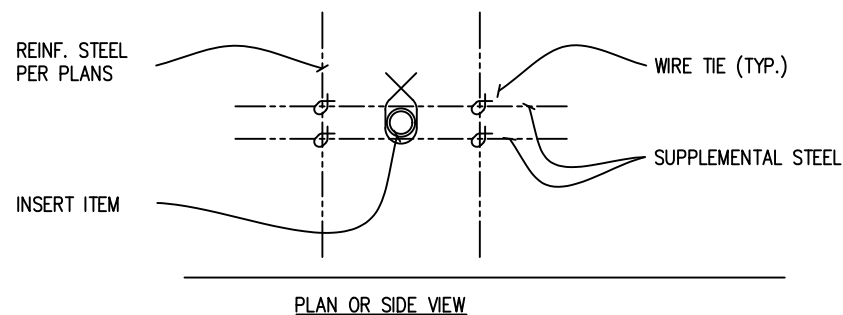
NOT REQUIRED.

SAFETY SLEEVE

NOT REQUIRED.

ANY ADDITIONAL EMBED MATERIALS

- SUPPLEMENTAL STEEL** - AS REQUIRED TO SECURE DUCT INTO PROPER POSITIONING IN A BEAM, #3 REBAR WILL BE TIED TO EACH SIDE OF INSERT AND TO NEARBY INTERIOR STEEL REINFORCING. SEE DETAIL BELOW

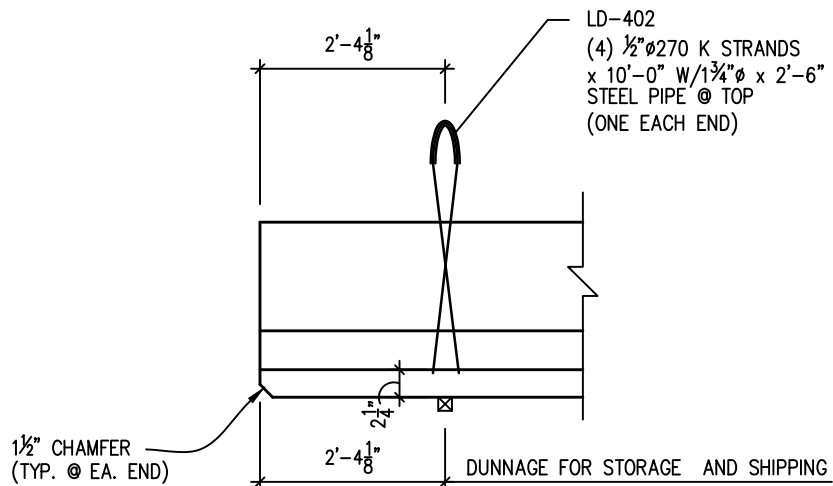


- CUT STRANDS AS SHOWN IN THIS SHEET.
- D/S SHALL PROVIDE MATERIAL SAMPLES TO UF/FDOT AS FOLLOWS :

(8) 6" DIA. x 12" CYLINDERS FROM EACH CONCRETE BATCH : (4) CYLINDERS CURE WITH GIRDER, (4) LAB CURE.

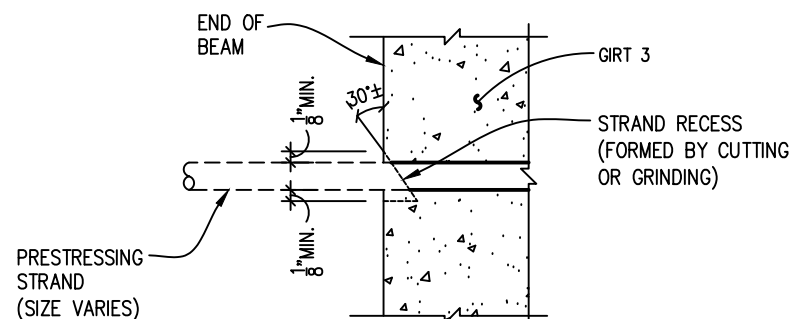
(16) 36" PIECES OF PRESTRESSING STRANDS FREE FROM SAND, DUST, ETC. SAMPLES TAKEN DIRECTLY OFF OF REEL.

(3) 36" PIECES OF EACH SIZE/BATCH OF REBAR.



HANDLING & DUNNAGE DIAGRAM FOR TYPES III (MOD.)
 TYP. EA. END OF ALL BEAMS

RESUBMITTED
 Dec 21, 2018
 FOR APPROVAL



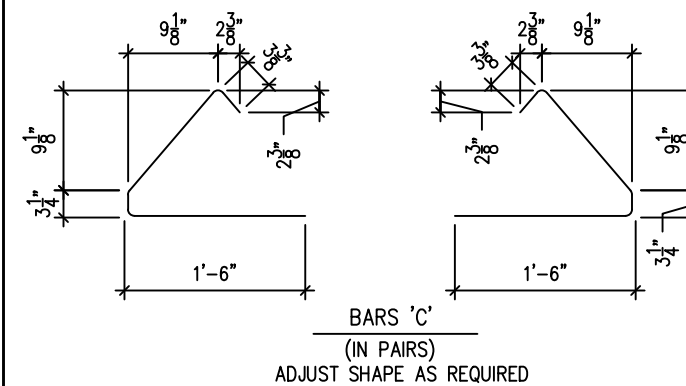
TYPICAL SECTION DURING BEAM CASTING
RECESSED STRAND DETAILS AT BEAM ENDS

BILL OF EMBED MATERIALS


FOR TYPE III (MOD.) ALL MEMBERS

BAR	D.S. I.D. #	SIZE	QTY.	LENGTH	REMARKS
A	RE-BAR 6	#6 BAR	40	24'-8"	STRAIGHT BAR
C	RE-BAR 3	#3 BAR	384	3'-3"	SEE BELOW
K1	RE-BAR 3	#3 BAR	128	3'-7"	SEE BELOW
K2	RE-BAR 4	#4 BAR	128	3'-9 5/8"	SEE BELOW
K3	RE-BAR 4	#4 BAR	64	3'-8 3/4"	SEE BELOW
K4	RE-BAR 4	#4 BAR	64	3'-9 7/8"	SEE BELOW
S	RE-BAR 4	#4 BAR	128	1'-8"	STRAIGHT BAR
T	RE-BAR 4	#4 BAR	52	2'-4 1/4"	SEE BELOW

ALL #3 BARS SHALL BE BENT AROUND A 1 1/2" DIA. PIN
 ALL #4 BARS SHALL BE BENT AROUND A 2" DIA. PIN
 ALL #5 BARS SHALL BE BENT AROUND A 2 1/2" DIA. PIN
 NOTE: ALL DIMENSIONS ARE OUT TO OUT



DS PART NO.
 GIRT 3 (MOD.)



DATE	12/21/18
BY	CHK. KK
REVISION	REVISAS SHOWN
REV	1

GENERAL NOTES AND MISC. MATERIALS
DURA-STRESS Inc.
 CA #6028
 P.O. BOX 490779 LEESBURG, FL 34749-0779
 PHONE (352) 787-1422 FAX (352) 787-0080
 STRUCTURAL PRESTRESSED AND ARCHITECTURAL PRECAST CONCRETE PRODUCTS

JOB NAME: FDOT RESEARCH	SHEAR BEHAVIOR OF WEBS
LOCATION: N/A	ARCHITECT: N/A
ENGINEER: N/A	CONTRACTOR: N/A
PROJ. NO: N/A	

DRAWN: NE	DS JOB NO: B1800
CHK'D.: POL	SHT: A1
APPR.:	
DATE : 11/13/18	
RELEASED:	



REV	DESCRIPTION	DATE	BY	CHK.
Δ	REVISED AS SHOWN	12/21/18	NE	KK

TYPE III (MOD.) BEAM SECTIONS AND DETAILS

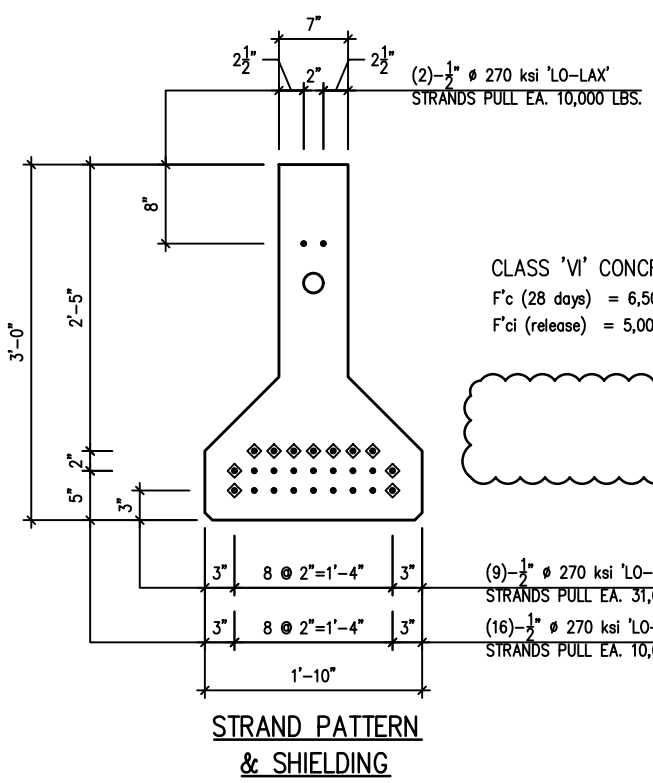
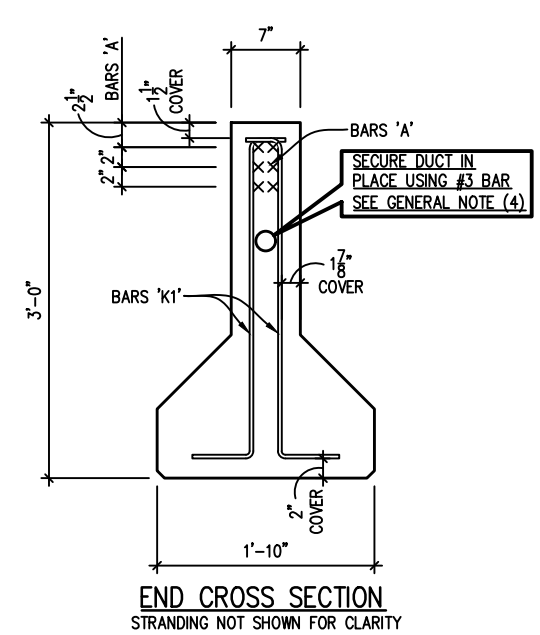
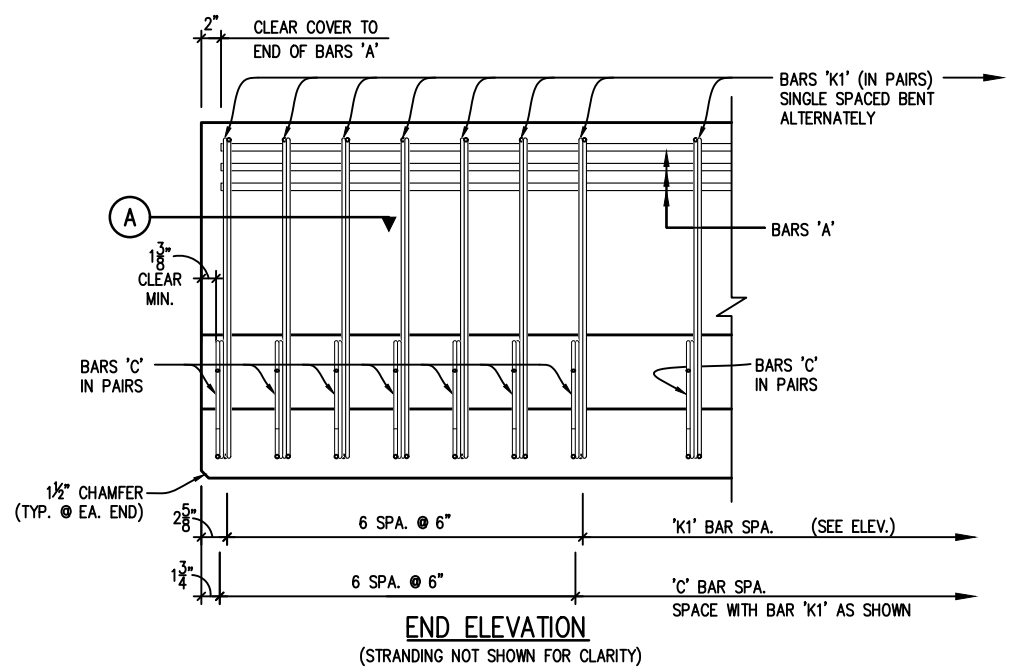
DURA-STRESS Inc.
 CA #6028
 P.O. BOX 490779 LEESBURG, FL 34749-0779
 PHONE (352) 787-1422 FAX (352) 787-0080
 STRUCTURAL PRESTRESSED AND ARCHITECTURAL PRECAST CONCRETE PRODUCTS



JOB NAME: FDOT RESEARCH SHEAR BEHAVIOR OF WEBS
 LOCATION: N/A
 ARCHITECT: N/A
 ENGINEER: N/A
 CONTRACTOR: N/A
 PROJ. NO: N/A

DRAWN: NE
 CHK'D.: POL
 APPR.:
 DATE: 11/13/18
 RELEASED:

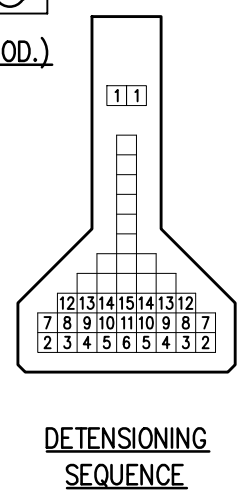
DS JOB NO: B1800
 SHT: SS1-1 OF 2



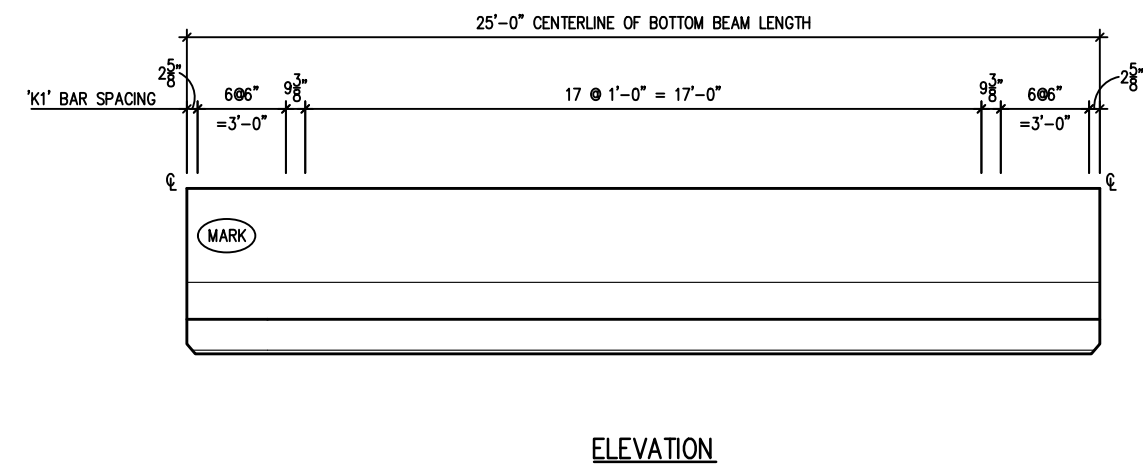
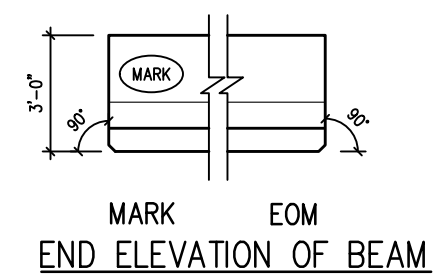
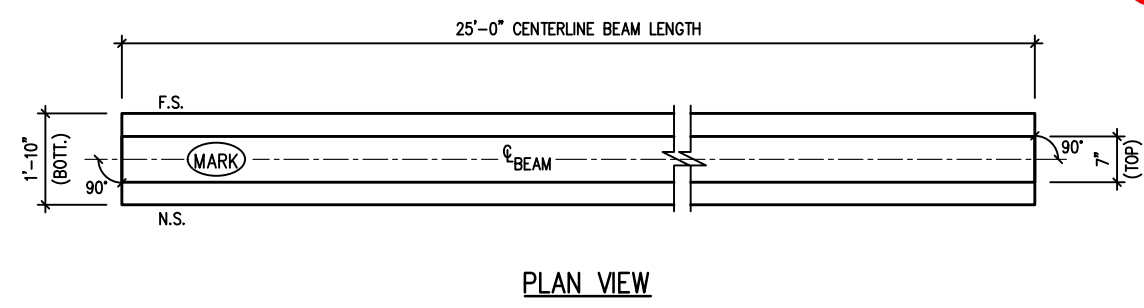
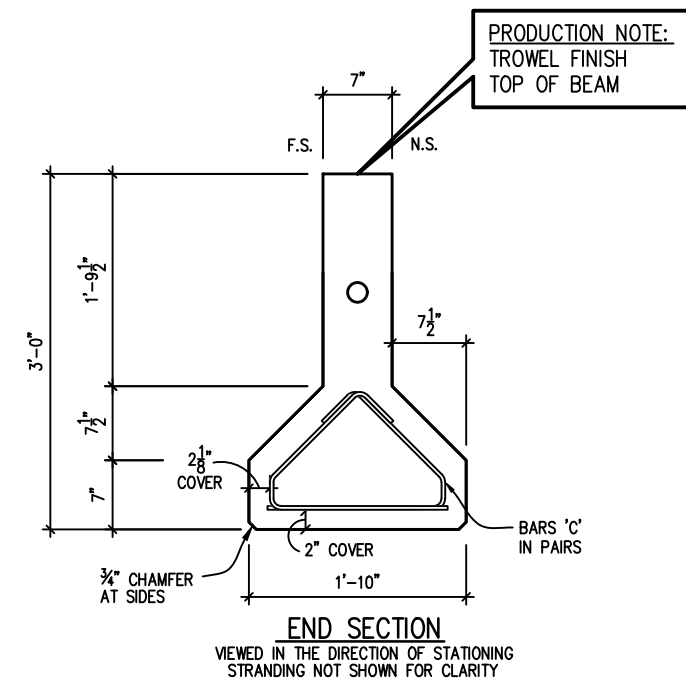
SHIELDING LEGEND

- - NONE REQUIRED
- ◊ - STRANDS DEBONDED 12'-0" FROM END OF BEAM

AASHTO TYPE III (MOD.)



RESUBMITTED
 Dec 21, 2018
 FOR APPROVAL



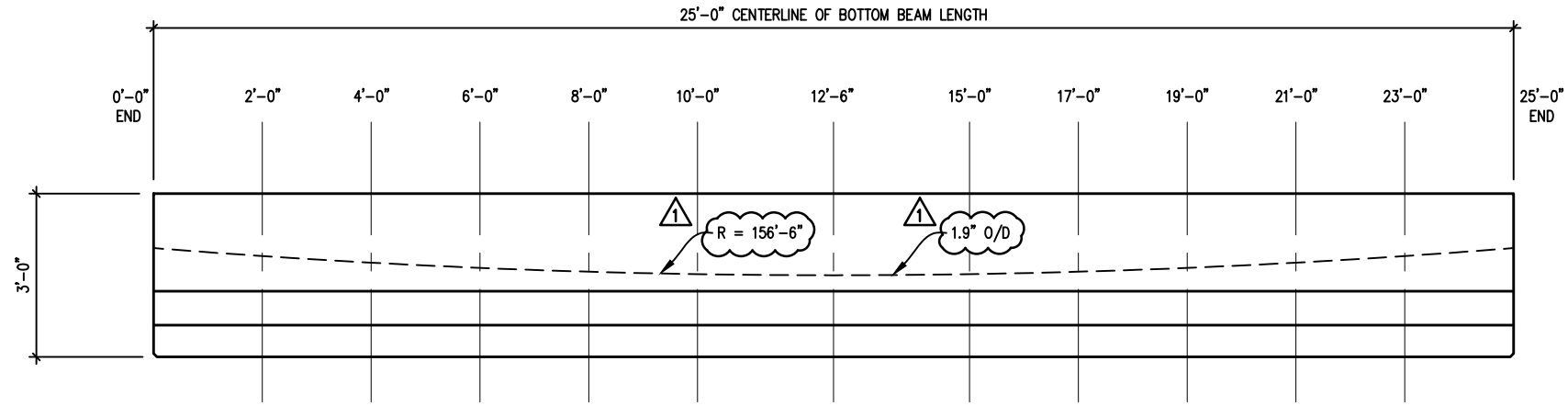
BILL OF EMBED MATERIALS FOR ONE MEMBER ONLY

BAR	D.S. I.D. #	SIZE	QTY.	LENGTH	REMARKS
A	RE-BAR 6	#6	6	24'-8"	STRAIGHT BAR
C	RE-BAR 3	#3	64	3'-3"	SEE SHEET 'A1'
K1	RE-BAR 3	#3	64	3'-7"	SEE SHEET 'A1'

MARK	QTY.	WEIGHT	CU. YDS	℄ LENGTH	BRG. PL. @ MK	BRG. PL. @ EOM
SS1	1	10,665#	2.63	25'-0"	-	-

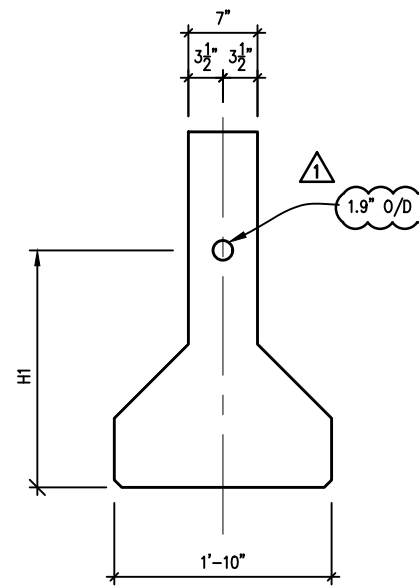
PRODUCTION NOTE: REFER TO SHEETS NO. A1 FOR ADDITIONAL NOTES NOT SHOWN, THAT APPLY TO BEAM DETAIL.

DS PART NO. GIRT 3 (MOD.)



DUCT LAYOUT

GIRDER	SS1													
DISTANCE FROM END OF GIRDER	0'-0"	2'-0"	4'-0"	6'-0"	8'-0"	10'-0"	12'-6"	15'-0"	17'-0"	19'-0"	21'-0"	23'-0"	25'-0"	
H1 (FT)	2'-0"	1'-10 1/4"	1'-8 3/4"	1'-7 5/8"	1'-6 3/4"	1'-6 1/4"	1'-6"	1'-6 1/4"	1'-6 3/4"	1'-7 5/8"	1'-8 3/4"	1'-10 1/4"	2'-0"	



BEAM SECTION

RESUBMITTED
Dec 21, 2018
FOR APPROVAL

DS PART NO.
GIRT 3 (MOD.)



REV	DESCRIPTION	DATE	BY	CHK.
1	REVISED AS SHOWN	12/21/18	NE	KK

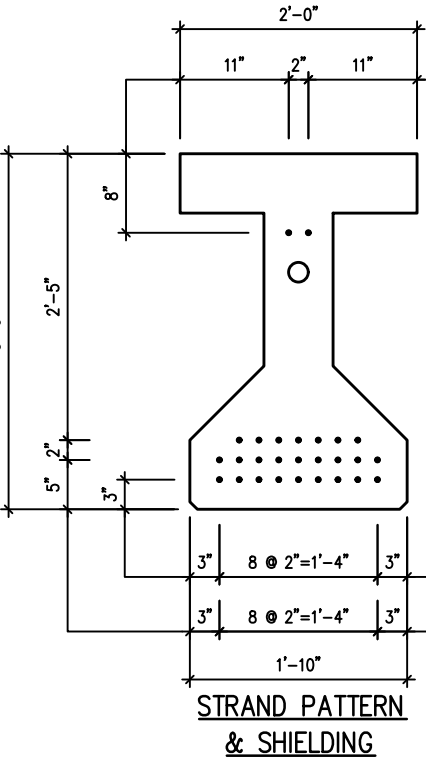
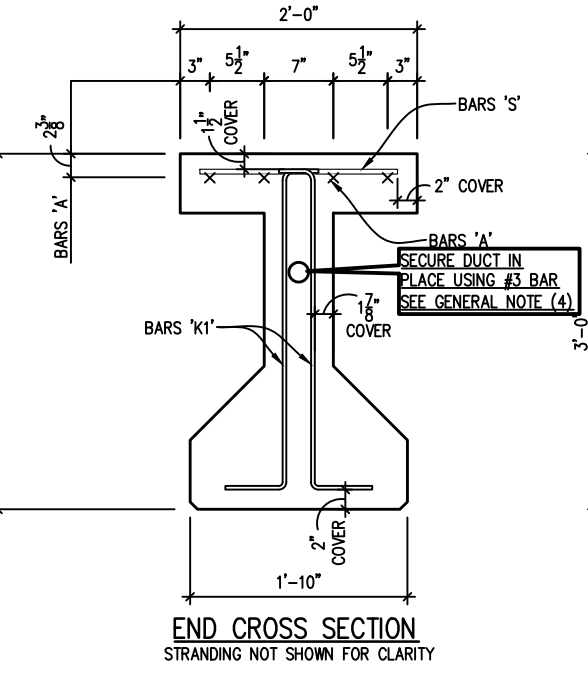
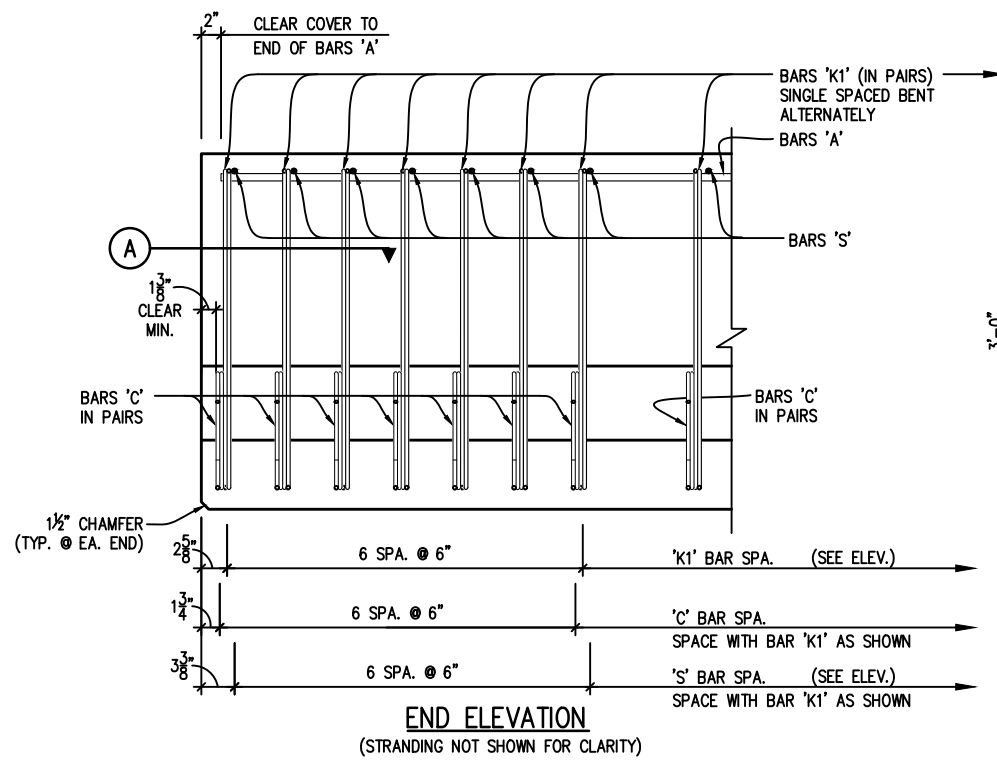
DUCT LOCATIONS

DURA-STRESS Inc.
CA #6028
P.O. BOX 490779 LEESBURG, FL 34749-0779
PHONE (352) 787-1422 FAX (352) 787-0080
STRUCTURAL PRESTRESSED AND ARCHITECTURAL PRECAST CONCRETE PRODUCTS

JOB NAME: FDOT RESEARCH SHEAR BEHAVIOR OF WEBS
LOCATION: N/A
ARCHITECT: N/A
ENGINEER: N/A
CONTRACTOR: N/A
PROJ. NO: N/A

DRAWN: NE
CHK'D.: POL
APPR.:
DATE: 11/13/18
RELEASED:

DS JOB NO:
B1800
SHT: SS1-2 OF 2



(2)-1/2" @ 270 ksi 'LO-LAX' STRANDS PULL EA. 10,000 LBS.

SHIELDING LEGEND

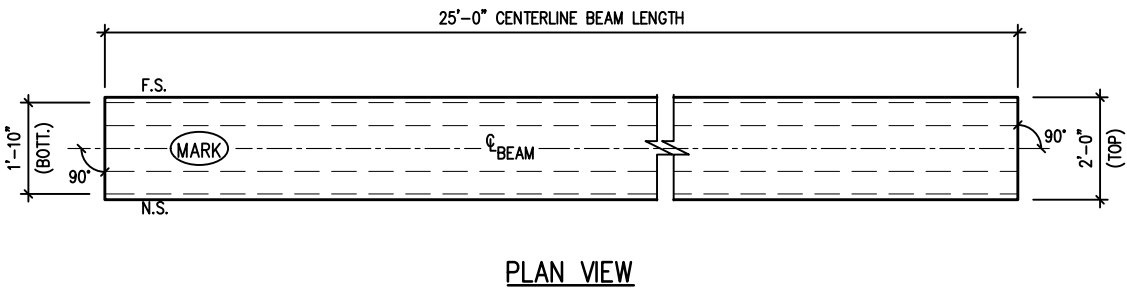
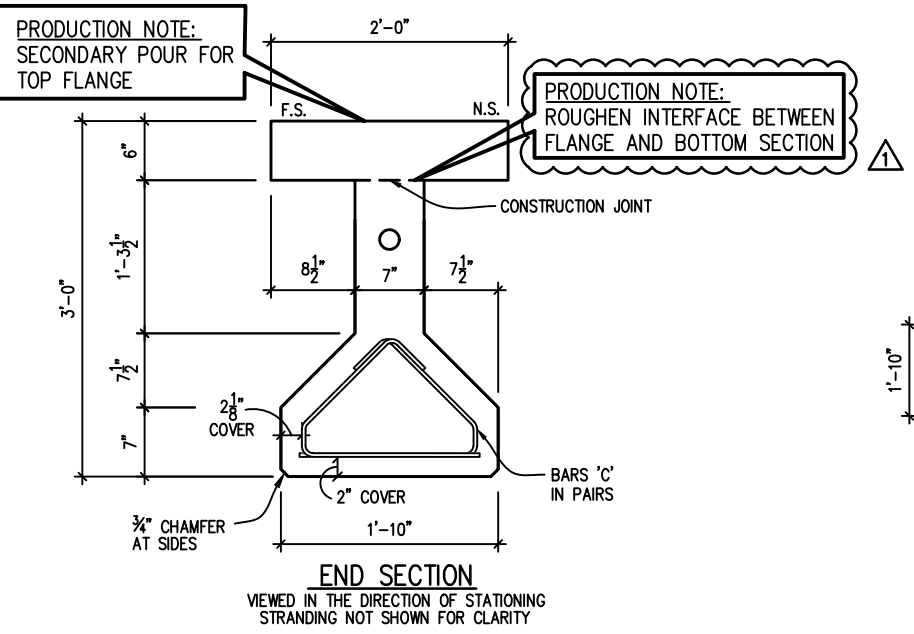
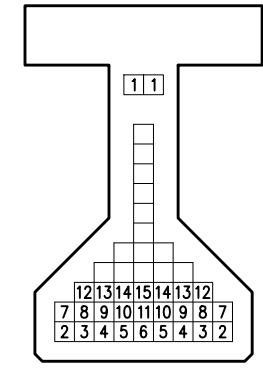
- - NONE REQUIRED

AASHTO TYPE III (MOD.)

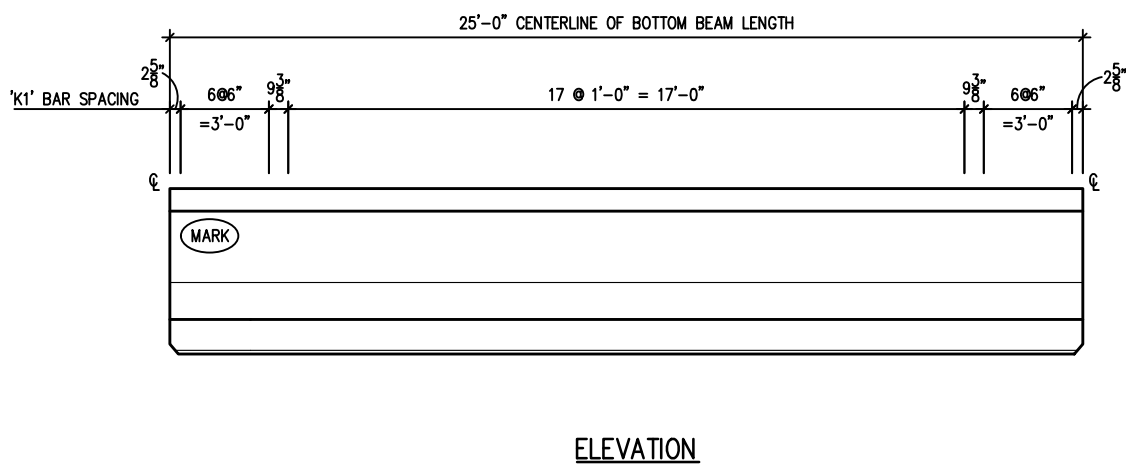
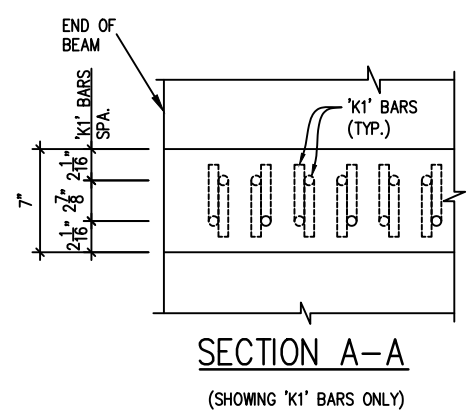
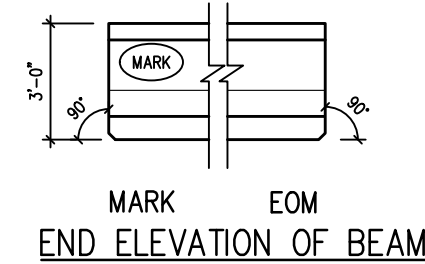
CLASS 'VI' CONCRETE

F'c (28 days) = 6,500 psi

F'ci (release) = 5,000 psi



RESUBMITTED
Dec 21, 2018
FOR APPROVAL



BILL OF EMBED MATERIALS FOR ONE MEMBER ONLY					
BAR	D.S. I.D. #	SIZE	QTY.	LENGTH	REMARKS
A	RE-BAR 6	#6	4	24'-8"	STRAIGHT BAR
C	RE-BAR 3	#3	64	3'-3"	SEE SHEET 'A1'
K1	RE-BAR 3	#3	64	3'-7"	SEE SHEET 'A1'
S	RE-BAR 4	#4	32	1'-8"	STRAIGHT BAR
MARK	QTY.	WEIGHT	CU.YDS	LENGTH	BRG. PL. @ MK
SS2	1	13,321#	3.29	25'-0"	-

PRODUCTION NOTE:
REFER TO SHEETS NO. A1
FOR ADDITIONAL NOTES NOT
SHOWN, THAT APPLY TO BEAM DETAIL.

DS PART NO.
GIRT 3 (MOD.)

REV	DESCRIPTION	DATE	BY	CHK.
Δ	REVISED AS SHOWN	12/21/18	NE	KK

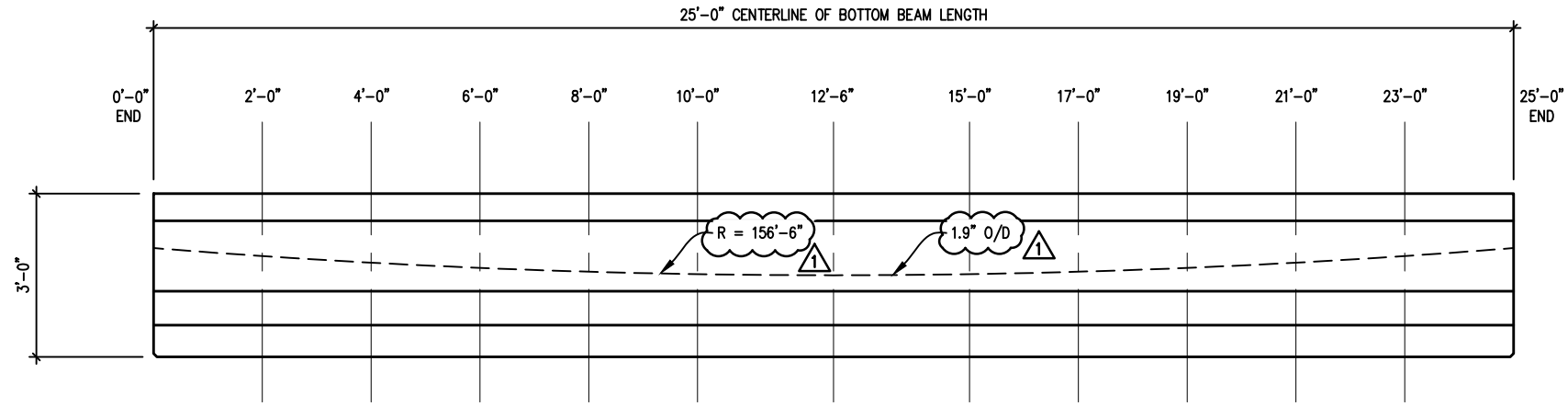
TYPE III (MOD.) BEAM SECTIONS AND DETAILS

DURA-STRESS Inc.
CA #6028
P.O. BOX 490779 LEESBURG, FL 34749-0779
PHONE (352) 787-1422 FAX (352) 787-0080
STRUCTURAL PRESTRESSED AND ARCHITECTURAL PRECAST CONCRETE PRODUCTS

JOB NAME: FDOT RESEARCH SHEAR BEHAVIOR OF WEBS
LOCATION: N/A
ARCHITECT: N/A
ENGINEER: N/A
CONTRACTOR: N/A
PROJ. NO: N/A

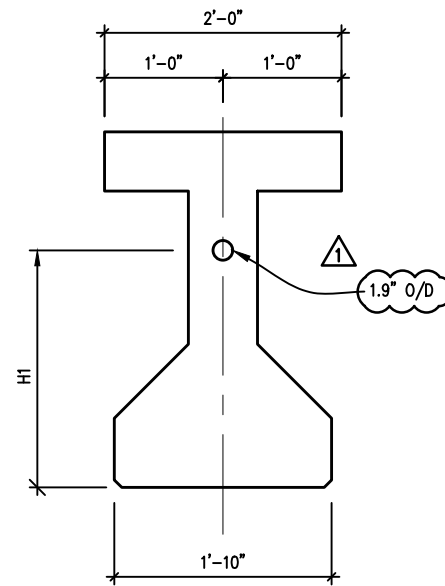
DRAWN: NE
CHK'D.: POL
APPR.:
DATE: 11/13/18
RELEASED:

DS JOB NO: B1800
SHT: SS2-1 OF 2



DUCT LAYOUT

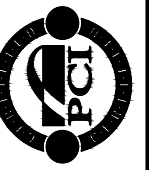
GIRDER	SS2													
DISTANCE FROM END OF GIRDER	0'-0"	2'-0"	4'-0"	6'-0"	8'-0"	10'-0"	12'-6"	15'-0"	17'-0"	19'-0"	21'-0"	23'-0"	25'-0"	
H1 (FT)	2'-0"	1'-10 1/4"	1'-8 3/4"	1'-7 5/8"	1'-6 3/4"	1'-6 1/4"	1'-6"	1'-6 1/4"	1'-6 3/4"	1'-7 5/8"	1'-8 3/4"	1'-10 1/4"	2'-0"	



BEAM SECTION

RESUBMITTED
 Dec 21, 2018
FOR APPROVAL

DS PART NO.
GIRT 3 (MOD.)



REV	DESCRIPTION	DATE	BY	CHK.
1	REVISED AS SHOWN	12/21/18	NE	KK

DUCT LOCATIONS
DURA-STRESS Inc.
 CA #6028
 P.O. BOX 490779 LEESBURG, FL 34749-0779
 PHONE (352) 787-1422 FAX (352) 787-0080
 STRUCTURAL PRESTRESSED AND ARCHITECTURAL PRECAST CONCRETE PRODUCTS

JOB NAME: FDOT RESEARCH
 SHEAR BEHAVIOR OF WEBS
 LOCATION: N/A
 ARCHITECT: N/A
 ENGINEER: N/A
 CONTRACTOR: N/A
 PROJ. NO: N/A

DRAWN: NE
 CHK'D.: POL
 APPR.:
 DATE: 11/13/18
 RELEASED:

DS JOB NO:
 B1800
 SHT: SS2-2 OF 2



REV	DESCRIPTION	DATE	BY	CHK.
Δ	REVISED AS SHOWN	12/21/18	NE	KK

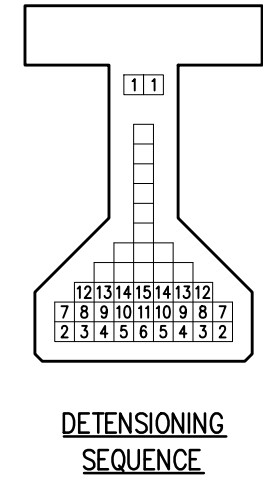
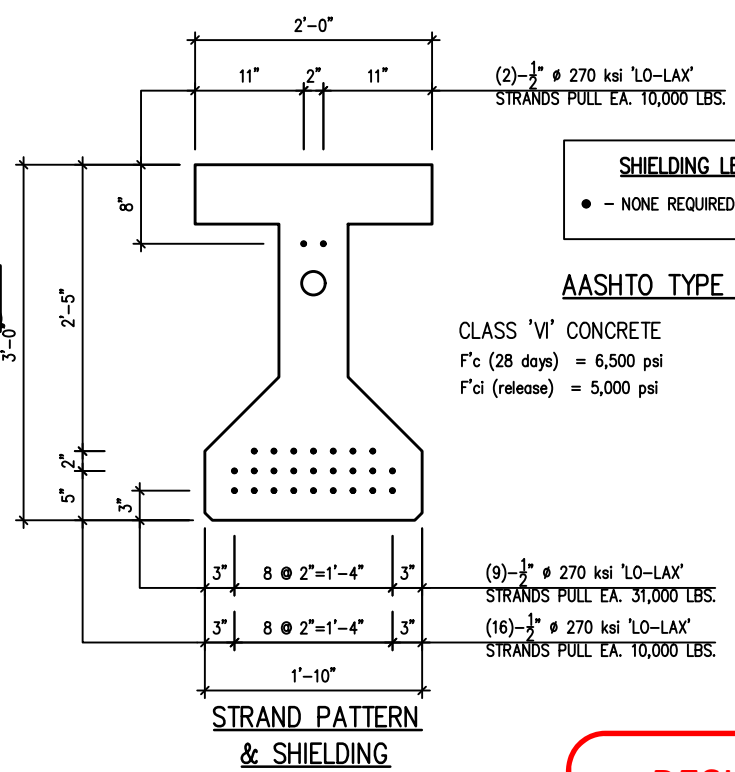
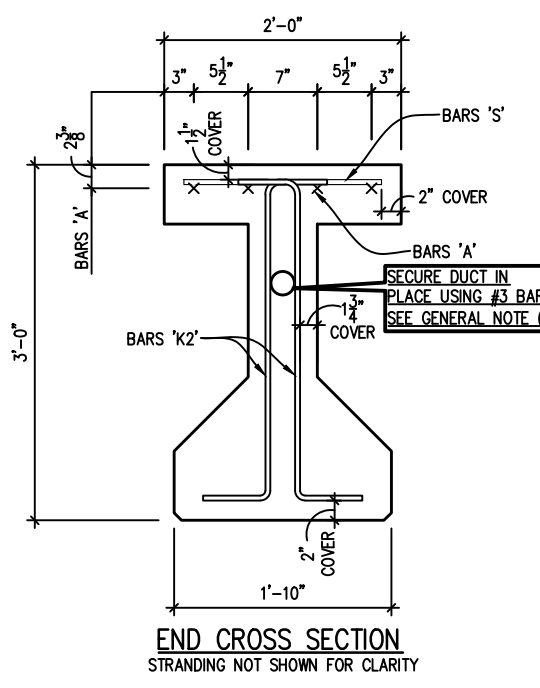
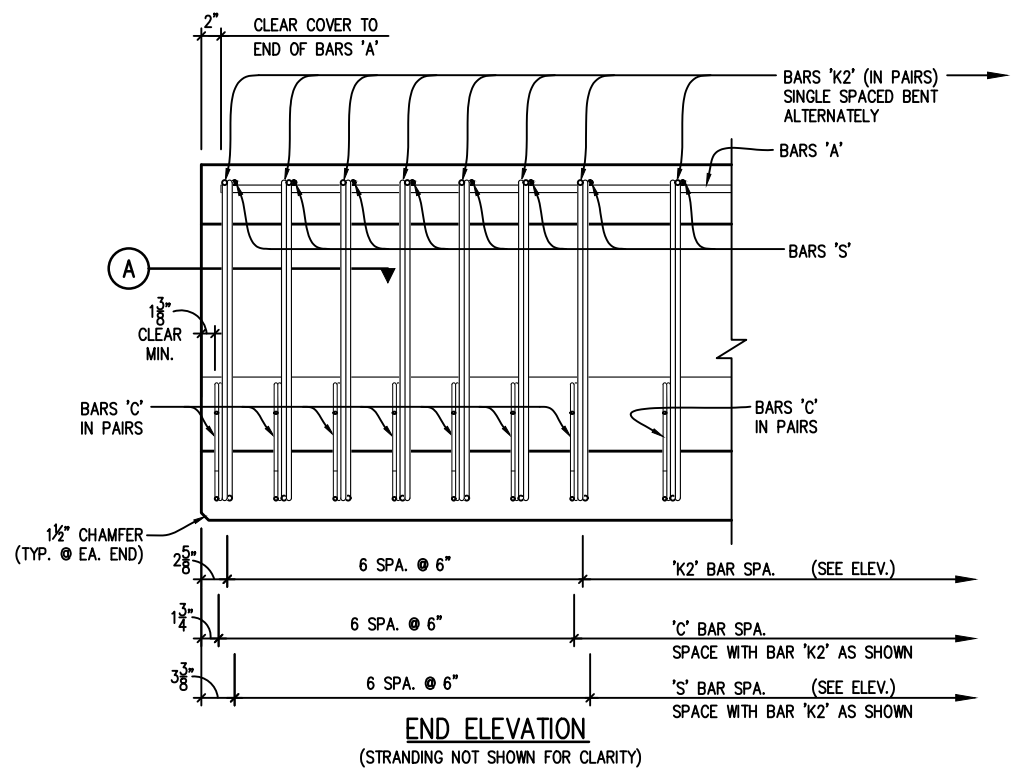
TYPE III (MOD.) BEAM SECTIONS AND DETAILS

DURA-STRESS Inc.
 CA #6028
 P.O. BOX 490779 LEESBURG, FL 34749-0779
 PHONE (352) 787-1422 FAX (352) 787-0080
 STRUCTURAL PRESTRESSED AND ARCHITECTURAL PRECAST CONCRETE PRODUCTS

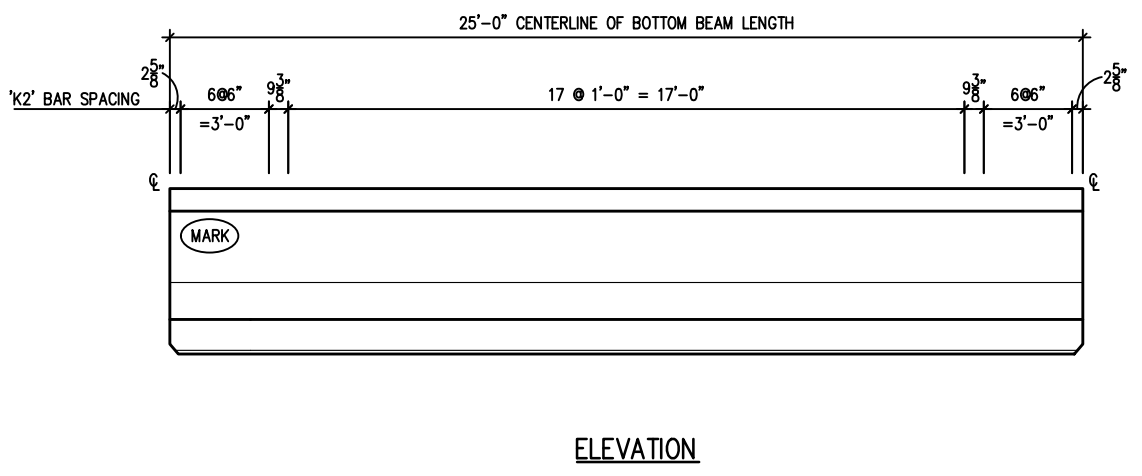
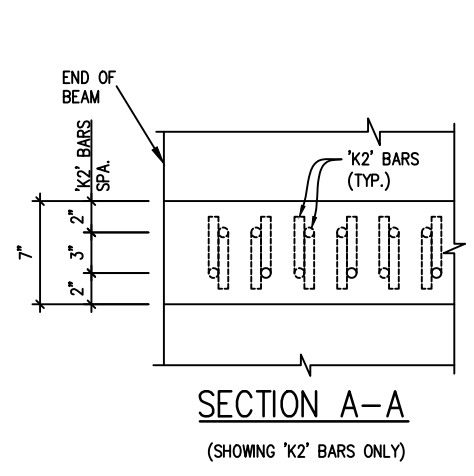
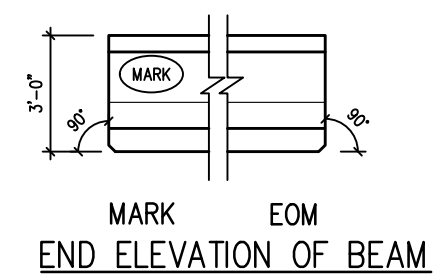
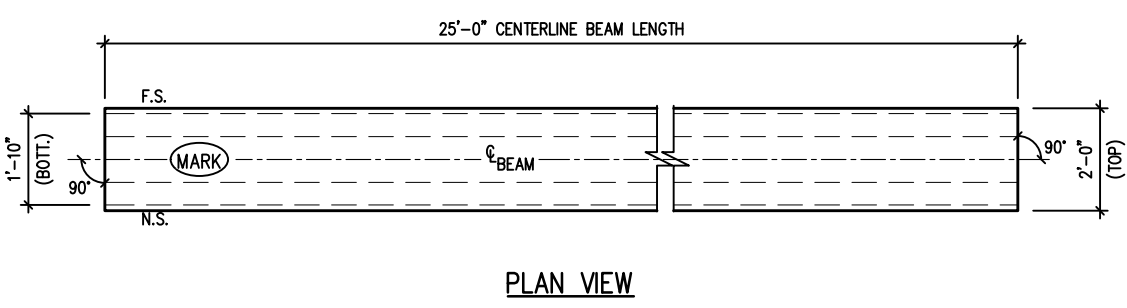
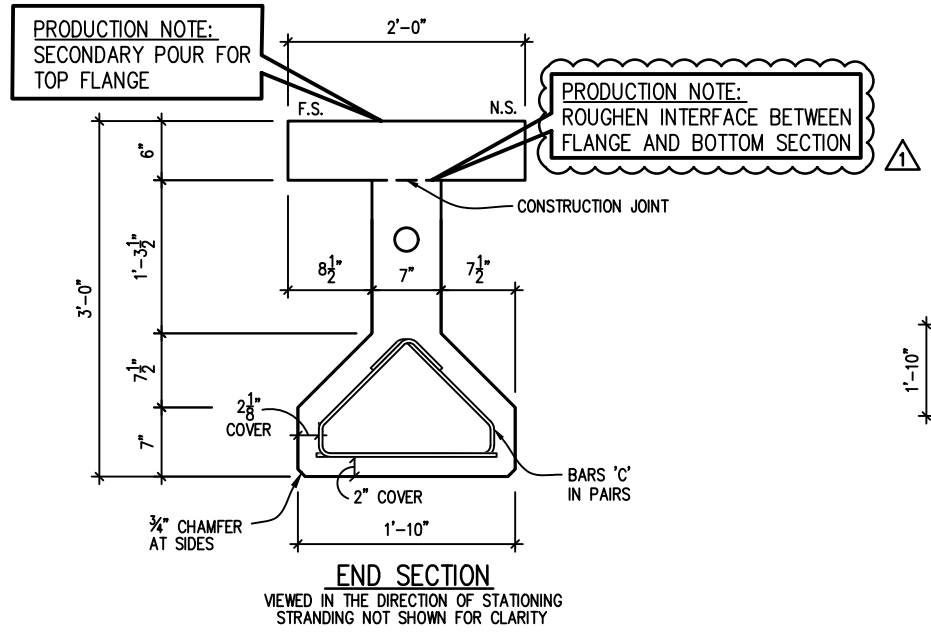
JOB NAME: FDOT RESEARCH SHEAR BEHAVIOR OF WEBS
 LOCATION: N/A
 ARCHITECT: N/A
 ENGINEER: N/A
 CONTRACTOR: N/A
 PROJ. NO: N/A

DRAWN: NE
 CHK'D.: POL
 APPR.:
 DATE: 11/13/18
 RELEASED:

DS JOB NO: B1800
 SHT: SS3-1 OF 2



RESUBMITTED
 Dec 21, 2018
 FOR APPROVAL



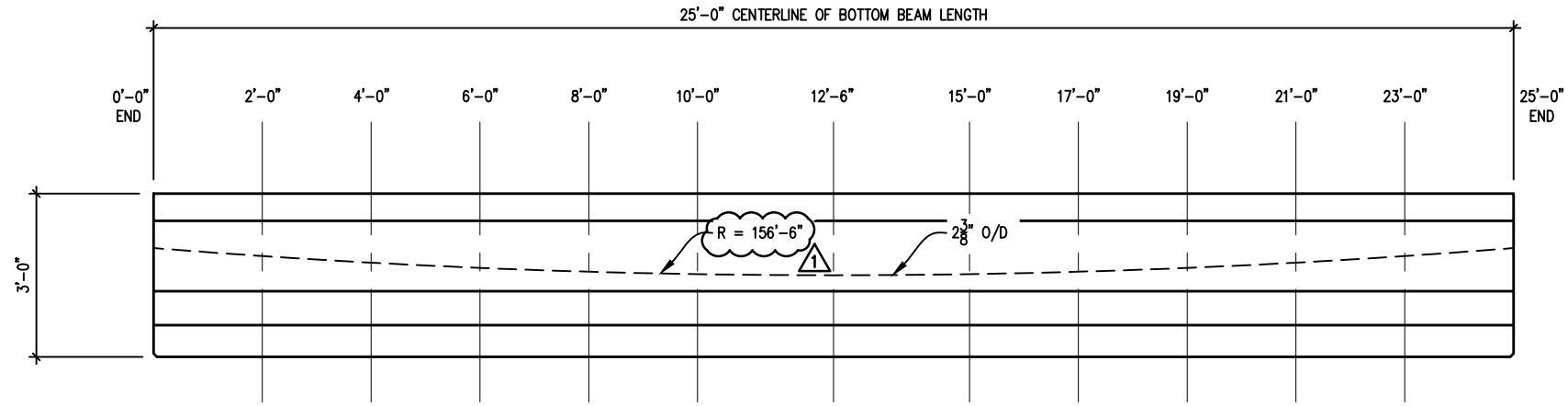
BILL OF EMBED MATERIALS FOR ONE MEMBER ONLY

BAR	D.S. I.D. #	SIZE	QTY.	LENGTH	REMARKS
A	RE-BAR 6	#6	4	24'-8"	STRAIGHT BAR
C	RE-BAR 3	#3	64	3'-3"	SEE SHEET 'A1'
K2	RE-BAR 4	#4	64	3'-9 3/8"	SEE SHEET 'A1'
S	RE-BAR 4	#4	32	1'-8"	STRAIGHT BAR

MARK	QTY.	WEIGHT	CU.YDS	LENGTH	BRG. PL. @ MK	BRG. PL. @ EOM
SS3	1	13,321#	3.29	25'-0"	-	-

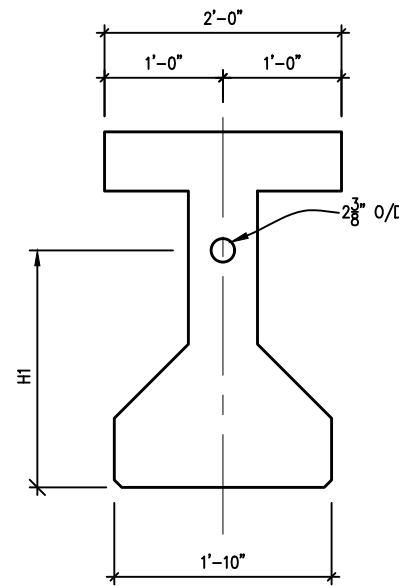
PRODUCTION NOTE:
 REFER TO SHEETS NO. A1
 FOR ADDITIONAL NOTES NOT
 SHOWN, THAT APPLY TO BEAM DETAIL.

DS PART NO.
 GIRT 3 (MOD.)



DUCT LAYOUT

GIRDER	SS3													
DISTANCE FROM END OF GIRDER	0'-0"	2'-0"	4'-0"	6'-0"	8'-0"	10'-0"	12'-6"	15'-0"	17'-0"	19'-0"	21'-0"	23'-0"	25'-0"	
H1 (FT)	2'-0"	1'-10 1/4"	1'-8 3/4"	1'-7 5/8"	1'-6 3/4"	1'-6 1/4"	1'-6"	1'-6 1/4"	1'-6 3/4"	1'-7 5/8"	1'-8 3/4"	1'-10 1/4"	2'-0"	



BEAM SECTION

RESUBMITTED
 Dec 21, 2018
FOR APPROVAL

DS PART NO.
 GIRT 3 (MOD.)



REV	DESCRIPTION	DATE	BY	CHK.
1	REVISED AS SHOWN	12/21/18	NE	KK

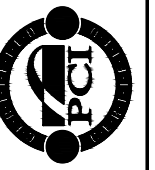
DUCT LOCATIONS

DURA-STRESS Inc.
 CA #6028
 P.O. BOX 490779 LEESBURG, FL 34749-0779
 PHONE (352) 787-1422 FAX (352) 787-0080
 STRUCTURAL PRESTRESSED AND ARCHITECTURAL PRECAST CONCRETE PRODUCTS

JOB NAME: FDOT RESEARCH SHEAR BEHAVIOR OF WEBS
 LOCATION: N/A
 ARCHITECT: N/A
 ENGINEER: N/A
 CONTRACTOR: N/A
 PROJ. NO: N/A

DRAWN: NE
 CHK'D.: POL
 APPR.:
 DATE: 11/13/18
 RELEASED:

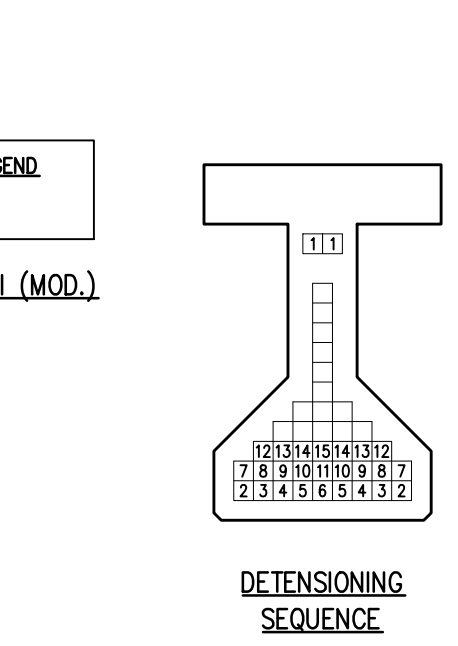
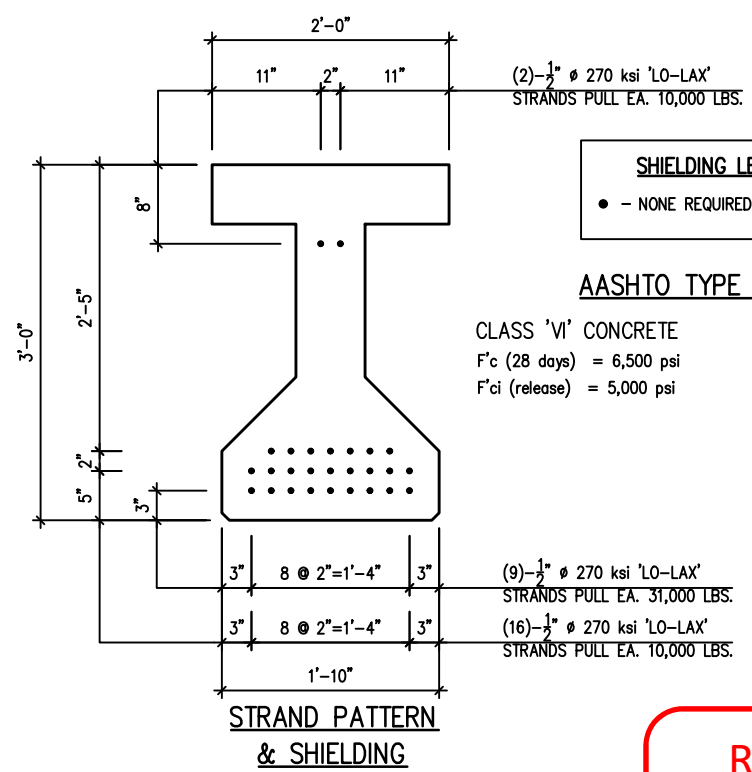
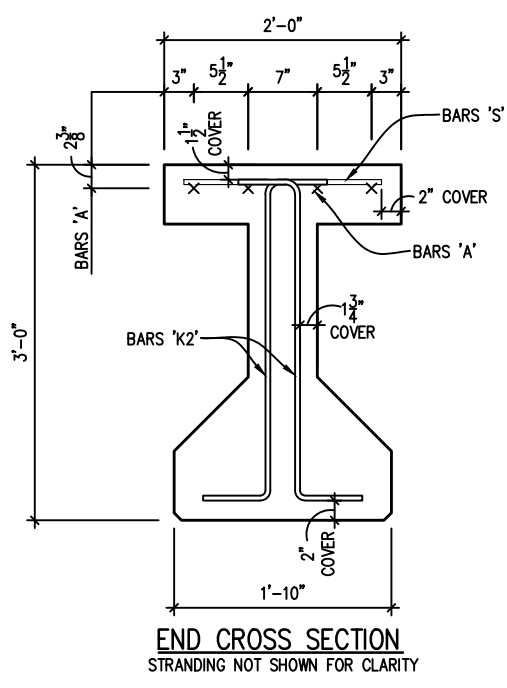
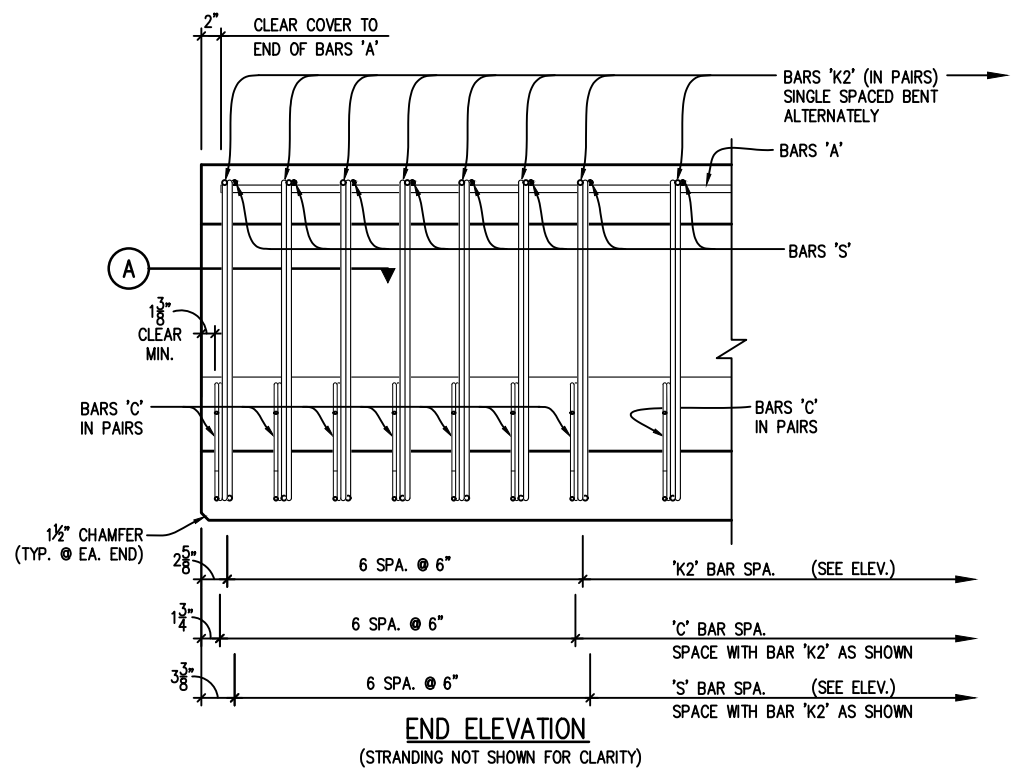
DS JOB NO:
 B1800
 SHT: SS3-2 OF 2



REV	DESCRIPTION	DATE	BY	CHK.
Δ	REVISED AS SHOWN	12/21/18	NE	KK

TYPE III (MOD.) BEAM SECTIONS AND DETAILS

DURA-STRESS Inc.
 CA #6028
 P.O. BOX 490779 LEESBURG, FL 34749-0779
 PHONE (352) 787-1422 FAX (352) 787-0080
 STRUCTURAL PRESTRESSED AND ARCHITECTURAL PRECAST CONCRETE PRODUCTS

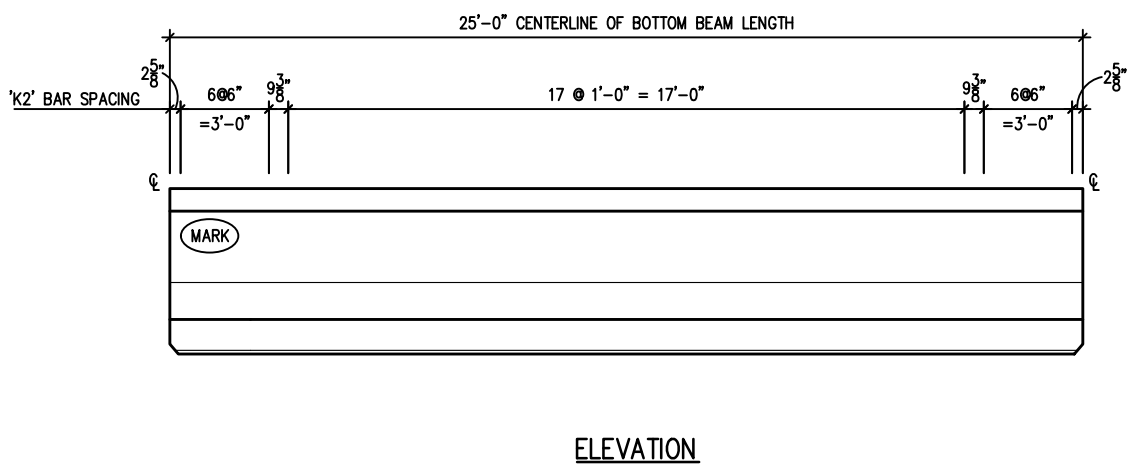
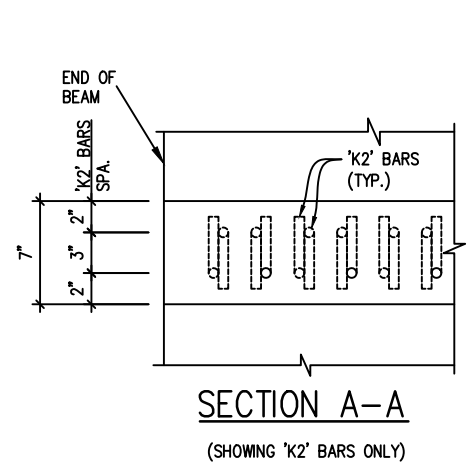
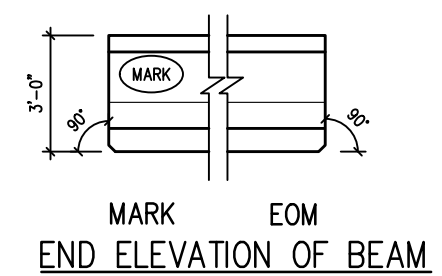
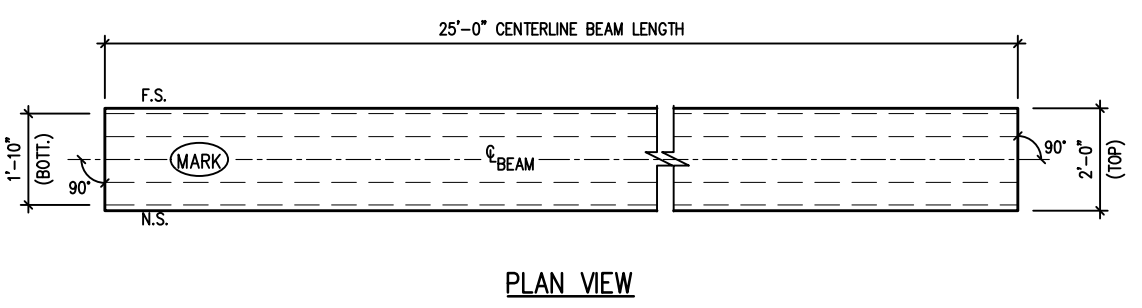
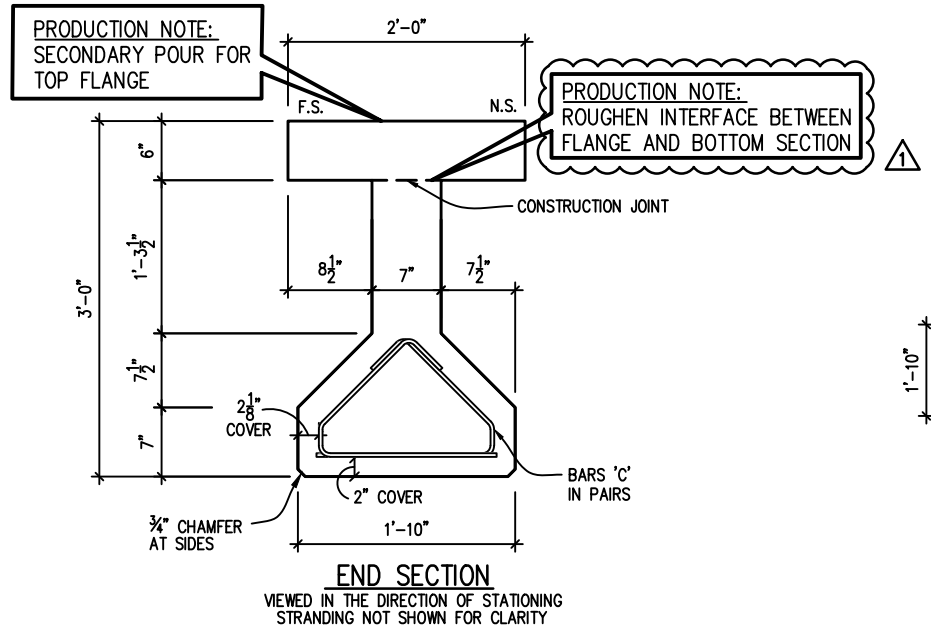


SHIELDING LEGEND
 • - NONE REQUIRED

AASHTO TYPE III (MOD.)

CLASS 'VI' CONCRETE
 F'c (28 days) = 6,500 psi
 F'ci (release) = 5,000 psi

RESUBMITTED
 Dec 21, 2018
FOR APPROVAL



BAR	D.S. I.D. #	SIZE	QTY.	LENGTH	REMARKS
A	RE-BAR 6	#6	4	24'-8"	STRAIGHT BAR
C	RE-BAR 3	#3	64	3'-3"	SEE SHEET 'A1'
K2	RE-BAR 4	#4	64	3'-9 3/8"	SEE SHEET 'A1'
S	RE-BAR 4	#4	32	1'-8"	STRAIGHT BAR

MARK	QTY.	WEIGHT	CU.YDS	ℓ LENGTH	BRG. PL. @ MK	BRG. PL. @ EOM
SS4	1	13,403#	3.31	25'-0"	-	-

PRODUCTION NOTE:
 REFER TO SHEETS NO. A1
 FOR ADDITIONAL NOTES NOT
 SHOWN, THAT APPLY TO BEAM DETAIL.

DS PART NO.
GIRT 3 (MOD.)

JOB NAME: FDOT RESEARCH SHEAR BEHAVIOR OF WEBS
 LOCATION: N/A
 ARCHITECT: N/A
 ENGINEER: N/A
 CONTRACTOR: N/A
 PROJ. NO: N/A

DRAWN: NE
 CHK'D.: POL
 APPR.:
 DATE: 11/13/18
 RELEASED:

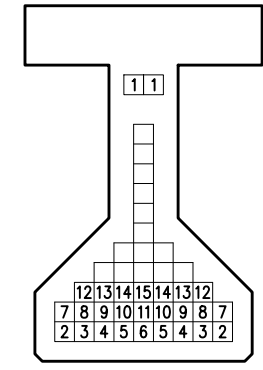
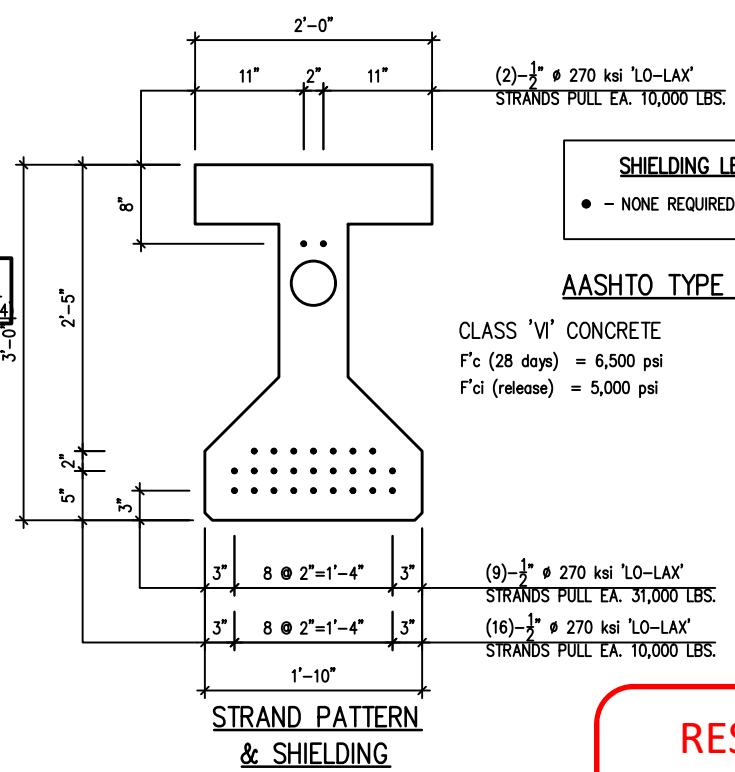
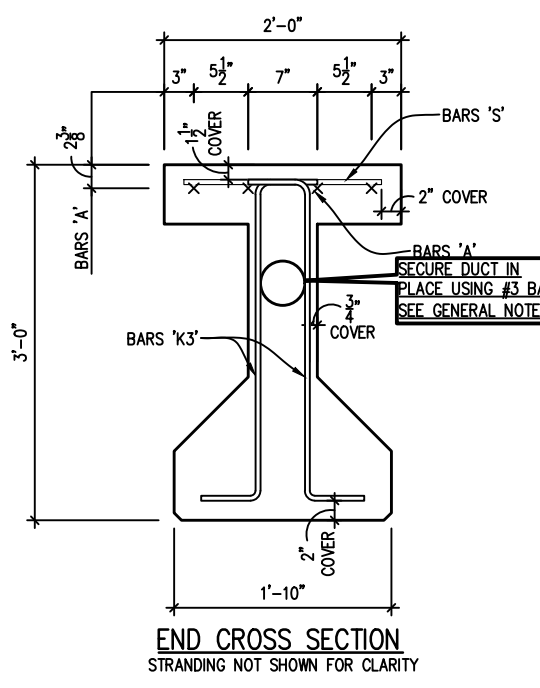
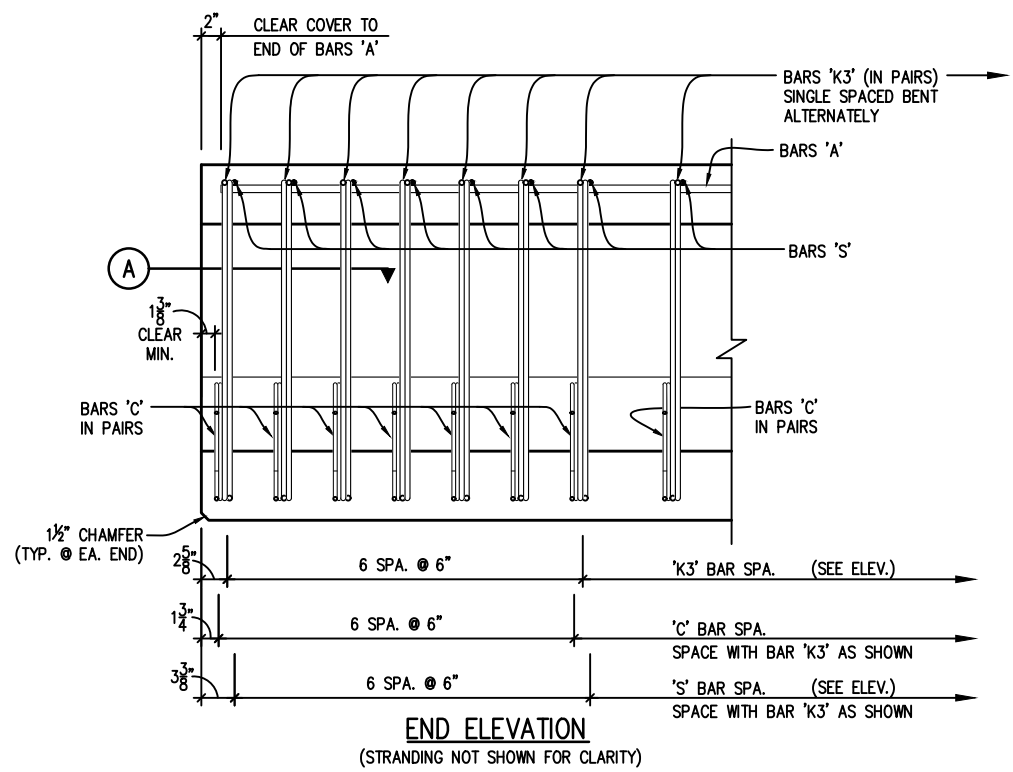
DS JOB NO:
B1800
 SHT: SS4



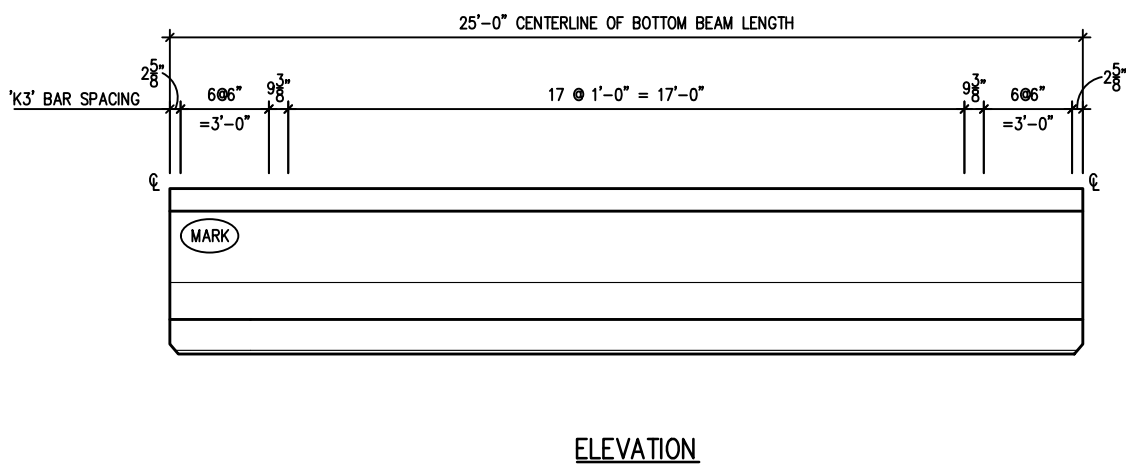
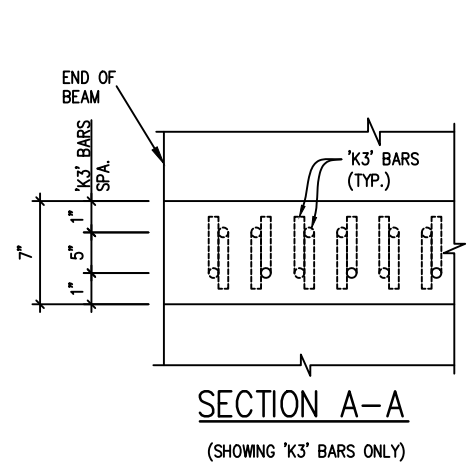
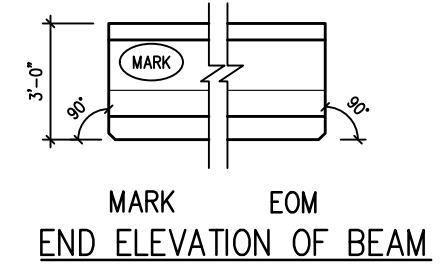
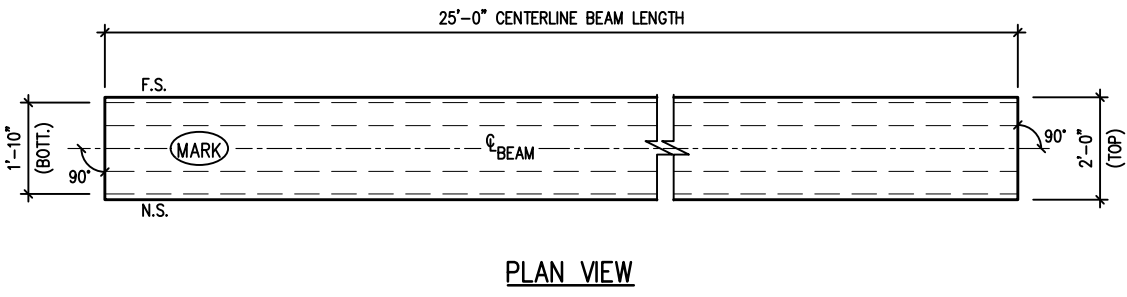
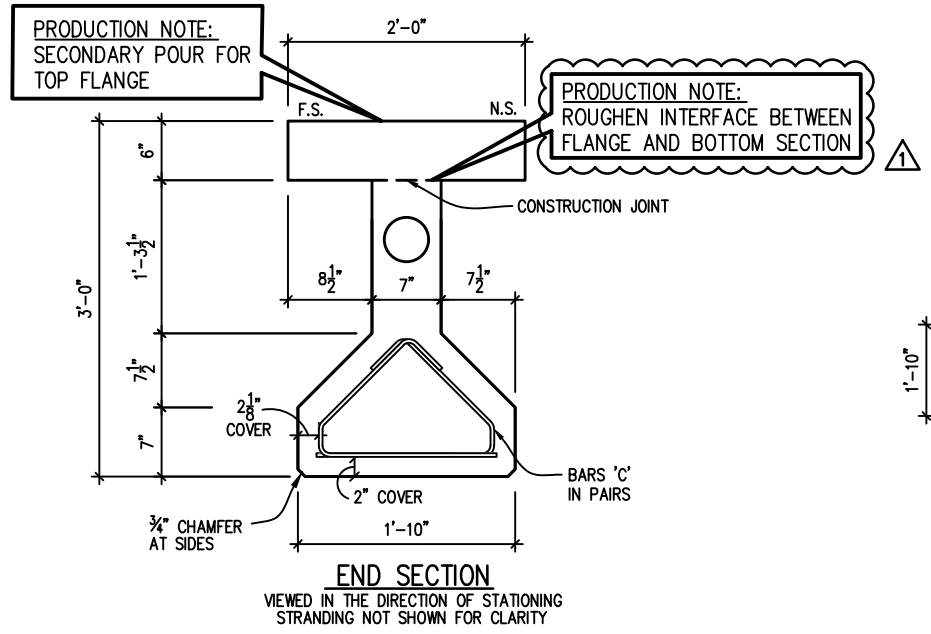
REV	DESCRIPTION	DATE	BY	CHK.
Δ	REVISED AS SHOWN	12/21/18	NE	KK

TYPE III (MOD.) BEAM SECTIONS AND DETAILS

DURA-STRESS Inc.
 CA #6028
 P.O. BOX 490779 LEESBURG, FL 34749-0779
 PHONE (352) 787-1422 FAX (352) 787-0080
 STRUCTURAL PRESTRESSED AND ARCHITECTURAL PRECAST CONCRETE PRODUCTS



RESUBMITTED
 Dec 21, 2018
 FOR APPROVAL



BILL OF EMBED MATERIALS FOR ONE MEMBER ONLY					
BAR	D.S. I.D. #	SIZE	QTY.	LENGTH	REMARKS
A	RE-BAR 6	#6	4	24'-8"	STRAIGHT BAR
C	RE-BAR 3	#3	64	3'-3"	SEE SHEET 'A1'
K3	RE-BAR 4	#4	64	3'-8 3/4"	SEE SHEET 'A1'
S	RE-BAR 4	#4	32	1'-8"	STRAIGHT BAR

MARK	QTY.	WEIGHT	CU. YDS	CL LENGTH	BRG. PL. @ MK	BRG. PL. @ EOM
SS5	1	12,989#	3.21	25'-0"	-	-

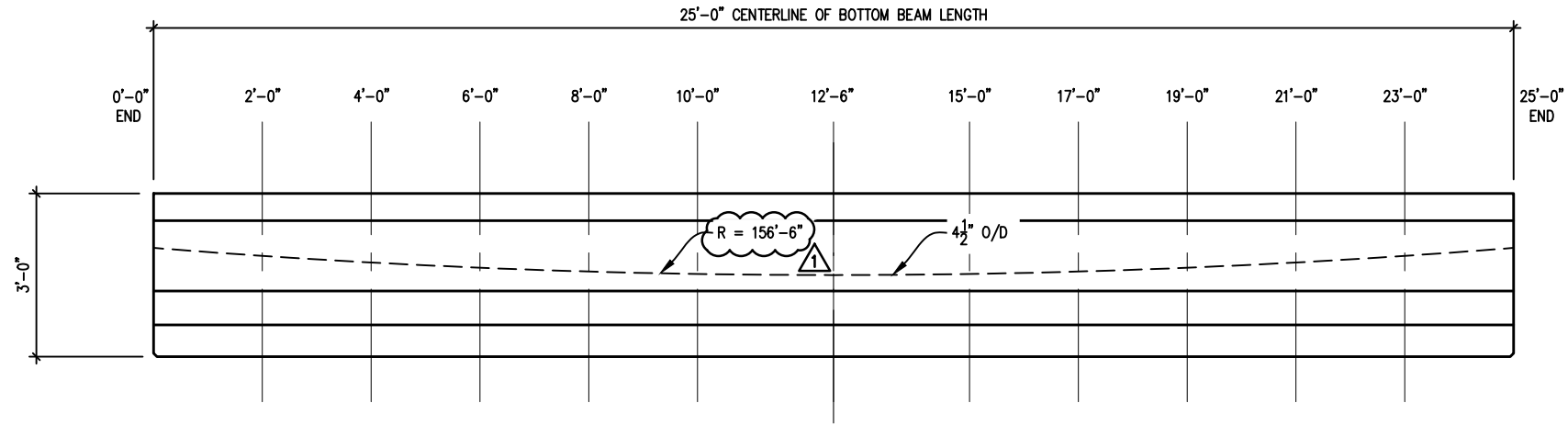
PRODUCTION NOTE:
 REFER TO SHEETS NO. A1 FOR ADDITIONAL NOTES NOT SHOWN, THAT APPLY TO BEAM DETAIL.

DS PART NO. GIRT 3 (MOD.)

JOB NAME: FDOT RESEARCH SHEAR BEHAVIOR OF WEBS
 LOCATION: N/A
 ARCHITECT: N/A
 ENGINEER: N/A
 CONTRACTOR: N/A
 PROJ. NO: N/A

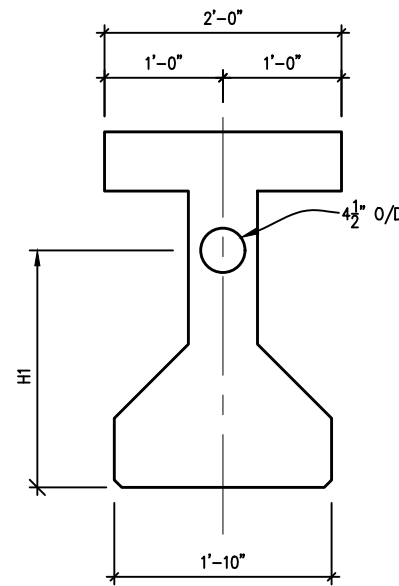
DRAWN: NE
 CHK'D.: POL
 APPR.:
 DATE: 11/13/18
 RELEASED:

DS JOB NO: B1800
 SHT: SS-1 OF 2



DUCT LAYOUT

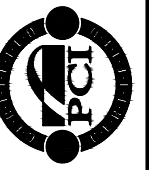
GIRDER	SS5													
DISTANCE FROM END OF GIRDER	0'-0"	2'-0"	4'-0"	6'-0"	8'-0"	10'-0"	12'-6"	15'-0"	17'-0"	19'-0"	21'-0"	23'-0"	25'-0"	
H1 (FT)	2'-0"	1'-10 1/4"	1'-8 3/4"	1'-7 5/8"	1'-6 3/4"	1'-6 1/4"	1'-6"	1'-6 1/4"	1'-6 3/4"	1'-7 5/8"	1'-8 3/4"	1'-10 1/4"	2'-0"	



BEAM SECTION

RESUBMITTED
 Dec 21, 2018
FOR APPROVAL

DS PART NO.
GIRT 3 (MOD.)



REV	DESCRIPTION	DATE	BY	CHK.
1	REVISED AS SHOWN	12/21/18	NE	KK

DUCT LOCATIONS
DURA-STRESS Inc.
 CA #6028
 P.O. BOX 490779 LEESBURG, FL 34749-0779
 PHONE (352) 787-1422 FAX (352) 787-0080
 STRUCTURAL PRESTRESSED AND ARCHITECTURAL PRECAST CONCRETE PRODUCTS

JOB NAME: FDOT RESEARCH SHEAR BEHAVIOR OF WEBS
 LOCATION: N/A
 ARCHITECT: N/A
 ENGINEER: N/A
 CONTRACTOR: N/A
 PROJ. NO: N/A

DRAWN: NE
 CHK'D.: POL
 APPR.:
 DATE: 11/13/18
 RELEASED:

DS JOB NO:
 B1800
 SHT: SS5-2 OF 2



REV	DESCRIPTION	DATE	BY	CHK.
1	REVISED AS SHOWN	12/21/18	NE	KK

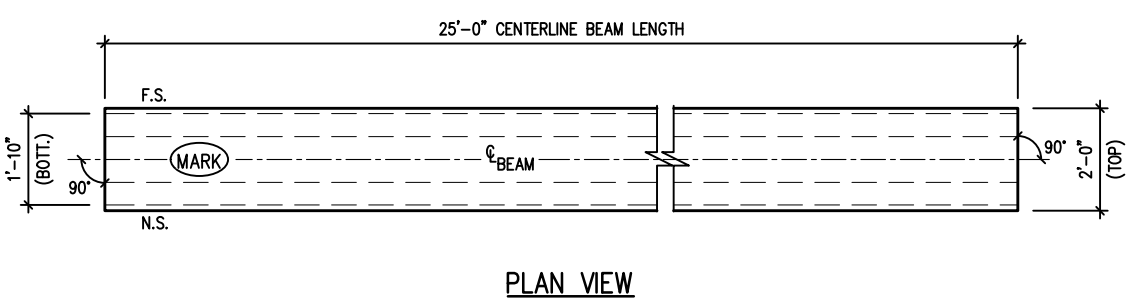
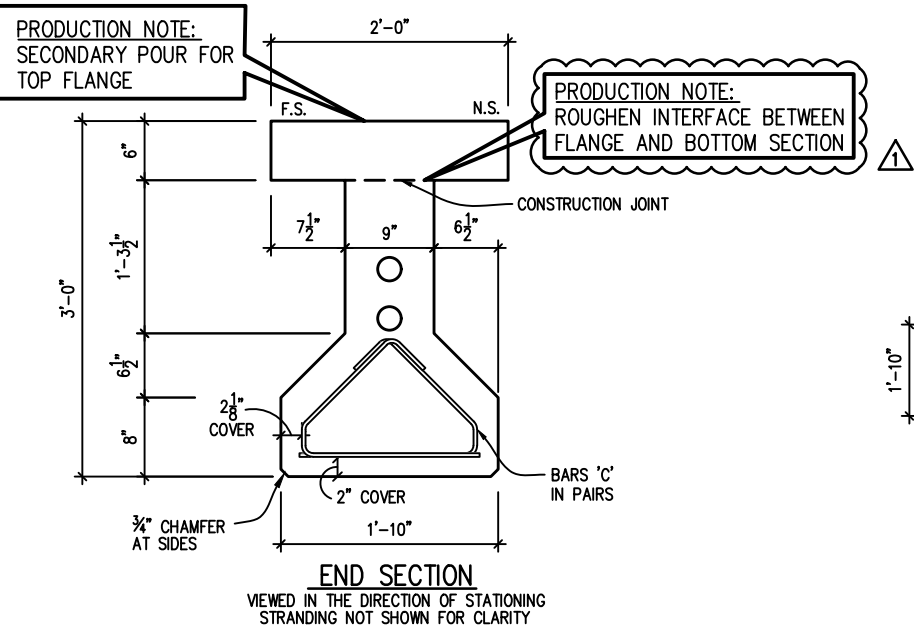
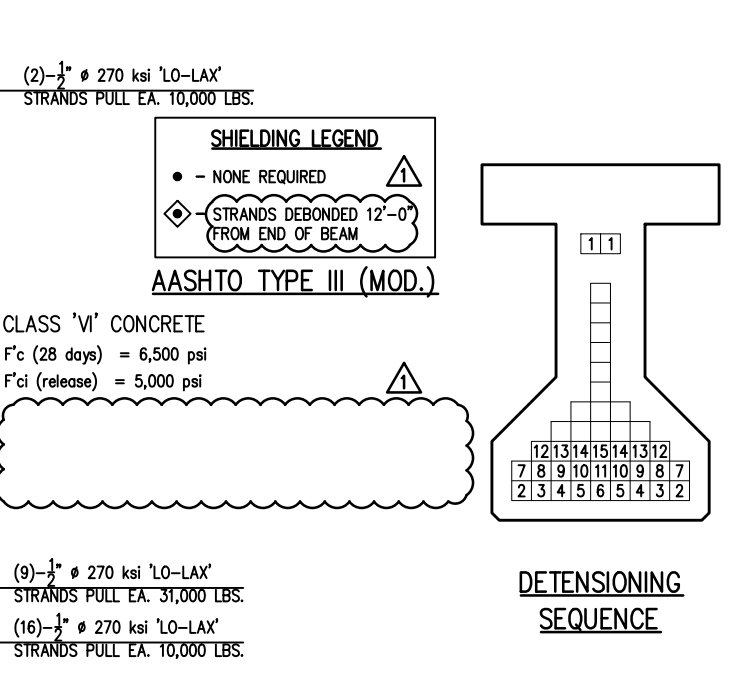
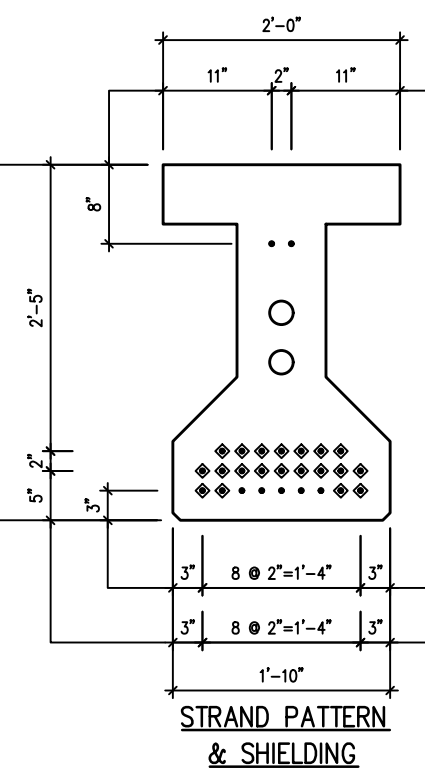
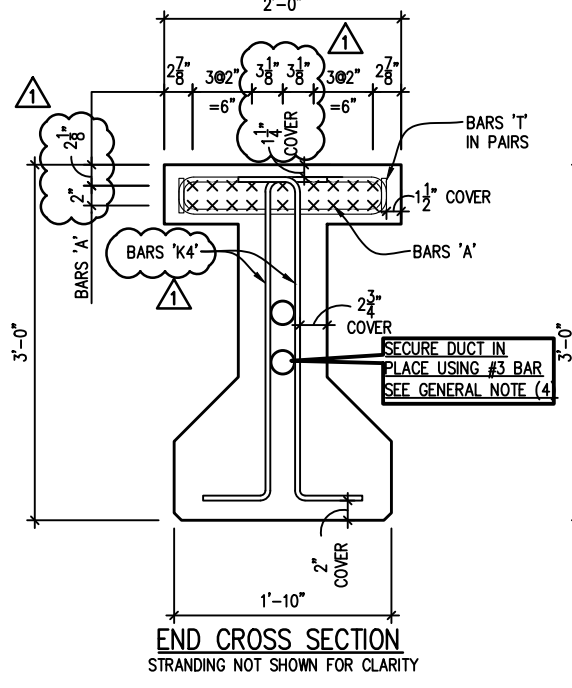
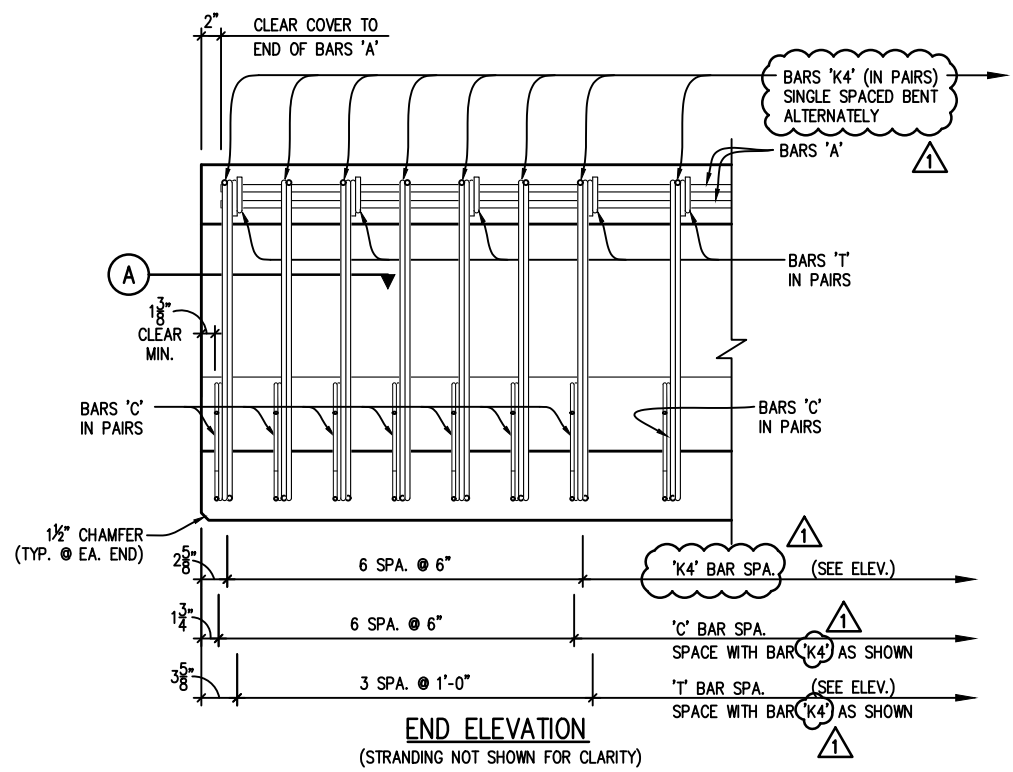
TYPE III (MOD.) BEAM SECTIONS AND DETAILS

DURA-STRESS Inc.
 CA #6028
 P.O. BOX 490779 LEESBURG, FL 34749-0779
 PHONE (352) 787-1422 FAX (352) 787-0080
 STRUCTURAL PRESTRESSED AND ARCHITECTURAL PRECAST CONCRETE PRODUCTS

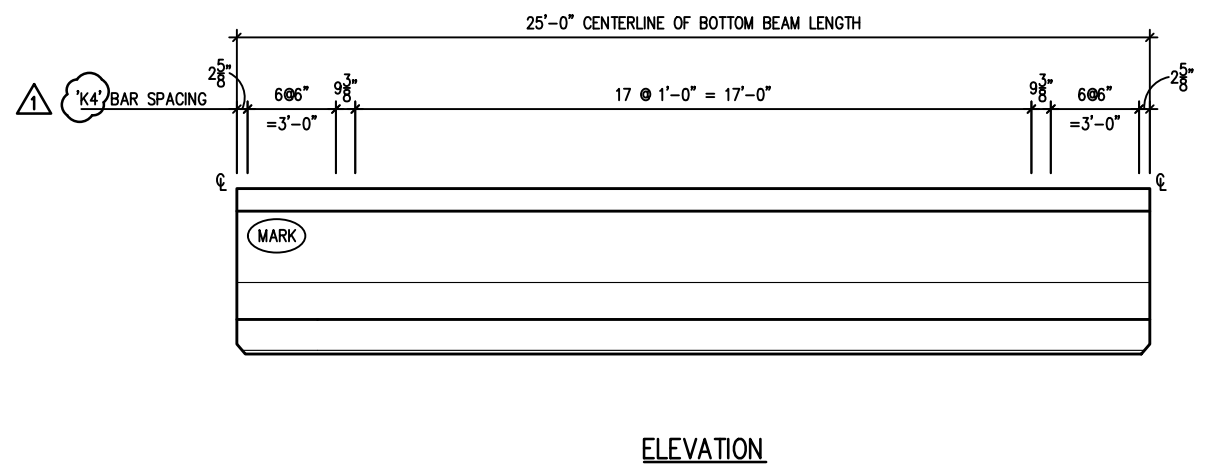
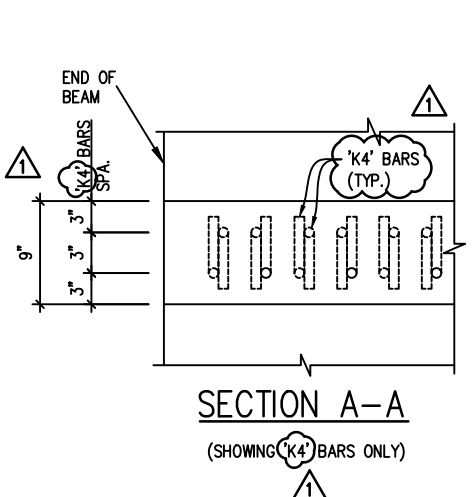
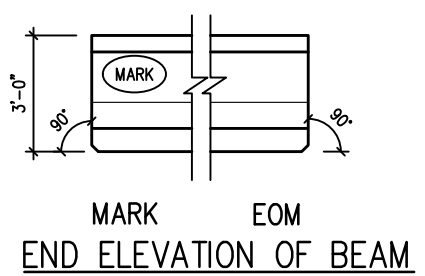
JOB NAME: FDOT RESEARCH SHEAR BEHAVIOR OF WEBS
 LOCATION: N/A
 ARCHITECT: N/A
 ENGINEER: N/A
 CONTRACTOR: N/A
 PROJ. NO: N/A

DRAWN: NE
 CHK'D.: POL
 APPR.:
 DATE: 11/13/18
 RELEASED:

DS JOB NO: B1800
 SHT: NB1-1 OF 2



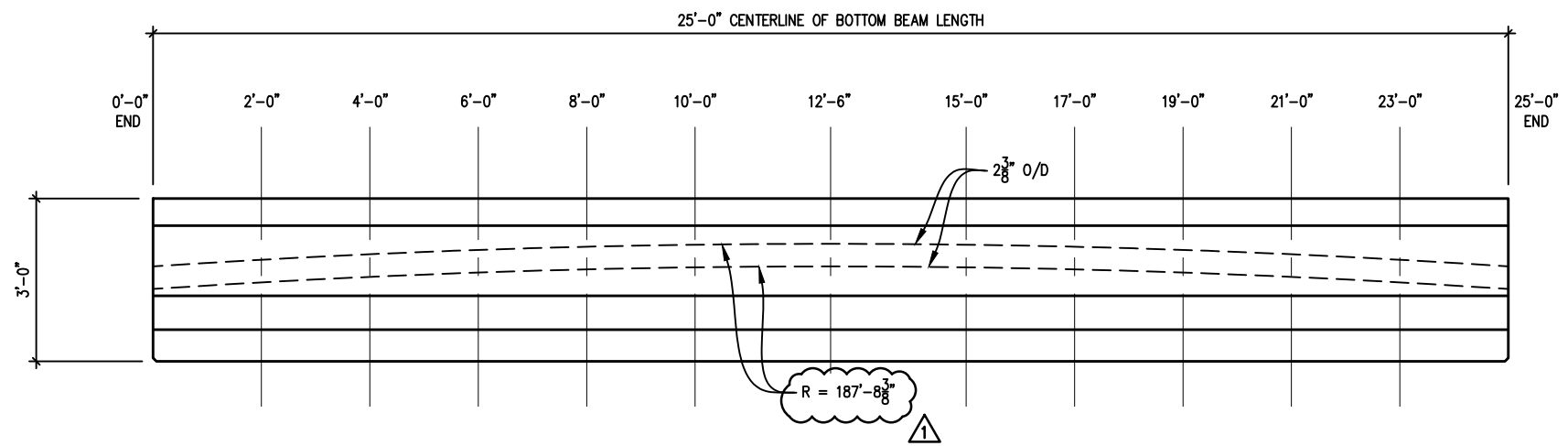
RESUBMITTED
 Dec 21, 2018
FOR APPROVAL



BILL OF EMBED MATERIALS FOR ONE MEMBER ONLY					
BAR	D.S. I.D. #	SIZE	QTY.	LENGTH	REMARKS
A	RE-BAR 6	#6	18	24'-8"	STRAIGHT BAR
C	RE-BAR 3	#3	64	3'-3"	SEE SHEET 'A1'
K4	RE-BAR 4	#4	64	3'-9 7/8"	SEE SHEET 'A1'
T	RE-BAR 4	#4	52	2'-4 1/4"	SEE SHEET 'A1'
MARK	QTY.	WEIGHT	CU.YDS	LENGTH	BRG. PL. @ MK
NB1	1	14,344#	3.54	25'-0"	BRG. PL. @ EOM

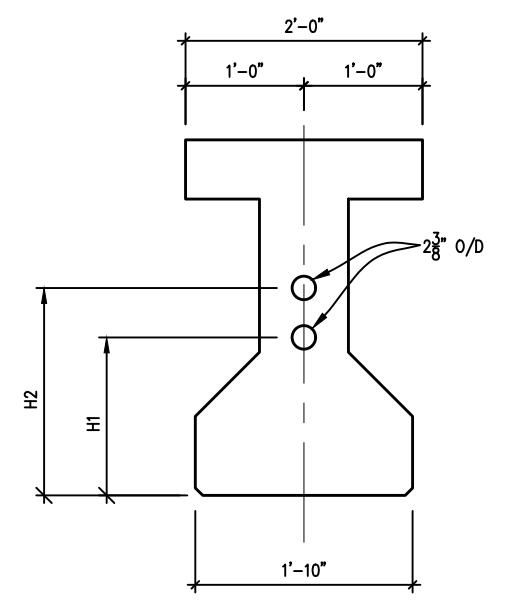
PRODUCTION NOTE:
 REFER TO SHEETS NO. A1
 FOR ADDITIONAL NOTES NOT
 SHOWN, THAT APPLY TO BEAM DETAIL.

DS PART NO.
GIRT 3 (MOD.)



DUCT LAYOUT

GIRDER	NB1												
DISTANCE FROM END OF GIRDER	0'-0"	2'-0"	4'-0"	6'-0"	8'-0"	10'-0"	12'-6"	15'-0"	17'-0"	19'-0"	21'-0"	23'-0"	25'-0"
H1 (FT)	1'-4"	1'-5 1/2"	1'-6 11/16"	1'-7 5/8"	1'-8 3/8"	1'-8 13/16"	1'-9"	1'-8 13/16"	1'-8 3/8"	1'-7 5/8"	1'-6 11/16"	1'-5 1/2"	1'-4"
H2 (FT)	1'-9"	1'-10 1/2"	1'-11 11/16"	2'-0 5/8"	2'-1 3/8"	2'-1 13/16"	2'-2"	2'-1 13/16"	2'-1 3/8"	2'-0 5/8"	1'-11 11/16"	1'-10 1/2"	1'-9"



BEAM SECTION

RESUBMITTED
Dec 21, 2018
FOR APPROVAL

REV	DESCRIPTION	DATE	BY	CHK.
1	REVISED AS SHOWN	12/21/18	NE	KK

DUCT LOCATIONS

DURA-STRESS Inc.
 CA #6028
 P.O. BOX 490779 LEESBURG, FL 34749-0779
 PHONE (352) 787-1422 FAX (352) 787-0080
 STRUCTURAL PRESTRESSED AND ARCHITECTURAL PRECAST CONCRETE PRODUCTS

JOB NAME: FDOT RESEARCH
 SHEAR BEHAVIOR OF WEBS
 LOCATION: N/A
 ARCHITECT: N/A
 ENGINEER: N/A
 CONTRACTOR: N/A
 PROJ. NO: N/A

DRAWN: NE
 CHK'D.: POL
 APPR.:
 DATE: 11/13/18
 RELEASED:

DS PART NO.
 GIRT 3 (MOD.)

DS JOB NO:
 B1800
 SHT: NB1-2 OF 2

GENERAL NOTES

(1) INDIVIDUAL PRECAST MEMBER PIECE DETAILS ARE NOT REQUIRED TO BE SUBMITTED FOR APPROVAL AS SUFFICIENT INFORMATION FOR THEIR FABRICATION IS CONTAINED IN THE CONTRACT DRAWINGS, F.D.O.T. STANDARD INDEX DRAWINGS AND SPECIFICATIONS FOR ROAD AND BRIDGE CONSTRUCTION. THESE DRAWINGS ARE INTENDED TO MEET THE REQUIREMENTS FOR PRECAST MEMBER SUBMITTALS AND ARE TO BE USED IN CONJUNCTION WITH THE PREVIOUSLY MENTIONED DOCUMENTS.

(2) THE COMPOSITE NEOPRENE BEARING PADS ARE TO BE FURNISHED AND INSTALLED BY THE G.C.

(3) PRIOR TO PRODUCTION OF PRECAST MEMBERS THE FOLLOWING INFORMATION NEEDS TO BE SUPPLIED REGARDING MATERIALS FURNISHED TO PRECASTER FOR EMBEDMENT INTO BEAMS.

S.I.P. FORM CLIPS

ARE THEY REQUIRED? NO

WHERE ARE THEY TO BE LOCATED? _____

WHAT IS THEIR SPACING? _____

WHAT IS THEIR EXACT TYPE? _____

WHAT ARE THEIR DIMENSIONS? _____

SLEEVE FOR OVERHANG BRACKETS

ARE THEY REQUIRED? NO

WHERE ARE THEY TO BE LOCATED? _____

WHAT IS THEIR SPACING? _____

WHAT IS THEIR EXACT TYPE? _____

WHAT ARE THEIR DIMENSIONS? _____

BRACING

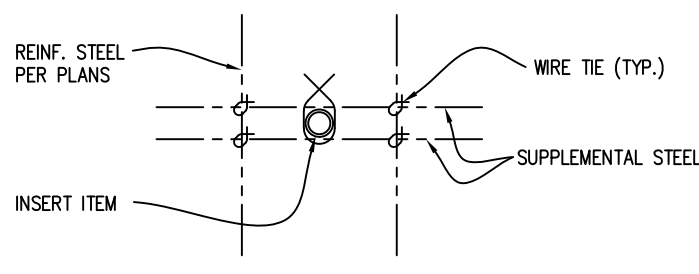
NOT REQUIRED.

SAFETY SLEEVE

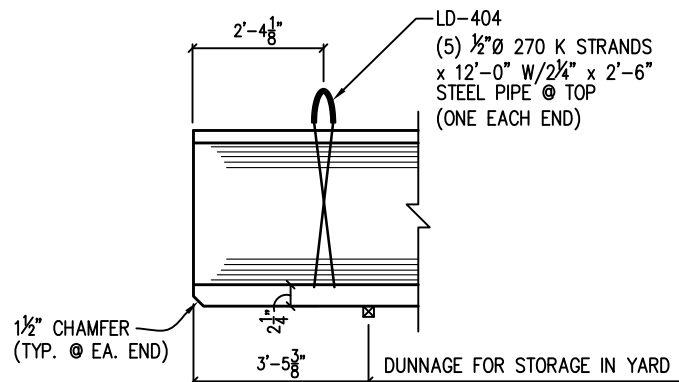
NOT REQUIRED.

ANY ADDITIONAL EMBED MATERIALS

(4) **SUPPLEMENTAL STEEL** - AS REQUIRED TO SECURE DUCT INTO PROPER POSITIONING IN A BEAM, #3 REBAR WILL BE TIED TO EACH SIDE OF INSERT AND TO NEARBY INTERIOR STEEL REINFORCING. SEE DETAIL BELOW



PLAN OR SIDE VIEW

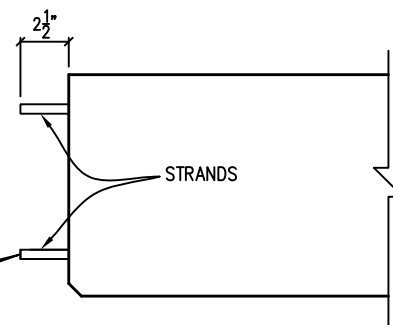


HANDLING & DUNNAGE

TYP. EA. END OF FIB 54 ALL BEAMS

DUCT TIES

AT 1 FOOT SPACING TO SECURE DUCT IN PROPER POSITION IN EACH SPECIMEN. W4/W4 WELDED WIRE MESH CUT AND USED TO SECURE EACH SIDE OF THE HDPE PIPE INSERT TO NEARBY INTERIOR STEEL REINFORCING. DETAIL IS SHOWN ON EACH PIECE DETAIL.



END ELEVATION

(5) ALL STRANDS SHALL PROJECT 2 1/2" BEYOND ENDS OF BEAMS.

(6) D/S SHALL PROVIDE MATERIAL SAMPLES TO UF/FDOT AS FOLLOWS :

- (8) 6"DIA. x 12" CYLINDERS FROM EACH CONCRETE BATCH :
- (4) CYLINDERS CURE WITH GIRDER, (4) LAB CURE.

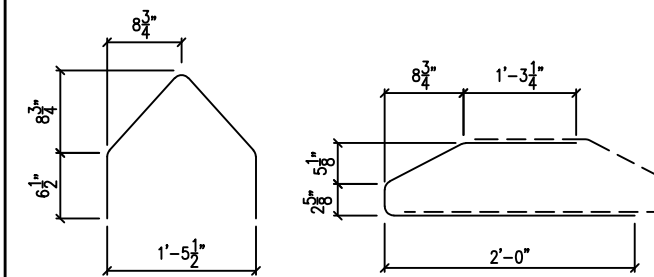
(16) 36" PIECES OF PRESTRESSING STRANDS FREE FROM SAND, DUST, ETC. SAMPLES TAKEN DIRECTLY OFF OF REEL.

(3) 36" PIECES OF EACH SIZE/BATCH OF REBAR.

BILL OF EMBED MATERIALS
FOR FLORIDA I-BEAM 54 ALL MEMBERS

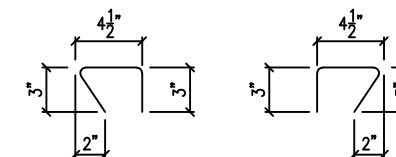
BAR	D.S. I.D. #	SIZE	QTY.	LENGTH	REMARKS
A	RE-BAR 5	#5 BAR	28	43'-9"	STRAIGHT BAR
C	RE-BAR 3	#3 BAR	112	3'-1 3/4"	SEE BELOW
D	RE-BAR 3	#3 BAR	756	4'-4"	SEE BELOW
H	RE-BAR 3	#3 BAR	90	9"	SEE BELOW
K	RE-BAR 4	#4 BAR	686	6'-5 5/8"	SEE BELOW
L	RE-BAR 4	#4 BAR	120	5'-10"	STRAIGHT BAR
M	RE-BAR 4	#4 BAR	350	3'-8"	STRAIGHT BAR
S1	RE-BAR 4	#4 BAR	2	43'-7"	SEE BELOW
S2	RE-BAR 4	#4 BAR	2	21'-0"	SEE BELOW
S3	RE-BAR 4	#4 BAR	2	20'-4"	SEE BELOW
S4	RE-BAR 4	#4 BAR	2	21'-10"	STRAIGHT BAR
Z	RE-BAR 4	#4 BAR	70	5'-11 1/4"	SEE BELOW

ALL #3 BARS SHALL BE BENT AROUND A 1 1/2" DIA. PIN
ALL #4 BARS SHALL BE BENT AROUND A 2" DIA. PIN
ALL #5 BARS SHALL BE BENT AROUND A 2 1/2" DIA. PIN
NOTE: ALL DIMENSIONS ARE OUT TO OUT

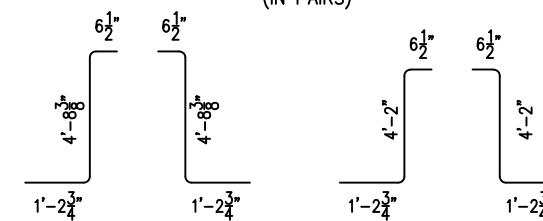


BARS 'C'

BARS 'D'
(IN PAIRS)

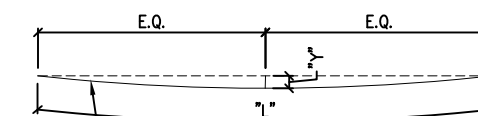


BARS 'H'
(IN PAIRS)



BARS 'K'

BARS 'Z'



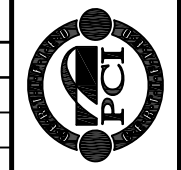
L = 43'-7", R = 199'-7 1/4", Y = 1'-2 3/4" (BARS S1)

L = 21'-10", R = 200'-4 3/4", Y = 3 5/8" (BARS S2)

L = 20'-4", R = 387'-8 1/2", Y = 2 3/8" (BARS S3)

BARS S1 THRU S3

DS PART NO.
FIB 54

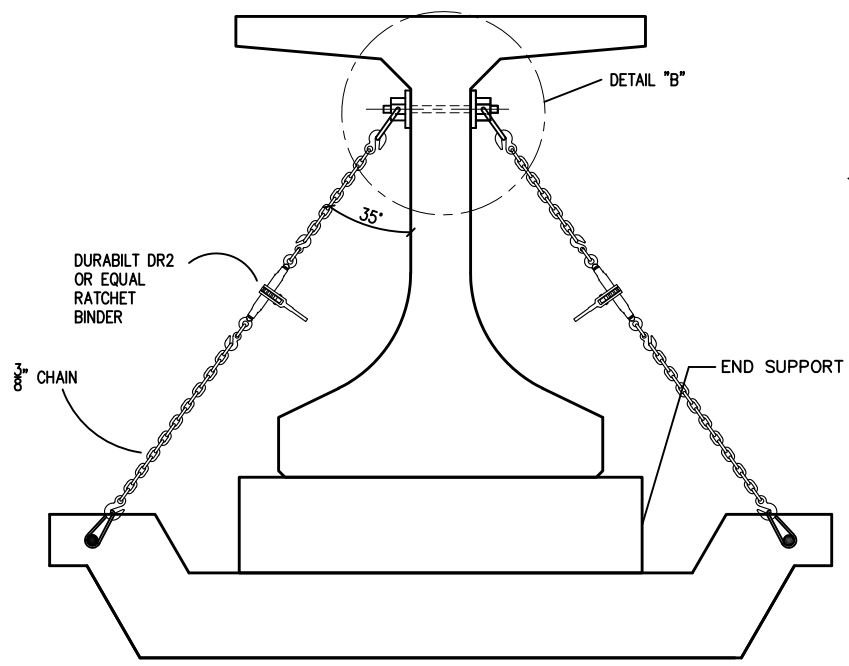
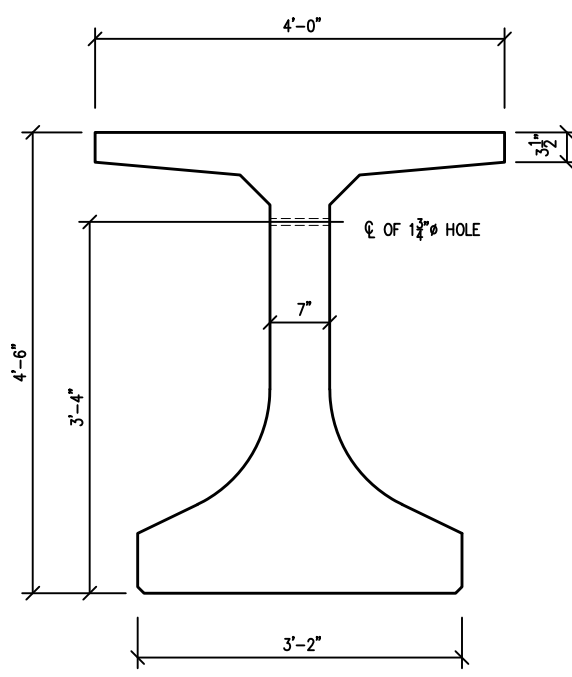


CHK.	BY	DATE	DESCRIPTION	REV

GENERAL NOTES & MISC. MATERIALS
DURA-STRESS Inc.
CA #6028
P.O. BOX 490779 LEESBURG, FL 34749-0779
PHONE (352) 787-1422 FAX (352) 787-0080
STRUCTURAL PRESTRESSED AND ARCHITECTURAL PRECAST CONCRETE PRODUCTS

JOB NAME: FDOT RESEARCH SHEAR BEHAVIOR OF WEBS BDV31-977-71
LOCATION: N/A
ARCHITECT: N/A
ENGINEER: N/A
CONTRACTOR: N/A
PROJ. NO.: N/A

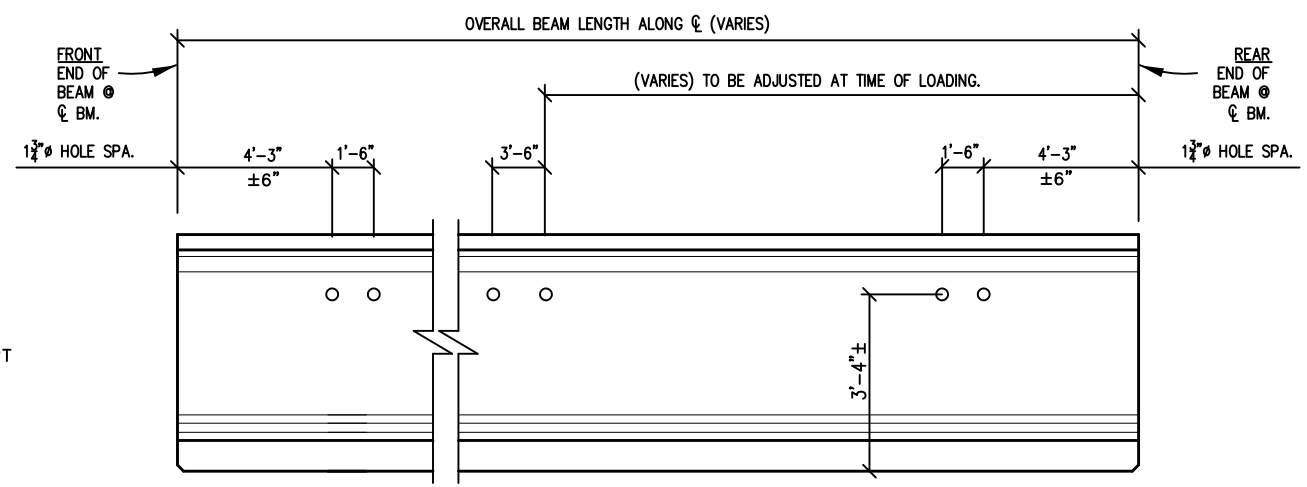
DRAWN: NE
CHK'D.: POL/TW
APPR.:
DATE: 1/21/2020
RELEASED:
DS JOB NO: B1824
SHT: A1



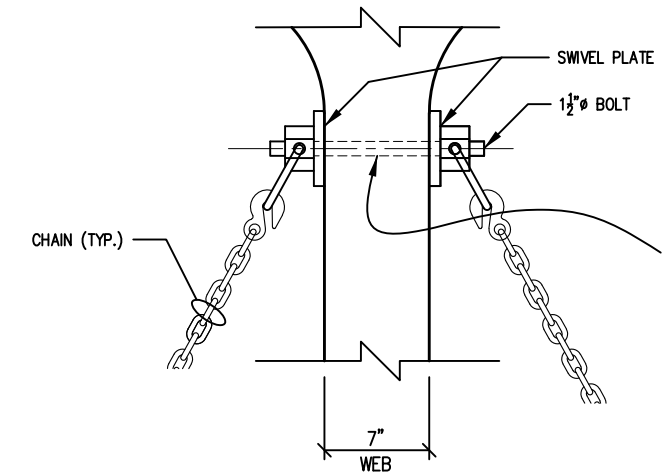
DETAIL "A"
 (END SUPPORT ON TRUCK DURING TRANSPORTATION)
 PROPOSED DETAIL
 REQUEST FOR APPROVAL

NOTE: D/S REQUESTS TO ADD 1 1/2" HOLES TO THE BEAM WEB. HOLES ARE TO BE USED FOR TIE DOWN PURPOSE DURING TRANSPORTATION OF BEAMS TO PREVENT DAMAGE TO THE TOP FLANGE. HOLES SHALL BE PATCHED AFTER BEAMS HAVE ARRIVED AT THE JOB SITE

D/S HAS USED THIS TIE DOWN PROCEDURE SUCCESSFULLY ON A PREVIOUS JOB, F.D.O.T. PROJECT#77002-3503. ALL BEAMS WERE NOT DAMAGED, NO SPALLING AT TOP OF FLANGE, AND NO SLIPPING OF BEAM DURING SHIPPING.



ELEVATION

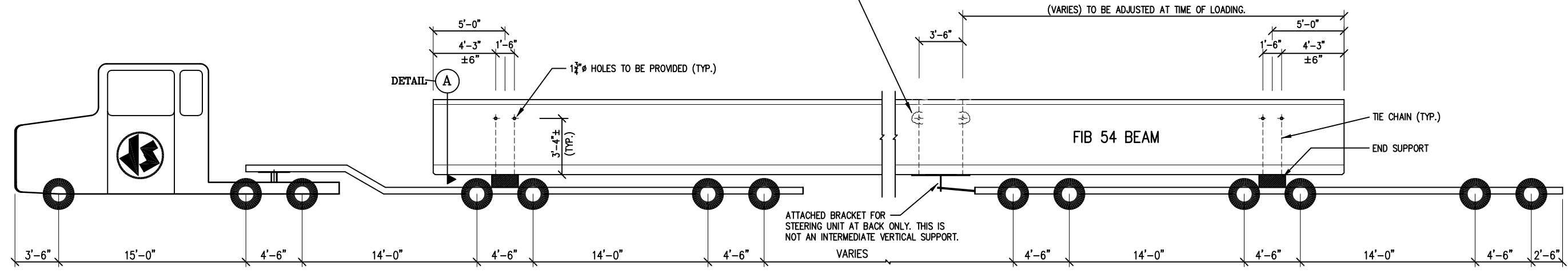


DETAIL "B" AT SWIVEL PLATE

G.C. NOTE:

- 1 1/2" HOLE TO BE PROVIDED IN BEAM WEB. HOLES ARE TO BE PATCHED AFTER THE REMOVAL OF BOLTS AND SWIVEL PLATES AT THE JOB SITE
- PATCHING PROCEDURE OF 1 1/2" HOLES**
- 1) REMOVE PVC PIPE FROM HOLE. HOLE SURFACE MUST BE CLEANED, FREE OF DUST AND OIL.
 - 2) APPLY EPOXY BONDING AGENT (PILGRIM EM 5-2 GEL OR EQUAL) ON HOLE SURFACE.
 - 3) FILL HOLE WITH VIBROPRUF # 11, A NON SHRINK GROUT (OR EQUAL)
 - 4) COSMETIC AS REQUIRED.

PRODUCTION NOTE:
 IF THESE TWO HOLES ARE TO BE PROVIDED AT TIME OF LOADING, DO NOT CUT REBAR OR STRAND. (TYP.)



ELEVATION OF FIB 54 BEAM DURING TRANSPORTATION
 (SHOWING LOCATION OF 1 1/2" HOLES AND CHAINS FOR BEAM TIE DOWN)

FOR ALL BEAMS

DS PART NO.
 FIB 54

REV	DESCRIPTION	DATE	BY	CHK.

TRANSPORTATION FOR TYPE FIB 54 BEAM

DURA-STRESS Inc.
 CA #6028
 P.O. BOX 490779 LEESBURG, FL 34749-0779
 PHONE (352) 787-1422 FAX (352) 787-0080
 STRUCTURAL PRESTRESSED AND ARCHITECTURAL PRECAST CONCRETE PRODUCTS

JOB NAME: FDOT RESEARCH SHEAR BEHAVIOR OF WEBS BDV31-977-71
 LOCATION: N/A
 ARCHITECT: N/A
 ENGINEER: N/A
 CONTRACTOR: N/A
 PROJ. NO.: N/A

DRAWN: NE
 CHK'D.: POL/TW
 APPR.:
 DATE: 1/21/2020
 RELEASED:

DS JOB NO:
 B1824
 SHT: A2



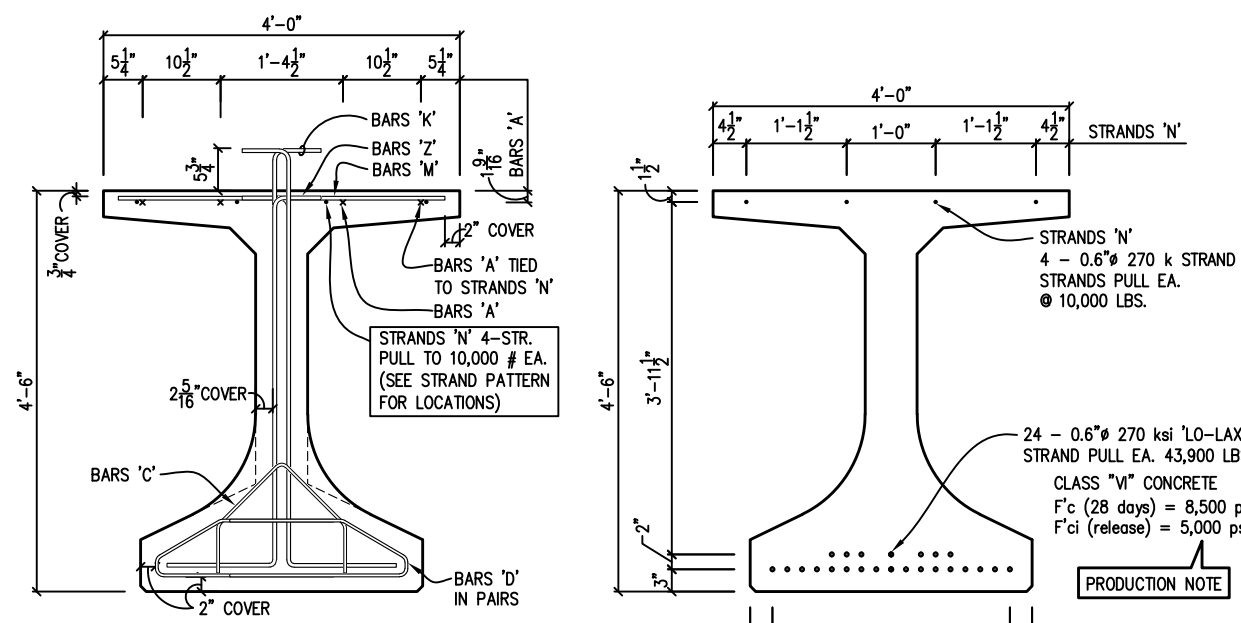
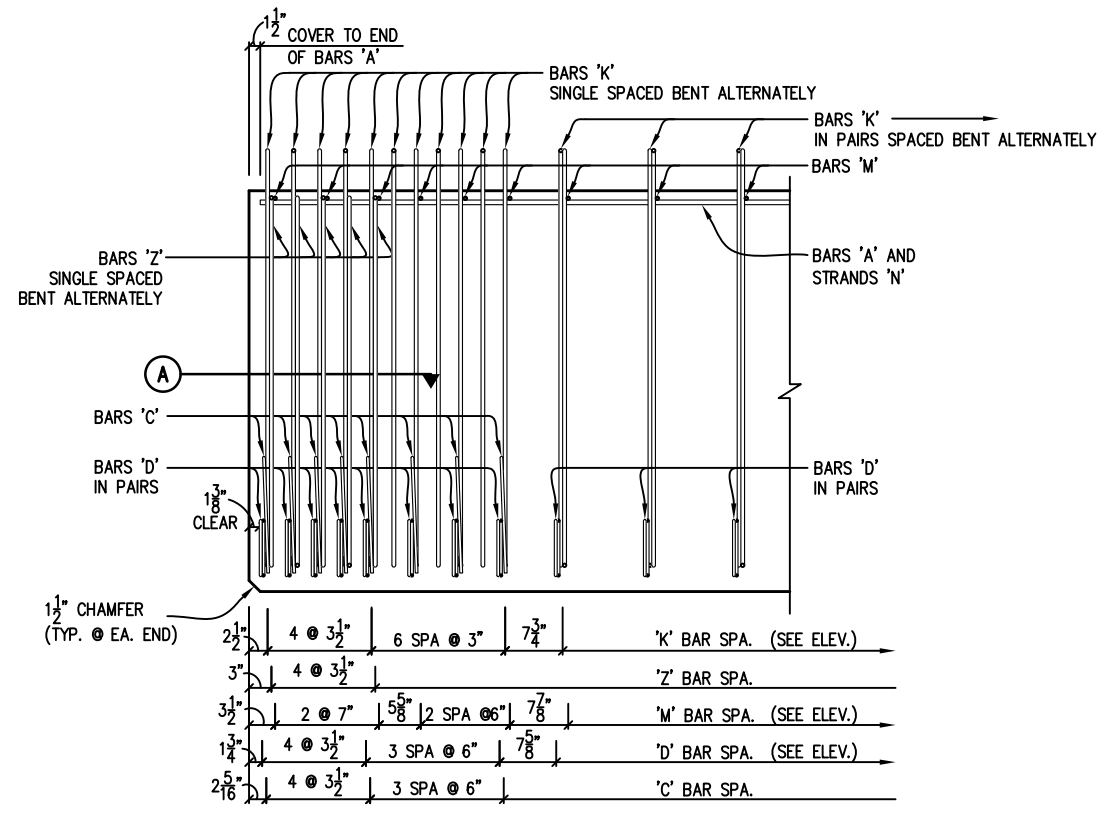
REV	DESCRIPTION	DATE	BY	CHK.

TYPE FIB 54 BEAM SECTIONS AND DETAILS

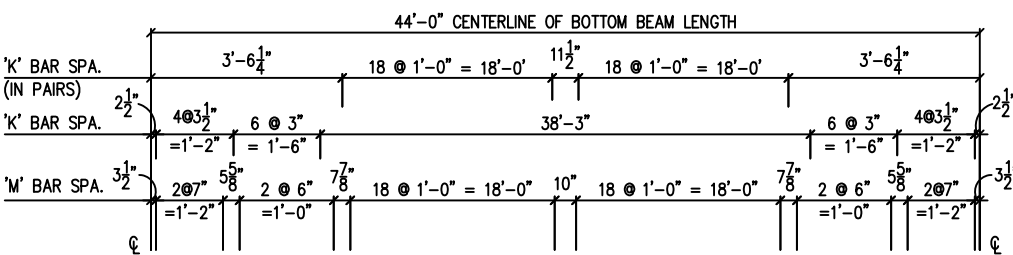
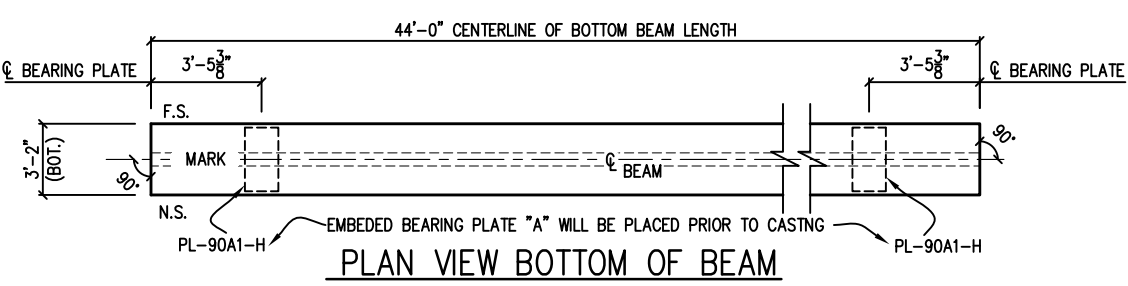
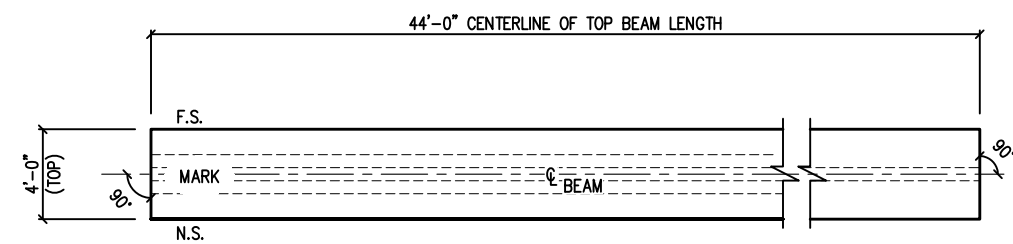
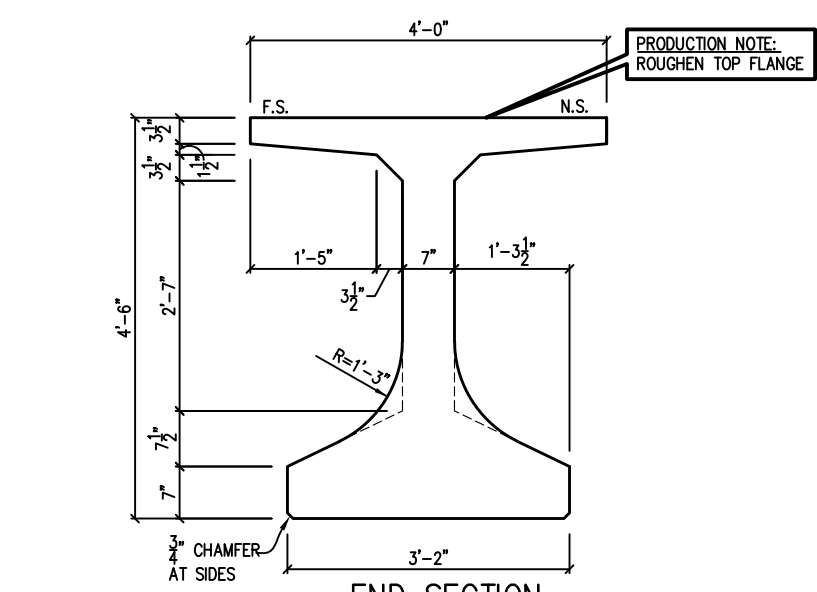
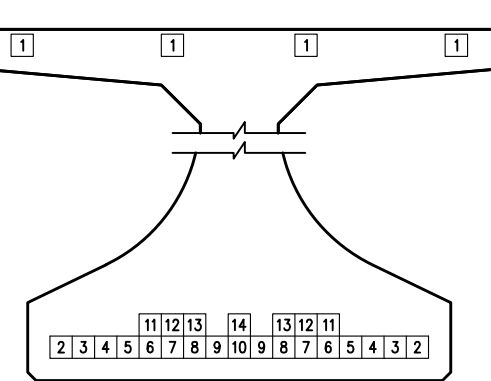
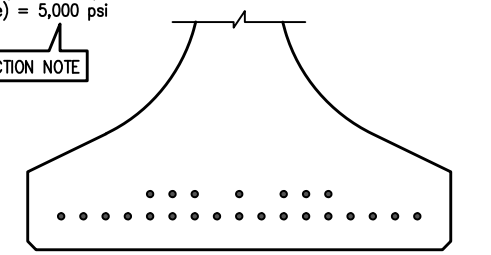
DURA-STRESS Inc.
 CA #6028
 P.O. BOX 490779 LEESBURG, FL 34749-0779
 PHONE (352) 787-1422 FAX (352) 787-0080
 STRUCTURAL PRESTRESSED AND ARCHITECTURAL PRECAST CONCRETE PRODUCTS

JOB NAME: FOOT RESEARCH SHEAR BEHAVIOR OF WEBS BDV31-977-71
 LOCATION: N/A
 ARCHITECT: N/A
 ENGINEER: N/A
 CONTRACTOR: N/A
 PROJ. NO.: N/A

DRAWN: NE
 CHK'D.: POL/TW
 APPR.:
 DATE: 1/21/2020
 RELEASED:
 DS JOB NO: B1824
 SHT: P00-1 OF 1



SHIELDING LEGEND
 • - NONE REQUIRED



PRODUCTION NOTE
 PLEASE PROVIDE 1 3/4" @ HOLE PER SHEET A2

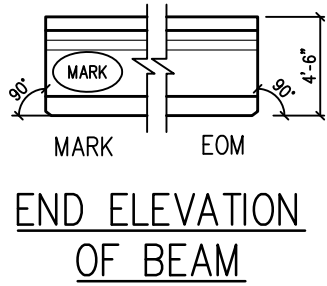
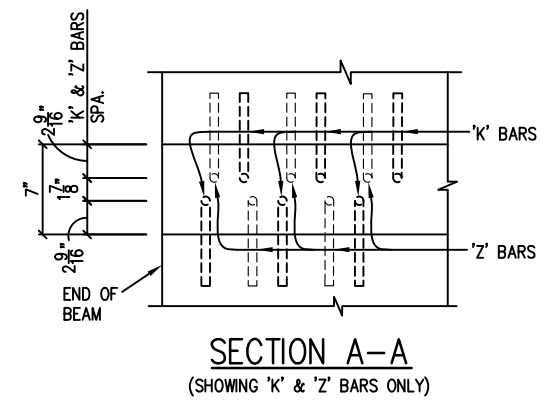
BILL OF EMBED MATERIALS
 FOR ONE MEMBER ONLY

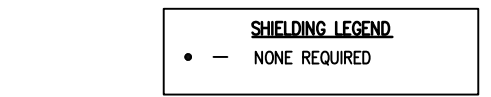
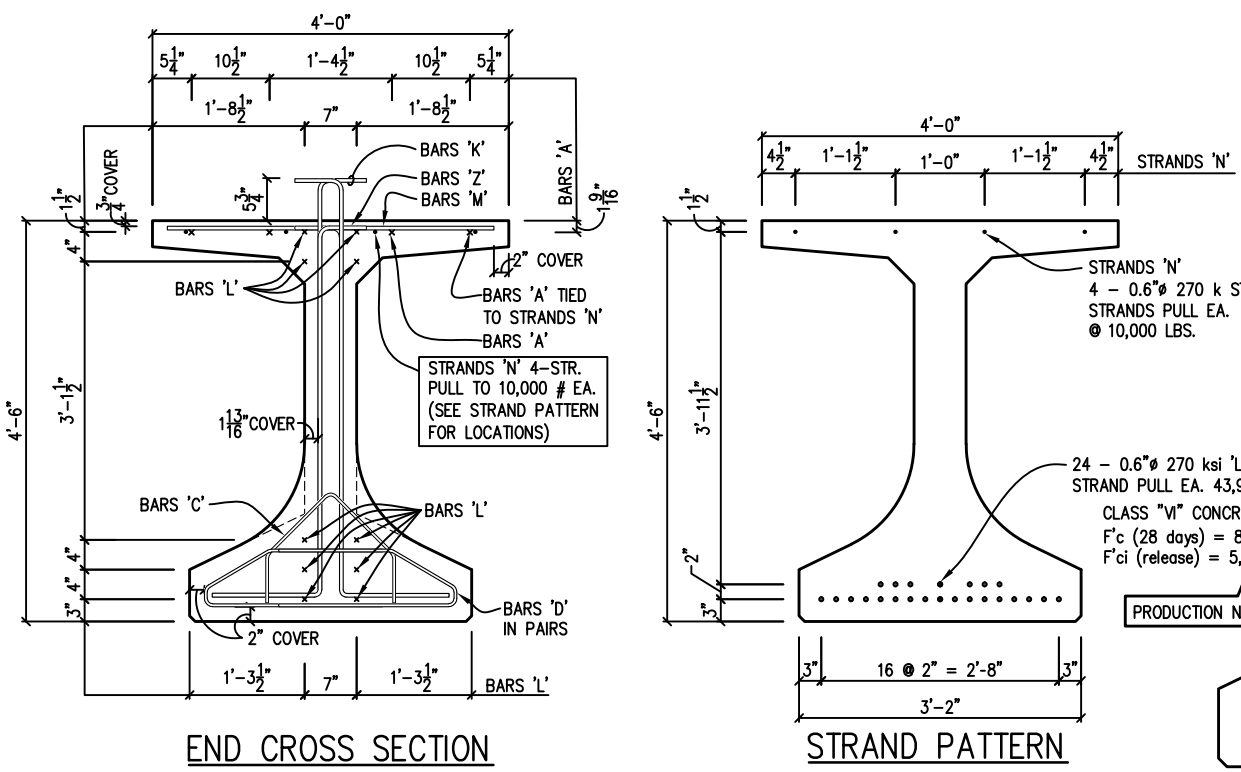
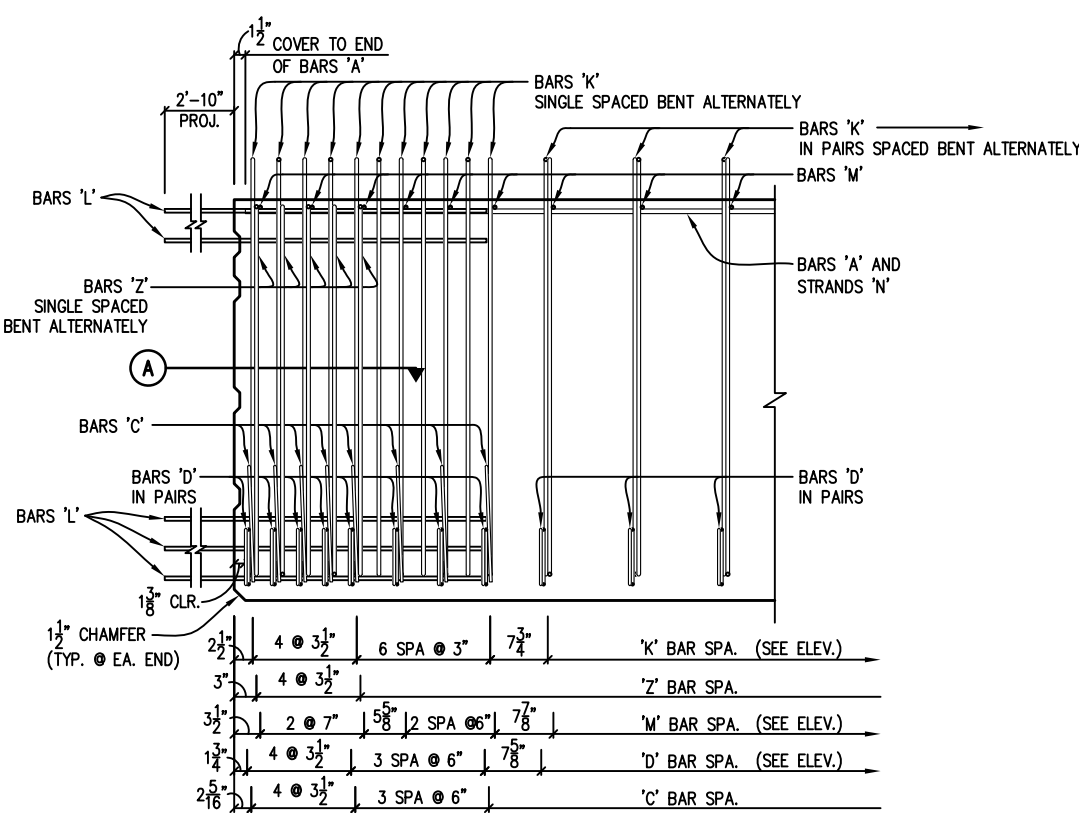
BAR	SIZE	D.S. I.D. #	QTY.	LENGTH	REMARKS
A	5	RE-BAR 5	4	43'-9"	STRAIGHT BAR
C	3	RE-BAR 3	16	3'-1 3/4"	SEE SHEET 'A1'
D	3	RE-BAR 3	108	4'-4"	SEE SHEET 'A1'
K	4	RE-BAR 4	98	6'-5 5/8"	SEE SHEET 'A1'
M	4	RE-BAR 4	50	3'-8"	STRAIGHT BAR
Z	4	RE-BAR 4	10	5'-11 1/4"	SEE SHEET 'A1'

MARK	QTY.	WEIGHT	CU. YDS.	MAX LENGTH	BRG. PL. @ MK	BRG. PL. @ EOM
P00	1	42,743#	10.55	44'-0"	PL-90A1-H	PL-90A1-H

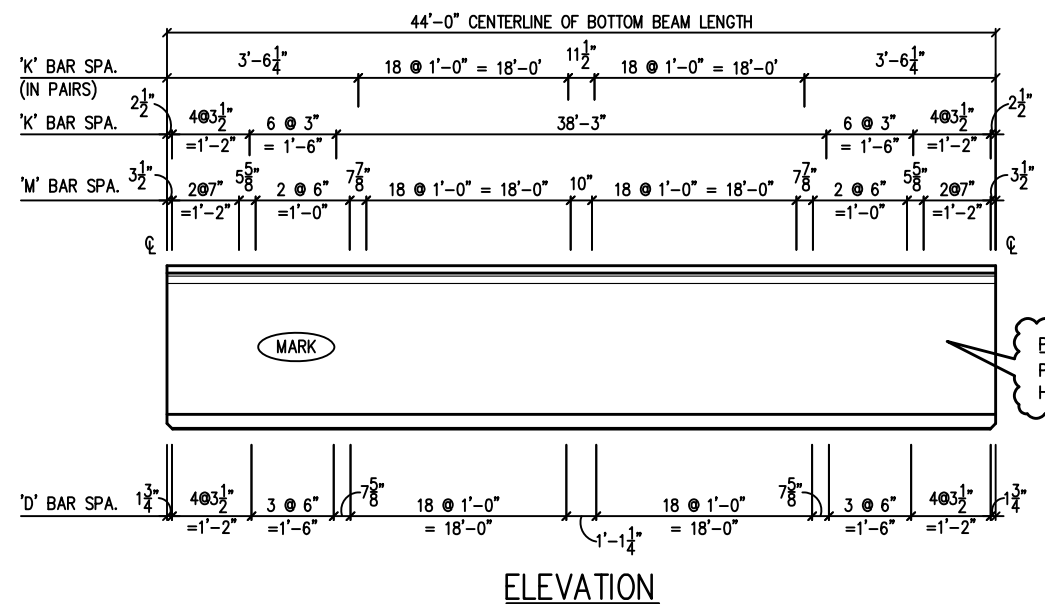
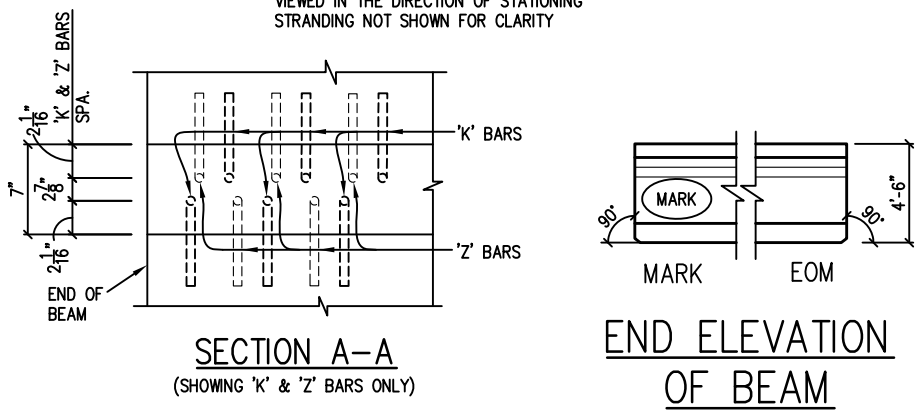
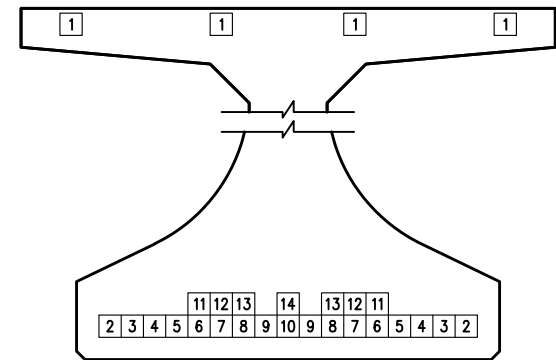
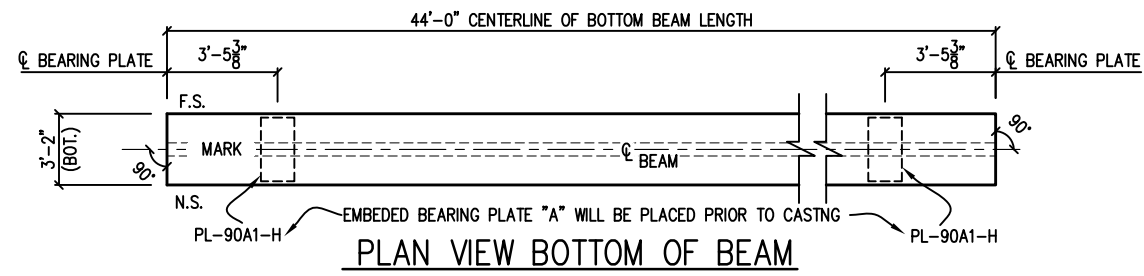
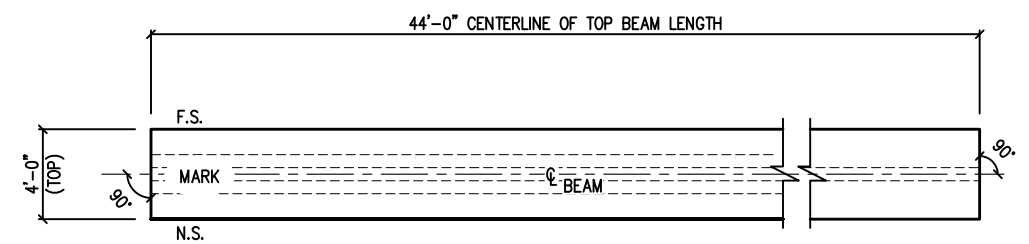
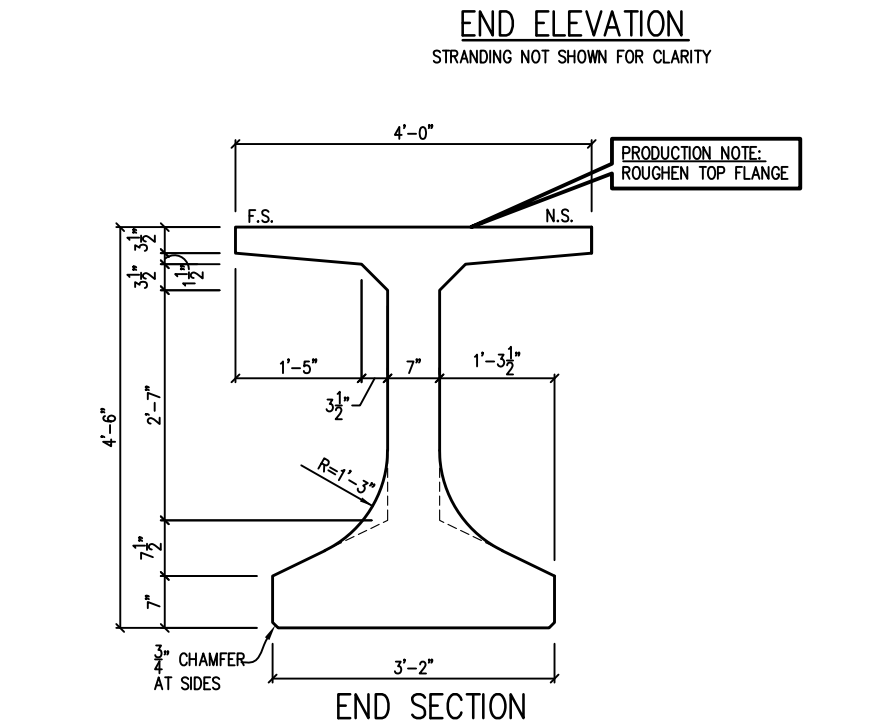
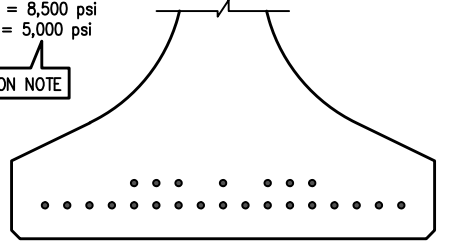
PRODUCTION NOTE:
 REFER TO SHEET NO. A1 FOR ADDITIONAL NOTES NOT SHOWN, THAT APPLY TO BEAM DETAIL.

DS PART NO.
FIB 54





PRODUCTION NOTE



BILL OF EMBED MATERIALS
FOR ONE MEMBER ONLY

BAR	SIZE	D.S. I.D. #	QTY.	LENGTH	REMARKS
A	5	RE-BAR 5	4	43'-9"	STRAIGHT BAR
C	3	RE-BAR 3	16	3'-1 3/4"	SEE SHEET 'A1'
D	3	RE-BAR 3	108	4'-4"	SEE SHEET 'A1'
K	4	RE-BAR 4	98	6'-5 5/8"	SEE SHEET 'A1'
L	4	RE-BAR 4	20	5'-10"	STRAIGHT BAR
M	4	RE-BAR 4	50	3'-8"	STRAIGHT BAR
Z	4	RE-BAR 4	10	5'-11 1/4"	SEE SHEET 'A1'

MARK	QTY.	WEIGHT	CU. YDS.	Ø MAX LENGTH	BRG. PL. @ MK	BRG. PL. @ EOM
P34	1	42,743#	10.55	44'-0"	PL-90A1-H	PL-90A1-H

PRODUCTION NOTE:
REFER TO SHEET NO. A1 FOR ADDITIONAL NOTES NOT SHOWN, THAT APPLY TO BEAM DETAIL.

DS PART NO.
FIB 54

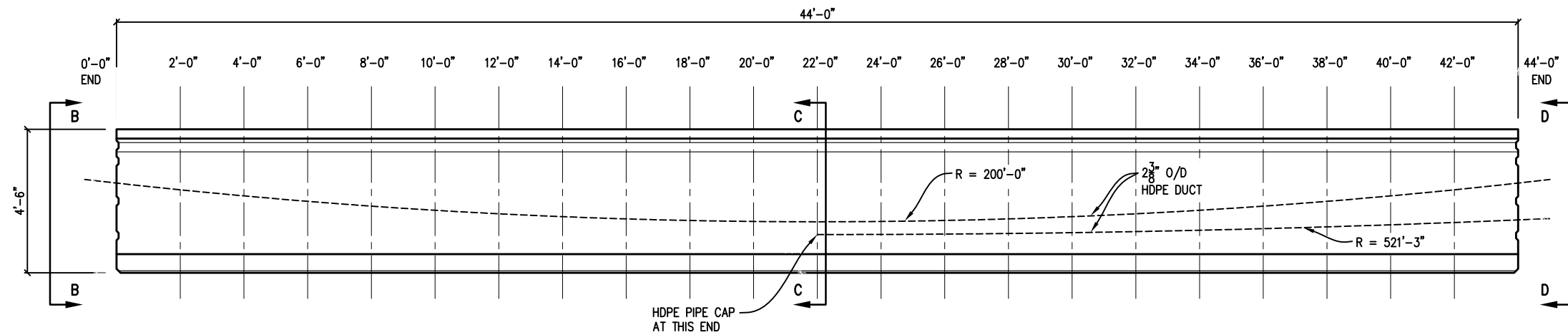
REV	DESCRIPTION	DATE	BY	CHK.

TYPE FIB 54 BEAM SECTIONS AND DETAILS

DURA-STRESS Inc.
CA #6028
P.O. BOX 490779 LEESBURG, FL 34749-0779
PHONE (352) 787-1422 FAX (352) 787-0080
STRUCTURAL PRESTRESSED AND ARCHITECTURAL PRECAST CONCRETE PRODUCTS

JOB NAME: FOOT RESEARCH SHEAR BEHAVIOR OF WEBS BDV31-977-71
LOCATION: N/A
ARCHITECT: N/A
ENGINEER: N/A
CONTRACTOR: N/A
PROJ. NO.: N/A

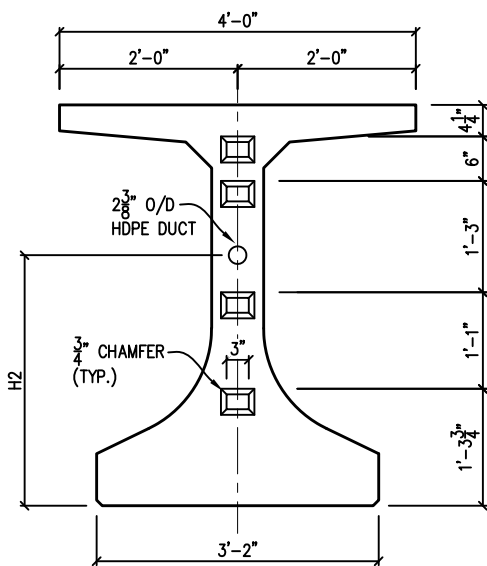
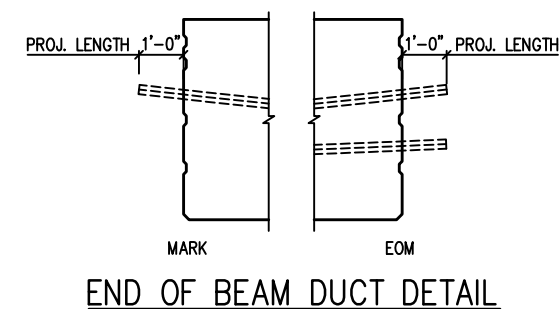
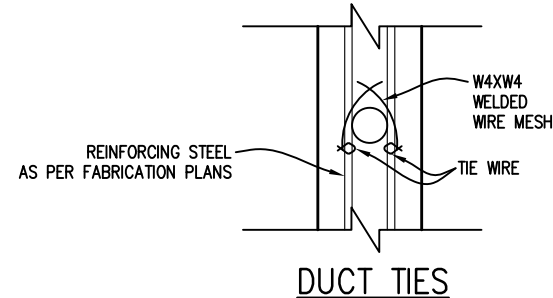
DRAWN: NE
CHK'D.: POL/TW
APPR.:
DATE: 1/21/2020
RELEASED:
DS JOB NO: B1824
SHT: P34-1 OF 2



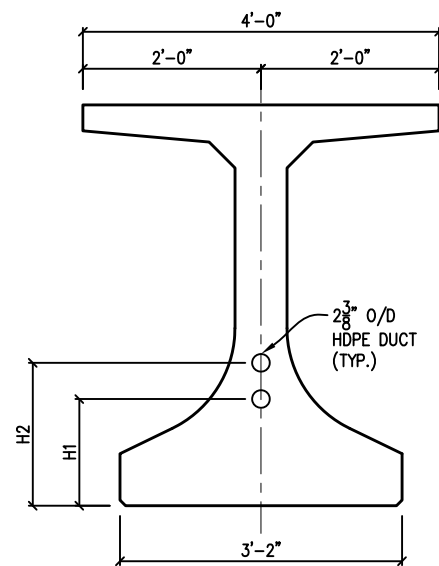
DUCT LAYOUT

GIRDER	P34																						
DISTANCE FROM END OF GIRDER	0'-0"	2'-0"	4'-0"	6'-0"	8'-0"	10'-0"	12'-0"	14'-0"	16'-0"	18'-0"	20'-0"	22'-0"	24'-0"	26'-0"	28'-0"	30'-0"	32'-0"	34'-0"	36'-0"	38'-0"	40'-0"	42'-0"	44'-0"
H1 (FT)	N/A	N/A	N/A	N/A	N/A	N/A	N/A	N/A	N/A	N/A	N/A	1'-2 3/8"	1'-2 3/8"	1'-2 1/2"	1'-2 3/4"	1'-3 1/8"	1'-3 1/2"	1'-4"	1'-4 5/8"	1'-5 1/4"	1'-6 1/8"	1'-7"	1'-7 7/8"
H2 (FT)	2'-9 3/4"	2'-7 1/4"	2'-5"	2'-2 7/8"	2'-1 1/8"	1'-11 1/2"	1'-10 1/4"	1'-9 1/8"	1'-8 1/4"	1'-7 3/4"	1'-7 3/8"	1'-7 1/4"	1'-7 3/8"	1'-7 3/4"	1'-8 1/4"	1'-9 1/8"	1'-10 1/4"	1'-11 1/2"	2'-1 1/8"	2'-2 7/8"	2'-5"	2'-7 1/4"	2'-9 3/4"

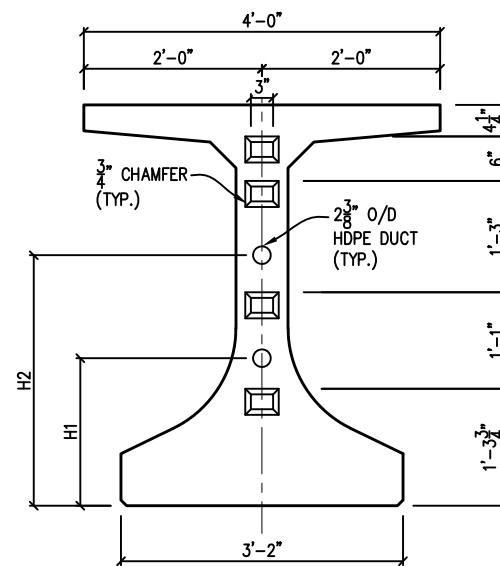
AT 1 FOOT SPACING, TYP.



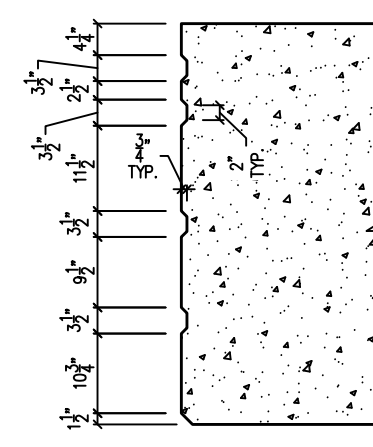
CROSS SECTION B-B



CROSS SECTION C-C



CROSS SECTION D-D



SHEAR KEY ELEVATION VIEW

MARK	QTY.	WEIGHT	CU. YDS.	Ø MAX LENGTH
P34	1	42,743#	10.55	44'-0"

DS PART NO.
FIB 54



REV	DESCRIPTION	DATE	BY	CHK.

TYPE FIB 54 BEAM SECTIONS AND DETAILS
DURA-STRESS Inc.
 CA #6028
 P.O. BOX 490779 LEESBURG, FL 34749-0779
 PHONE (352) 787-1422 FAX (352) 787-0080
 STRUCTURAL PRESTRESSED AND ARCHITECTURAL PRECAST CONCRETE PRODUCTS

JOB NAME: FOOT RESEARCH SHEAR BEHAVIOR OF WEBS BDV31-977-71
 LOCATION: N/A
 ARCHITECT: N/A
 ENGINEER: N/A
 CONTRACTOR: N/A
 PROJ. NO.: N/A

DRAWN: NE
 CHK'D.: POL/TW
 APPR.:
 DATE: 1/21/2020
 RELEASED:

DS JOB NO:
B1824
 SH: P34-2 OF 2

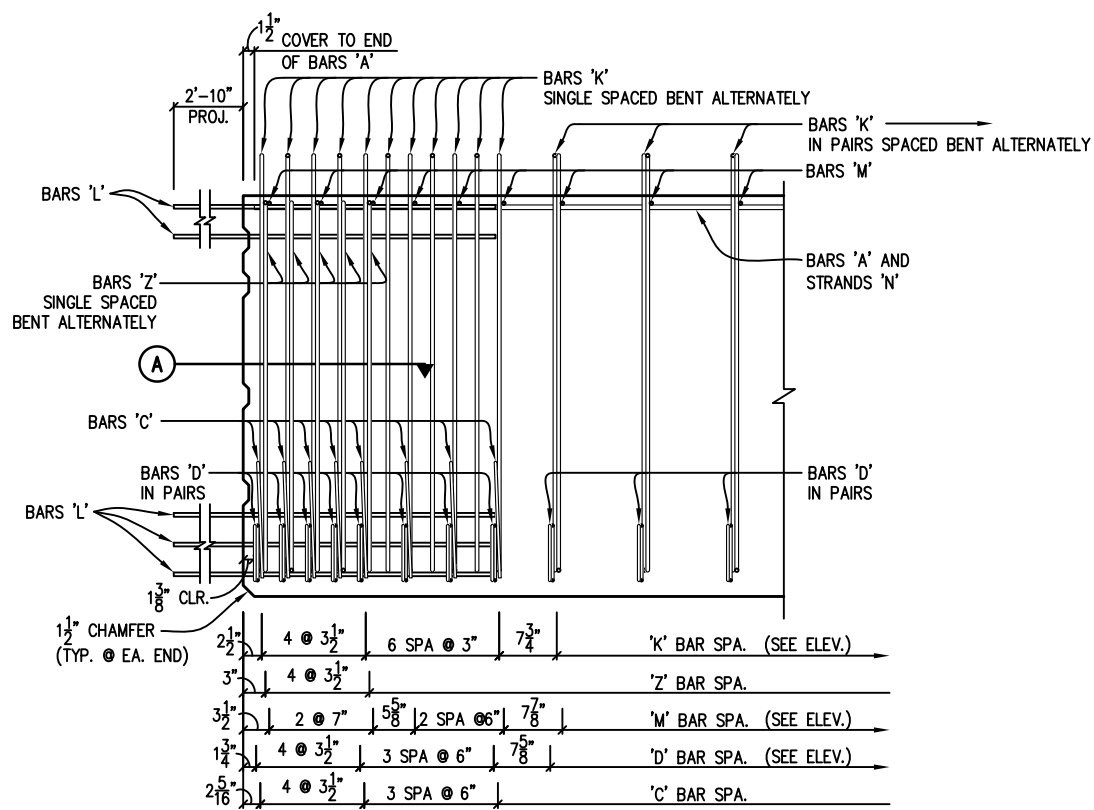


REV	DESCRIPTION	DATE	BY	CHK.

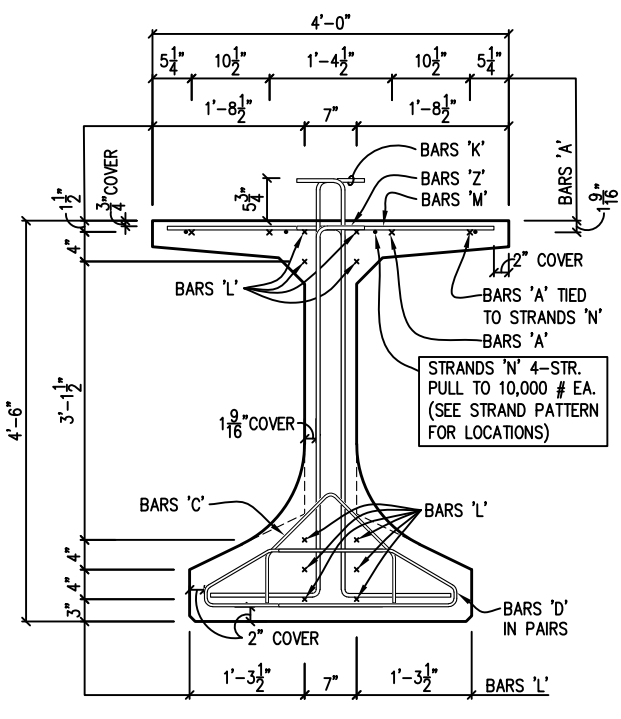
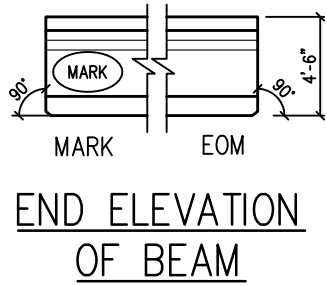
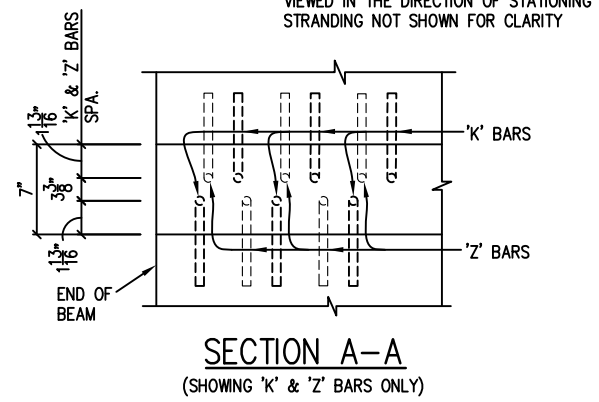
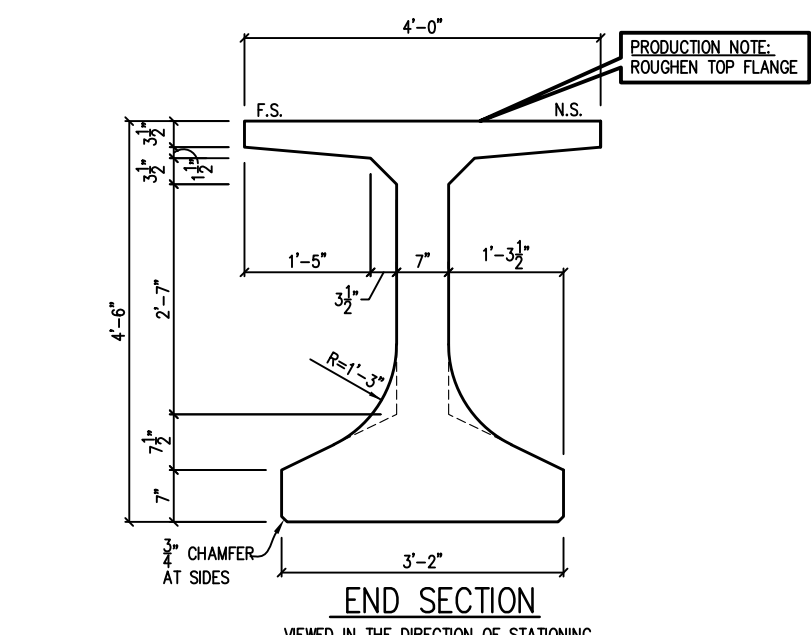
BRACING LOCATIONS
DURA-STRESS Inc.
 CA #6028
 P.O. BOX 490779 LEESBURG, FL 34749-0779
 PHONE (352) 787-1422 FAX (352) 787-0080
 STRUCTURAL PRESTRESSED AND ARCHITECTURAL PRECAST CONCRETE PRODUCTS

JOB NAME: FOOT RESEARCH SHEAR BEHAVIOR OF WEBS BDV31-977-71
 LOCATION: N/A
 ARCHITECT: N/A
 ENGINEER: N/A
 CONTRACTOR: N/A
 PROJ. NO.: N/A

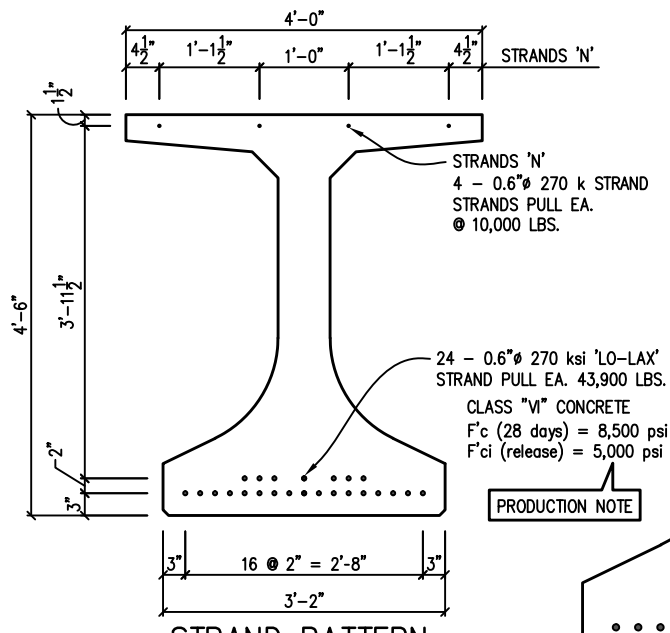
DRAWN: NE
 CHK'D.: POL/TW
 APPR.:
 DATE: 1/21/2020
 RELEASED:
 DS JOB NO: B1824
 SHT: P41-1 OF 2



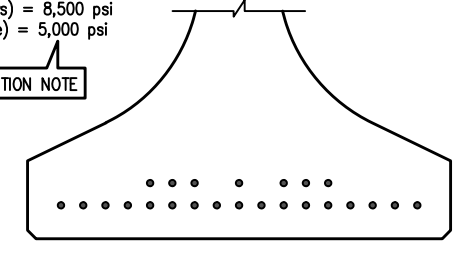
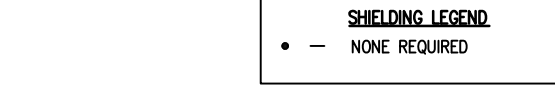
END ELEVATION
 STRANDING NOT SHOWN FOR CLARITY



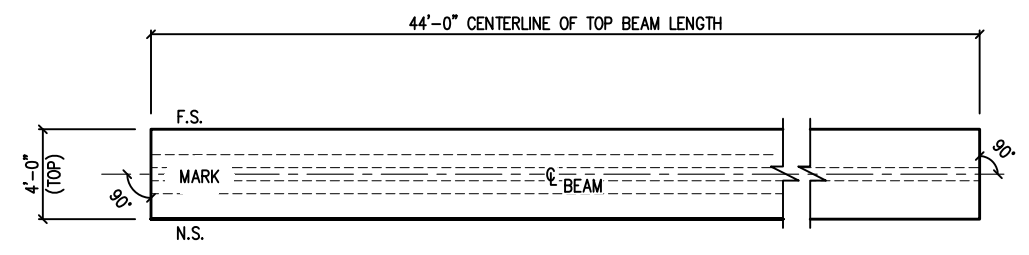
END CROSS SECTION



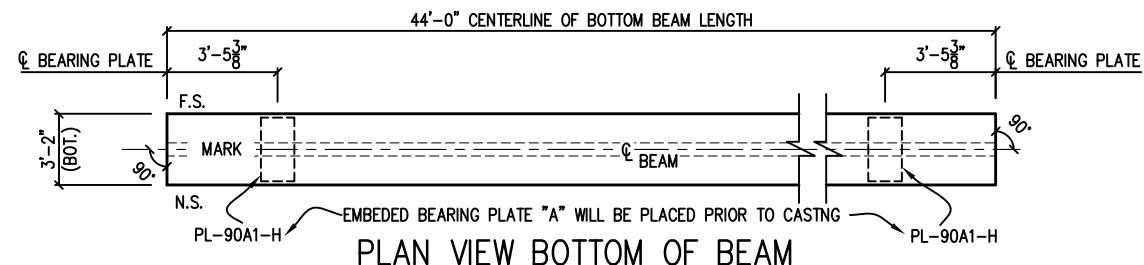
STRAND PATTERN



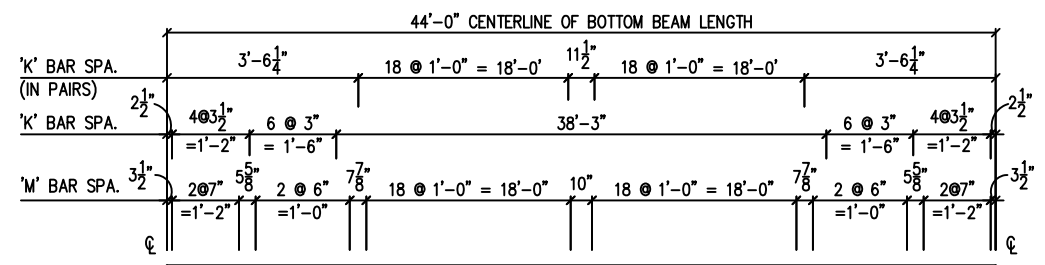
SHIELDING



PLAN VIEW TOP OF BEAM



PLAN VIEW BOTTOM OF BEAM



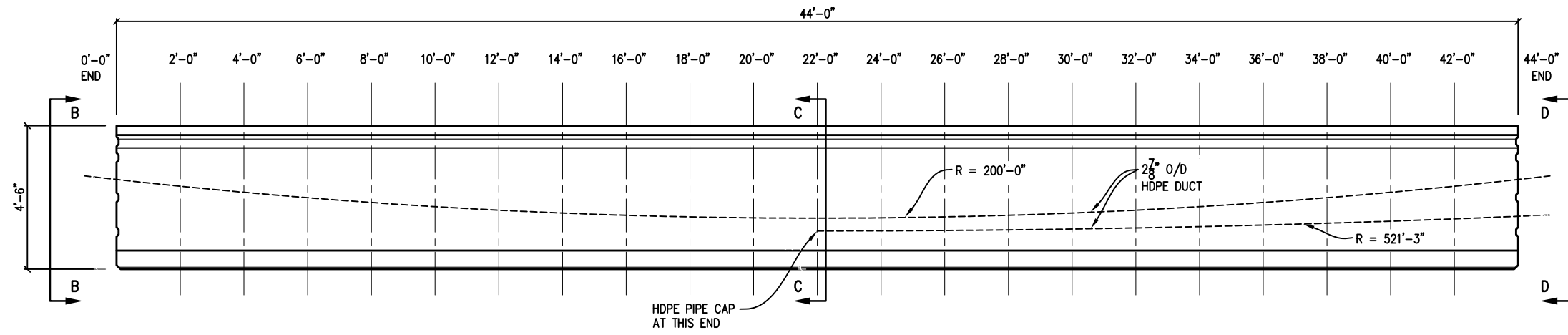
ELEVATION

BILL OF EMBED MATERIALS FOR ONE MEMBER ONLY					
BAR	SIZE	D.S. I.D. #	QTY.	LENGTH	REMARKS
A	5	RE-BAR 5	4	43'-9"	STRAIGHT BAR
C	3	RE-BAR 3	16	3'-1 3/4"	SEE SHEET 'A1'
D	3	RE-BAR 3	108	4'-4"	SEE SHEET 'A1'
K	4	RE-BAR 4	98	6'-5 5/8"	SEE SHEET 'A1'
L	4	RE-BAR 4	20	5'-10"	STRAIGHT BAR
M	4	RE-BAR 4	50	3'-8"	STRAIGHT BAR
Z	4	RE-BAR 4	10	5'-11 1/4"	SEE SHEET 'A1'

MARK	QTY.	WEIGHT	CU. YDS.	Ø MAX LENGTH	BRG. PL. @ MK	BRG. PL. @ EOM
P41	1	42,743#	10.55	44'-0"	PL-90A1-H	PL-90A1-H

PRODUCTION NOTE:
 REFER TO SHEET NO. A1 FOR ADDITIONAL NOTES NOT SHOWN, THAT APPLY TO BEAM DETAIL.

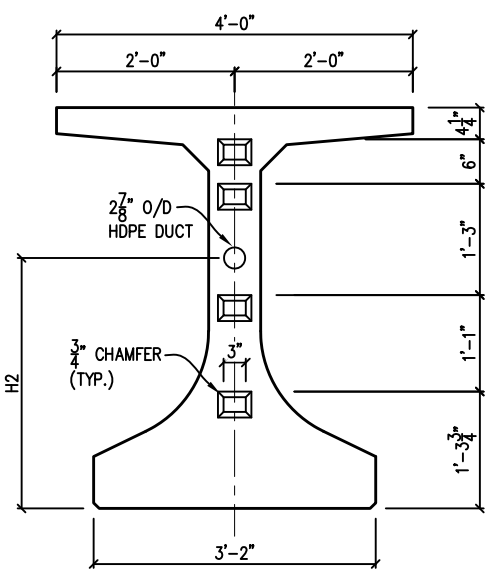
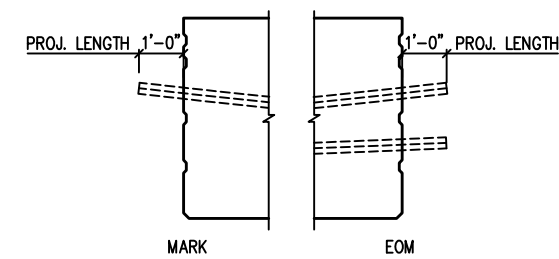
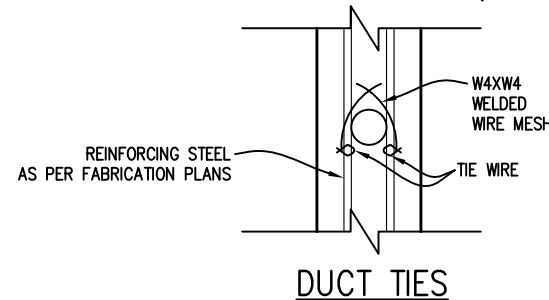
DS PART NO.
FIB 54



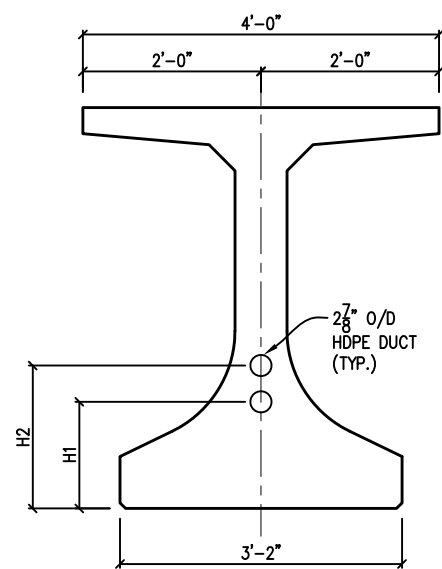
DUCT LAYOUT

GIRDER	P41																						
DISTANCE FROM END OF GIRDER	0'-0"	2'-0"	4'-0"	6'-0"	8'-0"	10'-0"	12'-0"	14'-0"	16'-0"	18'-0"	20'-0"	22'-0"	24'-0"	26'-0"	28'-0"	30'-0"	32'-0"	34'-0"	36'-0"	38'-0"	40'-0"	42'-0"	44'-0"
H1 (FT)	N/A	N/A	N/A	N/A	N/A	N/A	N/A	N/A	N/A	N/A	N/A	1'-2 3/8"	1'-2 3/8"	1'-2 1/2"	1'-2 3/4"	1'-3 1/8"	1'-3 1/2"	1'-4"	1'-4 5/8"	1'-5 1/4"	1'-6 1/8"	1'-7"	1'-7 7/8"
H2 (FT)	2'-9 3/4"	2'-7 1/4"	2'-5"	2'-2 7/8"	2'-1 1/8"	1'-11 1/2"	1'-10 1/4"	1'-9 1/8"	1'-8 1/4"	1'-7 3/4"	1'-7 3/8"	1'-7 1/4"	1'-7 3/8"	1'-7 3/4"	1'-8 1/4"	1'-9 1/8"	1'-10 1/4"	1'-11 1/2"	2'-1 1/8"	2'-2 7/8"	2'-5"	2'-7 1/4"	2'-9 3/4"

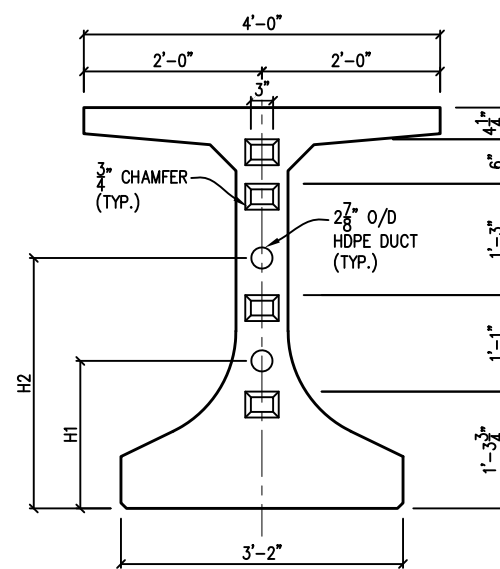
AT 1 FOOT SPACING, TYP.



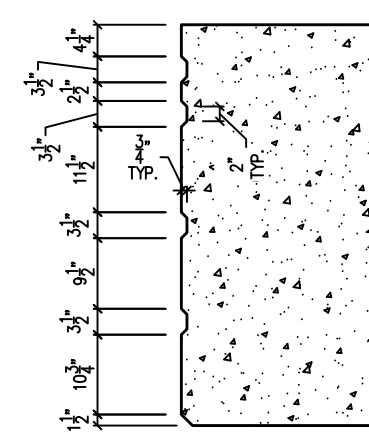
CROSS SECTION B-B



CROSS SECTION C-C



CROSS SECTION D-D



SHEAR KEY ELEVATION VIEW

MARK	QTY.	WEIGHT	CU. YDS.	Ø MAX LENGTH
P41	1	42,743#	10.55	44'-0"

DS PART NO.
FIB 54



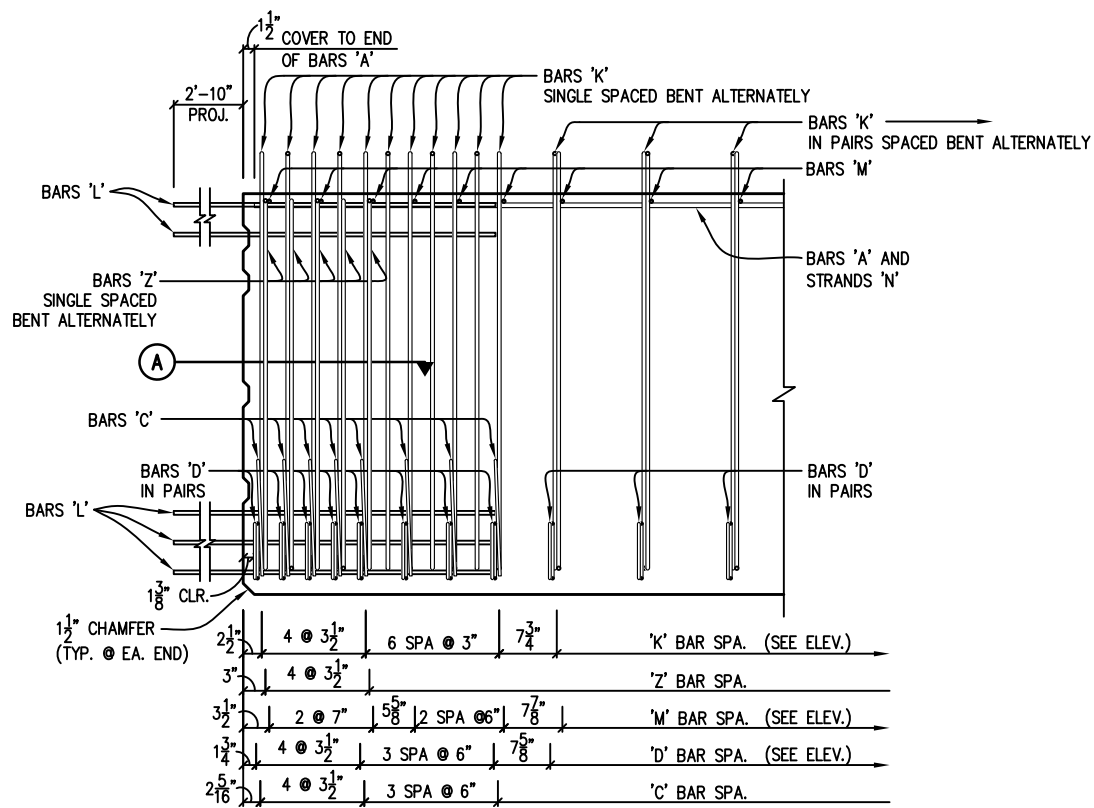
REV	DESCRIPTION	DATE	BY	CHK.

BRACING LOCATIONS
DURA-STRESS Inc.
 CA #6028
 P.O. BOX 490779 LEESBURG, FL 34749-0779
 PHONE (352) 787-1422 FAX (352) 787-0080
 STRUCTURAL PRESTRESSED AND ARCHITECTURAL PRECAST CONCRETE PRODUCTS

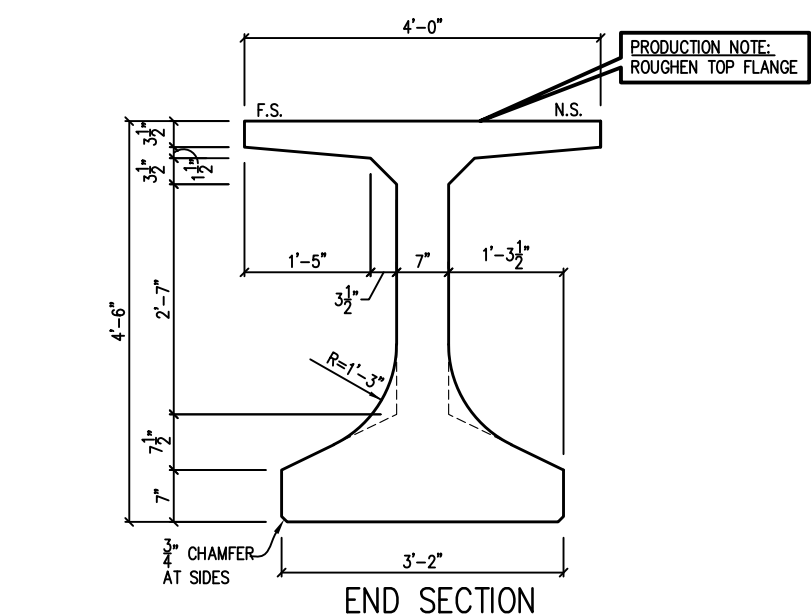
JOB NAME: FOOT RESEARCH SHEAR BEHAVIOR OF WEBS BDV31-977-71
 LOCATION: N/A
 ARCHITECT: N/A
 ENGINEER: N/A
 CONTRACTOR: N/A
 PROJ. NO.: N/A

DRAWN: NE
 CHK'D.: POL/TW
 APPR.:
 DATE: 1/21/2020
 RELEASED:

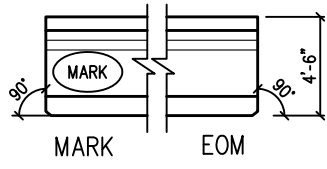
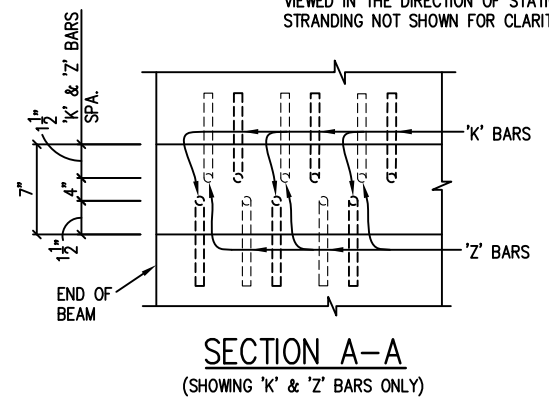
DS JOB NO:
B1824
 SHT: P41-2 OF 2



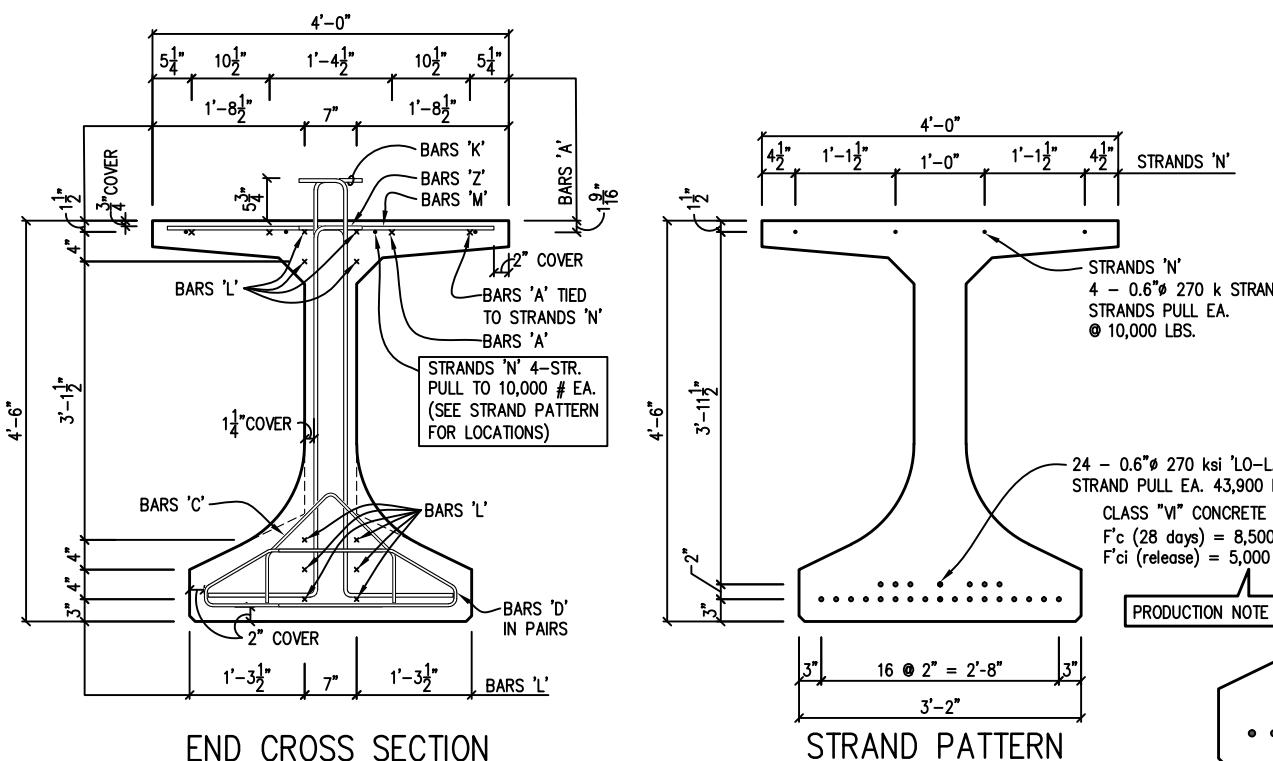
END ELEVATION
STRANDING NOT SHOWN FOR CLARITY



END SECTION
VIEWED IN THE DIRECTION OF STATIONING
STRANDING NOT SHOWN FOR CLARITY



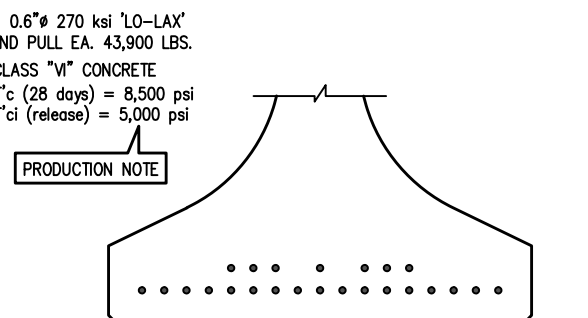
END ELEVATION
OF BEAM



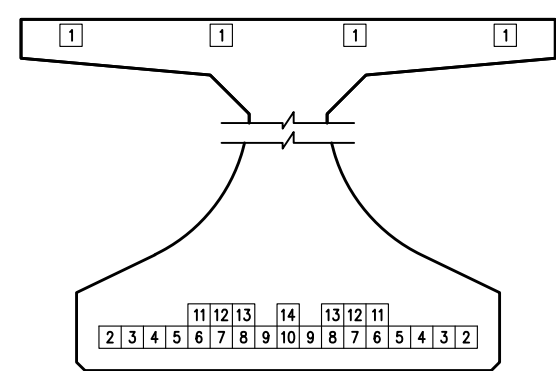
END CROSS SECTION

STRAND PATTERN

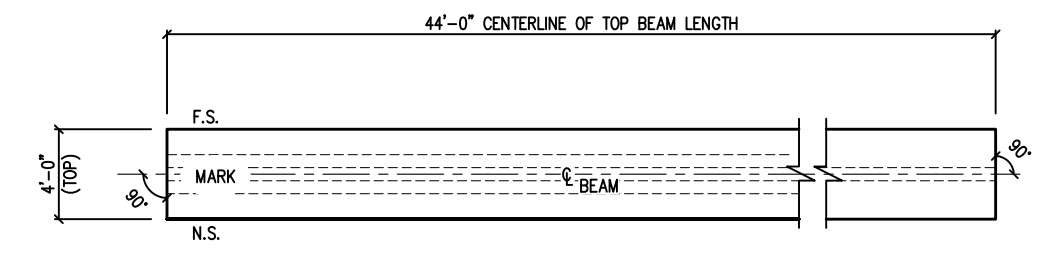
SHIELDING LEGEND
• - NONE REQUIRED



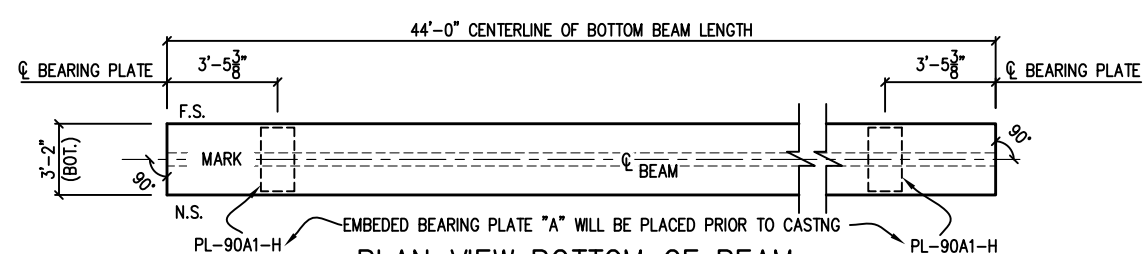
SHIELDING



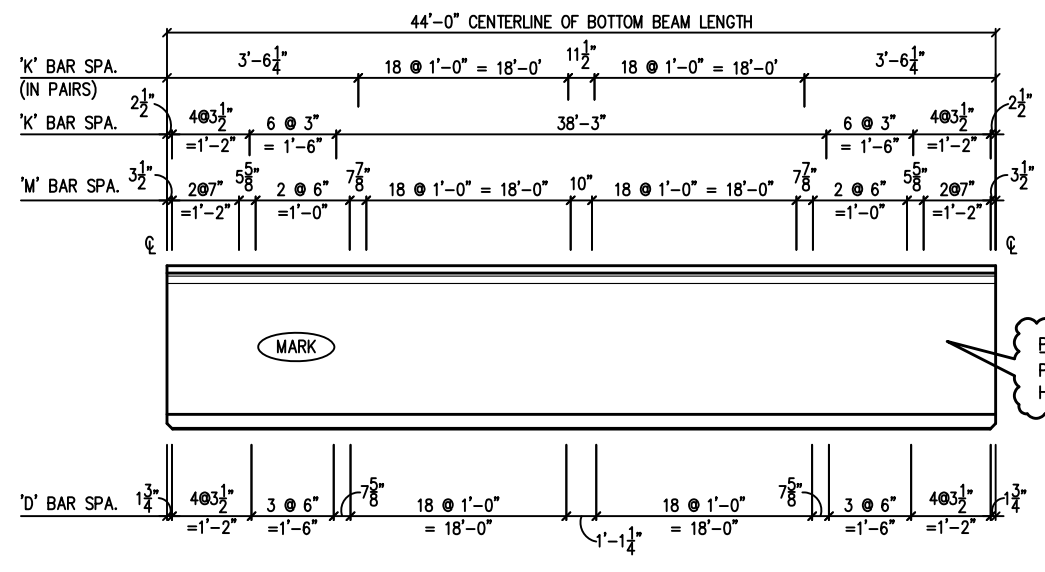
DETENSIONING SEQUENCE



PLAN VIEW TOP OF BEAM



PLAN VIEW BOTTOM OF BEAM



ELEVATION

BAR	SIZE	D.S. I.D. #	QTY.	LENGTH	REMARKS
A	5	RE-BAR 5	4	43'-9"	STRAIGHT BAR
C	3	RE-BAR 3	16	3'-1 3/4"	SEE SHEET 'A1'
D	3	RE-BAR 3	108	4'-4"	SEE SHEET 'A1'
K	4	RE-BAR 4	98	6'-5 5/8"	SEE SHEET 'A1'
L	4	RE-BAR 4	20	5'-10"	STRAIGHT BAR
M	4	RE-BAR 4	50	3'-8"	STRAIGHT BAR
Z	4	RE-BAR 4	10	5'-11 1/4"	SEE SHEET 'A1'

PRODUCTION NOTE:
REFER TO SHEET NO. A1
FOR ADDITIONAL NOTES NOT
SHOWN, THAT APPLY TO BEAM DETAIL.

DS PART NO.
FIB 54

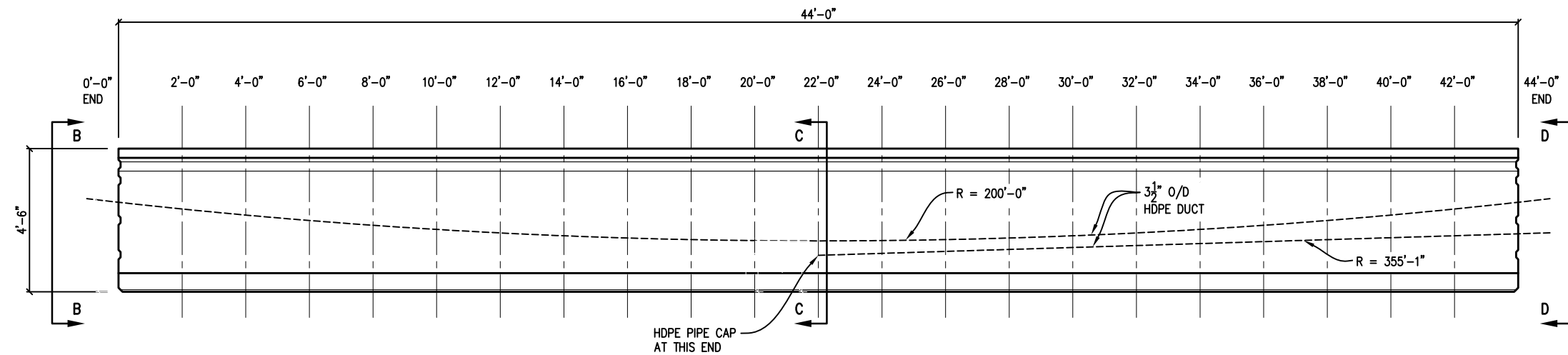
REV	DESCRIPTION	DATE	BY	CHK.

BRACING LOCATIONS

DURA-STRESS Inc.
CA #0028
P.O. BOX 490779 LEESBURG, FL 34749-0779
PHONE (352) 787-1422 FAX (352) 787-0080
STRUCTURAL PRESTRESSED AND ARCHITECTURAL PRECAST CONCRETE PRODUCTS

JOB NAME: FOOT RESEARCH SHEAR BEHAVIOR OF WEBS BDV31-977-71
LOCATION: N/A
ARCHITECT: N/A
ENGINEER: N/A
CONTRACTOR: N/A
PROJ. NO.: N/A

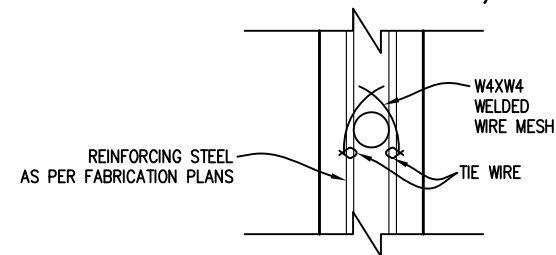
DRAWN: NE
CHK'D.: POL/TW
APPR.:
DATE: 1/21/2020
RELEASED:
DS JOB NO:
B1824
SHT: P50-1 OF 2



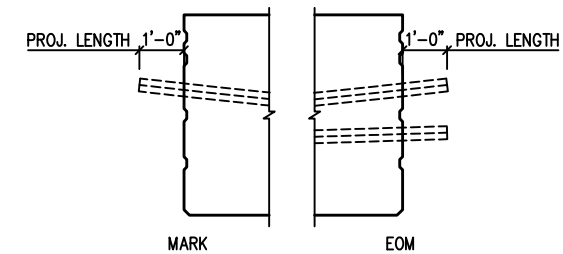
DUCT LAYOUT

GIRDER	P50																						
DISTANCE FROM END OF GIRDER	0'-0"	2'-0"	4'-0"	6'-0"	8'-0"	10'-0"	12'-0"	14'-0"	16'-0"	18'-0"	20'-0"	22'-0"	24'-0"	26'-0"	28'-0"	30'-0"	32'-0"	34'-0"	36'-0"	38'-0"	40'-0"	42'-0"	44'-0"
H1 (FT)	N/A	N/A	N/A	N/A	N/A	N/A	N/A	N/A	N/A	N/A	N/A	1'-1 3/4"	1'-1 3/4"	1'-2"	1'-2 3/8"	1'-2 3/4"	1'-3 1/2"	1'-4 1/8"	1'-5"	1'-6"	1'-7 1/4"	1'-8 1/2"	1'-9 7/8"
H2 (FT)	2'-9 3/4"	2'-7 1/4"	2'-5"	2'-2 7/8"	2'-1 1/8"	1'-11 1/2"	1'-10 1/4"	1'-9 1/8"	1'-8 1/4"	1'-7 3/4"	1'-7 3/8"	1'-7 1/4"	1'-7 3/8"	1'-7 3/4"	1'-8 1/4"	1'-9 1/8"	1'-10 1/4"	1'-11 1/2"	2'-1 1/8"	2'-2 7/8"	2'-5"	2'-7 1/4"	2'-9 3/4"

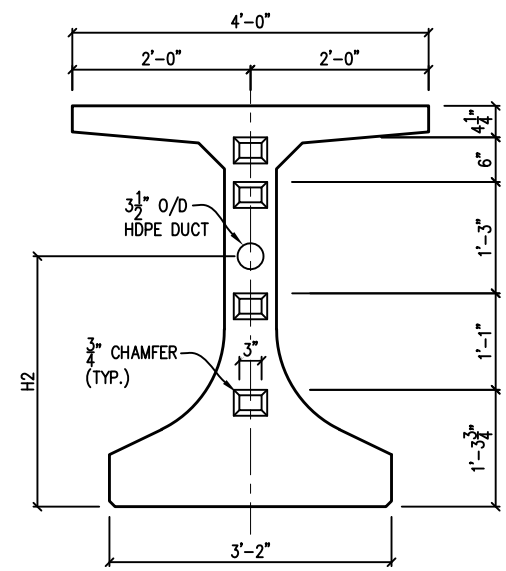
AT 1 FOOT SPACING, TYP.



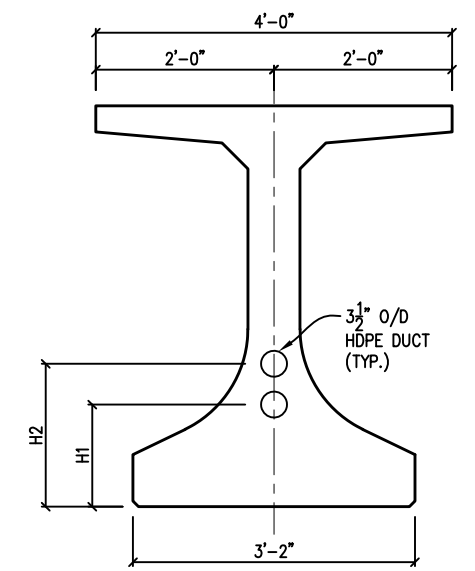
DUCT TIES



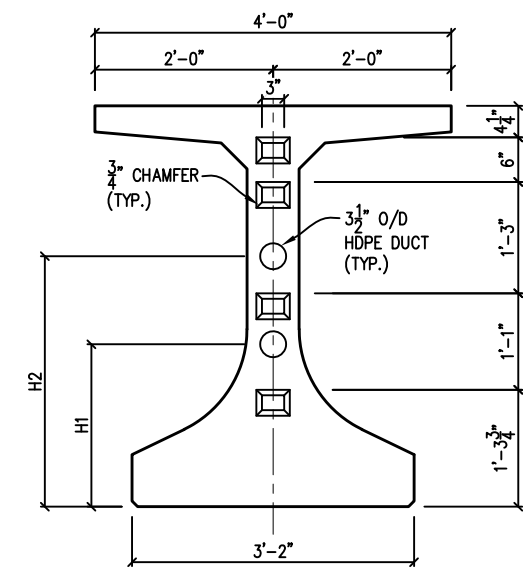
END OF BEAM DUCT DETAIL



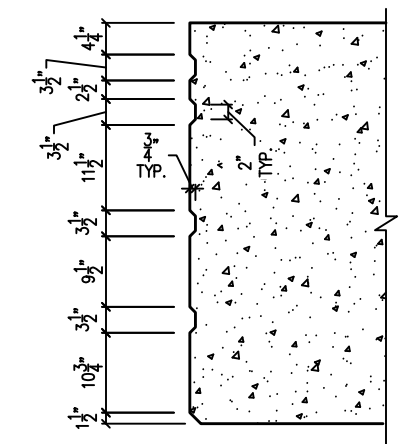
CROSS SECTION B-B



CROSS SECTION C-C



CROSS SECTION D-D



SHEAR KEY ELEVATION VIEW

MARK	QTY.	WEIGHT	CU. YDS.	Ø MAX LENGTH
P50	1	42,743#	10.55	44'-0"

DS PART NO.
FIB 54

REV	DESCRIPTION	DATE	BY	CHK.

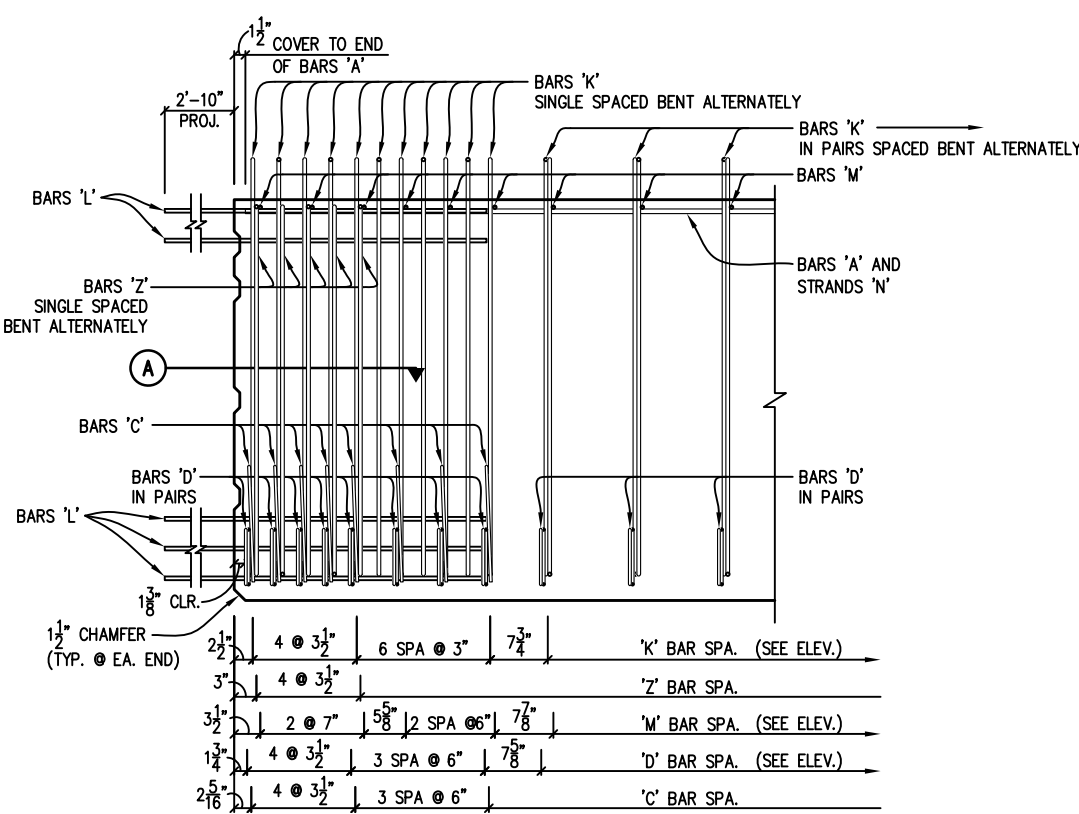
TYPE FIB 54 BEAM SECTIONS AND DETAILS

DURA-STRESS inc.
CA #6028
P.O. BOX 490779 LEESBURG, FL 34749-0779
PHONE (352) 787-1422 FAX (352) 787-0080
STRUCTURAL PRESTRESSED AND ARCHITECTURAL PRECAST CONCRETE PRODUCTS

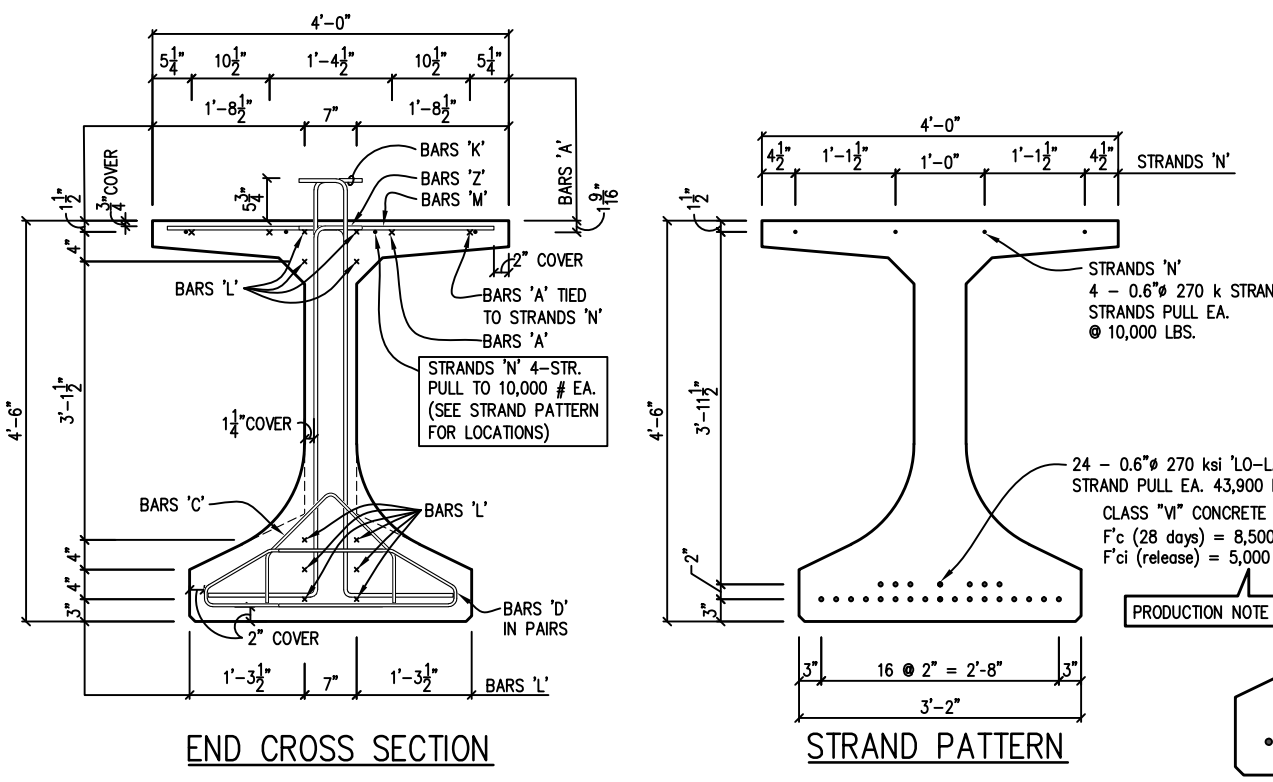
JOB NAME: FOOT RESEARCH SHEAR BEHAVIOR OF WEBS BDV31-977-71
LOCATION: N/A
ARCHITECT: N/A
ENGINEER: N/A
CONTRACTOR: N/A
PROJ. NO.: N/A

DRAWN: NE
CHK'D.: POL/TW
APPR.:
DATE: 1/21/2020
RELEASED:

DS JOB NO:
B1824
SHT: P50-2 OF 2



END ELEVATION
STRANDING NOT SHOWN FOR CLARITY



END CROSS SECTION

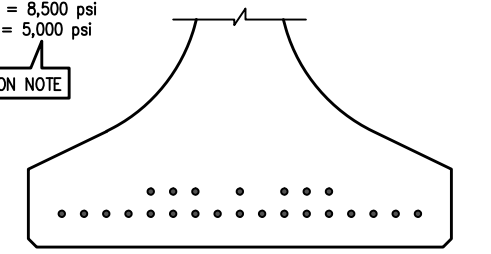
STRAND PATTERN

STRANDS 'N'
4 - 0.6"Ø 270 k STRAND
STRANDS PULL EA.
Ø 10,000 LBS.

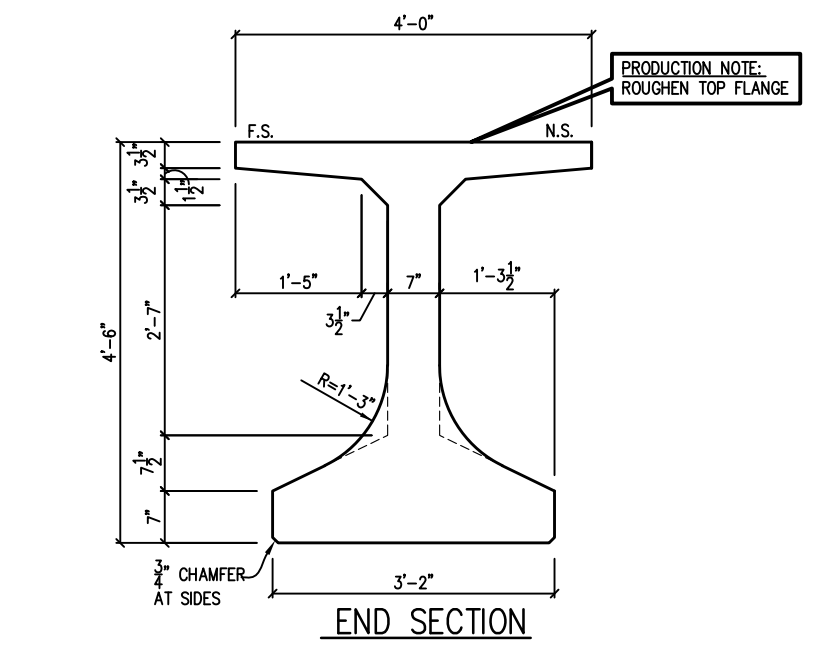
24 - 0.6"Ø 270 ksi 'LO-LAX'
STRAND PULL EA. 43,900 LBS.
CLASS "M" CONCRETE
F'c (28 days) = 8,500 psi
F'ci (release) = 5,000 psi

PRODUCTION NOTE

SHIELDING LEGEND
• - NONE REQUIRED

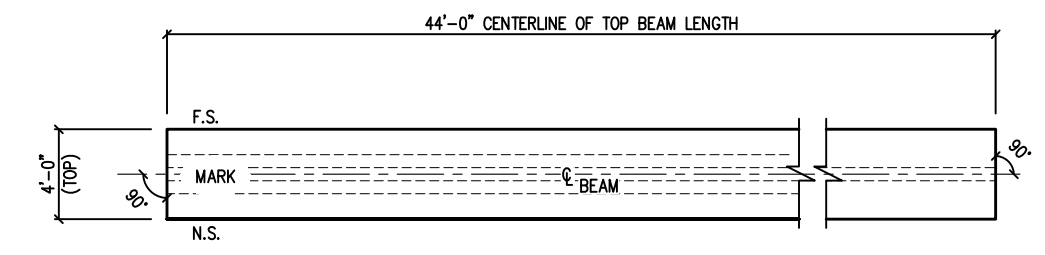


SHIELDING

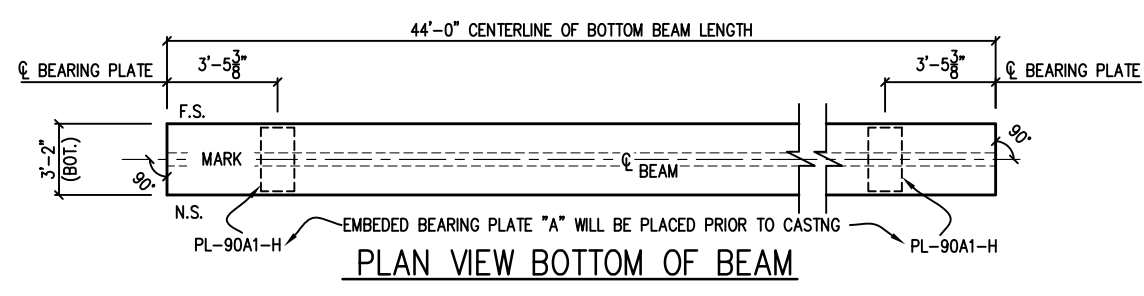


END SECTION
VIEWED IN THE DIRECTION OF STATIONING
STRANDING NOT SHOWN FOR CLARITY

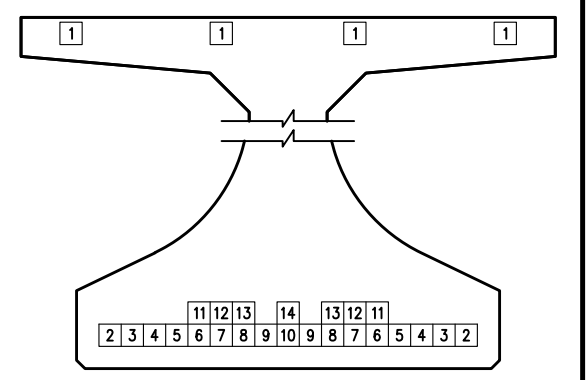
PRODUCTION NOTE:
ROUGHEN TOP FLANGE



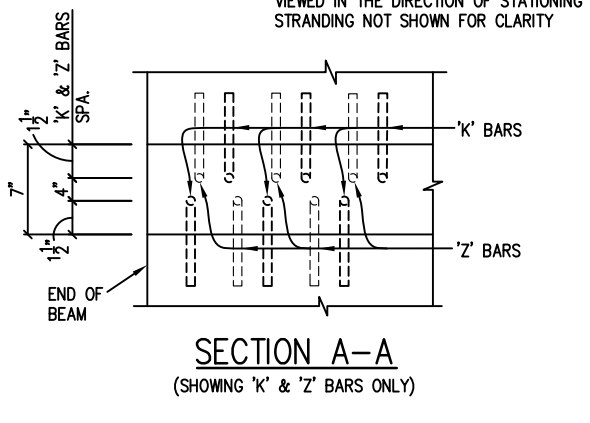
PLAN VIEW TOP OF BEAM



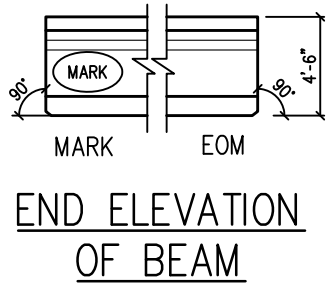
PLAN VIEW BOTTOM OF BEAM



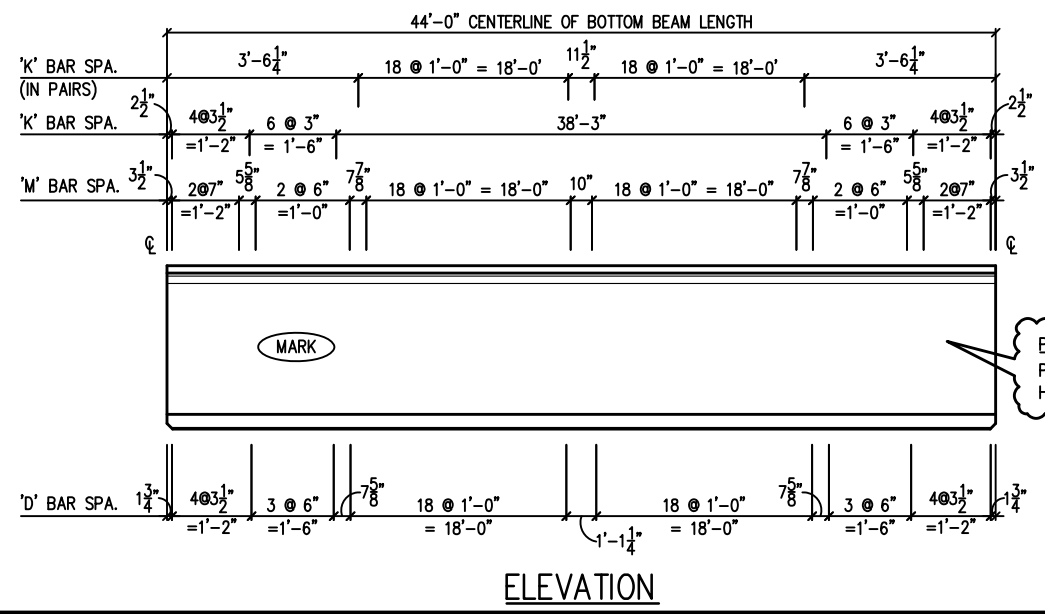
DETENSIONING SEQUENCE



SECTION A-A
(SHOWING 'K' & 'Z' BARS ONLY)



END ELEVATION OF BEAM



ELEVATION

PRODUCTION NOTE:
PLEASE PROVIDE 1 3/4"Ø
HOLE PER SHEET A2

BILL OF EMBED MATERIALS FOR ONE MEMBER ONLY					
BAR	SIZE	D.S. I.D. #	QTY.	LENGTH	REMARKS
A	5	RE-BAR 5	4	43'-9"	STRAIGHT BAR
C	3	RE-BAR 3	16	3'-1 3/4"	SEE SHEET 'A1'
D	3	RE-BAR 3	108	4'-4"	SEE SHEET 'A1'
K	4	RE-BAR 4	98	6'-5 5/8"	SEE SHEET 'A1'
L	4	RE-BAR 4	20	5'-10"	STRAIGHT BAR
M	4	RE-BAR 4	50	3'-8"	STRAIGHT BAR
Z	4	RE-BAR 4	10	5'-11 1/4"	SEE SHEET 'A1'

MARK	QTY.	WEIGHT	CU. YDS.	Ø MAX LENGTH	BRG. PL. Ø MK	BRG. PL. Ø EOM
P50R	1	42,743#	10.55	44'-0"	PL-90A1-H	PL-90A1-H

PRODUCTION NOTE:
REFER TO SHEET NO. A1
FOR ADDITIONAL NOTES NOT
SHOWN, THAT APPLY TO BEAM DETAIL.

DS PART NO.
FIB 54

REV	DESCRIPTION	DATE	BY	CHK.

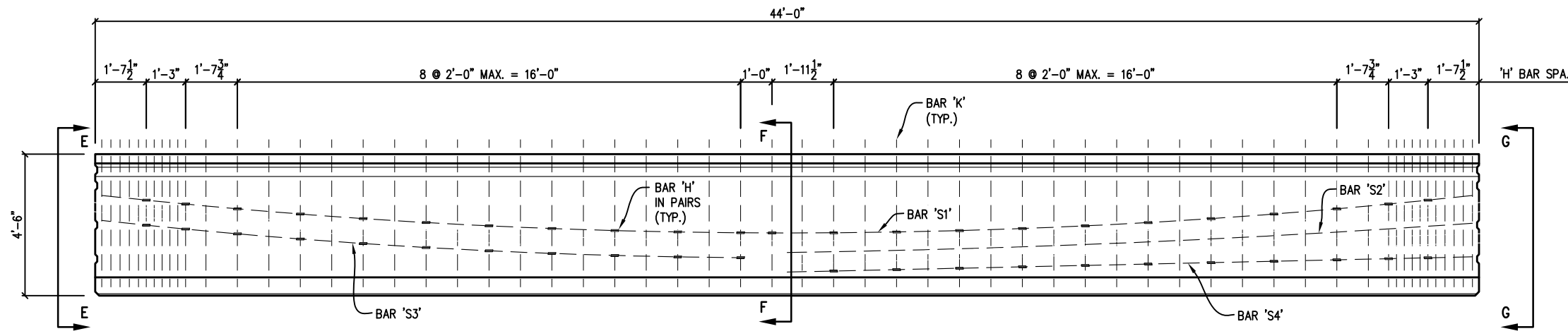
BRACING LOCATIONS

DURA-STRESS Inc.
CA #6028
P.O. BOX 490779 LEESBURG, FL 34749-0779
PHONE (352) 787-1422 FAX (352) 787-0080
STRUCTURAL PRESTRESSED AND ARCHITECTURAL PRECAST CONCRETE PRODUCTS

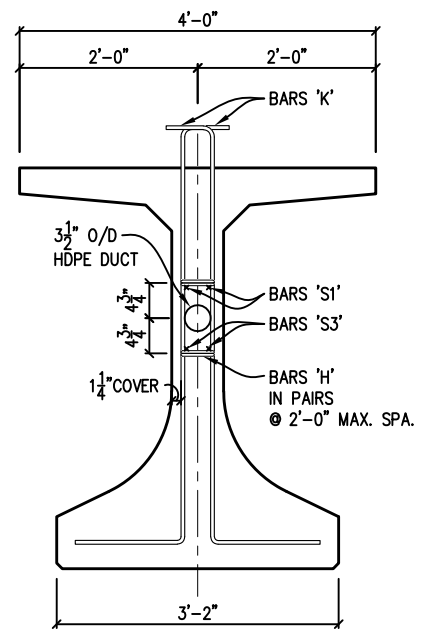
JOB NAME: FOOT RESEARCH SHEAR BEHAVIOR OF WEBS BDV31-977-71
LOCATION: N/A
ARCHITECT: N/A
ENGINEER: N/A
CONTRACTOR: N/A
PROJ. NO.: N/A

DRAWN: NE
CHK'D.: POL/TW
APPR.:
DATE: 1/21/2020
RELEASED:

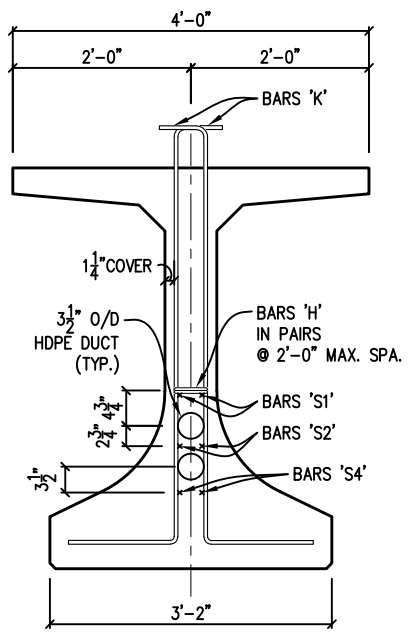
DS JOB NO:
B1824
SHT: P50R-1 OF 3



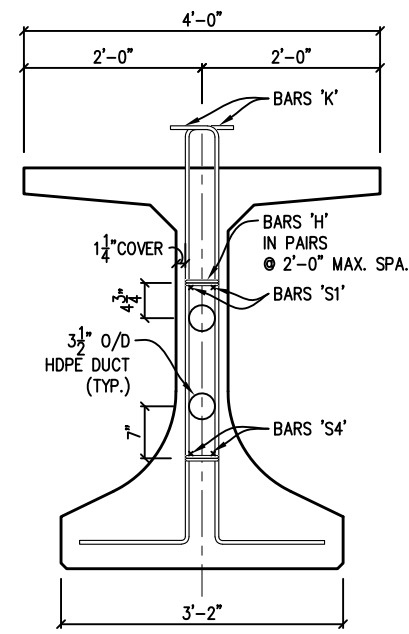
ELEVATION
(SHOWING 'S1' THRU 'S4' & H BARS ONLY)



CROSS SECTION E-E



CROSS SECTION F-F



CROSS SECTION G-G

BILL OF EMBED MATERIALS FOR ONE MEMBER ONLY					
BAR	SIZE	D.S. I.D. #	QTY.	LENGTH	REMARKS
H	3	RE-BAR 3	90	9"	SEE SHEET 'A1'
S1	4	RE-BAR 4	2	43'-7"	SEE SHEET 'A1'
S2	4	RE-BAR 4	2	21'-10"	SEE SHEET 'A1'
S3	4	RE-BAR 4	2	20'-4"	SEE SHEET 'A1'
S4	4	RE-BAR 4	2	21'-10"	STRAIGHT BAR

MARK	QTY.	WEIGHT	CU. YDS.	Q. MAX LENGTH	BRG. PL. @ MK	BRG. PL. @ EOM
P50R	1	42,743#	10.55	44'-0"	PL-90A1-H	PL-90A1-H

DS PART NO.
FIB 54

REV	DESCRIPTION	DATE	BY	CHK.

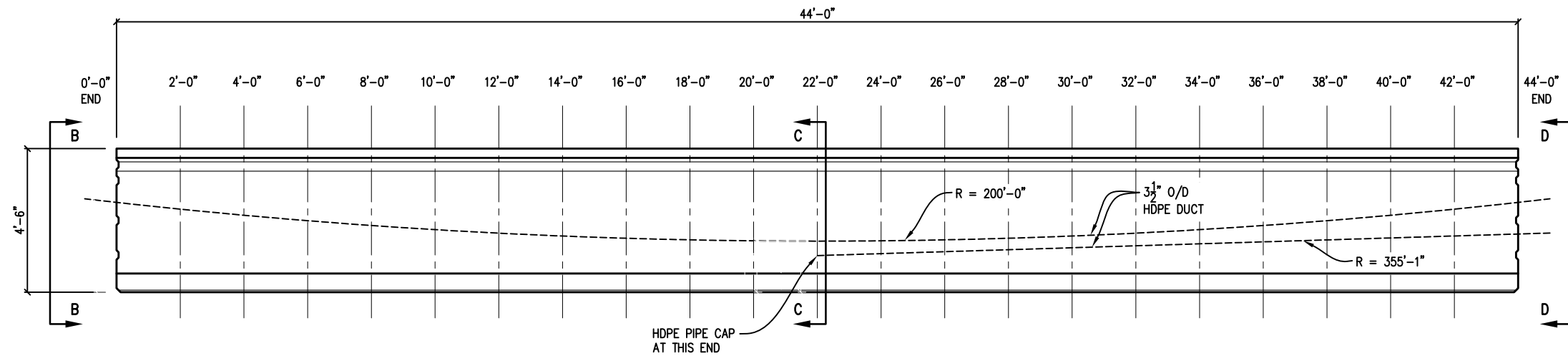
TYPE FIB 54 BEAM SECTIONS AND DETAILS

DURA-STRESS Inc.
CA #6028
P.O. BOX 490779 LEESBURG, FL 34749-0779
PHONE (352) 787-1422 FAX (352) 787-0080
STRUCTURAL PRESTRESSED AND ARCHITECTURAL PRECAST CONCRETE PRODUCTS

JOB NAME: FOOT RESEARCH SHEAR BEHAVIOR OF WEBS BDV31-977-71
LOCATION: N/A
ARCHITECT: N/A
ENGINEER: N/A
CONTRACTOR: N/A
PROJ. NO.: N/A

DRAWN: NE
CHK'D.: POL/TW
APPR.:
DATE: 1/21/2020
RELEASED:

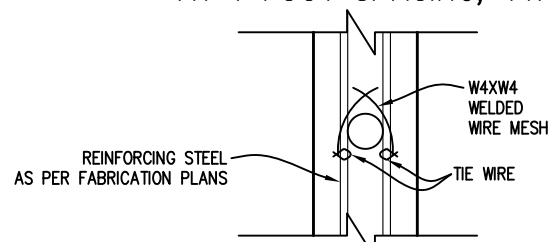
DS JOB NO:
B1824
SHT: P50R-2 OF 3



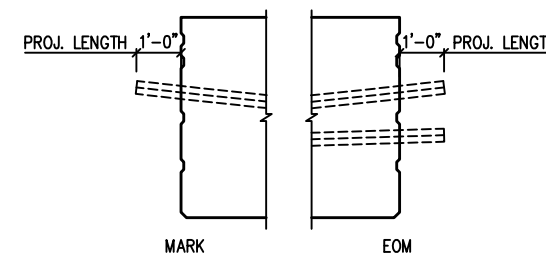
DUCT LAYOUT

GIRDER	P50R																						
DISTANCE FROM END OF GIRDER	0'-0"	2'-0"	4'-0"	6'-0"	8'-0"	10'-0"	12'-0"	14'-0"	16'-0"	18'-0"	20'-0"	22'-0"	24'-0"	26'-0"	28'-0"	30'-0"	32'-0"	34'-0"	36'-0"	38'-0"	40'-0"	42'-0"	44'-0"
H1 (FT)	N/A	N/A	N/A	N/A	N/A	N/A	N/A	N/A	N/A	N/A	N/A	1'-1 3/4"	1'-1 3/4"	1'-2"	1'-2 3/8"	1'-2 3/4"	1'-3 1/2"	1'-4 1/8"	1'-5"	1'-6"	1'-7 1/4"	1'-8 1/2"	1'-9 7/8"
H2 (FT)	2'-9 3/4"	2'-7 1/4"	2'-5"	2'-2 7/8"	2'-1 1/8"	1'-11 1/2"	1'-10 1/4"	1'-9 1/8"	1'-8 1/4"	1'-7 3/4"	1'-7 3/8"	1'-7 1/4"	1'-7 3/8"	1'-7 3/4"	1'-8 1/4"	1'-9 1/8"	1'-10 1/4"	1'-11 1/2"	2'-1 1/8"	2'-2 7/8"	2'-5"	2'-7 1/4"	2'-9 3/4"

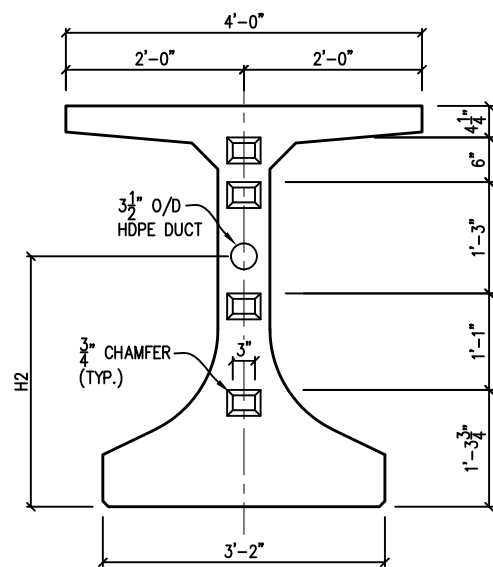
AT 1 FOOT SPACING, TYP.



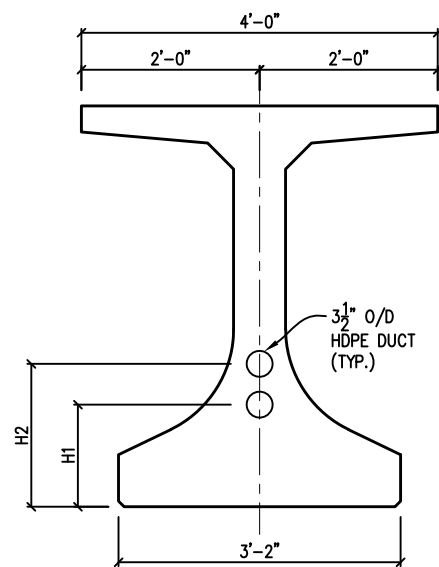
DUCT TIES



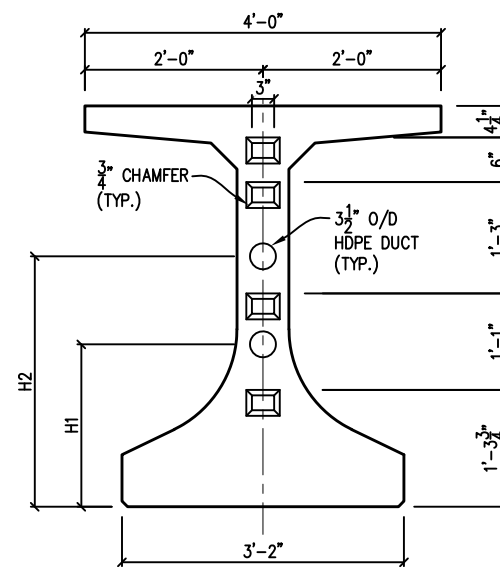
END OF BEAM DUCT DETAIL



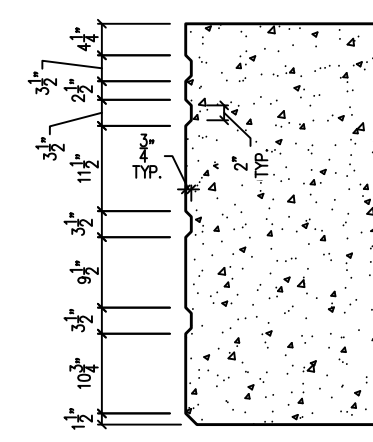
CROSS SECTION B-B



CROSS SECTION C-C



CROSS SECTION D-D



SHEAR KEY ELEVATION VIEW

MARK	QTY.	WEIGHT	CU. YDS.	Ø MAX LENGTH
P50R	1	42,743#	10.55	44'-0"

DS PART NO.
FIB 54



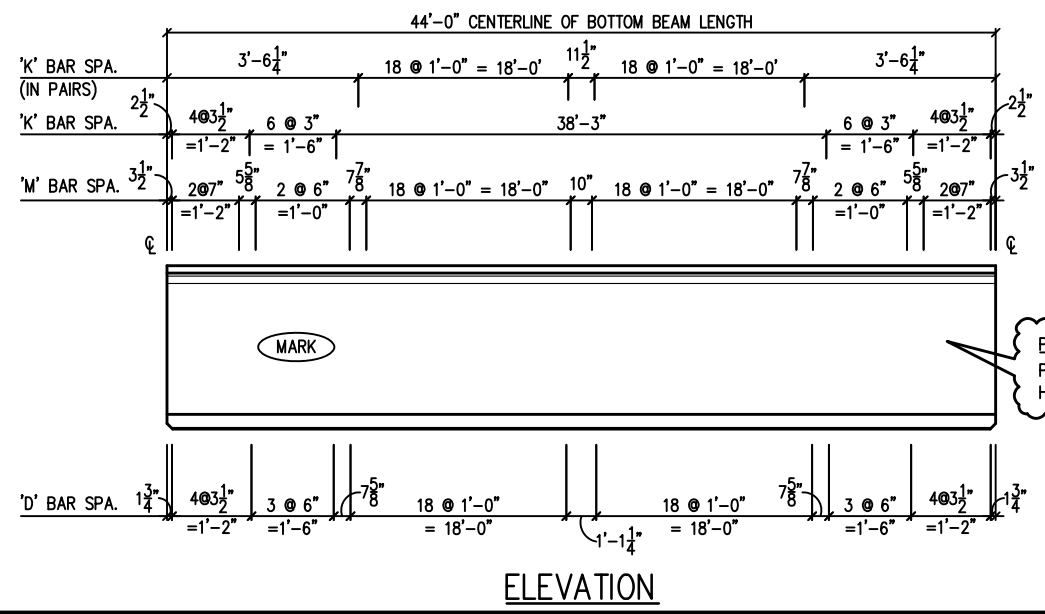
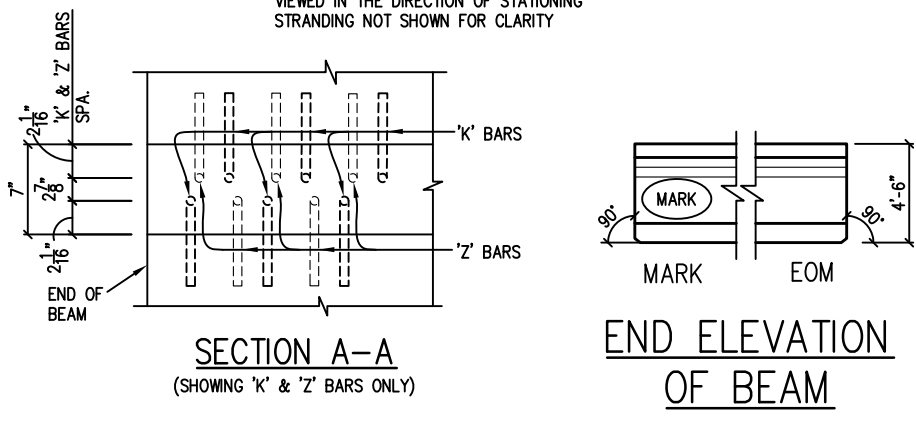
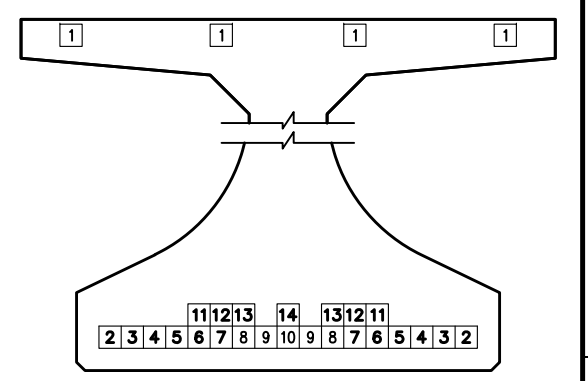
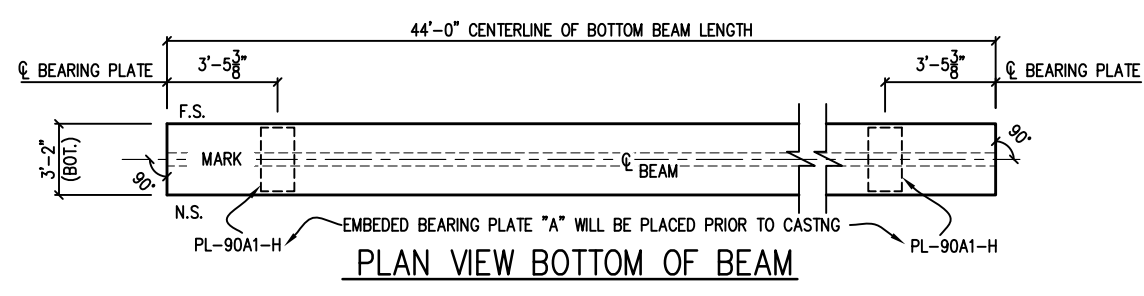
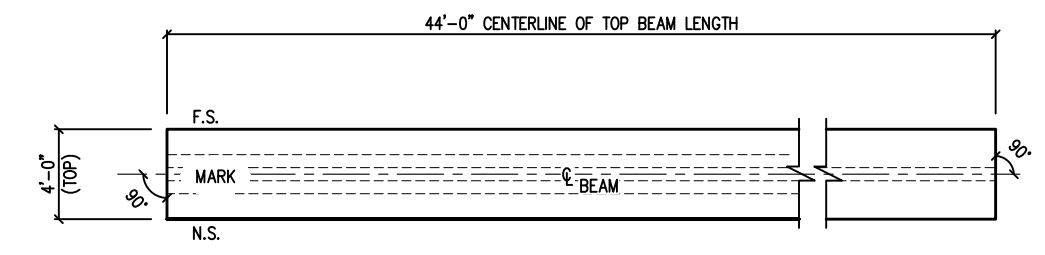
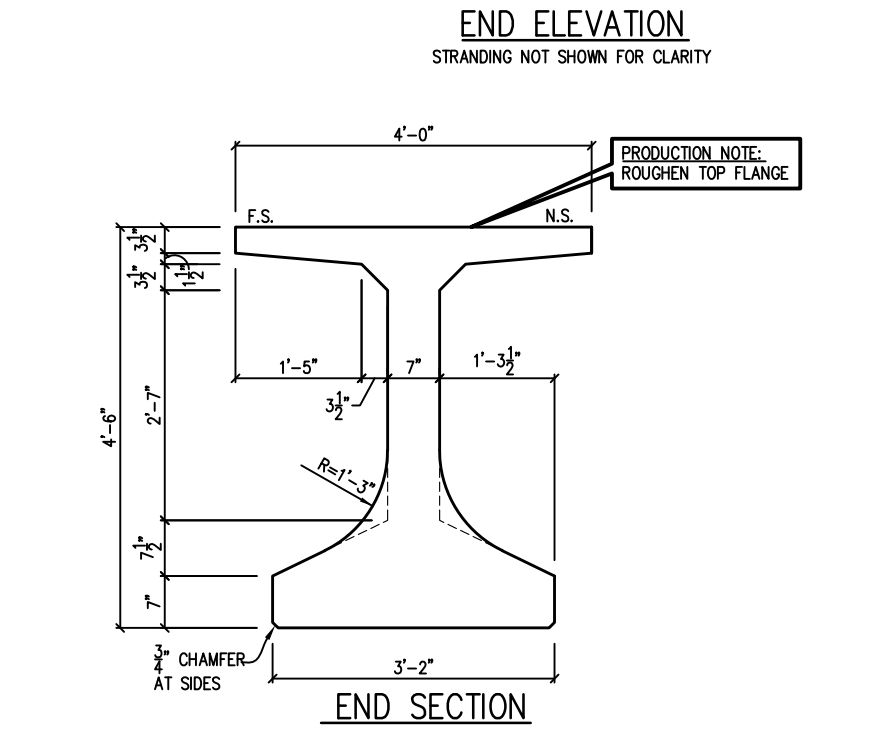
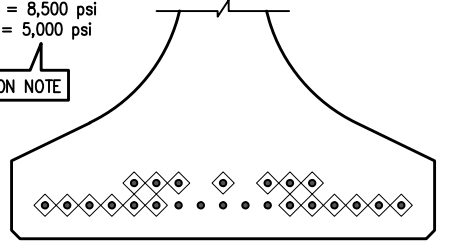
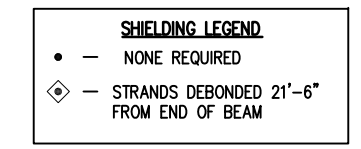
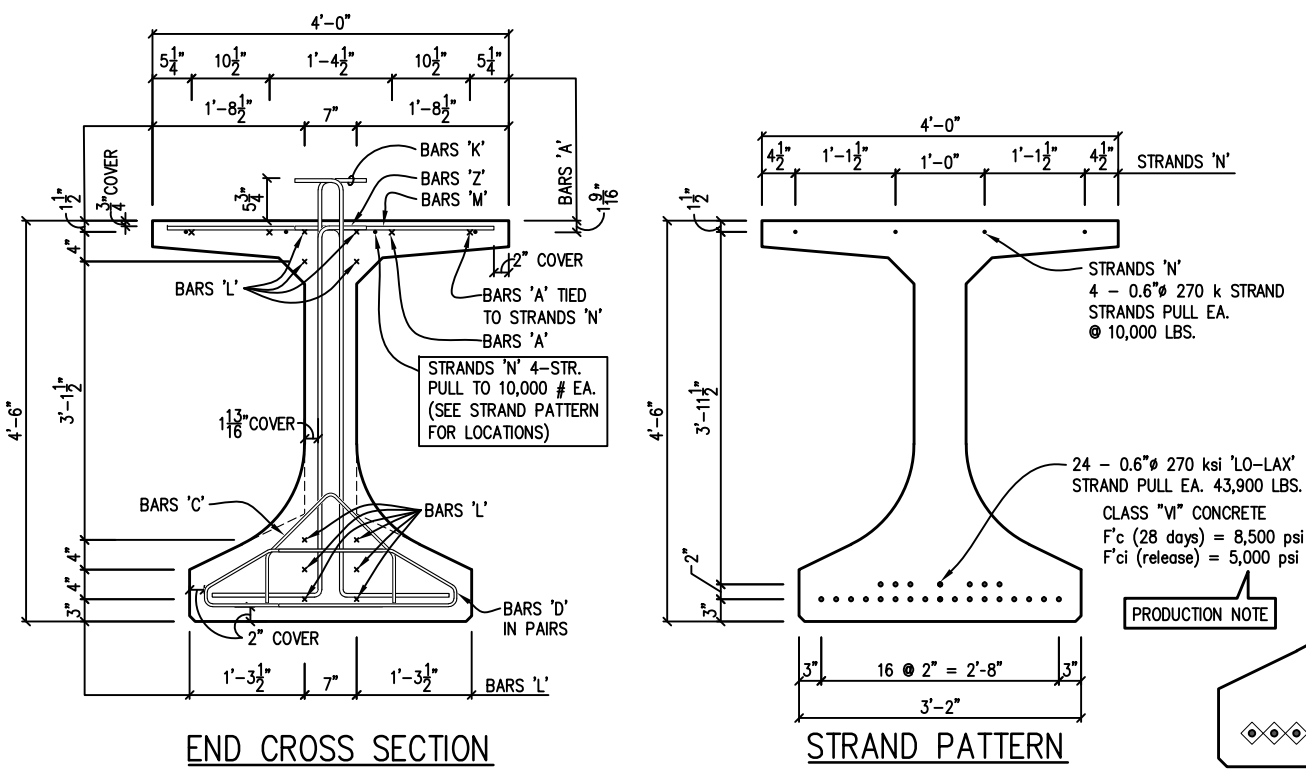
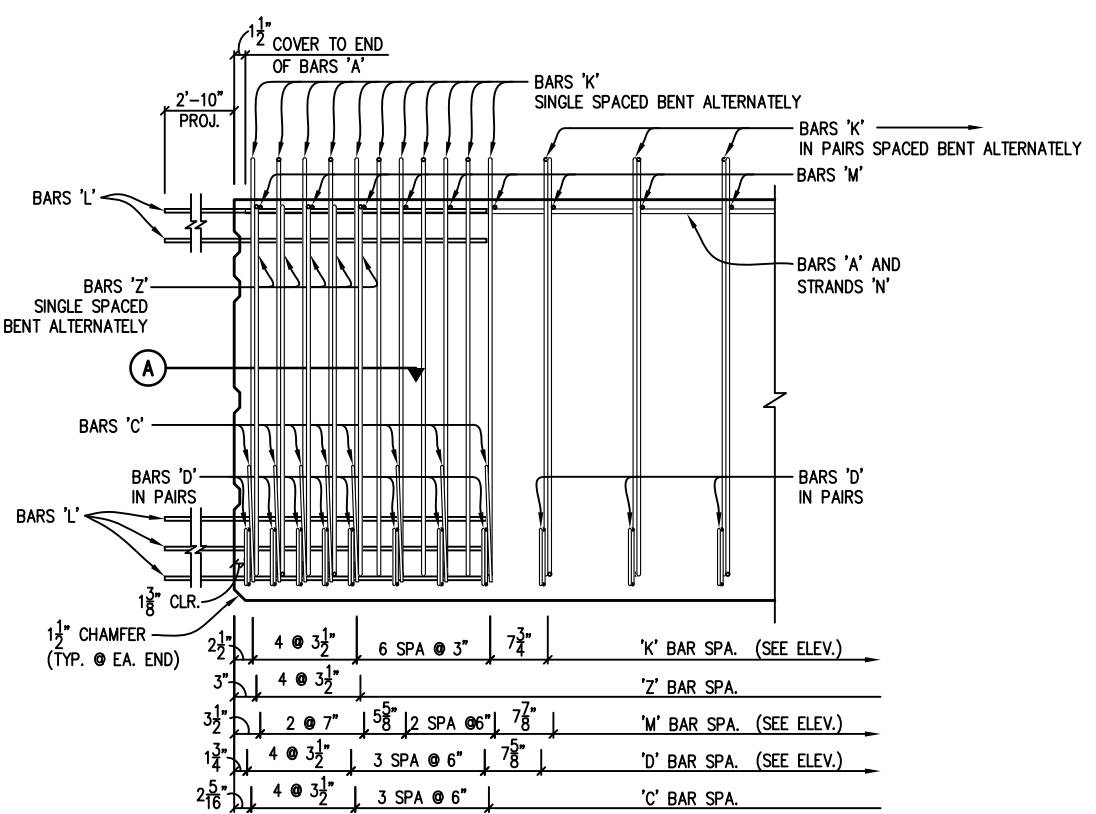
REV	DESCRIPTION	DATE	BY	CHK.

TYPE FIB 54 BEAM SECTIONS AND DETAILS
DURA-STRESS inc.
 CA #6028
 P.O. BOX 490779 LEESBURG, FL 34749-0779
 PHONE (352) 787-1422 FAX (352) 787-0080
 STRUCTURAL PRESTRESSED AND ARCHITECTURAL PRECAST CONCRETE PRODUCTS

JOB NAME: FOOT RESEARCH SHEAR BEHAVIOR OF WEBS BDV31-977-71
 LOCATION: N/A
 ARCHITECT: N/A
 ENGINEER: N/A
 CONTRACTOR: N/A
 PROJ. NO.: N/A

DRAWN: NE
 CHK'D.: POL/TW
 APPR.:
 DATE: 1/21/2020
 RELEASED:

DS JOB NO:
B1824
 SHT:P50R-3 OF 3



BILL OF EMBED MATERIALS
FOR ONE MEMBER ONLY

BAR	SIZE	D.S. I.D. #	QTY.	LENGTH	REMARKS
A	5	RE-BAR 5	4	43'-9"	STRAIGHT BAR
C	3	RE-BAR 3	16	3'-1 3/4"	SEE SHEET 'A1'
D	3	RE-BAR 3	108	4'-4"	SEE SHEET 'A1'
K	4	RE-BAR 4	98	6'-5 5/8"	SEE SHEET 'A1'
L	4	RE-BAR 4	20	5'-10"	STRAIGHT BAR
M	4	RE-BAR 4	50	3'-8"	STRAIGHT BAR
Z	4	RE-BAR 4	10	5'-11 1/4"	SEE SHEET 'A1'

MARK	QTY.	WEIGHT	CU. YDS.	Ø MAX LENGTH	BRG. PL. @ MK	BRG. PL. @ EOM
N34	1	42,743#	10.55	44'-0"	PL-90A1-H	PL-90A1-H

PRODUCTION NOTE:
REFER TO SHEET NO. A1 FOR ADDITIONAL NOTES NOT SHOWN, THAT APPLY TO BEAM DETAIL.

DS PART NO.
FIB 54

REV	DESCRIPTION	DATE	BY	CHK.

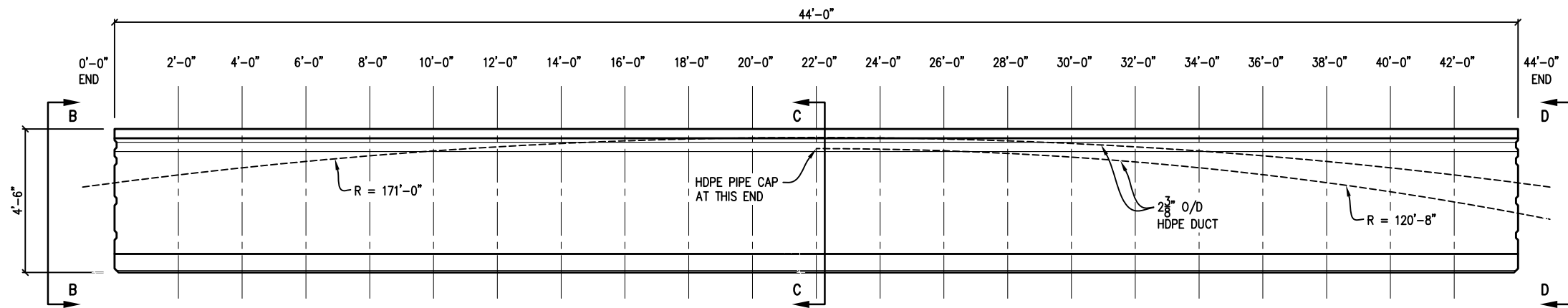
TYPE FIB 54 BEAM SECTIONS AND DETAILS

DURA-STRESS Inc.
CA #6028
P.O. BOX 490779 LEESBURG, FL 34749-0779
PHONE (352) 787-1422 FAX (352) 787-0080
STRUCTURAL PRESTRESSED AND ARCHITECTURAL PRECAST CONCRETE PRODUCTS

JOB NAME: FOOT RESEARCH SHEAR BEHAVIOR OF WEBS BDV31-977-71
LOCATION: N/A
ARCHITECT: N/A
ENGINEER: N/A
CONTRACTOR: N/A
PROJ. NO.: N/A

DRAWN: NE
CHK'D.: POL/TW
APPR.:
DATE: 1/21/2020
RELEASED:

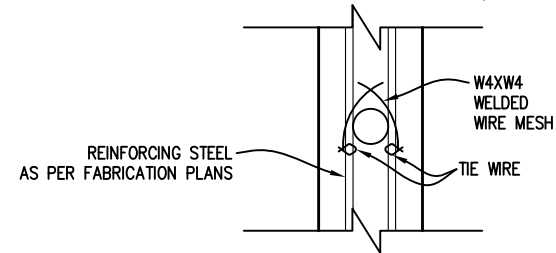
DS JOB NO: B1824
SHT: N34-1 OF 2



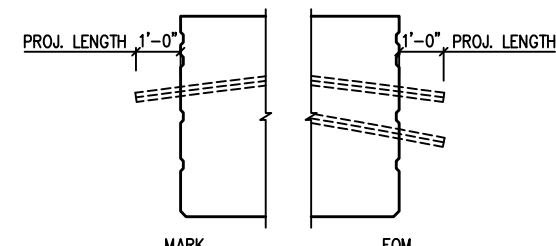
DUCT LAYOUT

GIRDER	N34																						
DISTANCE FROM END OF GIRDER	0'-0"	2'-0"	4'-0"	6'-0"	8'-0"	10'-0"	12'-0"	14'-0"	16'-0"	18'-0"	20'-0"	22'-0"	24'-0"	26'-0"	28'-0"	30'-0"	32'-0"	34'-0"	36'-0"	38'-0"	40'-0"	42'-0"	44'-0"
H1 (FT)	N/A	N/A	N/A	N/A	N/A	N/A	N/A	N/A	N/A	N/A	N/A	3'-10 5/8"	3'-10 3/8"	3'-9 3/4"	3'-8 3/4"	3'-7 3/8"	3'-5 5/8"	3'-3 3/8"	3'-0 7/8"	2'-9 3/4"	2'-6 3/8"	2'-2 1/2"	1'-10 3/8"
H2 (FT)	2'-9 7/8"	3'-0 7/8"	3'-3 5/8"	3'-6"	3'-8 1/8"	3'-9 7/8"	3'-11 1/2"	4'-0 3/4"	4'-1 3/4"	4'-2 3/8"	4'-2 7/8"	4'-3"	4'-2 7/8"	4'-2 3/8"	4'-1 3/4"	4'-0 3/4"	3'-11 1/2"	3'-9 7/8"	3'-8 1/8"	3'-6"	3'-3 5/8"	3'-0 7/8"	2'-9 7/8"

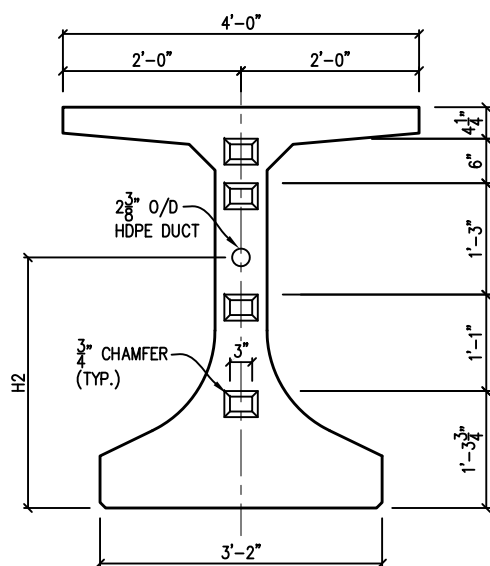
AT 1 FOOT SPACING, TYP.



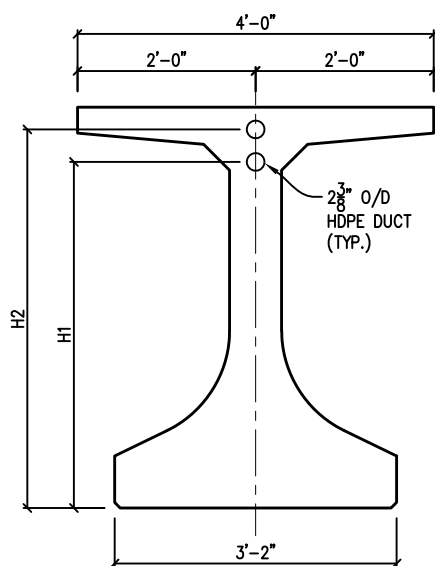
DUCT TIES



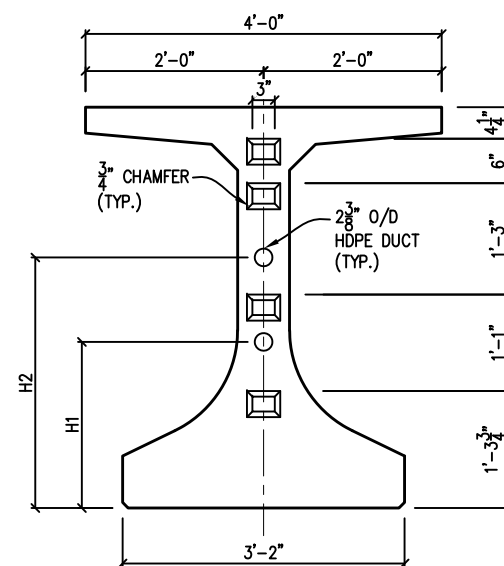
END OF BEAM DUCT DETAIL



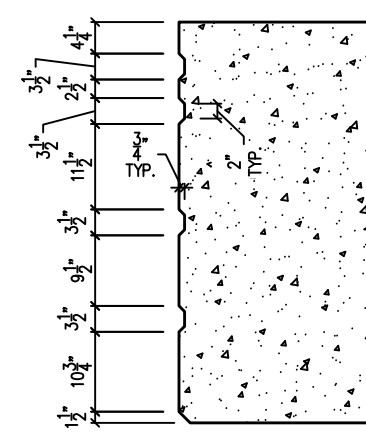
CROSS SECTION B-B



CROSS SECTION C-C



CROSS SECTION D-D



SHEAR KEY ELEVATION VIEW

MARK	QTY.	WEIGHT	CU. YDS.	Q MAX LENGTH
N34	1	42,743#	10.55	44'-0"

DS PART NO.
FIB 54



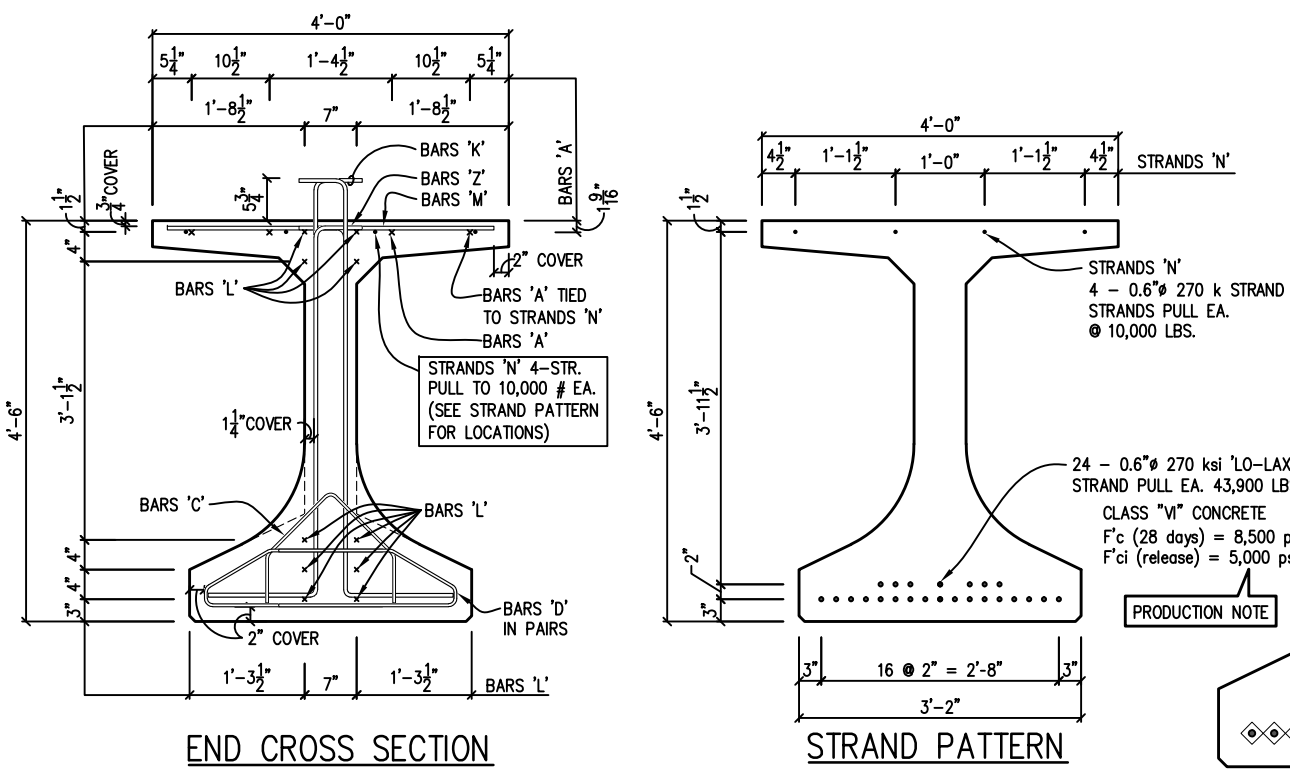
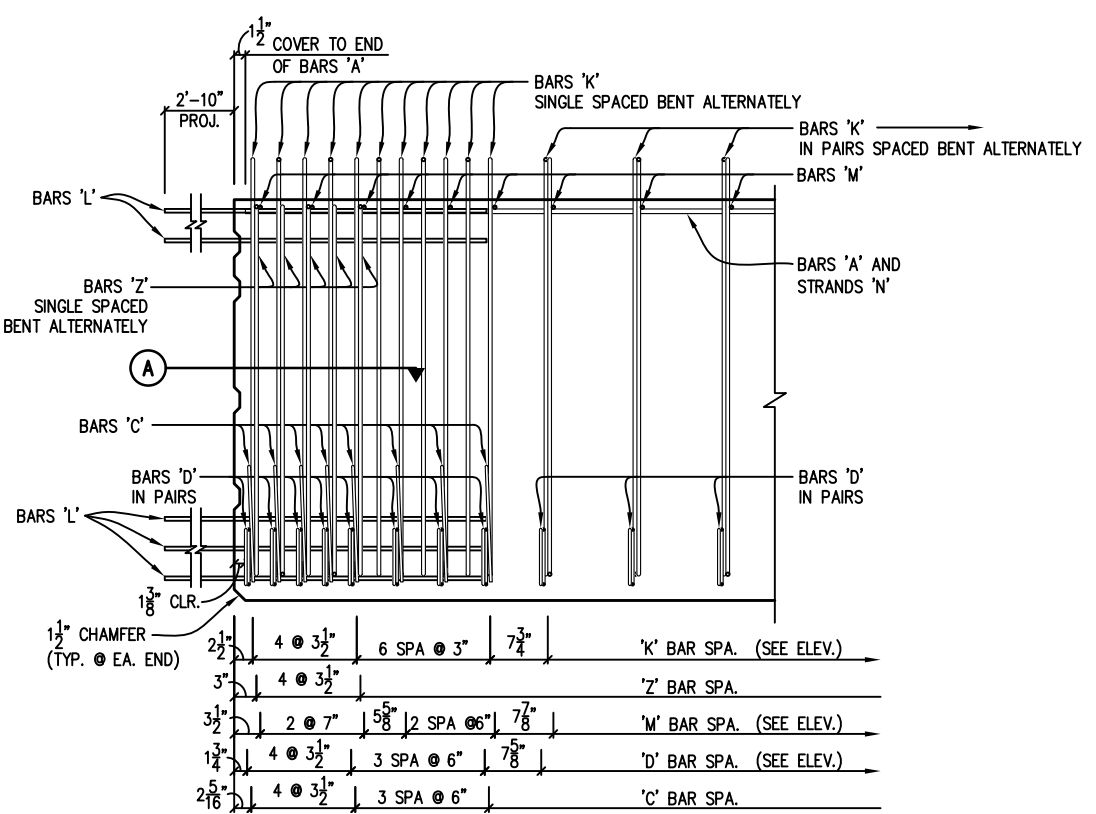
REV	DESCRIPTION	DATE	BY	CHK.

TYPE FIB 54 BEAM SECTIONS AND DETAILS
DURA-STRESS inc.
 CA #6028
 P.O. BOX 490779 LEESBURG, FL 34749-0779
 PHONE (352) 787-1422 FAX (352) 787-0080
 STRUCTURAL PRESTRESSED AND ARCHITECTURAL PRECAST CONCRETE PRODUCTS

JOB NAME: FOOT RESEARCH SHEAR BEHAVIOR OF WEBS BDV31-977-71
 LOCATION: N/A
 ARCHITECT: N/A
 ENGINEER: N/A
 CONTRACTOR: N/A
 PROJ. NO.: N/A

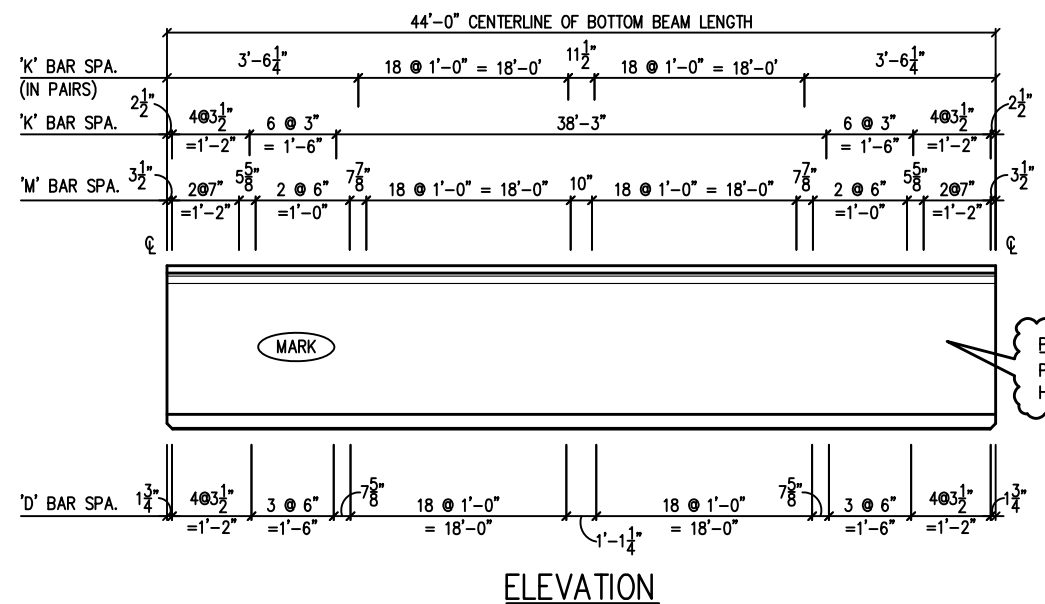
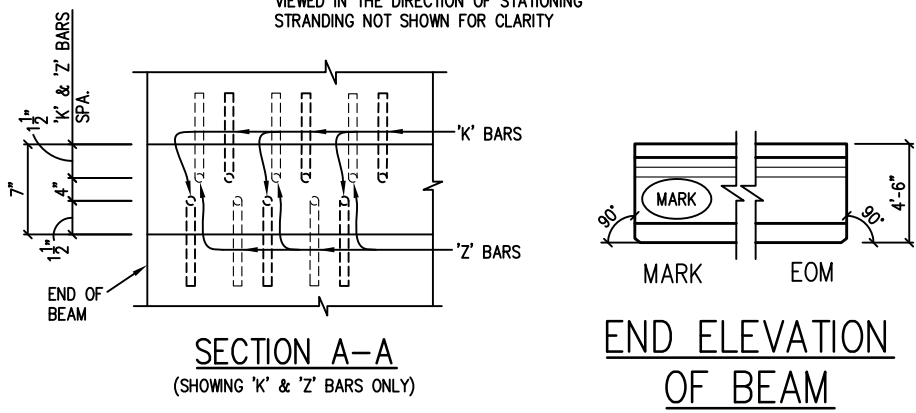
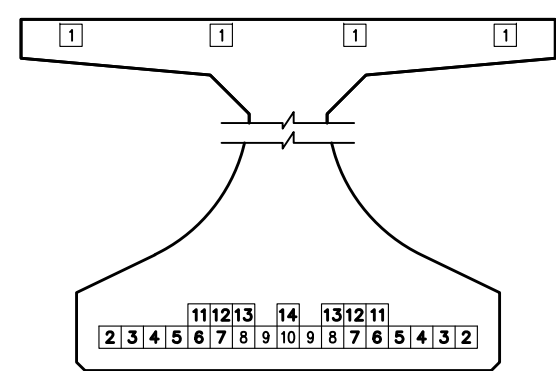
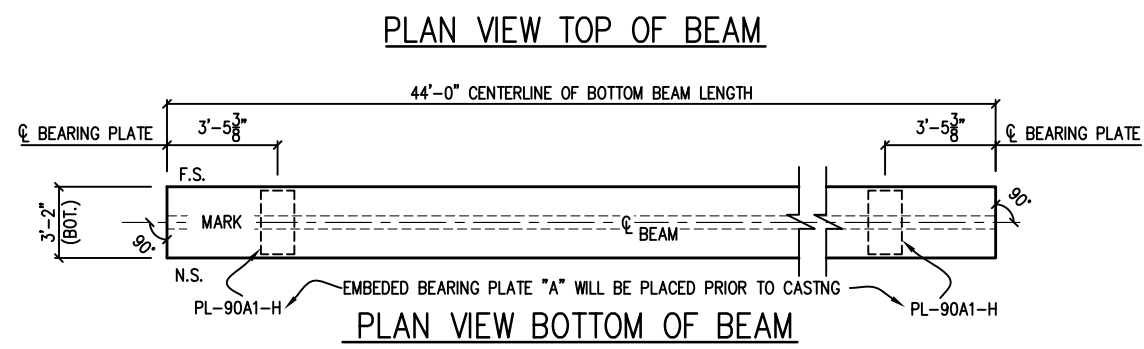
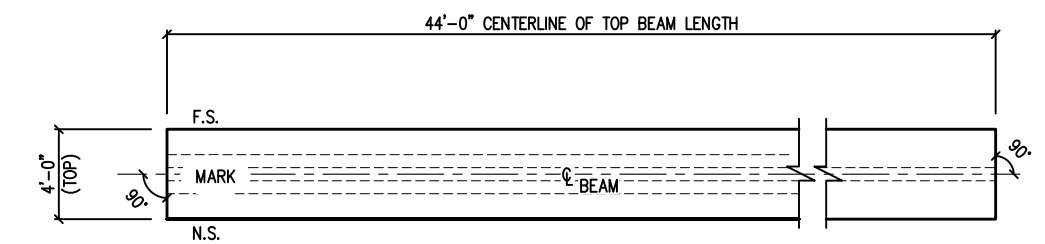
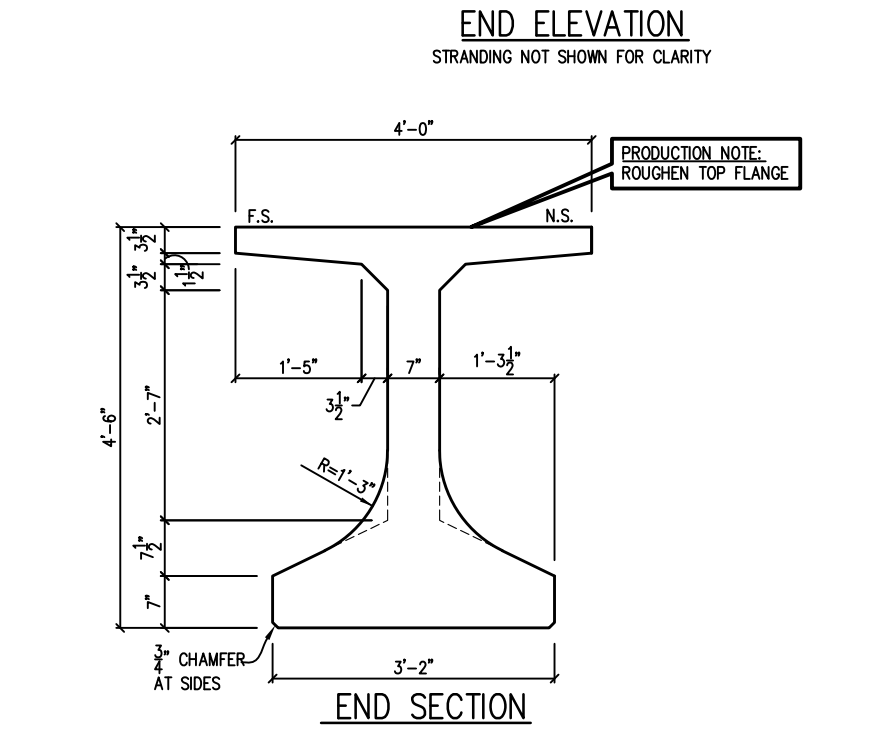
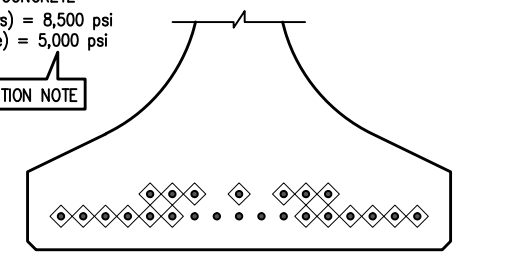
DRAWN: NE
 CHK'D.: POL/TW
 APPR.:
 DATE: 1/21/2020
 RELEASED:

DS JOB NO:
B1824
 SH: N34-2 OF 2



SHIELDING LEGEND

- - NONE REQUIRED
- ◊ - STRANDS DEBONDED 21'-6" FROM END OF BEAM



BILL OF EMBED MATERIALS FOR ONE MEMBER ONLY

BAR	SIZE	D.S. I.D. #	QTY.	LENGTH	REMARKS
A	5	RE-BAR 5	4	43'-9"	STRAIGHT BAR
C	3	RE-BAR 3	16	3'-1 3/4"	SEE SHEET 'A1'
D	3	RE-BAR 3	108	4'-4"	SEE SHEET 'A1'
K	4	RE-BAR 4	98	6'-5 5/8"	SEE SHEET 'A1'
L	4	RE-BAR 4	20	5'-10"	STRAIGHT BAR
M	4	RE-BAR 4	50	3'-8"	STRAIGHT BAR
Z	4	RE-BAR 4	10	5'-11 1/4"	SEE SHEET 'A1'

MARK	QTY.	WEIGHT	CU. YDS.	Ø MAX LENGTH	BRG. PL. @ MK	BRG. PL. @ EOM
N50	1	42,743#	10.55	44'-0"	PL-90A1-H	PL-90A1-H

PRODUCTION NOTE:
REFER TO SHEET NO. A1 FOR ADDITIONAL NOTES NOT SHOWN, THAT APPLY TO BEAM DETAIL.

DS PART NO. FIB 54

REV	DESCRIPTION	DATE	BY	CHK.

DURA-STRESS Inc.
CA #6028
P.O. BOX 490779 LEESBURG, FL 34749-0779
PHONE (352) 787-1422 FAX (352) 787-0080
STRUCTURAL PRESTRESSED AND ARCHITECTURAL PRECAST CONCRETE PRODUCTS

JOB NAME: FOOT RESEARCH SHEAR BEHAVIOR OF WEBS BDV31-977-71
LOCATION: N/A
ARCHITECT: N/A
ENGINEER: N/A
CONTRACTOR: N/A
PROJ. NO.: N/A

DRAWN: NE
CHK'D.: POL/TW
APPR.:
DATE: 1/21/2020
RELEASED:

DS JOB NO: B1824
SHT: N50-1 OF 2



DURA-STRESS Inc.

CA#6028

P.O. BOX 490779 LEESBURG, FL 34749-0779

PHONE (352) 787-1422 FAX. (352) 787-0080

STRUCTURAL PRESTRESSED AND ARCHITECTURAL PRECAST CONCRETE PRODUCTS

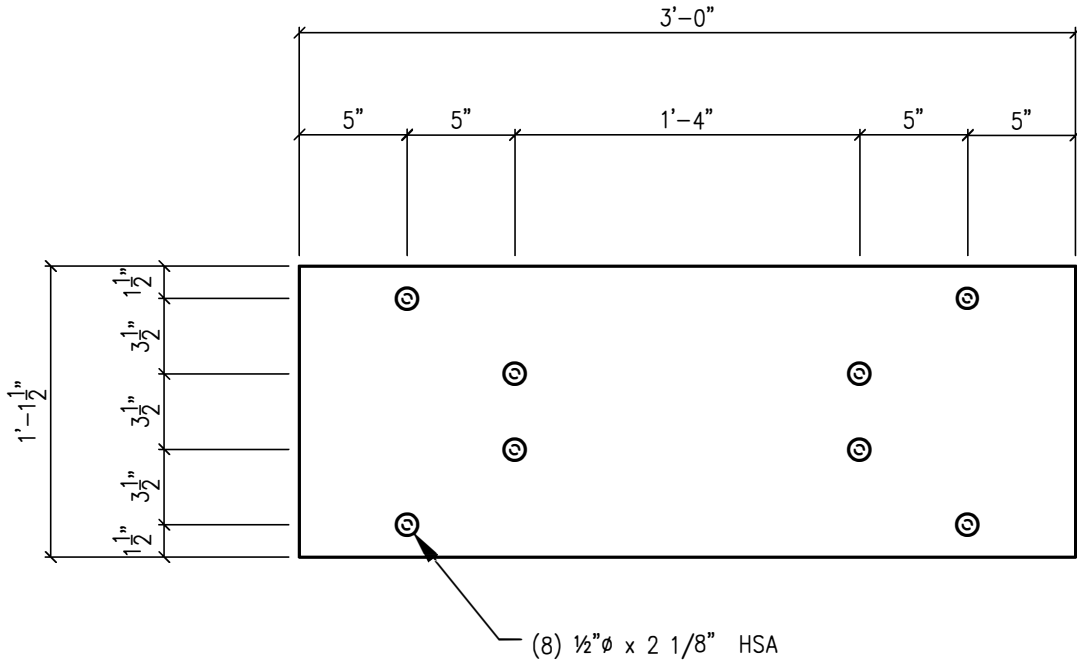
REV	DESCRIPTION	BY	CK	DATE

PART NUMBER:
PL-414-H

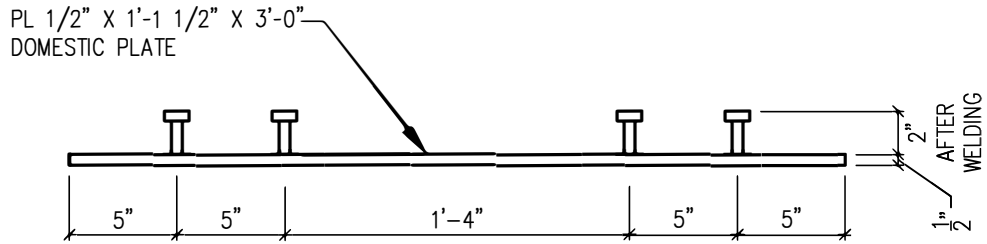
DESIGNED: FDOT-2014	DRAWN: YT	CHECKED: EW
-------------------------------	---------------------	-----------------------

**STANDARD
HARDWARE**

EMBEDDED BEARING PLATE A
FOR FLORIDA-I BEAM



PLAN



SIDE VIEW

PRODUCTION NOTE
HOT DIP GALVANIZE AFTER
FABRICATION ASTM 123

FINISH SUFFIX	NOTES	JOB NUMBER
-B BLACK (NO FINISH) -E ELECTROPLATED -G GALVANIZE PAINTED	1. ALL PLATE STEEL TO BE A36 OR ASTM A709 U.O.N. 2. ALL REBAR TO BE GRADE 60 WELDABLE OR WELDED IN ACCORDANCE WITH D 1.4.79 (E70 ELECTRODE) PREHEATED AS REQUIRED UNLESS NOTED OTHERWISE	B1824
-H HOT DIP GALVANIZED -P PRIMER PAINTED -S STAINLESS STEEL		

Materials

End Block concrete shall be FDOT class V mix
 f_c (28 day) = 6500 psi

Deck concrete shall be FDOT class II mix
 f_c (28 day) = 4500 psi

Mild reinforcement shall be ASTM A615 grade 60 (f_y 60 ksi).

Fabricator shall provide data sheets from concrete, strand, threaded rod, and rebar suppliers.

Fabricator shall provide material samples to UF/FDOT as follows:

(8) 6" dia x 12" cylinders from each concrete batch: (4) cylinders cure with girder, (4) lab cure.

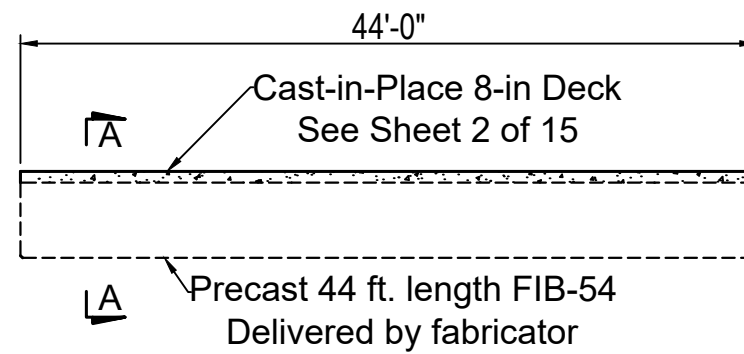
(3) 36" pieces of each size/batch of rebar.

Other

Girders will be received from fabricator.

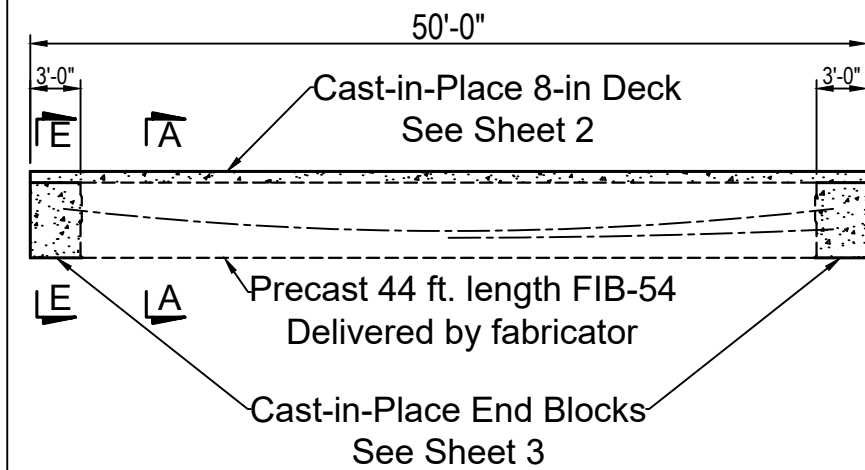
Cover beams with heavy tarp during curing.

Girder P00



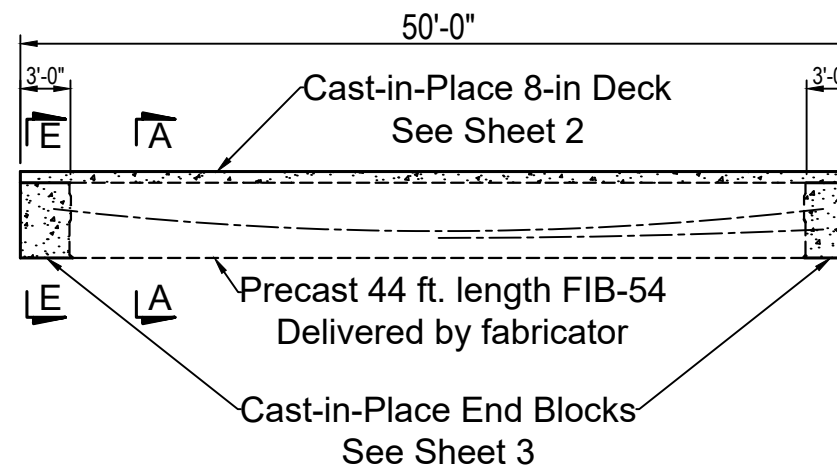
See sheet 5 for rebar schedule

Girder P34



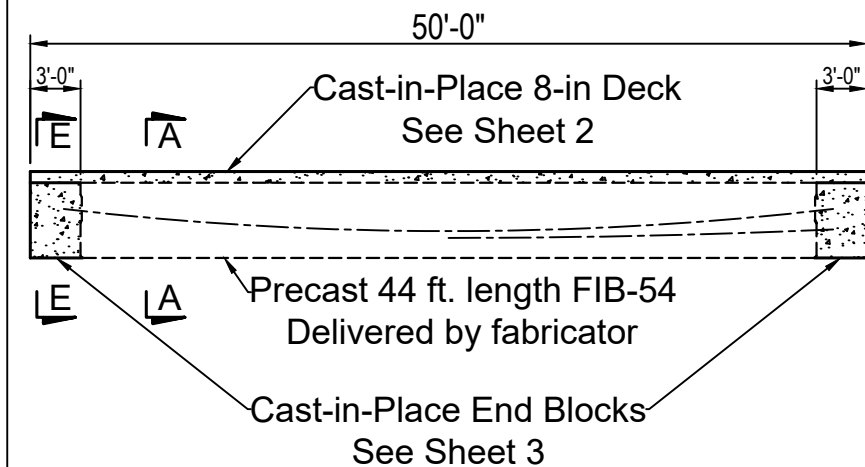
See sheet 6 for rebar schedule

Girder P41



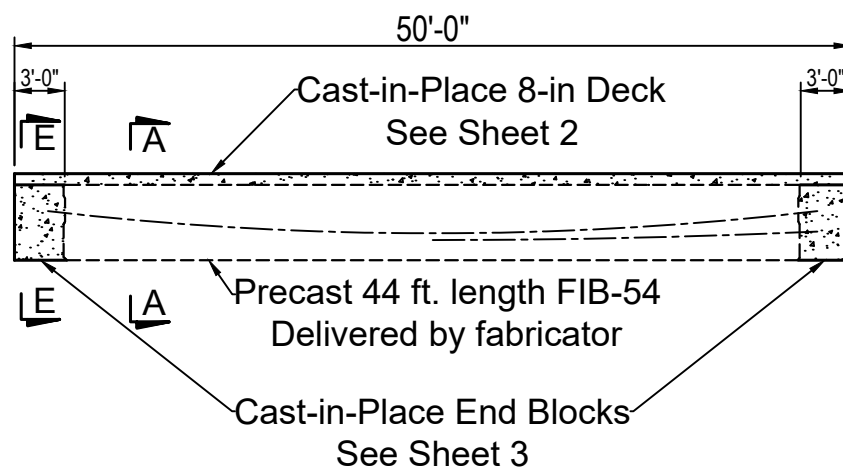
See sheet 6 for rebar schedule

Girder P50



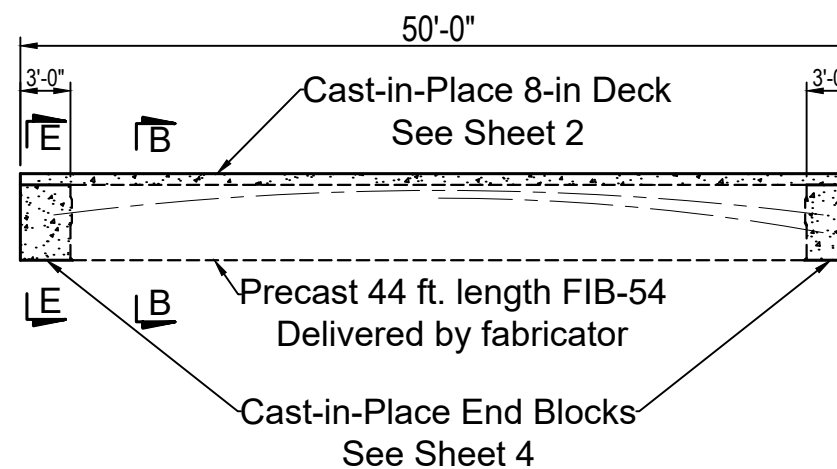
See sheet 6 for rebar schedule

Girder P50R



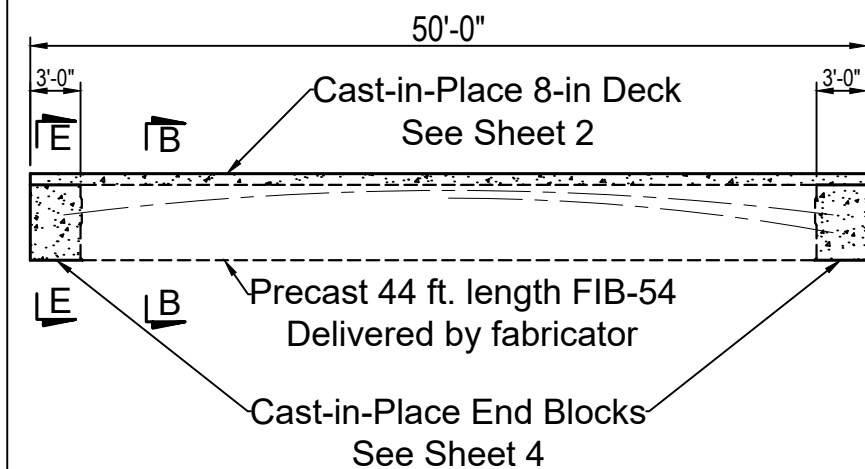
See sheet 6 for rebar schedule

Girder N34

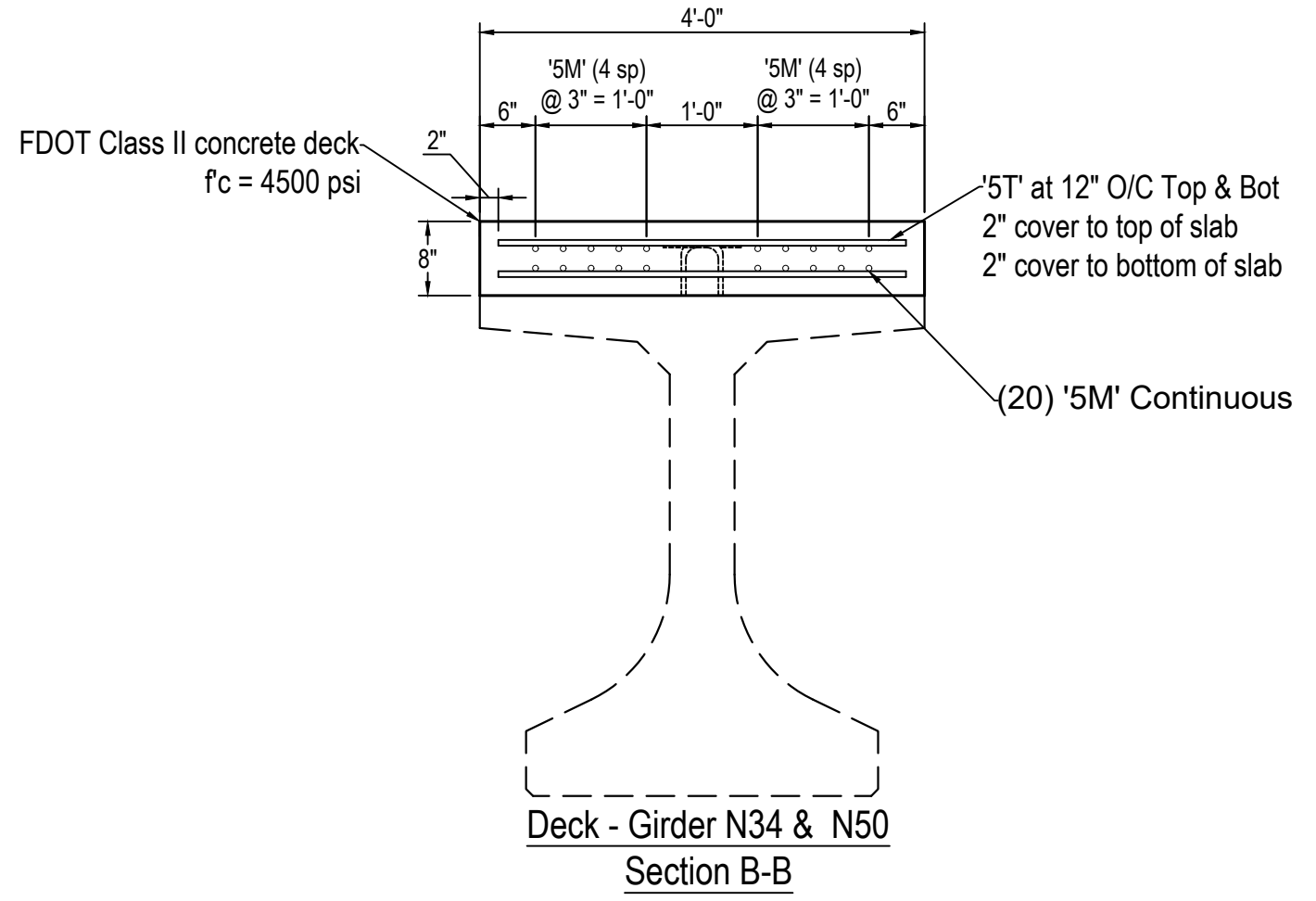
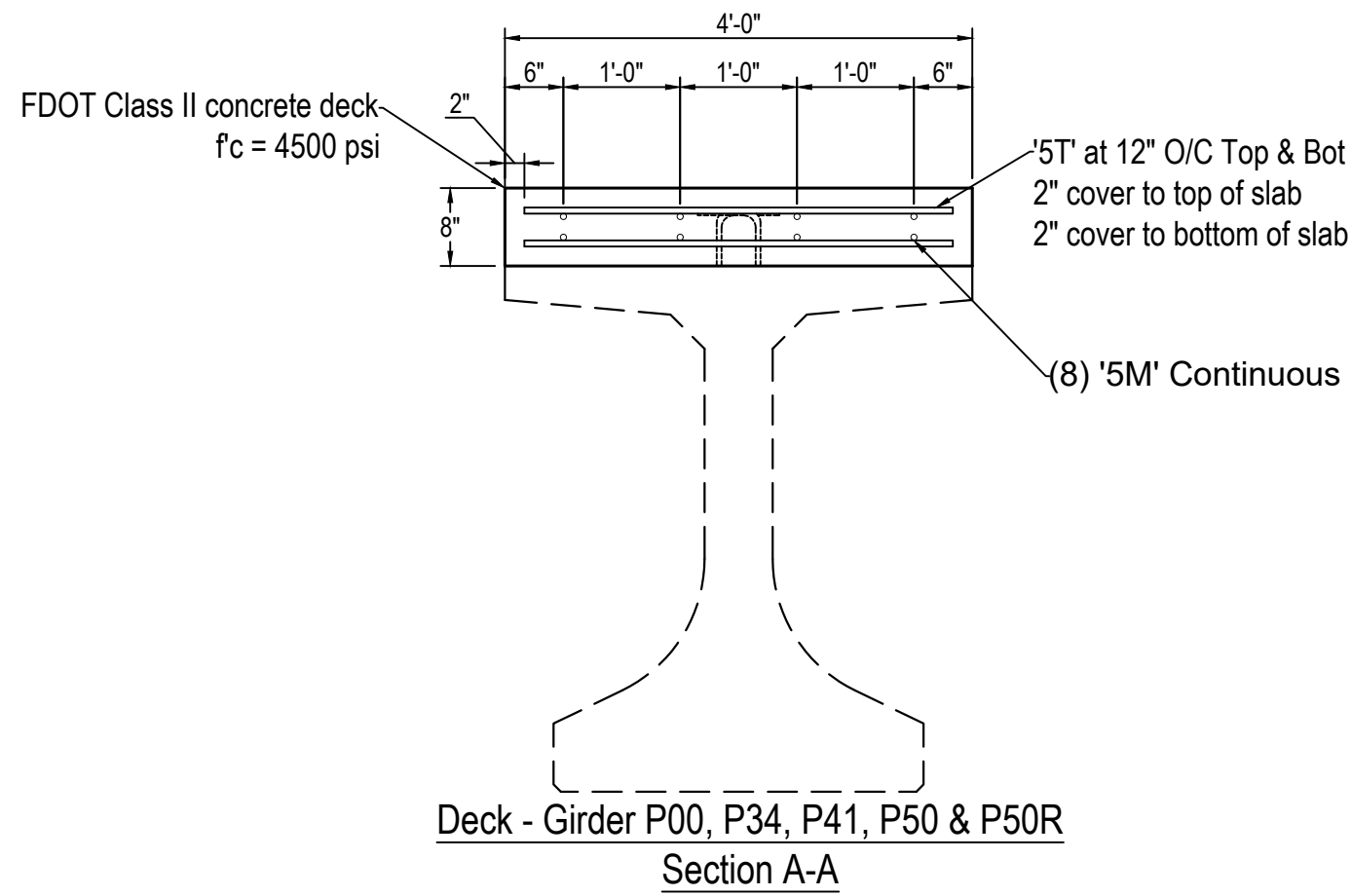


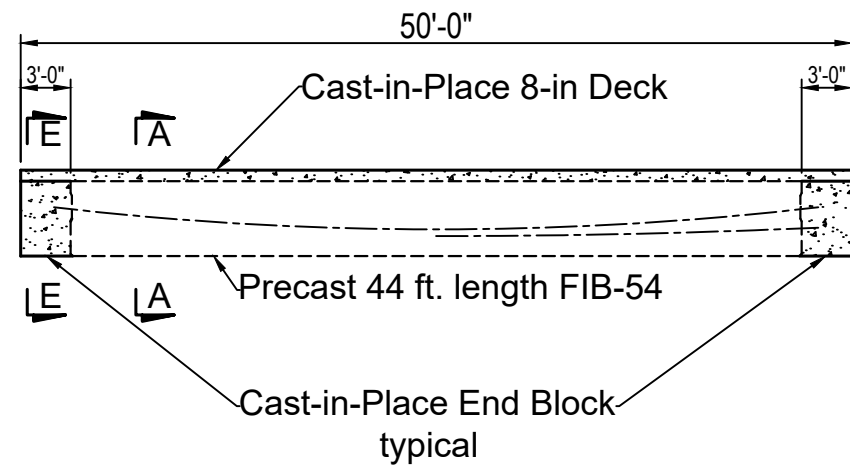
See sheet 7 for rebar schedule

Girder N50

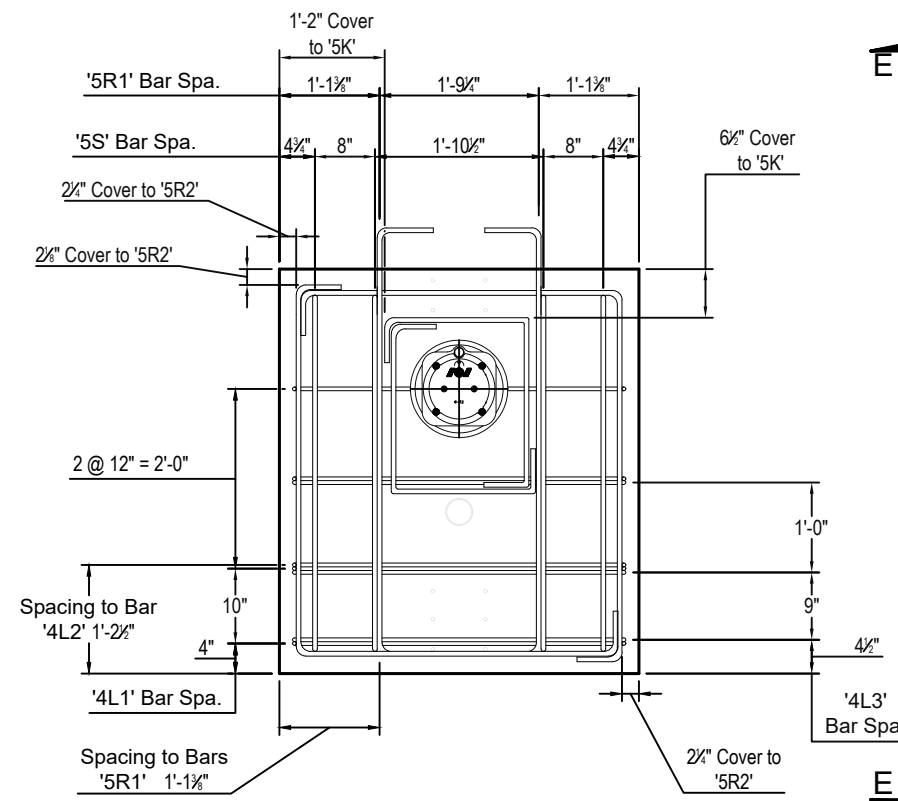


See sheet 7 for rebar schedule

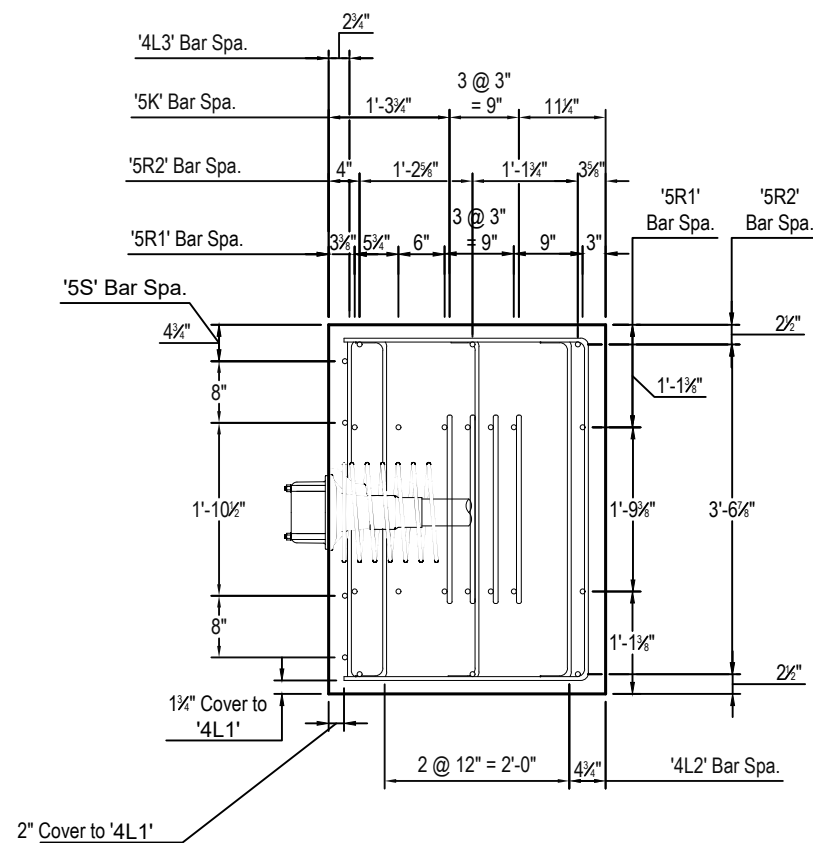




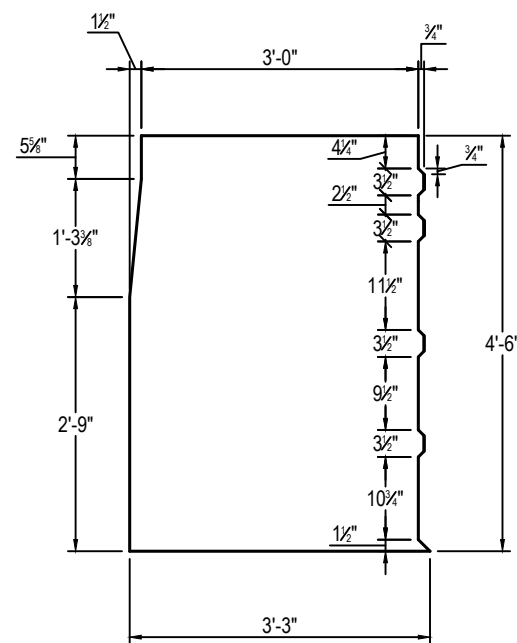
Typical Girder Layout - Girder P34, P41, P50 & P50R



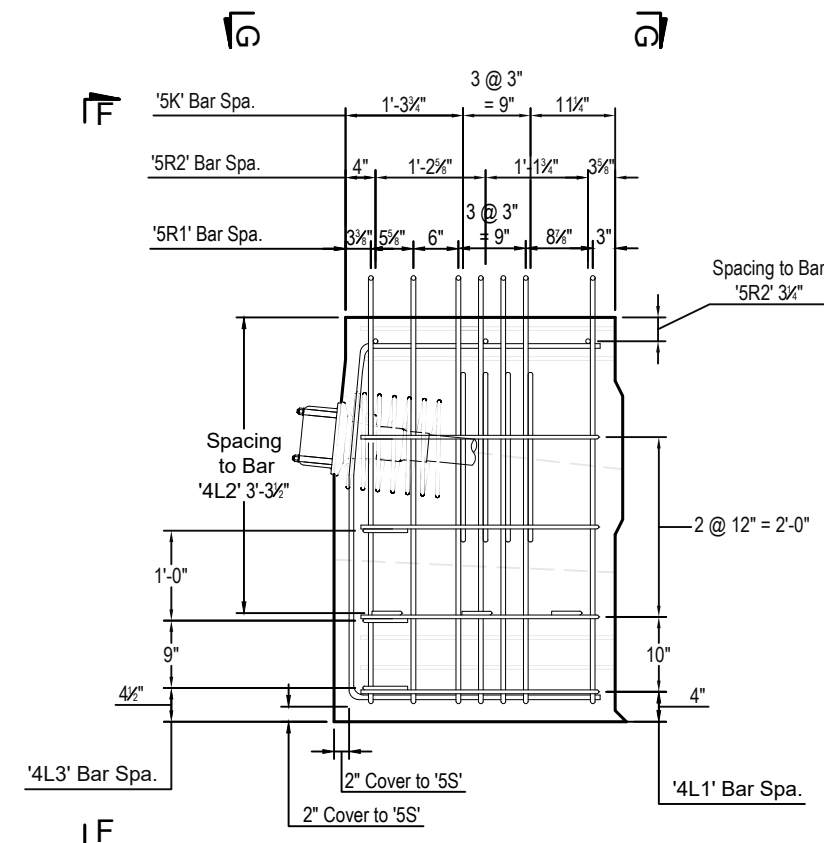
End Block - Girder P34, P41, P50 & P50R
Section F-F



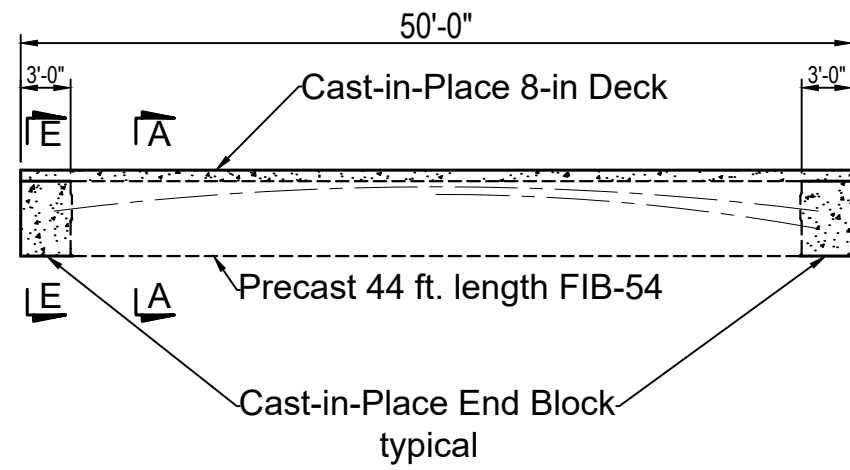
End Block - Girder P34, P41, P50 & P50R
Section G-G



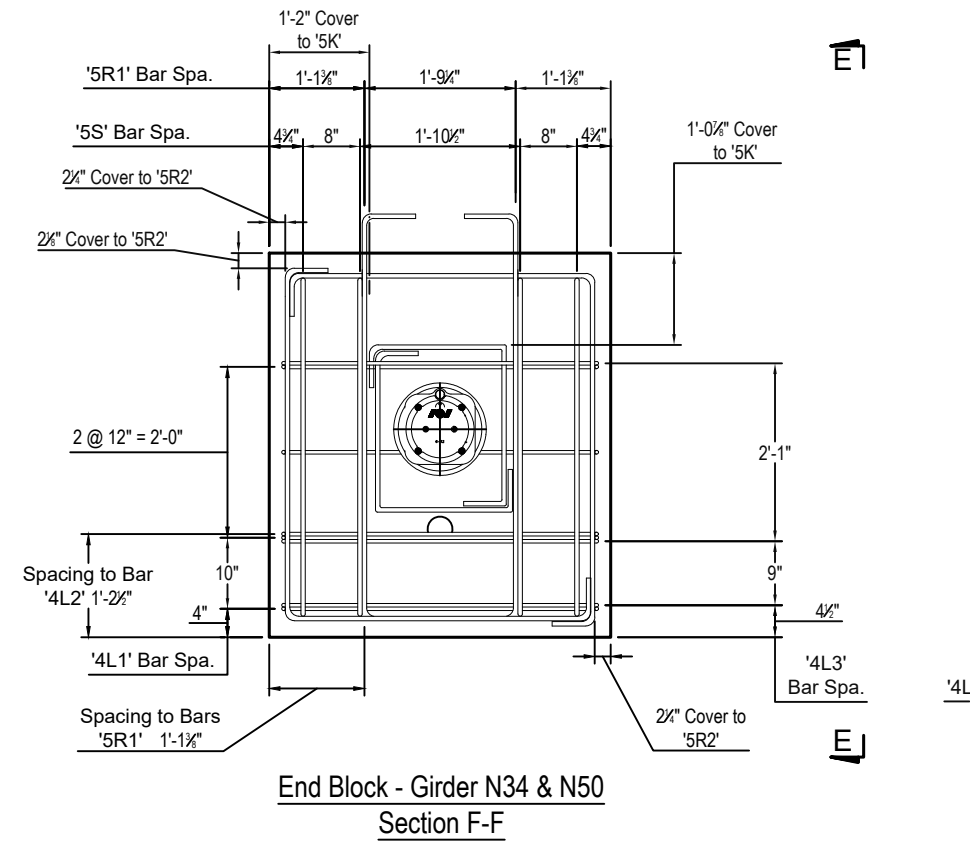
End Block - Girder P34, P41, P50 & P50R
End Block Dimensions



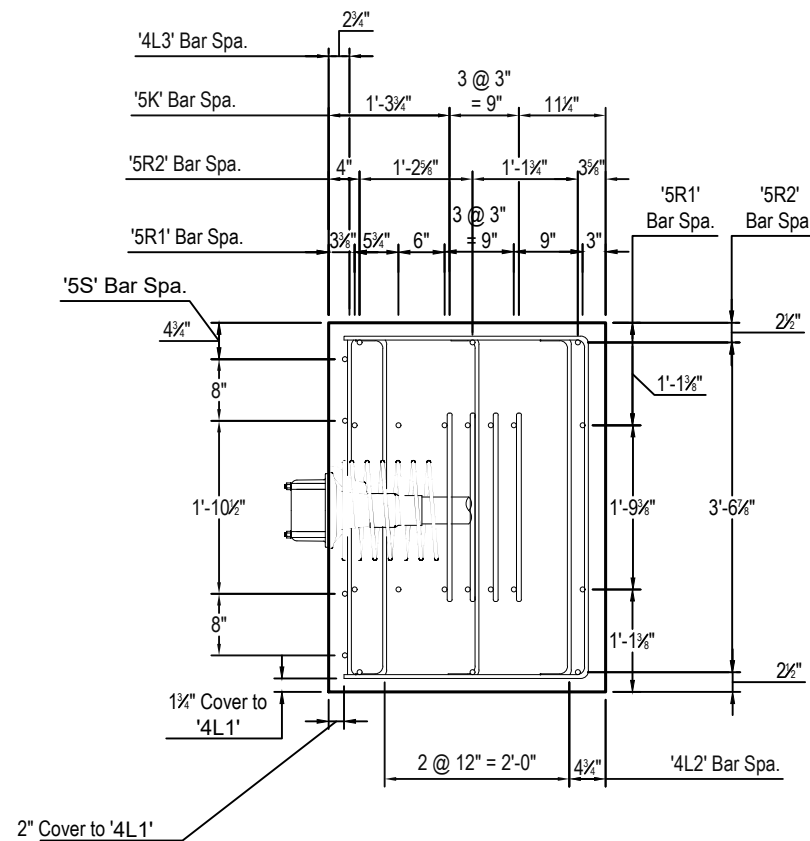
End Block - Girder P34, P41, P50 & P50R
Section E-E



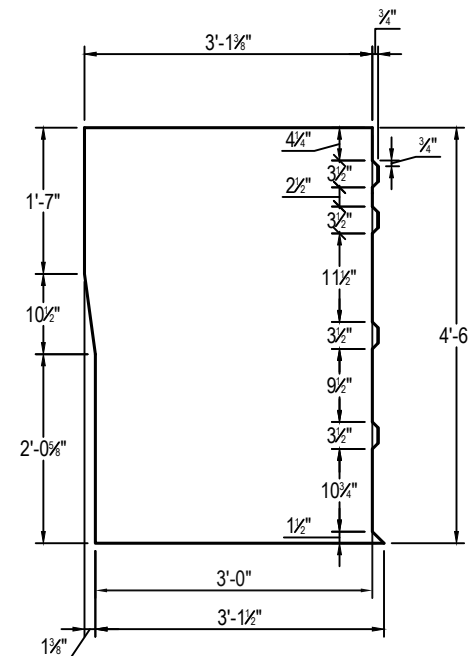
Typical Girder Layout - Girder N34 & N50



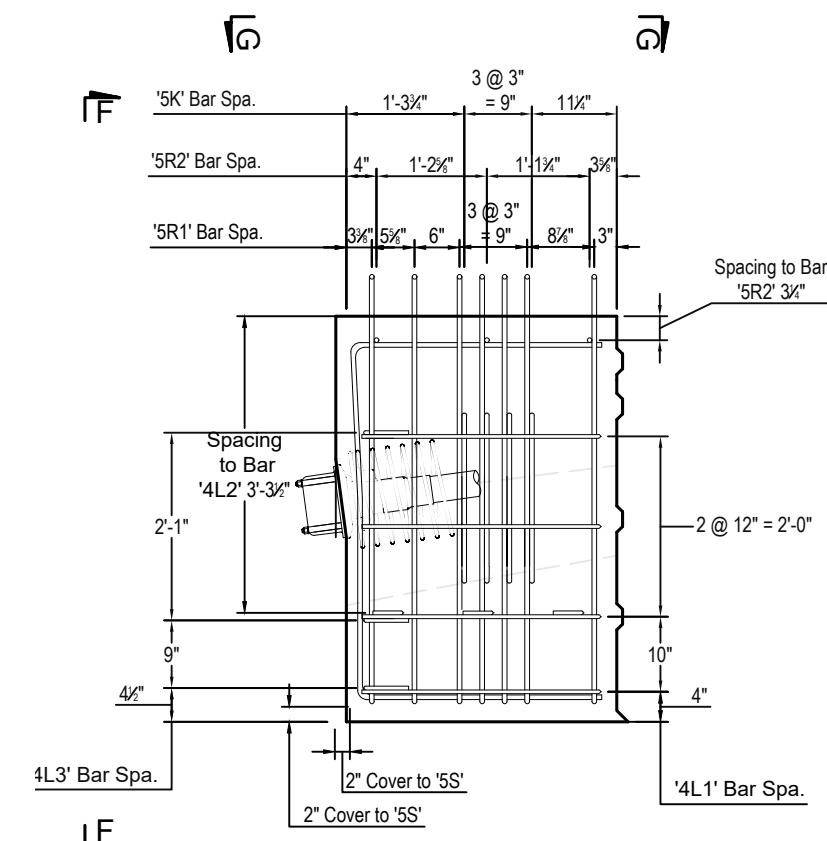
End Block - Girder N34 & N50
Section F-F



End Block - Girder N34 & N50
Section G-G



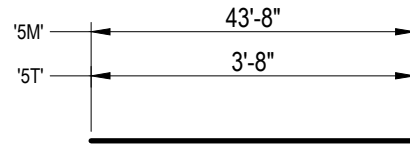
End Block - Girder N34 & N50
End Block Dimensions



End Block - Girder N34 & N50
Section E-E

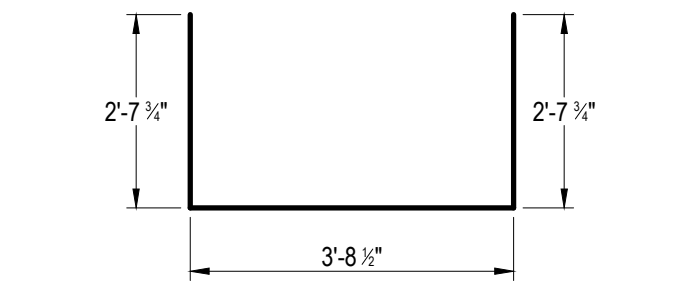
Bill of material: P00

Piece	Size	Qty.	Length	Notes
5T	#5	88	3'-8"	
5M	#5	8	43'-8"	

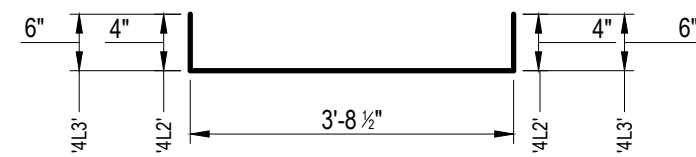


5T, 5M

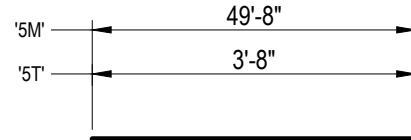
Bar Bending
 #3 Bars : bend around 1 1/2" dia. pin
 #4 Bars : bend around 2" dia. pin
 #5 Bars : bend around 2 1/2" dia. pin
 All dims are out-to-out



4L1



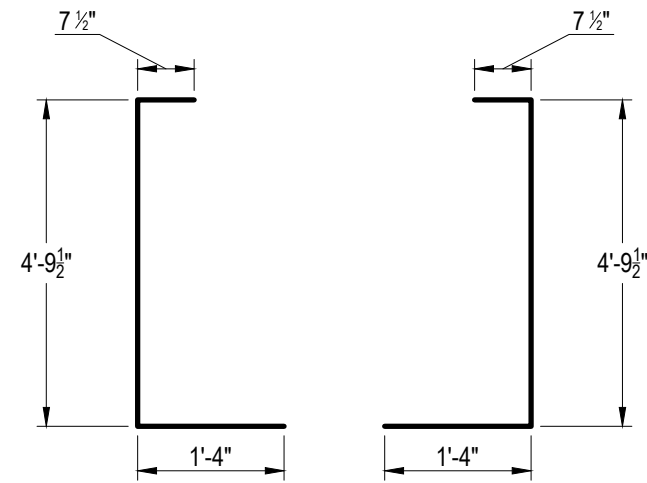
4L2, 4L3



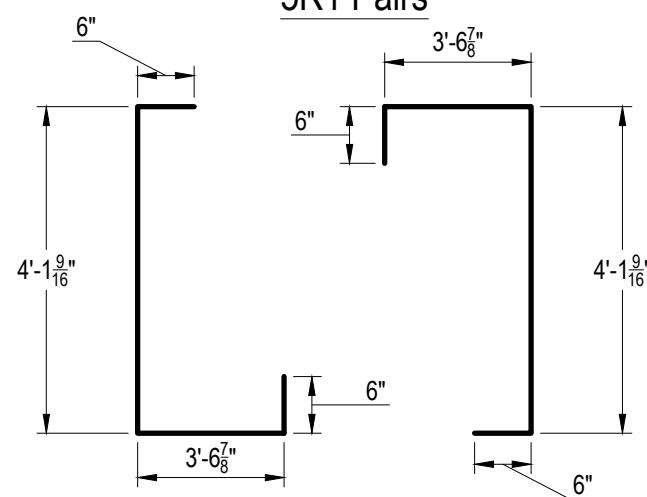
5T, 5M

Bill of mat.: P34, P41, P50, P50R

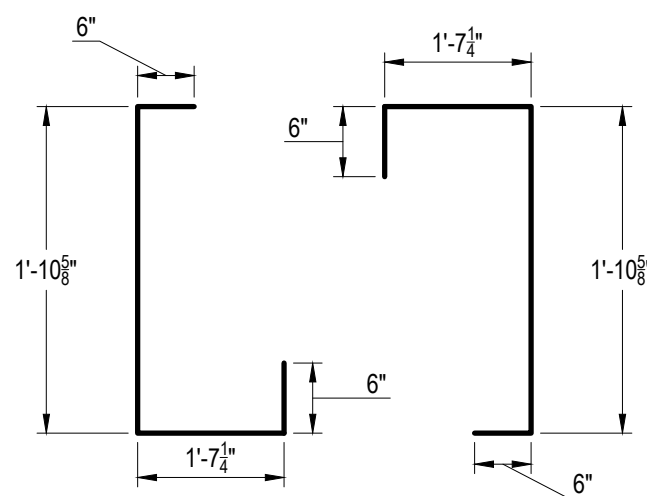
Piece	Size	Qty.	Length	Notes
5R1	#5	28	6'-9"	
5R2	#5	12	8'-8 7/16"	
5T	#5	100	3'-8"	
5M	#5	8	49'-8"	
5K	#5	16	4'-5 7/8"	
5S	#5	8	9'-6 9/16"	
4L1	#4	8	9'-0"	
4L2	#4	6	4'-4 1/2"	
4L3	#4	6	4'-6 1/2"	



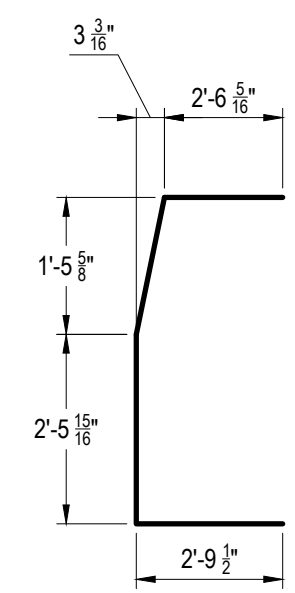
5R1 Pairs



5R2 Pairs

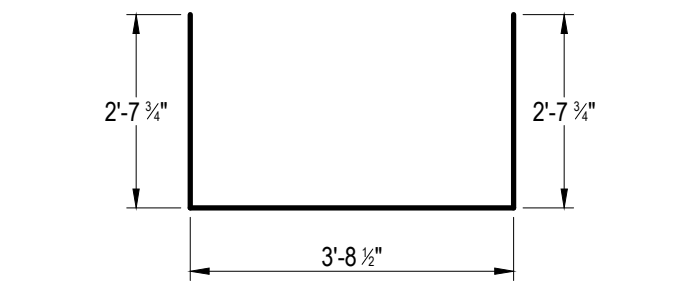


5K Pairs

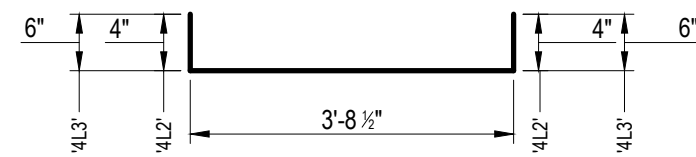


5S

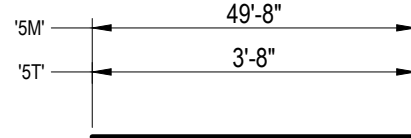
Bar Bending
 #3 Bars : bend around 1 1/2" dia. pin
 #4 Bars : bend around 2" dia. pin
 #5 Bars : bend around 2 1/2" dia. pin
 All dims are out-to-out



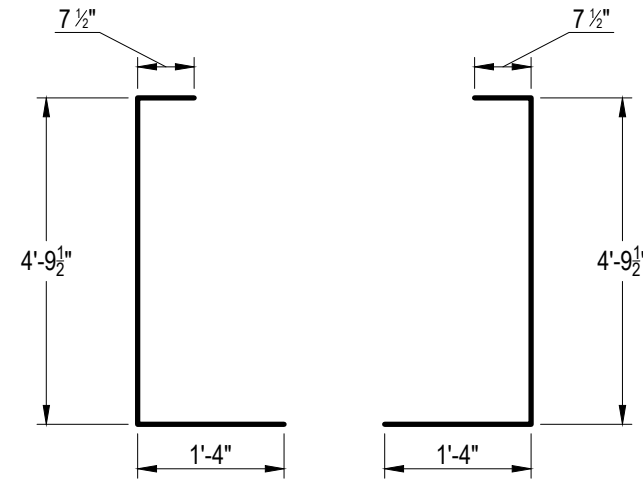
4L1



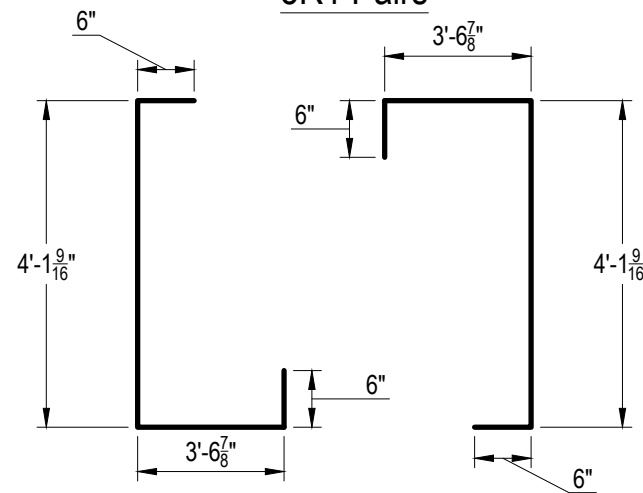
4L2, 4L3



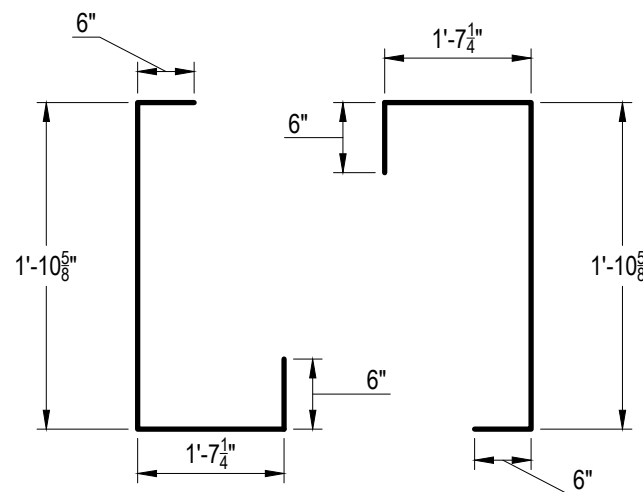
5T, 5M



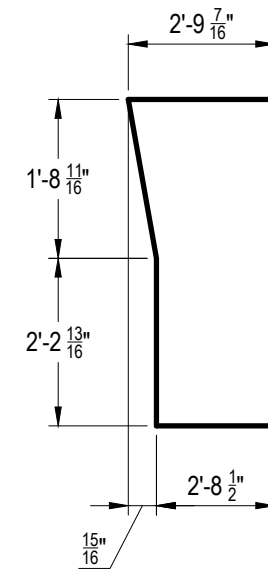
5R1 Pairs



5R2 Pairs



5K Pairs



5S

Bill of mat.: N34, N50

Piece	Size	Qty.	Length	Notes
5R1	#5	28	6'-9"	
5R2	#5	12	8'-8 7/16"	
5T	#5	100	3'-8"	
5M	#5	20	49'-8"	
5K	#5	16	4'-5 7/8"	
5S	#5	8	9'-6 3/8"	
4L1	#4	8	9'-0"	
4L2	#4	6	4'-4 1/2"	
4L3	#4	6	4'-6 1/2"	

Bar Bending
 #3 Bars : bend around 1 1/2" dia. pin
 #4 Bars : bend around 2" dia. pin
 #5 Bars : bend around 2 1/2" dia. pin
 All dims are out-to-out